In presenting the dissertation as a partial fulfillment of the requirements for an advanced degree from the Georgia Institute of Technology, I agree that the Library of the Institute shall make it available for inspection and circulation in accordance with its regulations governing materials of this type. I agree that permission to copy from, or to publish from, this dissertation may be granted by the professor under whose direction it was written, or, in his absence, by the Dean of the Graduate Division when such copying or publication is solely for scholarly purposes and does not involve potential financial gain. It is understood that any copying from, or publication of, this dissertation which involves potential financial gain will not be allowed without written permission.

3/17/65
b

A STUDY OF FREE MOLECULAR AND NEARLY-FREE MOLECULAR INTERNAL FLOW PROBLEMS

A THESIS

Presented to

The Faculty of the Graduate Division

by

Joseph Daniel Stewart

In Partial Fulfillment

of the Requirements for the Degree

Doctor of Philosophy

in the School of Aerospace Engineering

Georgia Institute of Technology

January, 1967

A STUDY OF FREE MOLECULAR AND NEARLY-FREE MOLECULAR INTERNAL FLOW PROBLEMS

Approved:

Chairman

Date approved by Chairman: 1/6/67

ACKNOWLEDGEMENTS

I would like to express my appreciation to my thesis advisor, Dr. A. Ben Huang, for his suggestion of the thesis topic and his willingness to discuss any difficulties encountered in the development of this work. I would also like to express my thanks to Professor J. E. Hubbartt and Dr. A. L. Ducoffe, who served on the reading committee, for their many helpful suggestions and careful review of the entire thesis.

I am also grateful to my friends for their encouragement throughout my stay at this institution. In particular, I express gratitude to Robert L. Stoy and Don P. Giddens, whose many discussions concerning the kinetic theory aspects of the problem were invaluable, and to Kenton D. Whitehead, Jerry A. Sills, and George W. Brown, whose comments concerning various aspects of the problem were quite helpful. I would also like to thank Miss Mary Dale for her patience during the typing of the final draft of this thesis.

I would also like to express gratitude for the financial assistance provided by a NASA Fellowship, NASA Research Grant NsG-657, and the Ford Foundation. This aid enabled me to pursue my graduate studies as a full-time student.

In conclusion, I am eternally grateful to my wife, Mary, whose support, patience, understanding, and encouragement have been instrumental to the attainment of my academic endeavor. Her devotion

has been an inspiration throughout my entire academic career. I would also like to thank her for her many hours of typing which went into the preparation of the rough draft of this thesis.

TABLE OF CONTENTS

LIST OF ILLUSTRATIONS

Figure Page

Figure Page

SUMMARY

A method for obtaining the complete free molecular solutions for internal flow problems is presented. This method consists of determining the distribution function for all boundaries of the flow field and obtaining the macroscopic moments of interest from the corresponding definitions. The usefulness of the method is illustrated by obtaining the complete free molecular solutions for the two dimensional channel and circular tube under the assumption of diffusely reflecting walls. These solutions include general expressions for the average flow rate and polynomial solutions for the nondimensional wall flux, as well as all of the common moments such as density, pressure, velocity components, heat flux components, etc. The procedure for obtaining the slit flow limits from the tube and channel results is outlined and a few of the limits presented. In addition, the method for obtaining the approximate results for a constant or linear wall flux variation over the entire channel or tube wall is described. To further illustrate the usefulness of the approach, the very difficult problem of free molecular flow through a rectangular channel is formulated for a few of the lower moments under the assumption of diffusely reflecting walls, and the general expression for the average mass flow rate and the integral equations for the boundary conditions are derived.

To obtain accurate numerical results it is necessary to solve the integral equations for the nondimensional wall flux. The collocation

method was applied and accurate results were obtained in the form of polynomial solutions for the two dimensional channel and circular tube. It is pointed out that the nondimensional wall flux can be determined to any desired degree of accuracy by this method. A series of linear segments is then fitted to the numerical results for the nondimensional wall flux and the contribution of each of these segments to the moment of interest is determined by analytically integrating over each of the linear wall flux segments. Any desired degree of accuracy for the moments can be attained by increasing the number of linear wall flux segments accordingly. The solutions for the two dimensional channel are expressed as a series of analytical functions which is suitable to numerical evaluation. For the two dimensional limits of constant and linear wall flux over the entire channel wall the solutions are analytical. However, in order to obtain numerical results for the circular tube, it was necessary to perform the integration with respect to one of the velocity angles numerically by Simpson's rule. Consequently, the circular tube solutions are expressed as a series of integrals which is also suitable to numerical evaluation.

Numerical results for several of the moments are presented for the two dimensional channel and circular tube for several flow conditions. Various results for a constant and linear wall flux over the entire channel or tube wall are compared with the accurate results obtained by linear wall flux segments in order to determine the range of validity of these solutions. The results are compared with the analytical results from other sources and experimental data, where such data were available.

Finally, the local and average mass flow rates for nearly-free molecular flow through a two dimensional slit for arbitrary pressure ratios are determined by the Willis iterative method. The free molecular solution required for this iterative scheme was obtained from the general solution for the two dimensional channel as a special case. The effect of a finite pressure ratio on the nearly-free molecular flow rates is studied, and results for the local and average flow rates for various pressure ratios and Reynolds numbers are presented.

The results of the investigation may be summarized in the following conclusions:

1. The method presented herein can be used to formulate the general problem of obtaining the local and average flow properties for free molecular flow through internal flow geometries, as illustrated for the cases of a two dimensional channel, a rectangular channel, and a circular tube.

2. Accurate numerical results for both local and average flow properties for free molecular internal flow problems can be obtained by using the collocation method to solve the integral equations for the wall flux. This method is a great improvement over all previous methods if the approximating functions weighted by the kernel can be analytically integrated.

3. The free molecular results obtained by previous investigators for the rectangular orifice, two dimensional channel, circular tube, and corresponding slit and orifice flows can be obtained as special cases of the general results presented herein, which are valid for arbitrary length-to-height ratios.

4. The results for a linear wall flux over the entire channel length are in worse agreement with the results for linear wall flux segments for intermediate values of length-to-height ratios. The limits of this range depend on the particular flow property of interest, the geometry considered, and the accuracy desired. For all practical purposes the linear wall flux solutions are good approximations for length-to-height ratios outside this intermediate range. For the circular tube case, the linear wall flux solutions for some of the flow properties are very accurate for the entire range of length-to-diameter ratios. Finally, the solutions for a constant wall flux over the entire channel length are accurate for only small length-to-height ratios.

5. The well-known long-channel and long-tube formulas of Clausing and Knudsen, respectively, for the average mass flow rate yield accurate results for sufficiently large length-to-height ratios.

6. The theoretical free-molecular values of average mass flow rate, as determined for the case of linear wall flux segments, agree quite well with the experimental values for the flow of a rarefied gas through a circular tube, even for inverse Knudsen numbers as large as one. The corresponding theoretical free-molecular average mass flow rates for a two dimensional channel do not agree well with the measured values for a rectangular channel whose width-to-height ratio is very large, even in the limit of very small inverse Knudsen numbers.

7. The backflow contribution for nearly-free molecular flow through a two dimensional slit is strongly dependent on the pressure

ratio for small pressure ratios, but for large pressure ratios the Reynolds number effect is predominant.

8. The nearly-free molecular flow rate through a two dimensional slit is larger than the corresponding free molecular value for all pressure ratios considered, and the magnitude of the difference continually increases with increasing Reynolds numbers.

NOMENCLATURE

Roman Symbols

$A_i(\, , \,)$	defined by equation (91) of Chapter III
a_1, a_2	defined by equations (25) and (26) of Chapter IV, respectively
$a_i(\,)$	defined by equation (83) of Chapter II or equation (88) of Chapter III
B^o	free-molecular nondimensional temperature, see equation (8) of Chapter IV
$B_i(\,)$	defined by equation (92) of Chapter III
$B_{2k-1}(\,)$	general coefficient in polynomial solution for wall flux
b_1	defined by equation (24) of Chapter IV
$b_i(\,)$	defined by equation (84) of Chapter II or equation (89) of Chapter III
C	magnitude of nondimensional total molecular velocity, see equation (8) of Chapter IV
c	magnitude of nondimensional planar molecular velocity, $h^{1/2}\lvert\vec{\xi}_r\rvert$
$\vec{c}$	nondimensional planar molecular velocity, $h^{1/2}\vec{\xi}_r$
$\bar{c}_1$	defined by equation (23) of Chapter IV
$D(\, , \,)$	defined by equation (40) of Chapter IV
d	height of channel or diameter of tube
$E(\, , \,)$	defined by equation (48) of Chapter IV
F	planar velocity distribution function
$F(\,)$	defined by equation (17) of Chapter II or equation (11) of Chapter III

$F_{\bar{x}'-\bar{x}}(\ ,\ )$	see equation (67) of Chapter II
f	velocity distribution function
$G_1(\ ,\ ), G_2(\ ,\ )$	defined by equations (28) and (29) of Chapter IV, respectively
$G_{0-\bar{x}}(\ )$	see equation (66) of Chapter II
g_w	nondimensional wall flux, see equation (12) of Chapter II
$g_{w_0}(\ )$	inlet value of nondimensional wall flux
$H_1(\ ,\ ), H_2(\ ,\ )$	defined by equations (30) and (35) of Chapter IV, respectively
h	$1/\sqrt{2RT}$
$I_n(\ ,\ )$	integral defined by equation (52) of Chapter IV
$K(\ ,\ )$	kernel for wall flux integral equation
$K^+(\ ), K^-(\ )$	two parts of kernel for circular tube, see equations (67) and (68) of Chapter III
L	length of tube or channel
M	number of terms in polynomial solution for wall flux
m	molecular mass
$\dot{m}$	Maxwellian equilibrium flux, $\rho\sqrt{8RT}/4\sqrt{\pi}$
$\dot{m}^{(1)}(\ )$	local mass flux for nearly-free molecular flow
$\overline{\dot{m}^{(1)}}(\ )$	average mass flux for nearly-free molecular flow, see equation (36) of Chapter IV
N	number of linear wall flux segments
N°	free-molecular nondimensional density, see equation (8) of Chapter IV
n	number density
P_1	static pressure in upstream tank

P_2	static pressure in downstream tank
P_{xx}, P_{yy}, P_{zz}	normal pressure components in the x-, y-, and z-directions, respectively
P_{yx}, P_{yz}	yx- and yz- components of shear stress tensor
p	static pressure
q_x, q_y, q_z	x-, y-, and z-components of heat flux vector
R	gas constant or radius of tube
Re	Reynolds number, see equation (11) of Chapter IV
T	thermodynamic temperature
U	nondimensional x-component of macroscopic velocity, $u/\sqrt{2RT}$
u	x-component of macroscopic velocity
V	nondimensional y-component of macroscopic velocity, $v/\sqrt{2RT}$
v	y-component of macroscopic velocity
$\vec{W}^o$	free-molecular nondimensional macroscopic velocity, see equation (9) of Chapter IV
w	z-component of macroscopic velocity
$\vec{w}^o$	free-molecular macroscopic velocity
x,y,z	position coordinates
$\bar{x}, \bar{y}, \bar{z}$	nondimensional position coordinates, defined in each chapter
$\bar{z}_r$	nondimensional z-coordinate, z/R

Greek Symbols

α	polar angle in ξ-η plane of velocity space
$\alpha_1, \alpha_2, \alpha_3, \alpha_4$	angles specifying a point in flow field for the two dimensional channel or slit

$\bar{\beta}(\ )$	denotes nondimensional distance measured in xy-plane of circular tube, see equation (3) of Chapter III
$\bar{\beta}_1(\ ), \bar{\beta}_2(\ )$	defined by equations (43) and (44) of Chapter III, respectively
δ	inverse Knudsen number
ζ	z-component of molecular velocity
η	y-component of molecular velocity
η', η''	nondimensional distances measured along particle path, see equation (9) of Chapter IV
θ	denotes polar angle for spherical velocity coordinates
θ_1, θ_2	defined by equations (41) and (42) of Chapter III, respectively
$\Lambda(\ )$	nondimensional average mass flow rate
ν	constant appearing in B-G-K model, see equation (6) of Chapter IV
ξ	x-component of molecular velocity
ξ_r	magnitude of planar molecular velocity, $\lvert\vec{\xi}_r\rvert$
ξ_ρ	magnitude of molecular velocity for spherical velocity coordinates
$\vec{\xi}_r$	planar molecular velocity
ρ	mass density
τ	length-to-height ratio, L/d, for channel or length-to-radius ratio, L/R, for tube
τ_d	length-to-diameter ratio for tube, L/d
$\Phi_{2k-1}(\ ), \Phi_{-1}(\ )$	defined by equations (73) and (74) of Chapter II, respectively
$\Phi^{+}_{2k-1}(\ ), \Phi^{+}_{-1}(\ )$	defined by equations (62) through (65) of Chapter III, respectively
φ	denotes azimuthal angle for spherical velocity coordinates

$\varphi_1(\ ),\ \varphi_2(\ )$	denote azimuthal angles for point on surface of discontinuity for velocity distribution functions
$\varphi_i(\ )$	defined by equation (93) of Chapter III
$\varphi_{2k-1}(\ )$	defined by equation (71) of Chapter II or equation (60) of Chapter III

Superscripts

f.m.	denotes free-molecular conditions
L,U	denote lower and upper walls, respectively
(o)	denotes results for free-molecular flow
(1)	denotes first iterative results for nearly-free molecular flow
'	denotes lower wall of channel or wall of tube
"	denotes upper wall of channel

Subscripts

1,2	denote upstream and downstream tanks, respectively
F.M.	denotes free-molecular conditions
i	denotes i-th wall flux segment
L,U	denote lower and upper walls of channel, respectively
W	denotes wall of tube or channel

CHAPTER I

INTRODUCTION

Discussion and Review of Literature

Discussion

Tsien [1] in 1946 rather arbitrarily divided the entire flow regime of gas dynamics into four parts: the continuum, the slip, the transition, and the free molecular flow regimes. The parameter used to define these regimes was the Knudsen number, which is defined as the ratio of the local mean free path to a representative dimension of the body under consideration or of the flow field. The continuum regime was defined for Knudsen numbers much smaller than unity ($Kn < 10^{-2}$). For this regime the intermolecular collisions are the predominant factor in determining the local flow properties and the interaction of the gas particles with the solid boundary is considered negligible. The slip flow regime was defined for Knudsen numbers less than unity but not extremely small ($10^{-2} < Kn < 1$). The intermolecular collisions are still predominant in determining the local flow properties in the core of the gas; however, near the solid boundaries this effect is of the same order of magnitude as the gas-surface interaction. For the transition flow regime, defined for Knudsen numbers greater than unity but not extremely large ($1 < Kn < 10$), both effects are of the same order of magnitude in determining the local flow properties. Finally, the free molecular regime was defined for large Knudsen numbers ($Kn > 10$).

This regime is governed solely by the gas-surface interaction in determining the local flow properties. Once the velocity distribution function is known for all boundaries of the flow field the local flow properties can be obtained. It should be noted that the term "nearly-free molecular" refers to that part of the transition flow region where first-order intermolecular collisional effects are considered.

Making use of the available continuum flow solutions for internal flow problems, a reasonable estimate of the transitional results based on the free molecular and continuum values can be made for the particular flow property of interest. It should be noted that the solution for the entire flow regime for the flow of a gas through a circular tube, two dimensional channel, etc. of finite length represents a formidable problem in the realm of the kinetic theory of gases. Analysis of the free molecular problem alone was begun in 1909 by Knudsen [2] and to date no complete analysis of the general problem of the flow of gas through finite length tubes and channels under free molecular conditions exists. Having solutions available for such problems should prove quite useful in more definitely defining the Knudsen number range within which the transition and slip flow regimes fall by comparing with experimental results as they become available.

With a growing interest in rarefied gas phenomena the kinetic theory solutions for application in low-density technology become quite important. For example, thermionic energy converters sometimes operate at conditions quite suitable for free molecular flow in that the mean free path of the gas passing through the converter is large compared to the distance between the converter walls. Perlmutter [3] has shown also

that the free molecular heat transfer of the gas is significant when compared to that of radiation for nominal operating conditions. Also, the problem of neutron diffusion is sometimes approximated by the free molecular flow of neutrons through an array of similar geometries such as circular tubes, etc. Still more examples of the application of free molecular flow solutions are propellent injection ducts for electric thrustors and in the realm of vacuum technology.

Due to the importance of gas dynamic solutions for all flow regimes there has been considerable emphasis in recent years on determining solutions of the Boltzmann transport equation. Unfortunately, however, only a few problems have been solved completely for all flow regimes, and these solutions have generally been restricted to linearized one-dimensional steady and unsteady problems; e.g., Couette flow, heat transfer between parallel plates, propagation of sound in monatomic gases, Rayleigh problem, etc. The exception is the plane shock-wave structure which has been studied by various iterative schemes. In an attempt to solve more general flow problems, many investigators have chosen to formulate the problem in the free molecular regime, obtain the complete solution for this region, and then use this solution in conjunction with various techniques for solving the Boltzmann equation to obtain the nearly-free molecular solution. The advantages of this approach are that a more general class of problems can be solved for the nearly-free molecular region and the non-linearity of the problem preserved. Since the complete free molecular solution is required in order to generate the nearly-free molecular solution via the iterative methods, it is desirable to have available methods whereby

the free molecular solution can be easily obtained. A method which has been successful in describing the nearly-free molecular flow regime accurately for a variety of problems is the Willis iterative method [4].

In view of the application of the free molecular and nearly-free molecular solutions for internal flow problems set forth in the preceding discussion, several internal flow problems will be analyzed in this work. In the free molecular part the general formulation of flow through circular tubes and two dimensional and rectangular channels will be presented. As special cases the corresponding orifice results can be obtained. In the nearly-free molecular part of this work the local and average mass flow rates through a two dimensional slit including backflow will be analyzed. The solutions of these problems provide rigorous theoretical results which can be used to compare with precise experimental measurements as they become available.

Review of Literature

Free Molecular Flow. The flow of a highly rarefied gas through cylindrical tubes of finite length has been a subject both of analytical and experimental interest for many years. In general, the various investigations have been concerned with determining the relationship between the average flow rate and the pressure potential which induces the flow. Only recently have there been any attempts at determining the local flow properties throughout the entire flow field. It should be noted that it is precisely the latter quantities which are of interest to gas dynamicists and which are needed for iterative schemes such as that proposed by Willis.

The relationship between the average flow rate and the pressure potential for free molecular flow through very long circular tubes was presented by Knudsen [2] in 1909. However, he used an unreliable method and some of his results were wrong. Smoluchowski [5] soon afterward obtained the general expression for the free-molecular average flow rate for very long cylindrical tubes with cross section of any nonreentrant shape. The most important assumptions made in deriving these expressions were those of small density gradient and diffusely reflecting walls. Smoluchowski [5] generalized his work to account for part of the particles being reflected specularly from the walls. It should be noted, however, that none of these results included end effects. Consequently, in 1918 the problem of the short circular tube was subjected to thorough study by Clausing [6] in his thesis. This same work appeared in the published literature [7] in 1929. In this paper Clausing also presented a formula derived by Smoluchowski for the free-molecular average flow rate through an infinitely long rectangular channel. In 1932 Clausing [8] presented his findings for the finite length circular tube of arbitrary length-to-diameter ratio. No accurate formula for the average flow rate could be obtained in terms of known functions, but he worked out a close approximation and presented numerical values for the entire range of length-to-diameter ratio. Clausing [8] also presented an approximate solution for the free-molecular average flow rate through rectangular channels for which the width was much larger than both the height and length and the length much larger than the height. During the same period experimental results were being obtained by Knudsen [2] in 1909 and

Gaede [9] in 1913. Both of these investigators studied the molecular flow of gases through circular glass tubes and measured the average flow rates. Gaede obtained agreement with the long tube formula within one per cent for hydrogen and two per cent for nitrogen for large Knudsen numbers. Similarly, Knudsen, experimenting with less refinement, got a similar agreement using hydrogen, oxygen, and carbon dioxide; in the case of hydrogen he found the formula to hold even for Knudsen numbers as small as six-tenths. However, since vacuum technology was in the preliminary stages of development during this period the accuracy of the results for large Knudsen numbers (i.e., low pressures) are considered questionable. Gaede [9] also measured the average rate of flow through a rectangular slit of 3.4-cm. width, 0.004-mm. height, and 0.12-cm. length. In 1937 Rasmussen [10] measured the average rate of flow through a rectangular channel of 0.97-cm. length, 1.32-cm. width, and 0.019-mm. height. A comparison with the theoretical value predicted by Clausing's rectangular channel formula showed that the experimental values for large Knudsen numbers were approximately twenty-five per cent low. However, since the width of the channel is only about one and one-half times the length, a comparison with Clausing's formula is questionable. It should also be noted that in the experiments of Gaede and Rasmussen the height of the channel was of such small dimensions that accurate measurements of these dimensions could not be obtained. Since the geometrical dimensions of the channel are the primary factors in determining the conductance of a tube or channel in free molecular flow, these experimental results should not be used to prove or disprove the validity of the theoretical free molecular formulas.

Since the pioneering efforts of Knudsen, Smoluchowski, Gaede, Clausing, and Rasmussen numerous analytical and experimental results have been reported. Bosanquet and Barrett [11] in 1944 derived expressions for the free-molecular average flow rate through infinitely long tubes and channels of various cross sections. In 1946 Brown, Di Nardo, Cheng, and Sherwood [12] presented experimental results for the average flow rate through straight copper and iron pipes. Data were obtained for nominal pipe diameters ranging from 5/8 in. to 8 in. and lengths ranging from 127 cm. to 1040 cm. They compare the nondimensional average flow rate at large Knudsen numbers through tubes of length-to-diameter ratios of 8.8, 4.8, and 2.9 with the theoretical free molecular results of Clausing [8]. The percentage differences based on the theoretical values are 8.3, 20.0, and 6.5 per cent, respectively. However, Clausing's results are only approximate and overestimate the exact values of average flow rate, as shown by Demarcus [13] and again shown by the results of the present investigation. Since the only special assumption made in deducing these theoretical values, in addition to the general results of kinetic theory, is that of diffuse reflection by the walls of the tube, the latter assumption seems to be definitely confirmed by these experimental results. The most complete experimental investigation into the flow of gases through various tubes and channels was reported in 1956 by Dong [14]. Data were obtained for the average flow rate for hydrogen, helium, air, carbon dioxide, and Freon-12 for copper tubes and channels. These tubes and channels included a circular section with a 3.64-cm. radius and 10.5-ft. length, two annular sections formed by inserting

cores of 1.905-cm. and 3.174-cm. radii into the circular section, respectively, and a rectangular section 0.324-cm. by 22.86-cm. and 50 in. in length. The Knudsen number range was sufficiently large to essentially include the free molecule and continuum limits for the circular and annular sections. However, the experimental values for the rectangular section fall about 30 per cent below the free molecular theoretical value, which was determined from the infinite rectangular channel formula. Dong also verified that the fraction of particles diffusely reflected from the tube walls was very close to unity for all gases considered. Therefore, it can be concluded that the assumption of diffuse reflection for free molecular internal flow problems is very good for moderate pressure ratios. Although Dong used only copper for the tube and channel walls, the same conclusion has been drawn from the work of Adzumi [15], Knudsen [2], Gaede [9], and Brown, et al. [12], as discussed above, using materials such as glass and iron.

The most recent analytical work for free molecular internal flow problems was begun by Demarcus and Hopper [16] in 1955 and Demarcus [13] in 1957. In these two works the emphasis is again on determining the conductance of finite length tubes and channels. Demarcus [13] uses a variational method to determine values of the conductance for circular tubes and two dimensional channels. He is able to determine upper and lower bounds for the conductance and presents results for several values of length-to-height ratios. Demarcus also proves rigorously that in the limit of very long circular tubes the formula of Smoluchowski [5] and Knudsen [2] is correct. In 1956 Dayton [17] determined analytically the gas flow patterns at the entrance and exit

of cylindrical tubes. This represented one of the first attempts in determining results for the local properties. It might be noted at this point that the Monte Carlo technique has also been used by many authors to calculate the free-molecular conductance through tubes and channels of various geometries. For example, see Levenson, Milleron, and Davis [18] and Davis [19]. Both of these works appeared in 1960. In 1963 Sparrow, Jonsson, and Lundgren [20] presented their results for the circular tube of finite length. These results consisted of the nondimensional wall flux, the average mass flow rate, and the adiabatic-wall temperature variation for values of the length-to-diameter ratio ranging from zero to 25. They utilized the analogy between the free molecular problem and the radiation problem. The results for the density, velocity, and temperature fields for free molecular flow through a circular orifice were reported in 1961 by Narasimha [21]. The corresponding density field for free molecular flow through a rectangular orifice was reported in 1961 by Howard [22], and later verified by a different method by Gustafson and Kiel [23]. These authors also presented the results for the circular orifice density field.

Very recently two experimental papers have appeared in the literature on the measurement of the local flux of particles downstream of short circular tubes. Gadamer [24] obtained the local flux across the diameter of a short circular tube of length-to-diameter ratio of unity at two stations just downstream of the exit for upstream Knudsen numbers based on the tube diameter of 2.3 and 1.0. A comparison with the free molecular solution showed fair agreement even for these

moderate Knudsen numbers. It should be noted that Gadamer was unable to give accurate error bounds for his results due to errors introduced by the use of a McLeod gage in the upstream chamber which was slightly inaccurate for the pressure range considered. Cook and Richley [25] measured the flux of particles for cesium vapor far downstream of the exit of circular tubes, which had length-to-diameter ratios from zero to four, for upstream Knudsen numbers based on tube diameter of 0.055 to 9.5. They also measured the average flow rate through the tubes. The measured distribution patterns for the local flux for large Knudsen numbers were in good agreement with the free-molecular theoretical patterns, which were derived for diffuse reflection from the wall, for length-to-diameter ratios of one-half, one, and two, and in fair agreement for three and four. The measured average flow rates of cesium vapor through the tubes were either equal to or less than those predicted by Clausing's free-molecular results for Knudsen numbers greater than about eight-tenths.

In 1964 a number of papers concerned with free molecular internal flow problems appeared. Perlmutter [3] determined several moments of the local properties for free molecular flow through finite length two-dimensional channels, but in order to perform the integrations analytically he assumed that the nondimensional wall flux varied linearly for the entire channel length. This approximation does not insure satisfaction of the boundary condition exactly, and as a result the moments are in greatest error at the walls. Since this is the region of greatest interest in many cases, a solution which would minimize this error, or completely remove it, is desirable. Also,

Perlmutter simplifies to the case of an isothermal system in determining most moments. It would be desirable to formulate the more general problem of arbitrary wall temperatures for all the macroscopic moments. Reynolds and Richley [26], [27] have presented numerical results for the nondimensional wall flux, the average flow rate, and the flux patterns downstream of the exit for free molecular flow through converging and diverging slots. They have also presented the results for wall flux and average flow rate for converging and diverging tubes. The length-to-inlet height ratio was varied from zero to eight. Their results for the wall flux are reported to three significant figures, but for the larger length-to-height ratios the results for the circular tube and two-dimensional channel with parallel walls are in slight error, since they do not satisfy the anti-symmetric property exactly. Sparrow and Haji-Sheikh [28] calculated the local axial velocity and formulated the density for free molecular flow through a circular tube. The results for axial velocity were obtained by numerical integration for length-to-diameter ratios of 0.25, 1.0, 4.0, and 10.0. Among other results obtained recently are those of Townsend [29] for the convection of mass, axial momentum, and kinetic energy through axi-symmetric tubes for free molecular conditions. Radial distributions of these flow quantities across the inlet and exit planes for several configurations are presented.

Nearly-Free Molecular Flow. Most of the experimental works discussed in the preceding section contain results for the nearly-free molecular regime. However, theoretical results to date for this regime for two-dimensional internal flow problems are limited. The two

dimensional slit and circular orifice are among the few which have been considered. Liepmann [30] has pointed out that orifice or slit flow offers the possibility of comparing theory and experiment without having to assume a particular gas-wall interaction model. Taking into account the effects of a finite wall for internal problems introduces the difficulty of a variable wall density, which is required in defining the velocity distribution function at the boundary, even in the free molecular limit, as opposed to a constant wall density for a body submerged in a free molecular stream or for free molecular flow through infinitely long tubes or channels. The only attempt to date, to the author's knowledge, at solving two-dimensional internal flow problems including the wall effects has been that of Wu [31]. He solves the integral equation for the wall density by matrix theory and formulates a probability model by a Markov chain process. Wu uses the iterative method of Willis [4] and presents some approximate results for the wall density and local density for nearly-free molecular flow through two parallel plates with length-to-height ratio of four. It should be noted, however, that a number of simplifying approximations are made throughout the entire analysis and the free molecular solution used in the iterative scheme is only an approximate one.

As pointed out earlier, the only method to date which has been applied with any success to two-dimensional internal flow problems is that of Willis [4]. The convergence of this iterative scheme has been proven for three simple linearized problems by Willis [4] and Pao [32]; however, convergence has not been proven in general. Consequently, it

is assumed that the scheme is convergent for more difficult problems. The final verification, of course, must be based on comparison with accurate experimental results.

In 1960 Narasimha [21] applied the Willis iterative method to the flow of gas through a circular orifice under nearly-free molecular conditions into a vacuum downstream. He made several simplifying approximations and obtained an expression for the average mass flow rate based solely on the value of the centerline velocity. A comparison with the experimental results of Liepmann [30] showed reasonable agreement. Narasimha concluded that the departure of the average flow rate from the free molecular value was linear in the inverse Knudsen number and that nearly-free molecular conditions prevailed up to an inverse Knudsen number of approximately unity. Willis [33] in 1965 reported his results for the same problem but made no simplifying approximations in obtaining the average flow rate based on the complete first iteration. In addition he solved the corresponding problem for the two dimensional slit. It should be noted that none of these analyses accounted for backflow since the gas was assumed to exit into a vacuum. Willis also compared his results for the circular orifice with the experimental data of Liepmann [30]. For sufficiently small inverse Knudsen numbers for which the theoretical first iteration is valid, the scatter in the experimental data was too large to draw any definite conclusions. At best he could only claim fair agreement with the complete first iterative results. However, it could clearly be seen that while Narasimha's results overestimated the average flow rate, Willis' results underestimated the flow rate. Very recently

Hurlbut, Lord, and Willis [34] reported experimental results for the average flow rate through a circular orifice at large Knudsen numbers. These results compare favorably with Liepmann's but are considered much more accurate. The complete first iteration for average flow rate, although slightly high, agreed well with these results in the nearly-free molecular regime. However, the axial measurements of the local flow rate did not compare favorably with the results of Willis' iteration. Whether or not the discrepancy exists in the theoretical or experimental results was not resolved. Other measurements for the average flow rate at large Knudsen numbers through circular orifices and very short circular tubes have been reported recently by Sreekanth [35], Smetana, Sherrill, and Schort [36], and Cook and Richley [25].

It should be noted at this point, in view of the above discussion, that the effects of the tube or channel walls and the backflow on the local and average flow rate through internal flow geometries have not been treated theoretically to date. Although these effects are considered to be small for very large pressure ratios and very thin orifices and slits, it would be helpful to determine for what range of variables the effects are considered significant.

Purpose

The purpose of the present work is:

1. To present a new approach which can be applied in a rather straight-forward manner to obtain all moments for internal free molecular flow problems by determining the distribution function for

the entire flow field and obtaining the moments directly from their definitions.

2. To illustrate the usefulness of this approach by obtaining solutions for the free molecular flow of gases through various tubes and channels, and to compare the theoretical results with the results of previous investigators and experimental results, where such results are available.

3. To study the effects of a finite pressure ratio on the local and average mass flow rates for nearly-free molecular flow through a two dimensional slit using the Willis iterative method.

CHAPTER II

FREE MOLECULAR FLOW THROUGH A TWO DIMENSIONAL CHANNEL OF ARBITRARY LENGTH

Statement of the Problem

The physical problem consists of the flow of gas between two reservoirs which, respectively, contain gas in equilibrium at P_1, T_1 and P_2, T_2, as shown in Figure 1. The wall temperatures are taken as constant at T_U, upper plate, and T_L, lower plate. The mean free path of the gas is assumed to be sufficiently large in comparison to the geometrical dimensions of the channel so that the effects of collisions between particles are negligible. It is also assumed that the gas particles which interact with the channel walls are completely accommodated to the appropriate wall temperature and are diffusely reflected. Therefore, by satisfying the boundary condition that there be no net flow normal to the channel walls at the walls, the local wall density can be determined for the gas particles leaving the channel walls and the corresponding distribution function can be obtained. The distribution functions for the gas particles leaving the channel walls, as well as for the gas particles emerging from the two reservoirs, are thus the equilibrium Maxwellian distribution functions. Since the reservoir temperatures and densities are constant, the corresponding Maxwellian distribution functions are independent of the physical coordinates. However, since the wall densities are not constant, the

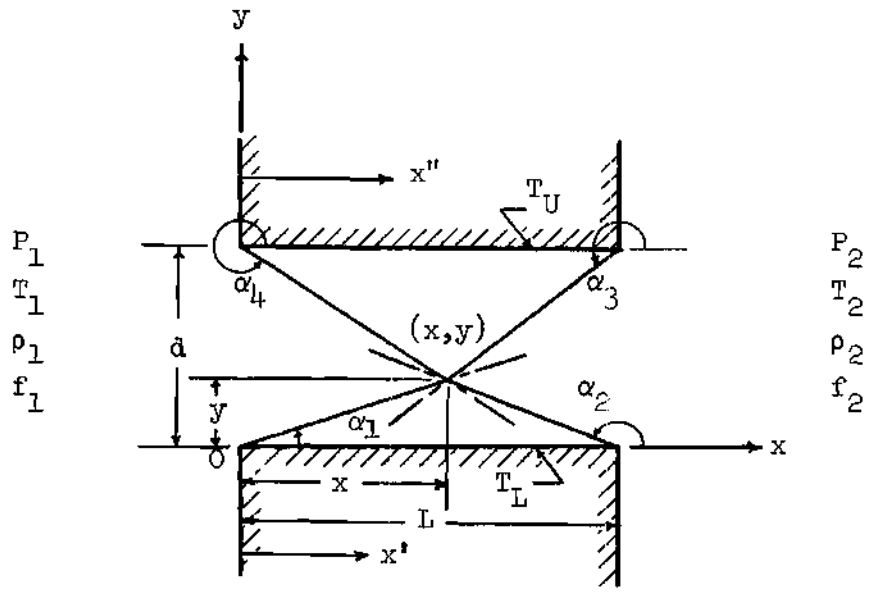

Two Dimensional Channel

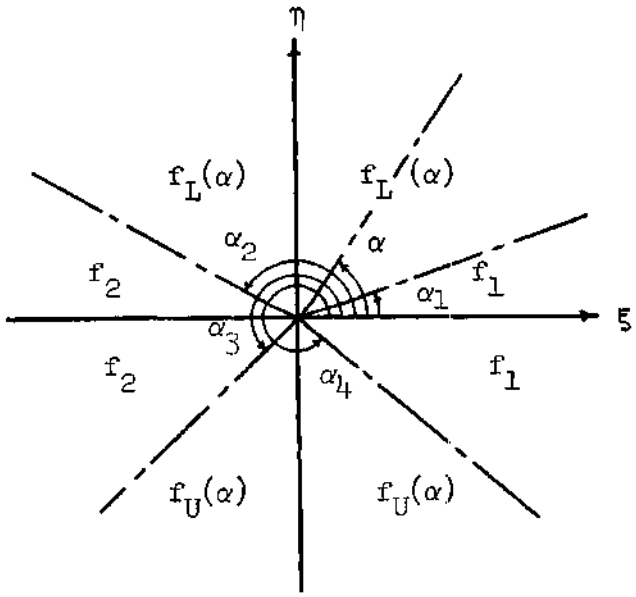

Velocity Space

Figure 1. Schematic of the Two Dimensional Channel and Division of Velocity Space for a General Point (x,y) of the Flow Field.

wall distribution functions do depend on the physical coordinates. Having determined the velocity distribution function for all boundaries in the flow field the distribution function for any arbitrary point, (x,y), as shown in Figure 1, is known since the distribution function is constant along a particle path in free molecular flow. The latter property enables one to trace each particle to a boundary where the distribution function is known. The flow field is therefore divided into four regions as illustrated in Figure 1. The corresponding velocity space is also presented in Figure 1 and the appropriate distribution function for each region is shown. By introducing the definitions for density, velocity, and higher moments the flow properties of interest at any point in the flow field can be determined by integrating the appropriately weighted distribution functions over the entire velocity space.

Since the wall distribution functions vary with the angle α, as illustrated in Figure 1, it is necessary to know the exact analytical expression for the wall density variation in order to determine the exact analytical expressions for the moments. However, the wall density must be obtained from an integral equation, which evolves from satisfying the boundary condition that there be no net flux of particles normal to the channel wall at the wall. Since the exact solution of the integral equation is not known, it becomes necessary to satisfy the integral equation for the boundary condition approximately, and then use these results to evaluate the moments.

The results presented in this chapter are only valid for the region defined by $0 \leq y \leq d$ and $-\infty < x < \infty$. The results for the

other parts of the flow field can be obtained from the results here by eliminating the appropriate wall effects and changing the limits of integration in velocity space. However, the results for slit flow are valid for the entire flow field. It should be noted that the two dimensional results presented in this chapter are special cases of the more general problem of free molecular flow through a rectangular channel. To illustrate the usefulness of the method to be presented herein, the general expressions for the density and velocity components were formulated for the more difficult problem of free molecular flow through a rectangular channel. In addition, the integral equations for the nondimensional wall fluxes and the general expression for the average mass flow rate were derived. The general formulation of these results is presented in Appendix A.

General Formulation

In the following sections the distribution functions for the flow field are determined, the integral equation representing the boundary condition is derived, the moments for density, velocity, pressure, etc. are determined in general by making no assumptions regarding the wall density variation, and the general relation for the average mass flow rate is derived. The results for slit flow are also presented as limiting cases by setting the length of the channel equal to zero.

Distribution Functions

Referring to Figure 1 it can be seen that the distribution function at any point in the flow field is composed of four separate Maxwellian distribution functions which are as follows:

$$f_1(\xi,\eta,\zeta) = \frac{n_1}{(2\pi RT_1)^{3/2}} e^{-\frac{[\xi^2+\eta^2+\zeta^2]}{2RT_1}} \quad \begin{cases} \alpha_4(\bar{x},\bar{y}) < \alpha \leq 2\pi \\ 0 \leq \alpha < \alpha_1(\bar{x},\bar{y}) \end{cases} \qquad (1)$$

$$f_2(\xi,\eta,\zeta) = \frac{n_2}{(2\pi RT_2)^{3/2}} e^{-\frac{[\xi^2+\eta^2+\zeta^2]}{2RT_2}} \qquad \alpha_2(\bar{x},\bar{y}) < \alpha < \alpha_3(\bar{x},\bar{y}) \qquad (2)$$

$$f_L(\bar{x},\bar{y},\xi,\eta,\zeta) = \frac{n_L(\bar{x}')}{(2\pi RT_L)^{3/2}} e^{-\frac{[\xi^2+\eta^2+\zeta^2]}{2RT_L}} \qquad \alpha_1(\bar{x},\bar{y}) < \alpha < \alpha_2(\bar{x},\bar{y}) \qquad (3)$$

$$f_U(\bar{x},\bar{y},\xi,\eta,\zeta) = \frac{n_U(\bar{x}'')}{(2\pi RT_U)^{3/2}} e^{-\frac{[\xi^2+\eta^2+\zeta^2]}{2RT_U}} \qquad \alpha_3(\bar{x},\bar{y}) < \alpha < \alpha_4(\bar{x},\bar{y}) \qquad (4)$$

where $\bar{x}$ and $\bar{y}$ are the nondimensional physical coordinates given by x/L and y/d, respectively, and

$$\text{Tan } \alpha_1(\bar{x},\bar{y}) = \frac{\bar{y}}{\tau\bar{x}} \qquad (5)$$

$$\text{Tan } \alpha_2(\bar{x},\bar{y}) = \frac{\bar{y}}{\tau(\bar{x} - 1)} \tag{6}$$

$$\text{Tan } \alpha_3(\bar{x},\bar{y}) = \frac{(\bar{y} - 1)}{\tau(\bar{x} - 1)} \tag{7}$$

$$\text{Tan } \alpha_4(\bar{x},\bar{y}) = \frac{(\bar{y} - 1)}{\tau\bar{x}} \tag{8}$$

The molecular velocities in the $\bar{x},\bar{y}$, and $\bar{z}$ directions are denoted by ξ, η, and ζ, respectively. The length-to-height ratio is given by τ, and the number densities of the tanks and walls are given as n_1, n_2, $n_U(\bar{x}'')$, and $n_L(\bar{x}')$, respectively. The upper and lower nondimensional wall coordinates, $\bar{x}''$ and $\bar{x}'$, respectively, are functions of $\bar{x}$ and $\bar{y}$, the point of interest within the flow field, and the direction of the velocity vector, α. Referring to Figure 1 it can be seen that the wall coordinates can be expressed in terms of the field coordinates and velocity coordinates by

$$\text{Tan } \alpha = \frac{\bar{y}}{\tau(\bar{x} - \bar{x}')} = \frac{\eta}{\xi} \quad \text{(Lower Wall)} \tag{9}$$

and

$$\text{Tan } \alpha = \frac{(\bar{y} - 1)}{\tau(\bar{x} - \bar{x}'')} = \frac{\eta}{\xi} \quad \text{(Upper Wall)} \tag{10}$$

The angle α is the direction of the velocity vector of the particles leaving the channel walls at $\bar{x}'$ or $\bar{x}''$ and passing through the point $(\bar{x},\bar{y})$

and, consequently, its tangent can be replaced with the ratio of molecular velocities, as shown in equations (9) and (10). Once the expressions for $n_L(\bar{x}')$ and $n_U(\bar{x}'')$ have been established, equations (9) and (10) can be used to eliminate the variables $\bar{x}'$ and $\bar{x}''$ in favor of the angle α, which turns out to be the polar angle in cylindrical velocity coordinates, and the physical coordinates of the point in the flow field, $\bar{x}$ and $\bar{y}$.

Boundary Condition

Introducing the definition for the velocity in the $\bar{y}$-direction, $v(\bar{x},\bar{y})$, the boundary condition that there be no net flux of particles normal to the walls at the walls can be expressed as follows for $0 \leq \bar{x} \leq 1$:

$$\rho(\bar{x},\bar{y} = \overset{0}{1}) \quad u(\bar{x},\bar{y} = \overset{0}{1}) \equiv m \int_{-\infty}^{\infty}\int_{-\infty}^{\infty}\int_{-\infty}^{\infty} \eta \, f(\bar{x},\bar{y} = \overset{0}{1}, \xi,\eta,\zeta)d\xi d\eta d\zeta = 0 \qquad (11)$$

where $\rho(\bar{x},\bar{y})$ is the local density and m is the molecular mass of the particle. By substituting equations (1) through (4) into equation (11), integrating over the appropriate regions of velocity space, which are illustrated in Figure 1, and introducing the nondimensional wall mass flux, defined as

$$g_w(\bar{x}') \equiv \frac{\dot{m}_w(\bar{x}') - \dot{m}_2}{\dot{m}_1 - \dot{m}_2} \qquad (12)$$

where $\dot{m}_1$, $\dot{m}_2$, and $\dot{m}_w(\bar{x}')$ are the equilibrium fluxes for the tanks and the walls, respectively, and are given by

$$\dot{m}_w(\bar{x}') = \frac{m\, n_U(\bar{x}')\sqrt{2\pi RT_U}}{2\pi} = \frac{m\, n_L(\bar{x}')\sqrt{2\pi RT_L}}{2\pi}$$

$$\dot{m}_1 = \frac{m\, n_1\sqrt{2\pi RT_1}}{2\pi} \tag{14}$$

$$\dot{m}_2 = \frac{m\, n_2\sqrt{2\pi RT_2}}{2\pi} \tag{15}$$

and R is the gas constant, the following single integral equation is obtained for the boundary conditions at $\bar{y} = 0$ and $\bar{y} = 1$:

$$g_w(\bar{x}') = F(\bar{x}') + \int_0^1 g_w(\bar{x}'')\, K(\bar{x}', \bar{x}'')\, d\bar{x}'' \tag{16}$$

where

$$F(\bar{x}') = \frac{1}{2}\left[1 - \frac{\tau\bar{x}'}{\sqrt{\tau^2\bar{x}'^2 + 1}}\right] \tag{17}$$

and

$$K(\bar{x}', \bar{x}'') = \frac{\tau}{2[\tau^2(\bar{x}' - \bar{x}'')^2 + 1]^{3/2}} \tag{18}$$

The details of the derivation of equation (16) are presented in Appendix B.

The function $g_w(\bar{x}')$ possesses the following property:

$$g_w(\bar{x}') = 1 - g_w(1 - \bar{x}') \tag{19}$$

Therefore,

$$g_w\left(\frac{1}{2}\right) = \frac{1}{2}$$

These relations are satisfied for all values of τ. In the limit of $\tau = 0$ and $\tau = \infty$ the solution of the integral equation is linear. However, the exact solution for arbitrary τ is not known.

Moments for Arbitrary Wall Flux

Density. By definition, in terms of cylindrical coordinates,

$$\rho(\bar{x},\bar{y}) \equiv m \int_{-\infty}^{\infty} \int_{0}^{\infty} \int_{0}^{2\pi} f(\bar{x},\bar{y},\alpha,\xi_r,\zeta)\, d\alpha \xi_r d\xi_r d\zeta \qquad (20)$$

where ξ_r is the total molecular velocity in the ξ - η plane and α is the polar angle measured from the ξ-direction. Substituting equations (1) through (4) into equation (20) yields

$$\rho(x,y) = \frac{\rho_1}{(2\pi RT_1)^{3/2}} \int_{-\infty}^{\infty} e^{-\frac{\zeta^2}{2RT_1}} d\zeta \int_{0}^{\infty} e^{-\frac{\xi_r^2}{2RT_1}} \xi_r d\xi_r \left[\int_{\alpha_4}^{2\pi} d\alpha + \int_{0}^{\alpha_1} d\alpha \right] + \qquad (21)$$

$$\frac{\rho_2}{(2\pi RT_2)^{3/2}} \int_{-\infty}^{\infty} e^{-\frac{\zeta^2}{2RT_2}} d\zeta \int_{0}^{\infty} e^{-\frac{\xi_r^2}{2RT_2}} \xi_r d\xi_r \int_{\alpha_2}^{\alpha_3} d\alpha +$$

$$\frac{m}{(2\pi RT_L)^{3/2}} \int_{-\infty}^{\infty} e^{-\frac{\zeta^2}{2RT_L}} d\zeta \int_{0}^{\infty} e^{-\frac{\xi_r^2}{2RT_L}} \xi_r d\xi_r \int_{\alpha_1}^{\alpha_2} n_L(\alpha)\, d\alpha +$$

$$\frac{m}{(2\pi RT_U)^{3/2}} \int_{-\infty}^{\infty} e^{-\frac{\zeta^2}{2RT_U}} d\zeta \int_{0}^{\infty} e^{-\frac{\xi_r^2}{2RT_U}} \xi_r d\xi_r \int_{\alpha_3}^{\alpha_4} n_U(\alpha)\, d\alpha$$

where ρ_1 and ρ_2 are the mass densities of the tanks. The angles α_1, α_2, etc. are functions of $\bar{x}$ and $\bar{y}$, but the functional notation is dropped for simplicity. Since

$$\int_{-\infty}^{\infty} e^{-ax^2} dx = \sqrt{\frac{\pi}{a}} \tag{22}$$

and

$$\int_{0}^{\infty} e^{-ax^2} x\, dx = \frac{1}{2a} \tag{23}$$

equation (21) can be written as

$$\rho(\bar{x},\bar{y}) = \frac{1}{2\pi}\left[\rho_1(2\pi - \alpha_4 - \alpha_1) + \rho_2(\alpha_3 - \alpha_2) + \int_{\alpha_1}^{\alpha_2} \rho_L(\alpha)\, d\alpha + \int_{\alpha_3}^{\alpha_4} \rho_U(\alpha)\, d\alpha\right] \tag{24}$$

where $\rho_L(\alpha)$ and $\rho_U(\alpha)$ are used to denote the wall mass densities. The wall densities can be expressed in terms of the nondimensional wall flux by combining equations (12) through (15) as

$$\rho_{L,U}(\alpha) = \left(\rho_1 \sqrt{\frac{T_1}{T_{L,U}}} - \rho_2 \sqrt{\frac{T_2}{T_{L,U}}}\right) g_w(\alpha) + \rho_2 \sqrt{\frac{T_2}{T_{L,U}}} \tag{25}$$

Substituting equation (25) into equation (24) and rearranging gives

$$\left[\frac{\rho(\bar{x},\bar{y}) - \rho_2}{\rho_1 - \rho_2}\right] = 1 + \frac{1}{2\pi(\rho_1 - \rho_2)}\left[\left(\rho_1 - \rho_2\sqrt{\frac{T_2}{T_L}}\right)\alpha_1 - \right. \tag{26}$$

$$\left(\rho_1 - \rho_2\sqrt{\frac{T_2}{T_U}}\right)\alpha_4 + \rho_2\left(1 - \sqrt{\frac{T_2}{T_U}}\right)\alpha_3 - \rho_2\left(1 - \sqrt{\frac{T_2}{T_L}}\right)\alpha_2 +$$

$$\left(\rho_1\sqrt{\frac{T_1}{T_U}} - \rho_2\sqrt{\frac{T_2}{T_U}}\right)\int_{\alpha_3}^{\alpha_4} g_w(\alpha)\,d\alpha + \left(\rho_1\sqrt{\frac{T_1}{T_L}} - \right.$$

$$\left.\left.\rho_2\sqrt{\frac{T_2}{T_L}}\right)\int_{\alpha_1}^{\alpha_2} g_w(\alpha)\,d\alpha\right]$$

Equation (26) is a general expression for the local density in the flow field in terms of the nondimensional wall flux defined by equation (12). Consider the two limits of equation (26) at $\bar{x} = \pm\infty$. As $\bar{x} \to +\infty$, α_1 and α_2 approach zero and α_3 and α_4 approach 2π. From equation (26) it is apparent that $\rho(\infty,\bar{y}) = \rho_2$. Similarly, as $\bar{x} \to -\infty$, α_1, α_2, α_3, and α_4 approach π. Again it is apparent from equation (26) that $\rho(-\infty, \bar{y}) = \rho_1$. It can also be shown that for an isothermal system, $T_w = T_1 = T_2$, the density distribution is anti-symmetric, or

$$\left[\frac{\rho(1 - \bar{x},\bar{y}) - \rho_2}{\rho_1 - \rho_2}\right] + \left[\frac{\rho(\bar{x},\bar{y}) - \rho_2}{\rho_1 - \rho_2}\right] = 1 \tag{27}$$

Similarly, the density, as well as all the other moments, is symmetric about the centerline $\bar{y} = 0.5$. As a final check, consider the slit flow limit of equation (26). Setting $\tau = 0$ and noting that $\alpha_2 = \alpha_1$ and $\alpha_3 = \alpha_4$, the density variation for a zero thickness slit is obtained as

$$\left[\frac{\rho(\bar{x},\bar{y}) - \rho_2}{\rho_1 - \rho_2}\right] = 1 + \frac{1}{2\pi}(\alpha_1 - \alpha_4) \qquad \text{for } \frac{\pi}{2} \le \alpha_4 \le 2\pi \tag{28}$$

and

$$\left[\frac{\rho(\bar{x},\bar{y}) - \rho_2}{\rho_1 - \rho_2}\right] = \frac{1}{2\pi}(\alpha_1 - \alpha_4) \qquad \text{for } 0 \le \alpha_4 \le \frac{\pi}{2} \tag{29}$$

Velocity Components. The $\bar{x}$-component of velocity, in terms of cylindrical coordinates, is defined as

$$\rho(\bar{x},\bar{y})u(\bar{x},\bar{y}) \equiv m\int_{-\infty}^{\infty}\int_{0}^{\infty}\int_{0}^{2\pi} f(\bar{x},\bar{y},\alpha,\xi_r,\zeta)\xi_r^{\,2}\,\mathrm{Cos}\,\alpha\, d\alpha d\xi_r d\zeta \tag{30}$$

Substituting the distribution functions from equations (1) through (4) into equation (30) gives

$$\rho(\bar{x},\bar{y})u(\bar{x},\bar{y}) = \frac{\rho_1}{(2\pi RT_1)^{3/2}}\int_{-\infty}^{\infty} e^{-\frac{\zeta^2}{2RT_1}} d\zeta \int_{0}^{\infty} e^{-\frac{\xi_r^{\,2}}{2RT_1}} \xi_r^{\,2} d\xi_r \left[\int_{\alpha_4}^{2\pi} \mathrm{Cos}\,\alpha\, d\alpha \right. \tag{31}$$

$$\left. + \int_{0}^{\alpha_1} \mathrm{Cos}\,\alpha\, d\alpha\right] + \frac{\rho_2}{(2\pi RT_2)^{3/2}}\int_{-\infty}^{\infty} e^{-\frac{\zeta^2}{2RT_2}} d\zeta \int_{0}^{\infty} e^{-\frac{\xi_r^{\,2}}{2RT_2}} \xi_r^{\,2} d\xi_r \int_{\alpha_2}^{\alpha_3} \mathrm{Cos}\,\alpha d\alpha$$

$$+ \frac{1}{(2\pi RT_L)^{3/2}} \int_{-\infty}^{\infty} e^{-\frac{\zeta^2}{2RT_L}} d\zeta \int_0^{\infty} e^{-\frac{\xi_r^2}{2RT_L}} \xi_r^2 d\xi_r \int_{\alpha_1}^{\alpha_2} \rho_L(\alpha) \operatorname{Cos} \alpha \, d\alpha +$$

$$\frac{1}{(2\pi RT_U)^{3/2}} \int_{-\infty}^{\infty} e^{-\frac{\zeta^2}{2RT_U}} d\zeta \int_0^{\infty} e^{-\frac{\xi_r^2}{2RT_U}} \xi_r^2 d\xi_r \int_{\alpha_3}^{\alpha_4} \rho_U(\alpha) \operatorname{Cos} \alpha \, d\alpha$$

Making use of the integral

$$\int_0^{\infty} e^{-ax^2} x^2 dx = \frac{1}{4\pi} \left(\frac{\pi}{a} \right)^{3/2} \tag{32}$$

and equation (22), substituting for the wall densities using equation (25), and introducing the definitions given in equations (12) through (15), equation (31) can be written as

$$\frac{\rho(\bar{x},\bar{y})u(\bar{x},\bar{y})}{(\dot{m}_1 - \dot{m}_2)} = \frac{1}{2} \left[\operatorname{Sin} \alpha_1 - \operatorname{Sin} \alpha_4 + \right. \tag{33}$$

$$\left. \int_{\alpha_1}^{\alpha_2} g_w(\alpha) \operatorname{Cos} \alpha \, d\alpha + \int_{\alpha_3}^{\alpha_4} g_w(\alpha) \operatorname{Cos} \alpha \, d\alpha \right]$$

Taking the limits for $\bar{x} = \pm \infty$, it is obvious that $u(\pm \infty, \bar{y}) = 0$. Similarly, setting $\tau = 0$ for slit flow and noting that $\alpha_2 = \alpha_1$ and $\alpha_3 = \alpha_4$, equation (33) becomes

$$\frac{\rho(\bar{x},\bar{y})u(\bar{x},\bar{y})}{(\dot{m}_1 - \dot{m}_2)} = \frac{1}{2}\left[\text{Sin } \alpha_1 - \text{Sin } \alpha_4\right] \tag{34}$$

The $\bar{y}$-component of velocity is similarly defined as

$$\rho(\bar{x},\bar{y})v(\bar{x},\bar{y}) \equiv m \int_{-\infty}^{\infty}\int_{0}^{\infty}\int_{0}^{2\pi} f(\bar{x},\bar{y},\alpha,\xi_r,\zeta)\xi_r^{\,2} \text{ Sin } \alpha \, d\alpha \, d\xi_r d\zeta \tag{35}$$

Following the same procedure as outlined for the $\bar{x}$-component of velocity the following equation is obtained:

$$\frac{\rho(\bar{x},\bar{y})v(\bar{x},\bar{y})}{(\dot{m}_1 - \dot{m}_2)} = \frac{1}{2}\left[\text{Cos } \alpha_4 - \text{Cos } \alpha_1 + \right. \tag{36}$$

$$\left. \int_{\alpha_1}^{\alpha_2} g_w(\alpha) \text{ Sin } \alpha \, d\alpha + \int_{\alpha_3}^{\alpha_4} g_w(\alpha) \text{ Sin } \alpha \, d\alpha \right]$$

Again it can be seen that the limits for $\bar{x} = \pm\infty$, $v(\pm\infty,\bar{y}) = 0$, are satisfied. In the limit of $\tau = 0$ the following relation is obtained for slit flow:

$$\frac{\rho(\bar{x},\bar{y})v(\bar{x},\bar{y})}{(\dot{m}_1 - \dot{m}_2)} = \frac{1}{2}\left[\text{Cos } \alpha_4 - \text{Cos } \alpha_1\right] \tag{37}$$

Both velocity components are symmetric about the centerline, $\bar{y} = 0.5$, and satisfy the following relations:

$$\frac{\rho(\bar{x},\bar{y})u(\bar{x},\bar{y})}{(\dot{m}_1 - \dot{m}_2)} = \frac{\rho(1 - \bar{x},\bar{y})u(1 - \bar{x},\bar{y})}{(\dot{m}_1 - \dot{m}_2)} \tag{38}$$

and

$$\frac{\rho(\bar{x},\bar{y})v(\bar{x},\bar{y})}{(\dot{m}_1 - \dot{m}_2)} = - \frac{\rho(1 - \bar{x},\bar{y})v(1 - \bar{x},\bar{y})}{(\dot{m}_1 - \dot{m}_2)} \tag{39}$$

Normal Pressure Components. By definition, the normal pressure component in the $\bar{x}$-direction is

$$P_{xx}(\bar{x},\bar{y}) \equiv m \int_{-\infty}^{\infty} \int_{0}^{\infty} \int_{0}^{2\pi} f(\bar{x},\bar{y},\alpha,\xi_r,\zeta) \xi_r^3 \cos^2 \alpha \, d\alpha \, d\xi_r \, d\zeta - \tag{40}$$

$$\rho(\bar{x},\bar{y})u^2(\bar{x},\bar{y})$$

Substituting equations (1) through (4) for the distribution functions into equation (40) and continuing as before, the normal pressure component in the $\bar{x}$-direction becomes

$$\left[\frac{P_{xx}(\bar{x},\bar{y}) - P_2}{P_1 - P_2}\right] = 1 + \frac{1}{4\pi(P_1 - P_2)} \left\{ \left(P_1 - P_2 \sqrt{\frac{T_L}{T_2}}\right) \left[2(\alpha_1 - \alpha_4) + \right. \right. \tag{41}$$

$$\left. (\sin 2\alpha_1 - \sin 2\alpha_4) \right] + P_2 \left(1 - \sqrt{\frac{T_L}{T_2}}\right) \left[2(\alpha_3 - \alpha_2) + \right.$$

$$\left. \left. (\sin 2\alpha_3 - \sin 2\alpha_2) \right] + P_2 \left(\sqrt{\frac{T_U}{T_2}} - \sqrt{\frac{T_L}{T_2}}\right) \left[2(\alpha_4 - \alpha_3) + \right.$$

$$(\text{Sin } 2\alpha_4 - \text{Sin } 2\alpha_3) \Big] + 4 \left(P_1 \sqrt{\frac{T_L}{T_1}} - P_2 \sqrt{\frac{T_L}{T_2}} \right) \cdot$$

$$\int_{\alpha_1}^{\alpha_2} g_w(\alpha) \text{ Cos}^2 \alpha \, d\alpha + 4 \left(P_1 \sqrt{\frac{T_U}{T_1}} - P_2 \sqrt{\frac{T_U}{T_2}} \right) \int_{\alpha_3}^{\alpha_4} g_w(\alpha) \text{ Cos}^2 \alpha \, d\alpha \Big]$$

$$- \frac{\rho(\bar{x},\bar{y}) u^2(\bar{x},\bar{y})}{(P_1 - P_2)}$$

Similarly, the definitions for the other two normal pressure components are

$$P_{yy}(\bar{x},\bar{y}) \equiv m \int_{-\infty}^{\infty} \int_{0}^{\infty} \int_{0}^{2\pi} f(\bar{x},\bar{y},\alpha,\xi_r,\zeta) \xi_r^3 \text{ Sin}^2 \alpha \, d\alpha \, d\xi_r \, d\zeta - \qquad (42)$$

$$\rho(\bar{x},\bar{y}) v^2(\bar{x},\bar{y})$$

and

$$P_{zz}(\bar{x},\bar{y}) \equiv m \int_{-\infty}^{\infty} \int_{0}^{\infty} \int_{0}^{2\pi} f(\bar{x},\bar{y},\alpha,\xi_r,\zeta) \, \zeta^2 \, \xi_r \, d\alpha d\xi_r d\zeta \qquad (43)$$

Again introducing the distribution functions from equations (1) through (4) and carrying out the required integrations, the following final forms are obtained for equations (42) and (43):

$$\left[\frac{P_{yy}(\bar{x},\bar{y}) - P_2}{P_1 - P_2} \right] = 1 + \frac{1}{4\pi(P_1 - P_2)} \left[\left(P_1 - P_2 \sqrt{\frac{T_L}{T_2}} \right) \left[2(\alpha_1 - \alpha_4) - \qquad (44) \right. \right.$$

$$\left. \left. (\text{Sin } 2\alpha_1 - \text{Sin } 2\alpha_4) \right] + P_2 \left(1 - \sqrt{\frac{T_L}{T_2}} \right) \left[2(\alpha_3 - \alpha_2) - \right. \right.$$

$$(\text{Sin } 2\alpha_3 - \text{Sin } 2\alpha_2)\Big] + P_2\left(\sqrt{\frac{T_U}{T_2}} - \sqrt{\frac{T_L}{T_2}}\right)\Big[2(\alpha_4 - \alpha_3) -$$

$$(\text{Sin } 2\alpha_4 - \text{Sin } 2\alpha_3)\Big] + 4\left(P_1\sqrt{\frac{T_L}{T_1}} - P_2\sqrt{\frac{T_L}{T_2}}\right)\int_{\alpha_1}^{\alpha_2} g_w(\alpha)\,\text{Sin}^2\,\alpha\,d\alpha$$

$$+ 4\left(P_1\sqrt{\frac{T_U}{T_1}} - P_2\sqrt{\frac{T_U}{T_2}}\right)\int_{\alpha_3}^{\alpha_4} g_w(\alpha)\,\text{Sin}^2\,\alpha\,d\alpha\Bigg] - \frac{\rho(\bar{x},\bar{y})v^2(\bar{x},\bar{y})}{(P_1 - P_2)}$$

$$\left[\frac{P_{zz}(\bar{x},\bar{y}) - P_2}{P_1 - P_2}\right] = 1 + \frac{1}{2\pi(P_1 - P_2)}\left[\left(P_1 - P_2\sqrt{\frac{T_L}{T_2}}\right)(\alpha_1 - \alpha_4) + \right. \tag{45}$$

$$P_2\left(1 - \sqrt{\frac{T_L}{T_2}}\right)(\alpha_3 - \alpha_2) + P_2\left(\sqrt{\frac{T_U}{T_2}} - \sqrt{\frac{T_L}{T_2}}\right)(\alpha_4 - \alpha_3) +$$

$$\left.\left(P_1\sqrt{\frac{T_U}{T_1}} - P_2\sqrt{\frac{T_U}{T_2}}\right)\int_{\alpha_3}^{\alpha_4} g_w(\alpha)\,d\alpha + \left(P_1\sqrt{\frac{T_L}{T_1}} - P_2\sqrt{\frac{T_L}{T_2}}\right)\int_{\alpha_1}^{\alpha_2} g_w(\alpha)\,d\alpha\right]$$

It can be shown that equations (41), (44), and (45) have the appropriate upstream and downstream limits. Similarly, the slit flow limits can be obtained by setting $\tau = 0$, $\alpha_2 = \alpha_1$, and $\alpha_3 = \alpha_4$.

Static or Thermodynamic Pressure. The definition for static or thermodynamic pressure is

$$p(\bar{x},\bar{y}) = \frac{1}{3}\left[\, P_{xx}(\bar{x},\bar{y}) + P_{yy}(\bar{x},\bar{y}) + P_{zz}(\bar{x},\bar{y}) \,\right] \qquad (46)$$

Substituting equations (41), (44), and (45) into equation (46) yields the following expression for the thermodynamic pressure:

$$\left[\frac{p(\bar{x},\bar{y}) - P_2}{P_1 - P_2}\right] = 1 + \frac{1}{2\pi(P_1 - P_2)}\left[\left(P_1 - P_2\sqrt{\frac{T_L}{T_2}}\right)(\alpha_1 - \alpha_4) + \right. \qquad (47)$$

$$P_2\left(1 - \sqrt{\frac{T_L}{T_2}}\right)(\alpha_3 - \alpha_2) + P_2\left(\sqrt{\frac{T_U}{T_2}} - \sqrt{\frac{T_L}{T_2}}\right)(\alpha_4 - \alpha_3) +$$

$$\left(P_1\sqrt{\frac{T_L}{T_1}} - P_2\sqrt{\frac{T_L}{T_2}}\right)\int_{\alpha_1}^{\alpha_2} g_w(\alpha)\, d\alpha + \left(P_1\sqrt{\frac{T_U}{T_1}} - P_2\sqrt{\frac{T_U}{T_2}}\right)\left.\int_{\alpha_3}^{\alpha_4} g_w(\alpha)\, d\alpha\right] -$$

$$\frac{\rho(\bar{x},\bar{y})}{3(P_1 - P_2)}\left[u^2(\bar{x},\bar{y}) + v^2(\bar{x},\bar{y})\right]$$

Since each of the normal pressure components satisfied the upstream and downstream limits, it is apparent from equation (46) that equation (47) will also satisfy the limits. In the slit flow limit equation (47) reduces to

$$\left[\frac{p(\bar{x},\bar{y}) - P_2}{P_1 - P_2}\right] = 1 + \frac{1}{2\pi}(\alpha_1 - \alpha_4) - \frac{\rho(\bar{x},\bar{y})}{3(P_1 - P_2)}\left[u^2(\bar{x},\bar{y}) + v^2(\bar{x},\bar{y})\right] \qquad (48)$$

for $\frac{\pi}{2} \leq \alpha_4 \leq 2\pi$, and

$$\left[\frac{p(\bar{x},\bar{y}) - P_2}{P_1 - P_2}\right] = \frac{1}{2\pi}(\alpha_1 - \alpha_4) - \frac{\rho(\bar{x},\bar{y})}{3(P_1 - P_2)}\left[u^2(\bar{x},\bar{y}) + v^2(\bar{x},\bar{y})\right] \quad (49)$$

for $0 \leq \alpha_4 \leq \frac{\pi}{2}$.

Thermodynamic Temperature. The thermodynamic temperature can be obtained from its definition or from the equation of state, since the pressure and density are already known. Since the two methods are equivalent, the latter method is chosen. From the equation of state the temperature can be written as

$$T(\bar{x},\bar{y}) = \frac{p(\bar{x},\bar{y})}{R\,\rho(\bar{x},\bar{y})}$$

or, in nondimensional form,

$$\left[\frac{T(\bar{x},\bar{y}) - T_2}{T_1 - T_2}\right] = \frac{1}{(T_1 - T_2)}\left[\frac{p(\bar{x},\bar{y})}{R\,\rho(\bar{x},\bar{y})} - T_2\right] \quad (50)$$

where the density and pressure are given by equations (26) and (47), respectively. The upstream and downstream limits for equation (50) are unity and zero, respectively. Since $p(\bar{x},\bar{y})$ and $\rho(\bar{x},\bar{y})$ already contain the correct upstream and downstream limits, it is obvious that equation (50) contains the correct limits. The temperature distribution for a two dimensional slit ($\tau = 0$) can be obtained by substituting the appropriate equations from equations (28), (29), (48), and (49) into equation (50).

A particularly simple form for the temperature distribution occurs for the case of an isothermal system. Setting all known temperatures equal to the common temperature T_1 and combining equations (26), (47), and (50) yield the following:

$$T(\bar{x},\bar{y}) = T_1 - \frac{1}{3R}\left[u^2(\bar{x},\bar{y}) + v^2(\bar{x},\bar{y}) \right] \tag{51}$$

This form of the temperature distribution is similar to that of continuum flow.

Shear Stress Components. The $\bar{y}\bar{x}$-component of the shear stress can be written in cylindrical coordinates from its definition as follows:

$$P_{yx}(\bar{x},\bar{y}) \equiv m \int_{-\infty}^{\infty}\int_{0}^{\infty}\int_{0}^{2\pi} f(\bar{x},\bar{y},\alpha,\xi_r,\zeta)\xi_r^3 \operatorname{Cos}\alpha \operatorname{Sin}\alpha \, d\alpha d\xi_r d\zeta - \tag{52}$$

$$\rho(\bar{x},\bar{y})u(\bar{x},\bar{y})v(\bar{x},\bar{y})$$

Introducing equations (1) through (4) for the distribution functions into equation (52) and performing the integrations yield

$$P_{yx}(\bar{x},\bar{y}) = \frac{1}{2\pi}\left[\left(P_1 - P_2\sqrt{\frac{T_L}{T_2}} \right)\left[\operatorname{Sin}^2\alpha_1 - \operatorname{Sin}^2\alpha_4 \right] + P_2\left(1 - \sqrt{\frac{T_L}{T_2}} \right)\right. \tag{53}$$

$$\cdot \left[\operatorname{Sin}^2\alpha_3 - \operatorname{Sin}^2\alpha_2 \right] + P_2\left(\sqrt{\frac{T_U}{T_2}} - \sqrt{\frac{T_L}{T_2}} \right)\left[\operatorname{Sin}^2\alpha_4 - \operatorname{Sin}^2\alpha_3 \right] +$$

$$2\left(P_1\sqrt{\frac{T_L}{T_1}} - P_2\sqrt{\frac{T_L}{T_2}} \right)\int_{\alpha_1}^{\alpha_2} g_w(\alpha) \operatorname{Sin}\alpha \operatorname{Cos}\alpha \, d\alpha + 2\left(P_1\sqrt{\frac{T_U}{T_1}} - \right.$$

$$P_2 \sqrt{\frac{T_U}{T_2}} \int_{\alpha_3}^{\alpha_4} g_w(\alpha) \text{ Sin } \alpha \text{ Cos } \alpha \, d\alpha \Bigg] - \rho(\bar{x},\bar{y})u(\bar{x},\bar{y})v(\bar{x},\bar{y})$$

The shear stress must vanish for $\bar{x} = \pm \infty$. Assigning the correct limits to the angles and noting that $v(\bar{x},\bar{y})$ and $u(\bar{x},\bar{y})$ approach zero for both limits, then it can be shown that equation (53) contains the correct upstream and downstream limits. The slit flow limit can be obtained by following the procedure outlined for the other moments. The $\bar{x}\bar{y}$-component of the shear stress is identical to the $\bar{y}\bar{x}$-component due to the symmetry of the pressure tensor. All other components of the shear stress are zero everywhere in the flow field.

Heat Flux Components. The heat flux components are defined in terms of cylindrical velocity coordinates as

$$2q_x(\bar{x},\bar{y}) \equiv m \int_{-\infty}^{\infty} \int_0^{\infty} \int_0^{2\pi} \left[\xi_r \text{ Cos } \alpha - u(\bar{x},\bar{y})\right] \Big\{ \left[\xi_r \text{ Cos } \alpha - u(\bar{x},\bar{y})\right]^2 + \quad (54)$$

$$\left[\xi_r \text{ Sin } \alpha - v(\bar{x},\bar{y})\right]^2 + \zeta^2 \Big\} f(\bar{x},\bar{y},\alpha,\xi_r,\zeta) \quad \xi_r d\alpha d\xi_r d\zeta$$

and

$$2q_y(\bar{x},\bar{y}) \equiv m \int_{-\infty}^{\infty} \int_0^{\infty} \int_0^{2\pi} \left[\xi_r \text{ Sin } \alpha - v(\bar{x},\bar{y})\right] \Big\{ \left[\xi_r \text{ Cos } \alpha - u(\bar{x},\bar{y})\right]^2 + \quad (55)$$

$$\left[\xi_r \text{ Sin } \alpha - v(\bar{x},\bar{y})\right]^2 + \zeta^2 \Big\} f(\bar{x},\bar{y},\alpha,\xi_r,\zeta) \xi_r \, d\alpha d\xi_r d\zeta$$

Expanding equations (54) and (55) and using the previous definitions, the following relations are obtained:

$$q_x(\bar{x},\bar{y}) = -\Big\{ \frac{3}{2} p(\bar{x},\bar{y})u(\bar{x},\bar{y}) + P_{xx}(\bar{x},\bar{y})u(\bar{x},\bar{y}) + P_{yx}(\bar{x},\bar{y})v(\bar{x},\bar{y}) + \tag{56}$$

$$\frac{1}{2}\ \rho(\bar{x},\bar{y})u(\bar{x},\bar{y})\Big[\ u^2(\bar{x},\bar{y}) + v^2(\bar{x},\bar{y})\Big]\Big\} + \frac{m}{2}\Bigg[\int_{-\infty}^{\infty}\int_{0}^{\infty}\int_{0}^{2\pi} f(\bar{x},\bar{y},\alpha,\xi_r,\zeta)\cdot$$

$$\xi_r^{\,4}\ \mathrm{Cos}^3\ \alpha\ d\alpha\ d\xi_r d\zeta + \int_{-\infty}^{\infty}\int_{0}^{\infty}\int_{0}^{2\pi} f(\bar{x},\bar{y},\alpha,\xi_r,\zeta)\xi_r^{\,4}\ \mathrm{Cos}\ \alpha\ \mathrm{Sin}^2\ \alpha\ d\alpha\ d\xi_r d\zeta$$

$$+ \int_{-\infty}^{\infty}\int_{0}^{\infty}\int_{0}^{2\pi} f(\bar{x},\bar{y},\alpha,\xi_r,\zeta)\xi_r^{\,2}\ \mathrm{Cos}\ \alpha\ \zeta^2\ d\alpha d\xi_r d\zeta\ \Bigg]$$

and

$$q_y(\bar{x},\bar{y}) = -\Big\{\frac{3}{2} p(\bar{x},\bar{y})v(\bar{x},\bar{y}) + P_{yy}(\bar{x},\bar{y})v(\bar{x},\bar{y}) + P_{yx}(\bar{x},\bar{y})u(\bar{x},\bar{y}) + \tag{57}$$

$$\frac{1}{2}\ \rho(\bar{x},\bar{y})v(\bar{x},\bar{y})\ \Big[\ u^2(\bar{x},\bar{y}) + v^2(\bar{x},\bar{y})\Big]\Big\} + \frac{m}{2}\cdot\Bigg[\int_{-\infty}^{\infty}\int_{0}^{\infty}\int_{0}^{2\pi} f(\bar{x},\bar{y},\alpha,\xi_r,\zeta)\cdot$$

$$\xi_r^{\,4}\ \mathrm{Cos}^2\ \alpha\ \mathrm{Sin}\ \alpha\ d\alpha\ d\xi_r d\zeta + \int_{-\infty}^{\infty}\int_{0}^{\infty}\int_{0}^{2\pi} f(\bar{x},\bar{y},\alpha,\xi_r,\zeta)\xi_r^{\,4}\ \mathrm{Sin}^3\ \alpha\ d\alpha\ d\xi_r d\zeta$$

$$+ \int_{-\infty}^{\infty}\int_{0}^{\infty}\int_{0}^{2\pi} f(\bar{x},\bar{y},\alpha,\xi_r,\zeta)\xi_r^{\,2}\ \mathrm{Sin}\ \alpha\ \zeta^2\ d\alpha d\xi_r d\zeta\ \Bigg]$$

The problem of determining the heat flux components has now been reduced to that of determining the integrals appearing on the right-hand side of equations (56) and (57). Substituting equations (1) through (4) for the distribution functions into equations (56) and (57), carrying out the resulting integrations, and simplifying yield the following results for the heat flux components:

$$q_x(\bar{x},\bar{y}) = -\left\{\frac{3}{2}\, p(\bar{x},\bar{y},)u(\bar{x},\bar{y}) + P_{xx}(\bar{x},\bar{y})u(\bar{x},\bar{y}) + P_{yx}(\bar{x},\bar{y})v(\bar{x},\bar{y}) + \right. \tag{58}$$

$$\left. \frac{1}{2}\,\rho(\bar{x},\bar{y})u(\bar{x},\bar{y}) \left[\, u^2(\bar{x},\bar{y}) + v^2(\bar{x},\bar{y})\right]\right\} + \frac{1}{4\sqrt{\pi}}\left\{\left[\, \rho_1(2RT_1)^{3/2} - \right.\right.$$

$$\rho_2(2RT_2)^{3/2}\left(\frac{T_L}{T_2}\right)\Big] \;(\mathrm{Sin}\;\alpha_1 - \mathrm{Sin}\;\alpha_4) + \rho_2(2RT_2)^{3/2}\left[\, 1 - \frac{T_L}{T_2}\,\right]\cdot$$

$$(\mathrm{Sin}\;\alpha_3 - \mathrm{Sin}\;\alpha_2) + \rho_2\,(2RT_2)^{3/2}\cdot\left[\,\frac{T_U}{T_2} - \frac{T_L}{T_2}\,\right]\;(\mathrm{Sin}\;\alpha_4 -$$

$$\mathrm{Sin}\;\alpha_3) + \left[\,\rho_1(2RT_1)^{3/2}\left(\frac{T_L}{T_1}\right) - \rho_2(2RT_2)^{3/2}\;\left(\frac{T_L}{T_2}\right)\right]\int_{\alpha_1}^{\alpha_2} g_w(\alpha)\;\mathrm{Cos}\;\alpha\;d\alpha$$

$$\left. + \left[\,\rho_1(2RT_1)^{3/2}\left(\frac{T_U}{T_1}\right) - \rho_2(2RT_2)^{3/2}\;\left(\frac{T_U}{T_2}\right)\right]\int_{\alpha_3}^{\alpha_4} g_w(\alpha)\;\mathrm{Cos}\;\alpha\;d\alpha\right\}$$

and

$$q_y(\bar{x},\bar{y}) = -\left\{\frac{3}{2}\; p(\bar{x},\bar{y})v(\bar{x},\bar{y}) + P_{yy}(\bar{x},\bar{y})v(\bar{x},\bar{y}) + P_{yx}(\bar{x},\bar{y})u(\bar{x},\bar{y}) + \right. \tag{59}$$

$$\frac{1}{2}\rho(\bar{x},\bar{y})v(\bar{x},\bar{y})\left[u^2(\bar{x},\bar{y}) + v^2(\bar{x},\bar{y})\right]\Big\} + \frac{1}{4\sqrt{\pi}}\Big\{\Big[\rho_1(2RT_1)^{3/2} -$$

$$\rho_2(2RT_2)^{3/2}\left(\frac{T_L}{T_2}\right)\Big](\cos\alpha_4 - \cos\alpha_1) + \rho_2(2RT_2)^{3/2}\left[1 - \frac{T_L}{T_2}\right].$$

$$(\cos\alpha_2 - \cos\alpha_3) + \rho_2(2RT_2)^{3/2}\left[\frac{T_U}{T_2} - \frac{T_L}{T_2}\right](\cos\alpha_3 - \cos\alpha_4) +$$

$$\left[\rho_1(2RT_1)^{3/2}\left(\frac{T_L}{T_1}\right) - \rho_2(2RT_2)^{3/2}\left(\frac{T_L}{T_2}\right)\right]\int_{\alpha_1}^{\alpha_2} g_w(\alpha)\,\sin\alpha\,d\alpha +$$

$$\left[\rho_1(2RT_1)^{3/2}\left(\frac{T_U}{T_1}\right) - \rho_2(2RT_2)^{3/2}\left(\frac{T_U}{T_2}\right)\right]\int_{\alpha_3}^{\alpha_4} g_w(\alpha)\,\sin\alpha\,d\alpha\Big\}$$

The $\bar{z}$-component of the heat flux vector is zero since the problem is two dimensional. By letting $\bar{x}$ approach positive and negative infinity it can be shown that equations (58) and (59) contain the appropriate limits of zero for the heat flux components. Similarly, setting $\alpha_2 = \alpha_1$, $\alpha_3 = \alpha_4$, and $\tau = 0$ in equations (58) and (59), the slit flow limits are easily obtained.

Average Mass Flow Rate

In order to obtain the average mass flow rate the axial mass velocity is averaged over the height of the channel. The following definitions are therefore introduced:

$$\overline{\rho(\bar{x},\bar{y})u(\bar{x},\bar{y})} \equiv \int_0^1 \rho(\bar{x},\bar{y})u(\bar{x},\bar{y})d\bar{y} \qquad (60)$$

and

$$\bigwedge(\bar{x},\tau) \equiv \frac{\overline{\rho(\bar{x},\bar{y})u(\bar{x},\bar{y})}}{(\dot{m}_1 - \dot{m}_2)} \tag{61}$$

Equation (60) can now be expressed as

$$\bigwedge(\bar{x},\tau) = \int_0^1 \frac{\rho(\bar{x},\bar{y})u(\bar{x},\bar{y})}{(\dot{m}_1 - \dot{m}_2)}\, d\bar{y} \tag{62}$$

Note that the nondimensional average mass flow rate, $\bigwedge(\bar{x},\tau)$, is expressed as a function of $\bar{x}$, the axial coordinate. It must be shown that the final form for the average mass flow rate is independent of $\bar{x}$ and dependent only on the length-to-height ratio, τ. This result is necessary in order to insure steady state conditions and the satisfaction of the conservation of mass principle.

Substituting equation (33) in equation (62) and performing the necessary integrations yield

$$\bigwedge(\bar{x},\tau) = \sqrt{\tau^2 \bar{x}^2 + 1} - \tau\bar{x} + \frac{1}{2}\int_0^1 \left[\int_{\alpha_1}^{\alpha_2} g_w(\alpha) \operatorname{Cos} \alpha\, d\alpha + \int_{\alpha_3}^{\alpha_4} g_w(\alpha) \operatorname{Cos} \alpha\, d\alpha \right] d\bar{y} \tag{63}$$

Note that the angles α_1, α_2, etc. are functions of $\bar{x}$ and $\bar{y}$. Since $\bar{x}$ and $\bar{y}$ are fixed, it can be seen from equations (9) and (10) that the variable α can be transformed to the wall coordinates, $\bar{x}'$ and $\bar{x}''$. Therefore, differentiating equations (9) and (10) yields

$$\tau d\bar{x}' = \bar{y}\ \mathrm{Csc}^2\ \alpha\ d\alpha \qquad \text{(Lower Wall)}$$

and

$$\tau d\bar{x}'' = (\bar{y} - 1)\ \mathrm{Csc}^2\ \alpha\ d\alpha \qquad \text{(Upper Wall)}$$

Since

$$\mathrm{Csc}^2\ \alpha = \frac{[\tau^2(\bar{x} - \bar{x}')^2 + \bar{y}^2]}{\bar{y}^2} \qquad \text{(Lower Wall)}$$

$$\mathrm{Csc}^2\ \alpha = \frac{[\tau^2(\bar{x} - \bar{x}'')^2 + (\bar{y} - 1)^2]}{(\bar{y} - 1)^2} \qquad \text{(Upper Wall)}$$

and

$$\mathrm{Cos}\ \alpha = \frac{\tau(\bar{x} - \bar{x}')}{\sqrt{\tau^2(\bar{x} - \bar{x}')^2 + \bar{y}^2}} \qquad \text{(Lower Wall)}$$

$$\mathrm{Cos}\ \alpha = \frac{\tau(\bar{x} - \bar{x}'')}{\sqrt{\tau^2(\bar{x} - \bar{x}'')^2 + (\bar{y} - 1)^2}} \qquad \text{(Upper Wall)}$$

equation (63) can be expressed as

$$\Lambda(\bar{x},\tau) = \sqrt{\tau^2\,\bar{x}^2 + 1} - \tau\bar{x} + \frac{1}{2}\left\{\int_0^1 \left[\int_0^1 g_w(\bar{x}')\,\frac{\tau^2\bar{y}(\bar{x}-\bar{x}')}{[\tau^2(\bar{x}-\bar{x}')^2 + \bar{y}^2]^{3/2}}\,dx' \right.\right. \qquad (64)$$

$$\left.\left. + \int_1^0 g_w(\bar{x}')\,\frac{\tau^2(\bar{y}-1)(\bar{x}-\bar{x}'')}{[\tau^2(\bar{x}-\bar{x}'')^2 + (\bar{y}-1)^2]^{3/2}}\,d\bar{x}'' \right] d\bar{y} \right\}$$

Finally, combining the integrals of equation (64) by defining one common variable of integration, $\bar{x}'$, and carrying out the integration over $\bar{y}$, the following equation is deduced for the nondimensional average mass flow at $\bar{x}$:

$$\Lambda(\bar{x},\tau) = G_{0-\bar{x}}(\bar{x}) - \tau \int_0^1 g_w(\bar{x}')\, F_{\bar{x}'-\bar{x}}(\bar{x},\bar{x}')\, d\bar{x}' \tag{65}$$

where

$$G_{0-\bar{x}}(\bar{x}) = \sqrt{\tau^2 \bar{x}^2 + 1} - \tau\bar{x} \tag{66}$$

and

$$F_{\bar{x}'-\bar{x}}(\bar{x},\bar{x}') = \tau(\bar{x}' - \bar{x}) \left[\frac{1}{|\tau(\bar{x} - \bar{x}')|} - \frac{1}{\sqrt{\tau^2(\bar{x} - \bar{x}')^2 + 1}} \right] \tag{67}$$

It was mentioned earlier that it is necessary to show that $\Lambda(\bar{x},\tau)$, as given by equation (65), is independent of $\bar{x}$. Therefore, differentiating equation (65) with respect to $\bar{x}$ and combining the resulting expression with the integral equation for the wall flux in equation (16), it can be shown that

$$\frac{\partial \Lambda(\bar{x},\tau)}{\partial \bar{x}} = 0 \tag{68}$$

Therefore, $\Lambda(\bar{x},\tau)$ must be a function of τ alone*, and the nondimensional average mass flow rate can be obtained from equation (65) for any value

---

* The author is indebted to Professor James H. Hubbartt for his discussions concerning this point and for the proof of equation (68).

of $\bar{x}$ ranging from zero to unity. Following the normal procedure and evaluating equations (65) through (67) at $\bar{x} = 0$ gives

$$\Lambda(\tau) = 1 - \tau\int_0^1 g_w(\bar{x}') \, F_{\bar{x}'-0}(0,\bar{x}') \, d\bar{x}' \tag{69}$$

where $\Lambda(0,\tau)$ has been replaced with $\Lambda(\tau)$ and $F_{\bar{x}'-0}(0,\bar{x}')$ can be obtained from equation (67). Note that in the slit flow limit, $\tau = 0$, equation (69) yields the correct limit of unity.

Consider equations (65) through (67). The function $G_{0-\bar{x}}(\bar{x})$ represents the fraction of the net flux crossing the channel height at $\bar{x}$ which came from the reservoirs at $\bar{x} = 0$ and $\bar{x} = 1$. Similarly, the function $F_{\bar{x}'-\bar{x}}(\bar{x},\bar{x}')$ represents the fraction of the flux originating at the walls at $\bar{x}'$ which crosses the channel height at $\bar{x}$. Combining the two quantities yields the net average mass flow rate at $\bar{x}$. Consequently, equation (65) could have been derived strictly by considering the fluxes as just mentioned. The derivation of the average mass flow rate by other authors has been based on this approach, but only the station at $\bar{x} = 0$ is considered and an equation identical to equation (69) is obtained.

Solution Technique for Linear Wall Flux Segments

Discussion

The general formulation for the flow properties was set forth in the first part of this chapter. In order to determine analytical expressions for these properties in terms of known quantities it becomes

necessary to describe the wall flux variation. A convenient representation is given by a series of linear segments for the wall flux (or density, since the wall temperatures are constant). The constants required for this representation can be obtained from the solution of the integral equation representing the boundary condition. Since all the moments can be evaluated analytically for a linear wall flux, the flow properties can be expressed in terms of a series of analytical expressions for the wall contribution, where each term of the series represents the results for a linear wall flux segment. The accuracy which can be attained depends on the accuracy with which the integral equation for the boundary condition can be solved and on the number of linear wall flux segments taken.

It was mentioned earlier that the solution of the integral equation for the boundary condition is linear in the limits of length-to-height ratios, τ, of zero and infinity. The zero limit solution is a constant. Consequently, in view of the nature of the solutions in these limits it is expected that a constant wall flux assumption will yield fairly accurate results for the moments for very small τ, and a linear wall flux for the entire channel length will yield fairly accurate results for small and very large τ.

In the following sections a polynomial solution of the integral equation for the boundary condition is presented, and the results for the moments for arbitrary wall flux variation, which were presented in the first part of this chapter, are determined in analytical form by integrating the wall contribution for the assumption of linear wall

flux segments. Expressions for the average mass flow rate based on the assumptions of linear wall flux segments and a constant or a linear wall flux over the entire channel length are also given. The other results for a constant or linear wall flux over the entire channel length are presented as special cases.

Polynomial Solution for Boundary Condition

Equation (16) is a Fredholm integral equation of the second kind. Its kernel, which is given by equation (18), is continuous and has continuous derivatives. For $\bar{x}'' = \bar{x}'$ it can be seen from equation (18) that the kernel takes on the value of $\tau/2$. For other values of $\bar{x}''$, however, the kernel is proportional to τ^{-2}. Consequently, for large values of τ the kernel is similar to a delta function in that it is very small everywhere except near $\bar{x}'' = \bar{x}'$, where it takes on its maximum value of $\tau/2$. It is this character of the kernel which makes numerical integration of the integral part of equation (16) very difficult for large values of τ when a reasonable degree of accuracy is required.

Several methods are available for obtaining numerical values of $g_w(\bar{x}')$ from equation (16). Two of these methods yield good results for small values of τ. The first method consists of replacing the integral of equation (16) with a numerical integration formula, evaluating the function to be found, $g_w(\bar{x}')$, at the same values of $\bar{x}'$ as used for $\bar{x}''$ in the numerical integration, and solving the system of equations for the unknown values of $g_w(\bar{x}')$. The second method, which has been used by most investigators, is that of successive

substitution. This method consists of substituting some initial guess for $g_w(\bar{x}'')$ into the integral of equation (16), evaluating the integral either numerically or analytically, and solving for the new function, $g_w(\bar{x}')$. The process is repeated until successive approximations satisfy some preassigned tolerance which has been specified for $g_w(\bar{x}')$ at discrete points. Since several iterations are required, it becomes convenient to use a digital computer for the computations. The integral is then evaluated numerically for each approximation, since analytical evaluation is usually not possible. For values of τ greater than about five the computational time required to obtain values of $g_w(\bar{x}')$ to four-place accuracy becomes exceedingly large since it becomes necessary to take a large number of points to evaluate the integral. Consequently, the collocation method was used to obtain solutions of equation (16). This method of solution is discussed in Hildebrand [37]. The advantages of this method over the two previous methods are that the integrations for each order of approximation can be performed analytically for a polynomial, which satisfies some preassigned tolerance at discrete points in the interval. The polynomial solutions are useful in evaluating the moments.

In order to obtain accurate results by the collocation method it is necessary to choose a polynomial to represent $g_w(\bar{x}')$ which satisfies all the properties of the solution of equation (16) and is integrable when weighted by the kernel. Such a polynomial approximation is contained in the series

$$g_w(\bar{x}') = \bar{x}' + \sum_{k=1}^{M} B_{2k-1}(\tau)\, \varphi_{2k-1}(\bar{x}') \tag{70}$$

where

$$\varphi_{2k-1}(\bar{x}') = \left(\bar{x}' - \frac{1}{2}\right)^{2k-1} \tag{71}$$

and the coefficients, $B_{2k-1}(\tau)$, are functions of τ and can be obtained by satisfying the integral equation at discrete points over the interval $0 \leq \bar{x}' < \frac{1}{2}$. Note that equation (70) satisfies the anti-symmetric property of equation (19) and has the value of $\frac{1}{2}$ at $\bar{x}' = \frac{1}{2}$.

By substituting equation (70) into equation (16) the following equation is obtained:

$$\sum_{k=1}^{M} B_{2k-1}(\tau) \left[\varphi_{2k-1}(\bar{x}') - \Phi_{2k-1}(\bar{x}') \right] \cong F(\bar{x}') + \Phi_{-1}(\bar{x}') - \bar{x}' \tag{72}$$

where $\Phi_{2k-1}(\bar{x}')$ and $\Phi_{-1}(\bar{x}')$ are defined as

$$\Phi_{2k-1}(\bar{x}') \equiv \int_0^1 \varphi_{2k-1}(\bar{x}'')\, K(\bar{x}', \bar{x}'')\, d\bar{x}'' \tag{73}$$

and

$$\Phi_{-1}(\bar{x}') \equiv \int_0^1 \bar{x}''\, K(\bar{x}', \bar{x}'')\, d\bar{x}'' \tag{74}$$

The coefficients, $B_{2k-1}(\tau)$, can be obtained from equation (72) by evaluating the equation at M points in the interval $0 \leq \bar{x}' < \frac{1}{2}$. The latter range has been chosen since $g_w(\bar{x}')$ satisfies the condition that $g_w(\frac{1}{2}) = \frac{1}{2}$ for all τ, and since $g_w(\bar{x}')$ is anti-symmetric about the value of $\frac{1}{2}$ at $\bar{x}' = \frac{1}{2}$.

The success of the collocation method in accurately describing the exact solution of the integral equation for arbitrary τ is due wholly to the analytical evaluation of equations (73) and (74). The details of the integrations are presented in Appendix B. The results are:

$$\Phi_{-1}(\bar{x}') = \frac{1}{2\tau}\left[A_1(\tau,\bar{x}') + \tau\bar{x}' A_0(\tau,\bar{x}')\right] \tag{75}$$

$$\Phi_{2k-1}(\bar{x}') = \frac{1}{2}\sum_{i=0}^{2k-1}\binom{2k-1}{i}\frac{(\bar{x}'-\frac{1}{2})^i}{\tau^{2k-1-i}} A_{2k-1-i}(\tau,\bar{x}') \qquad k \geq 1 \tag{76}$$

where

$$A_{2k-1-i}(\tau,\bar{x}') = \frac{1}{(2k-3-i)}\left\{\frac{[\tau(1-\bar{x}')]^{2k-2-i}}{\sqrt{\tau^2(1-\bar{x}')^2+1}} - \frac{[-\tau\bar{x}']^{2k-2-i}}{\sqrt{\tau^2\bar{x}'^2+1}} - \right. \tag{77}$$

$$\left. (2k-2-i)\, A_{2k-3-i}(\tau,\bar{x}')\right\} \qquad (2k-1-i) \geq 4$$

and

$$A_0(\tau,\bar{x}') = \frac{\tau(1-\bar{x}')}{\sqrt{\tau^2(1-\bar{x}')^2+1}} + \frac{\tau\bar{x}'}{\sqrt{\tau^2\bar{x}'^2+1}} \tag{78}$$

$$A_1(\tau,\bar{x}') = \frac{1}{\sqrt{\tau^2\bar{x}'^2 + 1}} - \frac{1}{\sqrt{\tau^2(1-\bar{x}')^2 + 1}} \tag{79}$$

$$A_2(\tau,\bar{x}') = \mathrm{LN}\left| \frac{\sqrt{\tau^2(1-\bar{x}')^2 + 1} + \tau(1-\bar{x}')}{\sqrt{\tau^2\bar{x}'^2 + 1} - \tau\bar{x}} \right| - A_0(\tau,\bar{x}') \tag{80}$$

$$A_3(\tau,\bar{x}') = \sqrt{\tau^2(1 - \bar{x}')^2 + 1} - \sqrt{\tau^2\bar{x}'^2 + 1} - A_1(\tau,\bar{x}') \tag{81}$$

The binomial coefficient, $\binom{2k-1}{i}$, is given by

$$\binom{n}{i} = \frac{n!}{(n - i)!\,i!}$$

If one specifies the number of terms, M, to be taken in the series of equation (70), then equation (72) can be evaluated at the M points in the interval $0 \leq \bar{x}' < \frac{1}{2}$. For example, if M = 4 then the points could be taken as equally spaced and given by $\bar{x}' = 0$, 0.125, 0.250, and 0.375. Once equation (72) has been evaluated at the appropriate points, and the known functions evaluated by using equations (17), (71), and (75) through (81), the only unknowns left are the M coefficients, $B_{2k-1}(\tau)$. Having solved the M x M system of equations for the coefficients, the polynomial solution for $g_w(\bar{x}')$ can be obtained from equation (70). It should be noted that as the accuracy desired for $g_w(\bar{x}')$ is increased more terms are required in the series of equation (70) and, consequently, the larger the system of equations

to be solved for the coefficients. Also, the integral equation has been satisfied for a prescribed tolerance at only M discrete points. It is necessary, therefore, to test the accuracy of the solution for a large number of points over the interval $0 \leq \bar{x}' < \frac{1}{2}$ in order to be assured that the accuracy of the solution has some uniformity.

The coefficients, $B_{2k-1}(\tau)$, can in theory be expressed in analytical form as functions of τ. However, the labor involved in solving a system of equations larger than three-by-three does not warrant the accuracy obtainable. Numerical values for the coefficients can be obtained for each value of τ by numerically solving the system of equations. Once the coefficients are known for a given τ, then the series solution of equation (70) is known for the same value of τ. If a large degree of accuracy is desired, then the numerical evaluation of the coefficients is recommended since a large system of equations must be solved. The analytical expression for the coefficient, $B_1(\tau)$, is given by equation (B-46) of Appendix B.

In order to derive analytical expressions for the moments, linear wall flux segments are used. The linear segments are fitted to the results for the polynomial solution as follows:

$$g_w(\bar{x}') = a_i(\tau)\bar{x}' + b_i(\tau) \quad \text{for} \quad \bar{x}'_i \leq \bar{x}' \leq \bar{x}'_{i+1} \tag{82}$$

where

$$a_i(\tau) = \frac{\left[g_{w_i}(\tau) - g_{w_{i+1}}(\tau)\right]}{\left[\bar{x}'_i - \bar{x}'_{i+1}\right]}. \tag{83}$$

$$b_i(\tau) = \frac{[g_{w_{i+1}}(\tau)\bar{x}'_i - g_{w_i}(\tau)\bar{x}'_{i+1}]}{[\bar{x}'_i - \bar{x}'_{i+1}]} \tag{84}$$

and $g_{w_i}(\tau)$ denotes the value of the wall flux at $\bar{x}'_i$. The subscript i varies from zero to N, where N is the number of linear wall flux segments. Expressing $g_w(\bar{x}')$ in terms of the polar angle α will prove useful in the following development. Thus, combining equations (9) and (10) with equation (82) yields

$$g_w(\alpha) = [a_i(\tau)\bar{x} + b_i(\tau)] - a_i(\tau)\frac{\bar{y}}{\tau}\operatorname{Cot}\alpha \quad \text{for } \alpha_i^L \le \alpha \le \alpha_{i+1}^L \tag{85}$$

and

$$g_w(\alpha) = [a_i(\tau)\bar{x} + b_i(\tau)] - a_i(\tau)\frac{(\bar{y}-1)}{\tau}\operatorname{Cot}\alpha \text{ for } \alpha_{i+1}^U \le \alpha \le \alpha_i^U \tag{86}$$

where

$$\operatorname{Tan}\alpha_i^L = \frac{\bar{y}}{\tau(\bar{x}-\bar{x}'_i)} \qquad \text{(Lower Wall)} \tag{87}$$

and

$$\operatorname{Tan}\alpha_i^U = \frac{(\bar{y}-1)}{\tau(\bar{x}-\bar{x}''_i)} \qquad \text{(Upper Wall)} \tag{88}$$

Since N denotes the number of linear segments, it can be seen from equations

(87) and (88) that $\alpha_0^L = \alpha_1$, $\alpha_{N+1}^L = \alpha_2$, $\alpha_0^U = \alpha_4$, and $\alpha_{N+1}^U = \alpha_3$. Note that each of the angles is a function of the coordinates, $\bar{x}$ and $\bar{y}$.

Moments for Linear Wall Flux Segments

In the following sections the wall contribution for all the moments is determined by using linear wall flux segments and analytically integrating to obtain the contribution for each segment. The total wall contribution for each moment is then determined by summing up the contributions of all the wall flux segments.

Density. The density distribution for an arbitrary wall flux variation is given by equation (26). The integrals for the wall contribution can be evaluated by introducing equations (85) and (86) for the nondimensional wall flux at the lower and upper walls, respectively, and integrating for each segment. The results are:

$$\int_{\alpha_1}^{\alpha_2} g_w(\alpha)\, d\alpha = \sum_{i=0}^{N} \int_{\alpha_i^L}^{\alpha_{i+1}^L} g_w(\alpha)\, d\alpha = \sum_{i=0}^{N} \left\{ [a_i(\tau)\bar{x} + b_i(\tau)](\alpha_{i+1}^L - \alpha_i^L) - a_i(\tau)\, \frac{\bar{y}}{\tau}\, LN \left| \frac{\sin \alpha_{i+1}^L}{\sin \alpha_i^L} \right| \right\} \tag{89}$$

$$\int_{\alpha_3}^{\alpha_4} g_w(\alpha)\, d\alpha = \sum_{i=0}^{N} \int_{\alpha_{i+1}^U}^{\alpha_i^U} g_w(\alpha)\, d\alpha = \sum_{i=0}^{N} \left\{ \left[a_i(\tau)\bar{x} + b_i(\tau) \right] (\alpha_i^U - \alpha_{i+1}^U) - a_i(\tau)\, \frac{(\bar{y}-1)}{\tau}\, LN \left| \frac{\sin \alpha_i^U}{\sin \alpha_{i+1}^U} \right| \right\} \tag{90}$$

Replacing the integrals of equation (26) with the expressions in equations (89) and (90) yields the final form for the local density.

Velocity Components. The integrals for the wall contribution of the velocity components, as presented in equations (33) and (36) for arbitrary wall flux variation, can be evaluated by substituting equations (85) and (86) for the nondimensional wall flux at the lower and upper walls, respectively, and performing the necessary integrations for each segment. The results can be expressed as follows:

$$\int_{\alpha_1}^{\alpha_2} g_w(\alpha)\,\mathrm{Cos}\,\alpha\,d\alpha = \sum_{i=0}^{N} \int_{\alpha_i^L}^{\alpha_{i+1}^L} g_w(\alpha)\,\mathrm{Cos}\,\alpha\,d\alpha = \sum_{i=0}^{N} \left\{ \left[a_i(\tau)\bar{x} + b_i(\tau) \right] \cdot \right. \tag{91}$$

$$(\mathrm{Sin}\,\alpha_{i+1}^L - \mathrm{Sin}\,\alpha_i^L) - a_i(\tau)\,\frac{\bar{y}}{\tau}\left[\mathrm{LN}\left| \frac{\mathrm{Tan}\left(\frac{\alpha_{i+1}^L}{2}\right)}{\mathrm{Tan}\left(\frac{\alpha_i^L}{2}\right)} \right| + \right.$$

$$\left. (\mathrm{Cos}\,\alpha_{i+1}^L - \mathrm{Cos}\,\alpha_i^L) \right] \Bigg\}$$

$$\int_{\alpha_3}^{\alpha_4} g_w(\alpha)\,\mathrm{Cos}\,\alpha\,d\alpha = \sum_{i=0}^{N} \int_{\alpha_{i+1}^U}^{\alpha_i^U} g_w(\alpha)\,\mathrm{Cos}\,\alpha\,d\alpha = \sum_{i=0}^{N} \left\{ \left[a_i(\tau)\bar{x} + b_i(\tau) \right] \cdot \right. \tag{92}$$

$$(\mathrm{Sin}\,\alpha_i^U - \mathrm{Sin}\,\alpha_{i+1}^U) - a_i(\tau)\,\frac{(\bar{y}-1)}{\tau}\left[\mathrm{LN}\left| \frac{\mathrm{Tan}\left(\frac{\alpha_i^U}{2}\right)}{\mathrm{Tan}\left(\frac{\alpha_{i+1}^U}{2}\right)} \right| + \right.$$

$$(\text{Cos } \alpha^{U}_{i} - \text{Cos } \alpha^{U}_{i+1}) \Big] \Big\}$$

$$\int_{\alpha_1}^{\alpha_2} g_w(\alpha) \text{ Sin } \alpha \, d\alpha = \sum_{i=0}^{N} \int_{\alpha_i^L}^{\alpha_{i+1}^L} g_w(\alpha) \text{ Sin } \alpha \, d\alpha = \sum_{i=0}^{N} \Big\{ \Big[a_i(\tau)\bar{x} + b_i(\tau) \Big] \cdot \quad (93)$$

$$(\text{Cos } \alpha^{L}_{i} - \text{Cos } \alpha^{L}_{i+1}) - a_i(\tau) \frac{\bar{y}}{\tau} (\text{Sin } \alpha^{L}_{i+1} - \text{Sin } \alpha^{L}_{i}) \Big\}$$

$$\int_{\alpha_3}^{\alpha_4} g_w(\alpha) \text{ Sin } \alpha \, d\alpha = \sum_{i=0}^{N} \int_{\alpha_{i+1}^U}^{\alpha_i^U} g_w(\alpha) \text{ Sin } \alpha \, d\alpha = \sum_{i=0}^{N} \Big\{ \Big[a_i(\tau)\bar{x} + b_i(\tau) \Big] \cdot \quad (94)$$

$$(\text{Cos } \alpha^{U}_{i+1} - \text{Cos } \alpha^{U}_{i}) - a_i(\tau) \frac{(\bar{y}-1)}{\tau} (\text{Sin } \alpha^{U}_{i} - \text{Sin } \alpha^{U}_{i+1}) \Big\}$$

The final expressions for the velocity components are obtained by replacing the integrals of equations (33) and (36) with the appropriate integrals of equations (91) through (94).

Normal Pressure Components. The general expressions for the normal pressure components are given by equations (41), (44), and (45) for arbitrary wall flux variation. Following the same procedure as outlined for the other moments, the integrals for the wall contribution can be expressed as follows:

$$\int_{\alpha_1}^{\alpha_2} g_w(\alpha)\ \mathrm{Cos}^2\ \alpha\ d\alpha = \sum_{i=0}^{N} \int_{\alpha_i^L}^{\alpha_{i+1}^L} g_w(\alpha)\ \mathrm{Cos}^2\ \alpha\ d\alpha = \sum_{i=0}^{N} \left\{ \left[a_i(\tau)\bar{x} + b_i(\tau) \right] \cdot \right. \quad (95)$$

$$\left[2(\alpha^L_{i+1} - \alpha^L_i) + (\mathrm{Sin}\ 2\alpha^L_{i+1} - \mathrm{Sin}\ 2\alpha^L_i) \right] - a_i(\tau)\ \frac{\bar{V}}{\tau} \cdot$$

$$\left. \left[4\,\mathrm{LN} \left| \frac{\mathrm{Sin}\ \alpha^L_{i+1}}{\mathrm{Sin}\ \alpha^L_i} \right| + 2\ (\mathrm{Cos}^2\ \alpha^L_{i+1} - \mathrm{Cos}^2\ \alpha^L_i) \right] \right\}$$

$$\int_{\alpha_3}^{\alpha_4} g_w(\alpha)\ \mathrm{Cos}^2\ \alpha\ d\alpha = \sum_{i=0}^{N} \int_{\alpha^U_{i+1}}^{\alpha^U_i} g_w(\alpha)\ \mathrm{Cos}^2\ \alpha\ d\alpha = \sum_{i=0}^{N} \left\{ \left[a_i(\tau)\bar{x} + b_i(\tau) \right] \cdot \right. \quad (96)$$

$$\left[2\ (\alpha^U_i - \alpha^U_{i+1}) + (\mathrm{Sin}\ 2\alpha^U_i - \mathrm{Sin}\ 2\alpha^U_{i+1}) \right] - a_i(\tau)\ \frac{(\bar{y}-1)}{\tau} \cdot$$

$$\left. \left[4\ \mathrm{LN} \left| \frac{\mathrm{Sin}\ \alpha^U_i}{\mathrm{Sin}\ \alpha^U_{i+1}} \right| + 2\ (\mathrm{Cos}^2\ \alpha^U_i - \mathrm{Cos}^2\ \alpha^U_{i+1}) \right] \right\}$$

$$\int_{\alpha_1}^{\alpha_2} g_w(\alpha)\ \mathrm{Sin}^2\ \alpha\ d\alpha = \sum_{i=0}^{N} \int_{\alpha^L_i}^{\alpha^L_{i+1}} g_w(\alpha)\ \mathrm{Sin}^2\ \alpha\ d\alpha = \sum_{i=0}^{N} \left\{ \left[a_i(\tau)\bar{x} + b_i(\tau) \right] \cdot \right. \quad (97)$$

$$\left[2\,(\alpha^{L}_{i+1} - \alpha^{L}_{i}) - (\sin 2\alpha^{L}_{i+1} - \sin 2\alpha^{L}_{i}) \right] -$$

$$a_i(\tau)\,\frac{\bar{v}}{\tau}\left[2(\cos^2 \alpha^{L}_{i} - \cos^2 \alpha^{L}_{i+1}) \right]\Big\}$$

$$\int_{\alpha_3}^{\alpha_4} g_w(\alpha)\,\sin^2\alpha\,d\alpha = \sum_{i=0}^{N} \int_{\alpha^{U}_{i+1}}^{\alpha^{U}_{i}} g_w(\alpha)\,\sin^2\alpha\,d\alpha = \sum_{i=0}^{N} \Big\{ \Big[a_i(\tau)\bar{x} + b_i(\tau) \Big] \cdot \quad (98)$$

$$\left[2\,(\alpha^{U}_{i} - \alpha^{U}_{i+1}) - (\sin 2\alpha^{U}_{i} - \sin 2\alpha^{U}_{i+1}) \right] -$$

$$a_i(\tau)\,\frac{(\bar{v}-1)}{\tau}\left[2\,(\cos^2 \alpha^{U}_{i+1} - \cos^2 \alpha^{U}_{i}) \right]\Big\}$$

The integrals for the wall contribution of the $\bar{z}$-component of the normal pressure are identical to the integrals appearing in the density, which are given by equations (89) and (90). The final expressions for the normal pressure components are obtained by substituting the appropriate integrals of equations (89), (90), and (95) through (98) for the integrals of equations (41), (44), and (45).

Thermodynamic Pressure and Temperature. The general expressions for the thermodynamic pressure and temperature for arbitrary wall flux variation are given by equations (47) and (50). The integrals for the

wall contribution are identical to those obtained for the density, which are given by equations (89) and (90). Therefore, the final expressions for the pressure and temperature can be obtained by combining the integrals of equations (89) and (90) with the general expressions of equations (47) and (50).

Shear Stress Components. The general expression for the shear stress is given by equation (53) for arbitrary wall flux variation. Substituting equations (85) and (86) for the wall flux variation over each segment of the lower and upper walls, respectively, into the integrals of equation (53) and performing the necessary integrations yield the following:

$$\int_{\alpha_1}^{\alpha_2} g_w(\alpha)\ \mathrm{Sin}\ \alpha\ \mathrm{Cos}\ \alpha\ d\alpha = \sum_{i=0}^{N} \int_{\alpha_i^L}^{\alpha_{i+1}^L} g_w(\alpha)\ \mathrm{Sin}\ \alpha\ \mathrm{Cos}\ \alpha\ d\alpha = \tag{99}$$

$$\sum_{i=0}^{N} \left\{ \left[a_i(\tau)\bar{x} + b_i(\tau) \right] \left[2(\mathrm{Sin}^2\ \alpha_{i+1}^L - \mathrm{Sin}^2\ \alpha_i^L) \right] - a_i(\tau)\frac{\bar{y}}{\tau} \left[2(\alpha_{i+1}^L - \alpha_i^L) + (\mathrm{Sin}\ 2\alpha_{i+1}^L - \mathrm{Sin}\ 2\alpha_i^L) \right] \right\}$$

$$\int_{\alpha_3}^{\alpha_4} g_w(\alpha)\ \mathrm{Sin}\ \alpha\ \mathrm{Cos}\ \alpha\ d\alpha = \sum_{i=0}^{N} \int_{\alpha_{i+1}^U}^{\alpha_i^U} g_w(\alpha)\ \mathrm{Sin}\ \alpha\ \mathrm{Cos}\ \alpha\ d\alpha = \tag{100}$$

$$\sum_{i=0}^{N} \left\{ [a_i(\tau)\bar{x} + b_i(\tau)] \left[2(\mathrm{Sin}^2 \alpha_i^U - \mathrm{Sin}^2 \alpha_{i+1}^U) \right] - \right.$$

$$\left. a_i(\tau)\frac{(\bar{y}-1)}{\tau} \left[2(\alpha_i^U - \alpha_{i+1}^U) + (\mathrm{Sin}\, 2\alpha_i^U - \mathrm{Sin}\, 2\alpha_{i+1}^U) \right] \right\}$$

Substituting the expressions from equations (99) and (100) for the integrals of equation (53) yields the final expression for the shear stress.

Heat Flux Components. The heat flux components are expressed in general for arbitrary wall flux variation by equations (58) and (59). The wall contribution is composed of the same integrals which appeared in the velocity components. Therefore, the final expressions for the heat flux components are obtained by replacing the integrals of equations (58) and (59) with the appropriate expressions of equations (91) through (94).

Moments for Constant or Linear Wall Flux Over Entire Channel Length

The expressions for a constant or linear wall flux over the entire channel length can be obtained as special cases of the results presented in the last section for linear wall flux segments. In order to determine the exact range of τ for which these approximate solutions are applicable, it is necessary to compare the results of the approximate solutions with the results of the accurate solution for linear wall flux segments. This comparison will be made in a subsequent section.

Constant Wall Flux. For the constant wall flux case $a_i(\tau)$,

defined by equation (83), and N, the number of linear wall flux segments, are set equal to zero. Noting that the index i is equal to zero and referring to equations (87) and (88), it can be seen that $\bar{x}_0' = \bar{x}_0'' = 0$ and $\bar{x}_1' = \bar{x}_1'' = 1$. Since for the constant wall flux case the nondimensional wall flux is assigned its value for $\tau = 0$, which is 1/2 (i.e., $g_{w_0}(\tau) = g_{w_1}(\tau) = 1/2$), $b_i(\tau)$ of equation (84) becomes 1/2. Substituting all of these values into the appropriate moments of interest, as presented for the case of linear wall flux segments, yields the moments for a constant nondimensional wall flux of 1/2.

Linear Wall Flux. The expressions for a linear wall flux over the entire channel length can be obtained by setting N equal to one and noting from equations (87) and (88) that $\bar{x}_0' = \bar{x}_0'' = 0$, $\bar{x}_1' = \bar{x}_1'' = 1/2$, and $\bar{x}_2' = \bar{x}_2'' = 1$, since i varies from zero to one. Substituting these values into equations (83) and (84) and making use of the anti-symmetric property of equation (19), $a_i(\tau)$ and $b_i(\tau)$ can be expressed in terms of $g_{w_0}(\tau)$, the nondimensional wall flux at the channel inlet. The inlet value of the wall flux, $g_{w_0}(\tau)$, can be obtained from the polynomial solutions for the boundary condition. Therefore, the accuracy of $g_{w_0}(\tau)$ depends on the order of the polynomial used to represent the wall flux. For example, for a first order polynomial solution (i.e., linear) $g_{w_0}(\tau)$ is given by

$$g_{w_0}(\tau) = -\frac{1}{2} B_1(\tau) \tag{101}$$

where $B_1(\tau)$ is given by equation (B-46) of Appendix B. Thus, the final expressions for the moments, based on a linear wall flux variation over the entire channel length, are obtained by substituting the results

presented above into the corresponding moments for linear wall flux segments.

Perlmutter [3] has also derived expressions for a linear wall flux over the entire channel length for the density, velocity components, temperature, and wall shear stress for an isothermal system. All of these expressions can be obtained as special cases of the general results obtained by following the procedure outlined in this section.

Average Mass Flow Rate

The average mass flow rate for the assumption of linear wall flux segments can be obtained by combining equations (67), (69), and (82). Performing the necessary integrations yields

$$\Lambda(\tau) = 1 + \sum_{i=0}^{N} \left\{ b_i(\tau) \left[\left(\sqrt{\tau^2 \bar{x}'^2_{i+1} + 1} - \tau \bar{x}'_{i+1} \right) - \left(\sqrt{\tau^2 \bar{x}'^2_{i} + 1} - \tau \bar{x}'_{i} \right) \right] + \frac{a_i(\tau)}{2\tau} \left[\ln \left| \frac{\sqrt{\tau^2 \bar{x}'^2_{i+1} + 1} - \tau \bar{x}'_{i+1}}{\sqrt{\tau^2 \bar{x}'^2_{i} + 1} - \tau \bar{x}'_{i}} \right| + \tau \bar{x}'_{i+1} \left(\sqrt{\tau^2 \bar{x}'^2_{i+1} + 1} - \tau \bar{x}'_{i+1} \right) - \tau \bar{x}'_{i} \left(\sqrt{\tau^2 \bar{x}'^2_{i} + 1} - \tau \bar{x}'_{i} \right) \right] \right\} \tag{102}$$

In order to obtain the results for the constant wall flux assumption set $N = 0$ and $a_i(\tau) = 0$ in equation (102). Noting that $\bar{x}'_0 = 0$, $\bar{x}'_1 = 1$, and $b_0(\tau) = 1/2$, one obtains

$$\Lambda(\tau) = \frac{1}{2}\left[\sqrt{\tau^2 + 1} - \tau + 1\right] \tag{103}$$

Similarly, setting N = 1 in equation (102) yields for the case of a linear wall flux over the entire channel length,

$$\Lambda(\tau) = \left[1 - g_{w_0}(\tau)\right] + \frac{1}{2\tau}\left\{\left[1 - 2\, g_{w_0}(\tau)\right] \mathrm{LN}\left|\sqrt{\tau^2+1} - \tau\right| + \right. \tag{104}$$

$$\left. \tau\left(\sqrt{\tau^2 + 1} - \tau\right)\right\}$$

where $g_{w_0}(\tau)$ is the nondimensional wall flux at the channel inlet and can be determined from any of the different order polynomial solutions for the wall flux, as discussed in the last section. Taking the limits for $\tau = 0$ and $\tau = \infty$, one obtains $\Lambda(0) = 1$ and $\Lambda(\infty) = 0$, respectively, for each of equations (102) and (104). Equation (103) yields $\Lambda(0) = 1$ and $\Lambda(\infty) = 1/2$.

Computational Procedures

Nondimensional Wall Flux

The nondimensional wall flux can be determined by the series approximation of equation (70) once the coefficients, $B_{2k-1}(\tau)$, are known. The coefficients are obtained by evaluating equation (72) at M points and solving the resulting M x M system of equations. In order to evaluate the nondimensional wall flux for a prescribed tolerance, the following procedure can be used:

(1) For a given number M the M x M system of equations resulting from evaluation of equation (72) at M equidistant points in the interval $0 \leq \bar{x}' < 1/2$ is solved for the M coefficients and the nondimensional wall flux calculated.

(2) M is replaced by M + 1 and the procedure outlined in (1) is repeated.

(3) The results for the nondimensional wall flux of (1) and (2) are compared at several points in the interval $0 \leq \bar{x}' < 1/2$. If the results satisfy the prescribed tolerance then the nondimensional wall flux is taken to be that of (2); if not, then the process is repeated until the tolerance is satisfied.

The tolerance for the computations of this work was taken to be 10^{-4} for $\tau \leq 100$ and 10^{-3} for $\tau > 100$ and was satisfied at ten equidistant points in the interval $0 \leq \bar{x}' < 1/2$. For the tolerance of 10^{-4}, the number of terms, M, for the polynomial varied from one for small τ to thirteen for $\tau = 100$. For the tolerance of 10^{-3}, M varied from one for small τ to a maximum of seven for τ of the order of 100, and then dropped to five for $\tau = 10^{4}$.

Local and Average Flow Properties

The local and average flow properties for the case of linear wall flux segments have been expressed in terms of a series of analytical functions, which represents the wall contribution, and a single analytical expression, which represents the contribution of the two reservoirs. The accuracy of the final results depends on the accuracy with which the

wall contribution is evaluated. Having specified some desired degree of accuracy consistent with the accuracy of the nondimensional wall flux results, the wall contribution of the flow properties can be evaluated by the following scheme:

(1) A single linear wall flux segment is used for the entire channel length by setting N equal to one, and the wall contribution is calculated.

(2) The procedure outlined for (1) is repeated for two linear wall flux segments by setting N equal to two.

(3) The results of (1) and (2) for the wall contribution are compared. If the results satisfy a prescribed tolerance, which is consistent with the accuracy desired, then the value of the wall contribution is taken to be that of (2); if not, then the process is repeated by successively adding wall flux segments until the tolerance is satisfied.

The flow property is then determined by combining the value obtained by the above procedure for the wall contribution with the value obtained for the reservoir contribution.

The approximate expressions for the cases of a constant or linear wall flux over the entire channel length can be evaluated directly since the wall contribution for each consists of a single analytical expression.

The tolerance for all local flow property calculations of this work was chosen as 10^{-4}. For the average mass flow rate calculations, the tolerance was 10^{-4} for $\tau \leq 100$ and 10^{-3} for $\tau > 100$.

All numerical calculations were performed using a Burroughs B5500 digital computer.

Results

Results are presented for three methods. For reference to the different results the following key is introduced:

Method 1 Results are obtained by using linear wall flux segments.

Method 2 Results are obtained for a linear wall flux over the entire channel length. The nondimensional wall flux at the inlet, $g_{w_0}(\tau)$, is determined by evaluating the nondimensional wall flux expression of Method 1 at the inlet.

Method 3 Results are obtained for a constant wall flux over the entire channel length. The nondimensional wall flux is assigned the constant value of 1/2.

In general, the local flow properties are plotted versus the axial coordinate for constant values of $\bar{y}$. This enables one to study the development region of the flow and slip velocity along the wall with relative ease.

Nondimensional Wall Flux

The results for the nondimensional wall flux for various values of τ are presented in Figure 2. For $\tau \leq 4.0$ the results were in agreement with the results of Reynolds and Richley [26] to all three significant figures which they present. For $\tau > 4.0$ the results of Reynolds and Richley [26] do not satisfy the anti-symmetric property

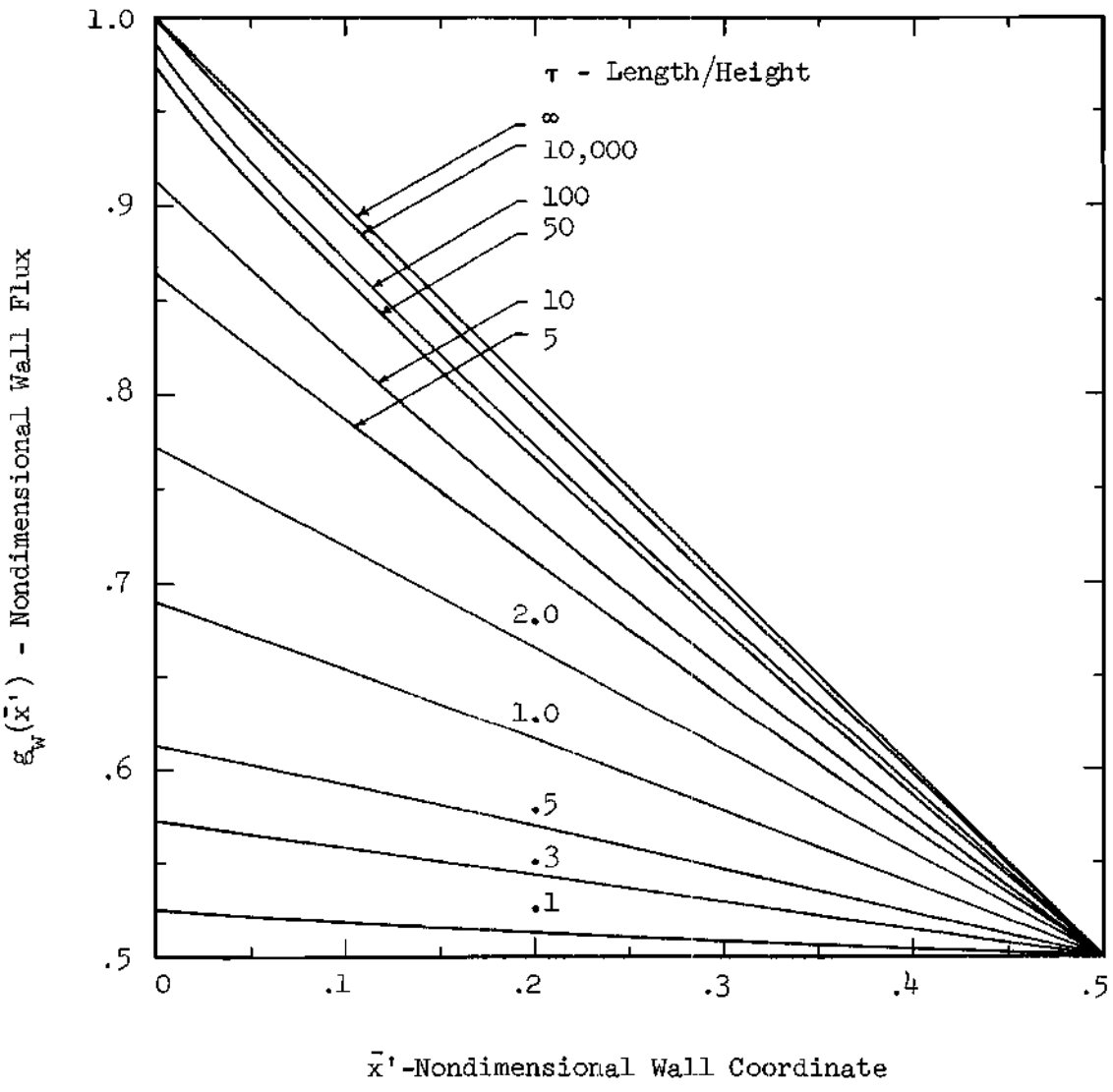

Figure 2. Nondimensional Wall Flux for Free Molecular Flow Through Two Dimensional Channels for Various Values of τ.

exactly to all three significant figures. For $\tau > 12.0$ there are no results available with which to compare. It can be seen that the approach to the linear solution for infinite τ is very slow. It should also be noted that for large τ the results deviate from a linear variation in the region near $\bar{x}' = 0$.

Average Mass Flow Rate

The results for Method 1 are presented in Figure 3 for τ ranging from 10^{-3} to 10^{3}. The results for $\tau \leq 10$ were compared with the results of Demarcus [13], which represent the most accurate calculations of $\Lambda(\tau)$ to date. Demarcus used a variational technique to determine the upper bounds for the values of $\Lambda(\tau)$ for $\tau \leq 10$. The comparison showed that the results of Method 1 agree with the results of Demarcus within $\pm 2 \times 10^{-4}$. For $\tau > 5$ the results of Method 1 were always less then the values given by Demarcus.

A comparison of the results of Method 2, Method 3, and Clausing's long channel formula with the results of Method 1 is also shown in Figure 3. It can be seen that Method 2 predicts $\Lambda(\tau)$ within 3 per cent for $\tau \leq 10$ and Clausing's long channel formula predicts $\Lambda(\tau)$ within 4 per cent for $\tau > 10$. Therefore, analytical expressions which predict the average mass flow rate within 4 per cent for the entire range of τ are available. In addition, the very simple expression of Method 3 predicts $\Lambda(\tau)$ within 3 per cent for $\tau \leq 1.0$.

A further comparison of the results of Method 2 and Clausing's long channel formula with the results of Method 1 for large τ is shown in the inset of Figure 3. It can be seen that Clausing's formula and

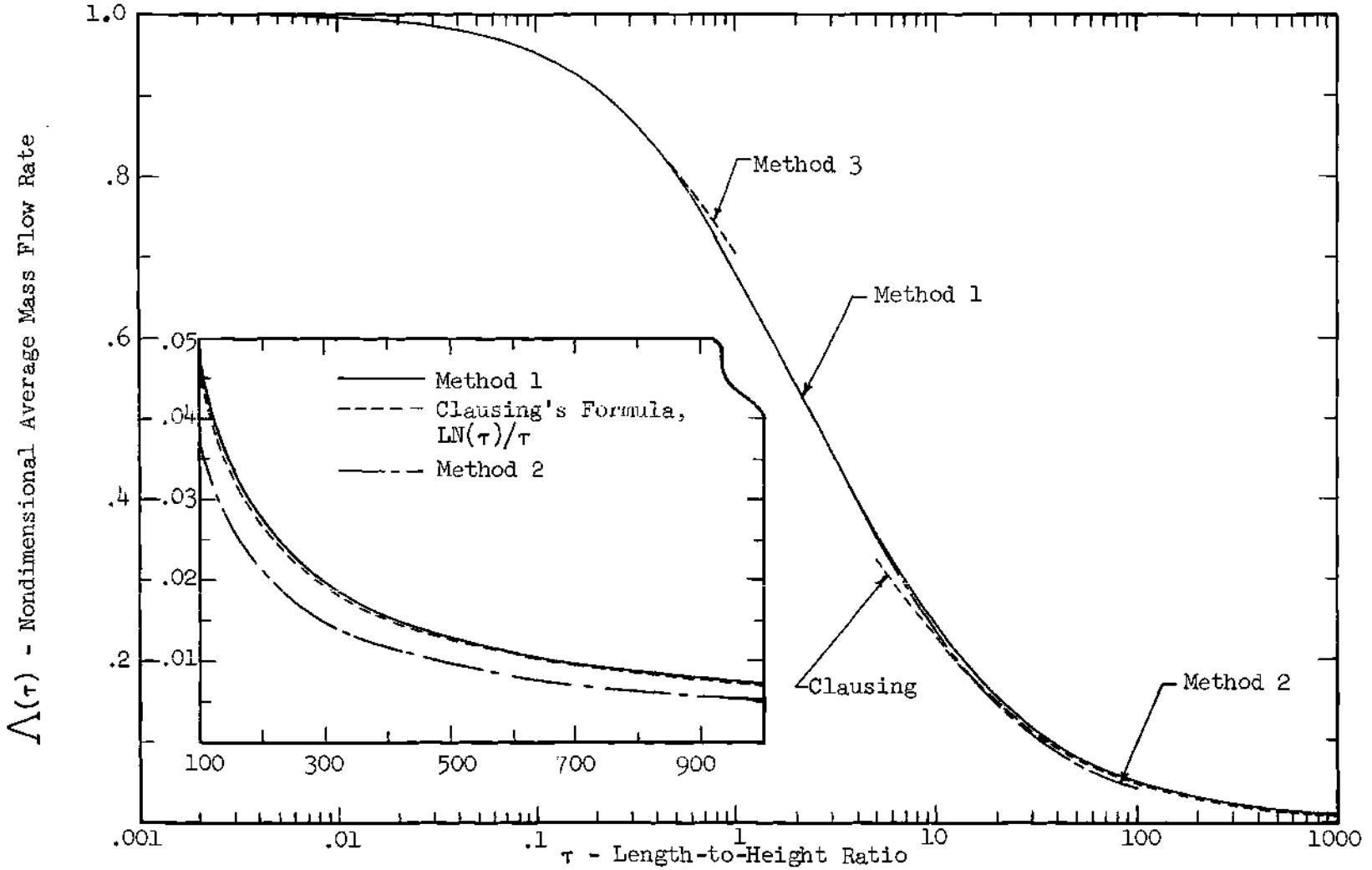

Figure 3. Average Mass Flow Rate for Free Molecular Flow Through Two Dimensional Channels for Various Values of τ, and Comparison of Results for Three Methods for Large τ.

Method 1 are in excellent agreement for large τ, and that Method 2 is slowly approaching Method 1 as τ increases.

Velocity Components

The velocity components have been expressed in universal form by dividing by the average mass flow rate as defined in equation (60). Due to the symmetric and anti-symmetric properties, as illustrated in equations (38) and (39), the results are presented for only half of the channel length.

The axial mass velocity component, as determined by Methods 1 and 2, is presented in Figures 4 through 7 for τ equal to 0.1, 2.0, 10.0, and 50.0, respectively. It should be noted that the results for the singular points, $(\bar{x},\bar{y}) = (0, 0)$ and $(\bar{x},\bar{y}) = (0, 1)$, are not shown. The comparison between Methods 1 and 2 is excellent for $\tau = 0.1$ but becomes progressively worse as τ increases. It can be seen in Figure 4 that for small τ the axial mass velocity is almost constant in the axial direction for points within the channel. For larger values of τ the axial variation becomes large as the wall effects become predominant. A more vivid illustration of the mass velocity profiles in the $\bar{y}$-direction is shown in Figure 8 for several axial stations and several values of τ. It can be seen that for large τ the velocity profiles do not vary significantly across the channel for points away from the inlet and exit regions. For points near the inlet or exit, as illustrated for the cases of $\tau = 0.1$ and $\tau = 2.0$, the mass velocity profiles are essentially flat everywhere except near the walls, where a large variation occurs. Finally, although the results are not shown, a

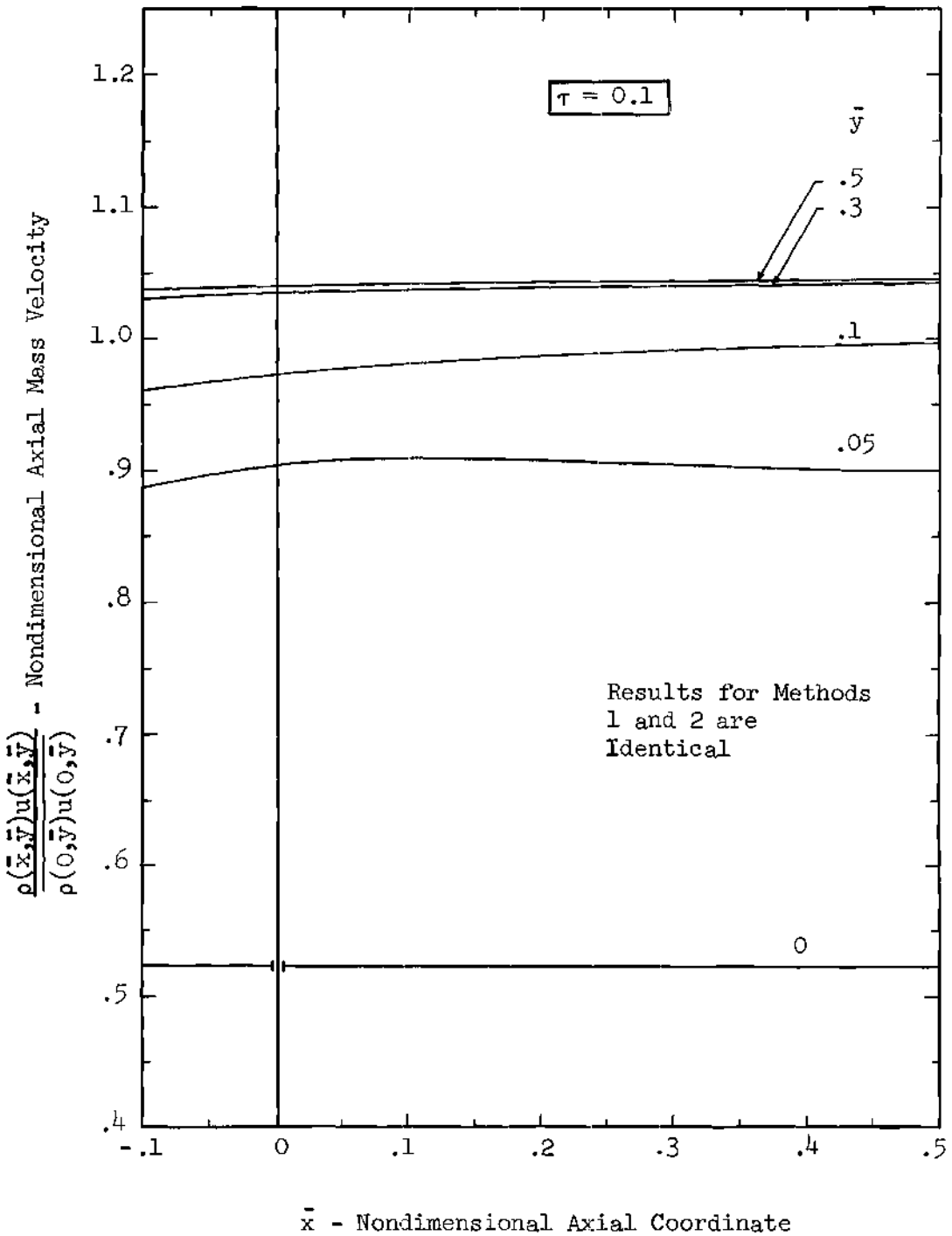

Figure 4. Nondimensional Axial Mass Velocity for Free Molecular Flow Through a Two Dimensional Channel with $\tau = 0.1$.

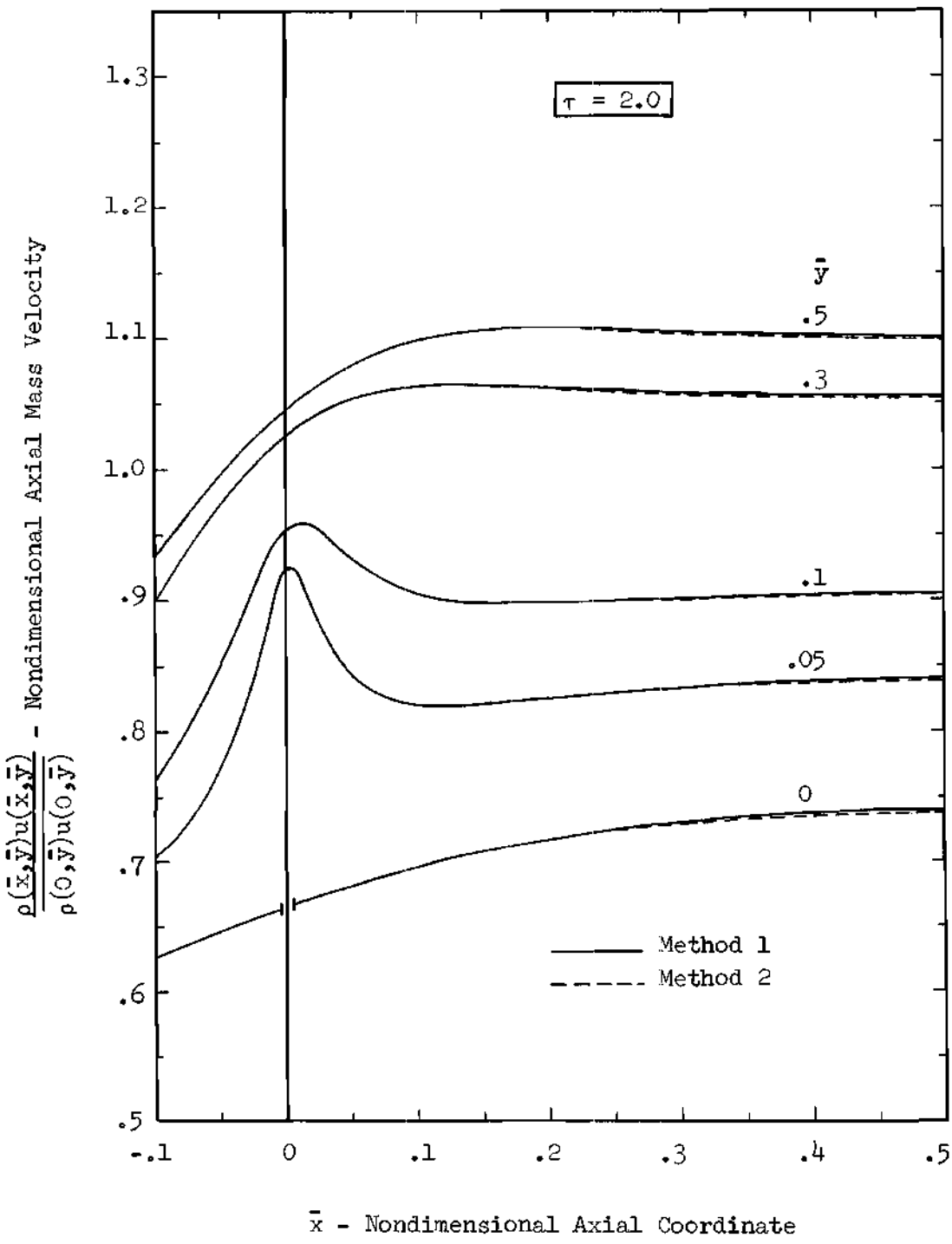

Figure 5. Nondimensional Axial Mass Velocity for Free Molecular Flow Through a Two Dimensional Channel with $\tau = 2$.

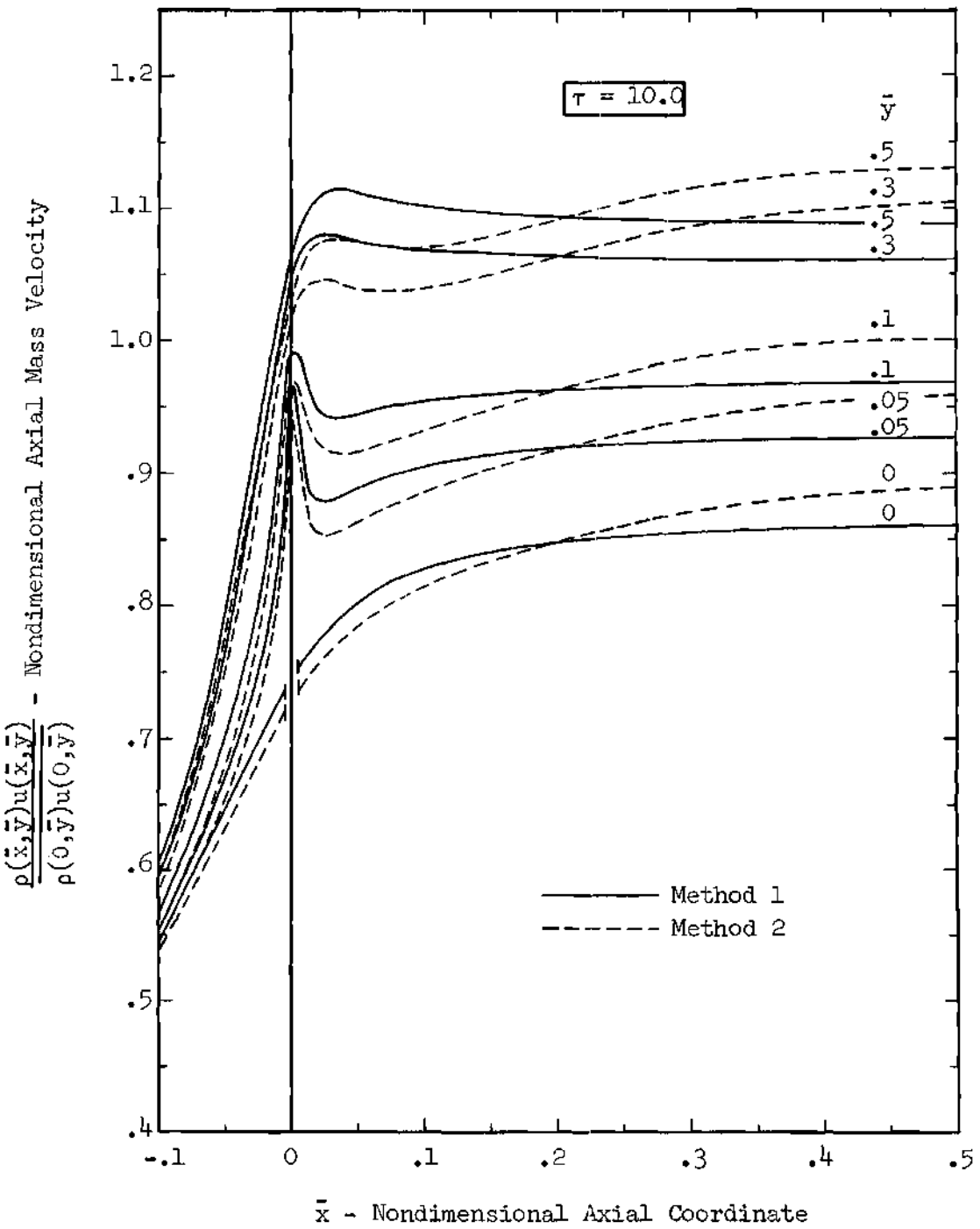

Figure 6. Nondimensional Axial Mass Velocity for Free Molecular Flow Through a Two Dimensional Channel with $\tau = 10$.

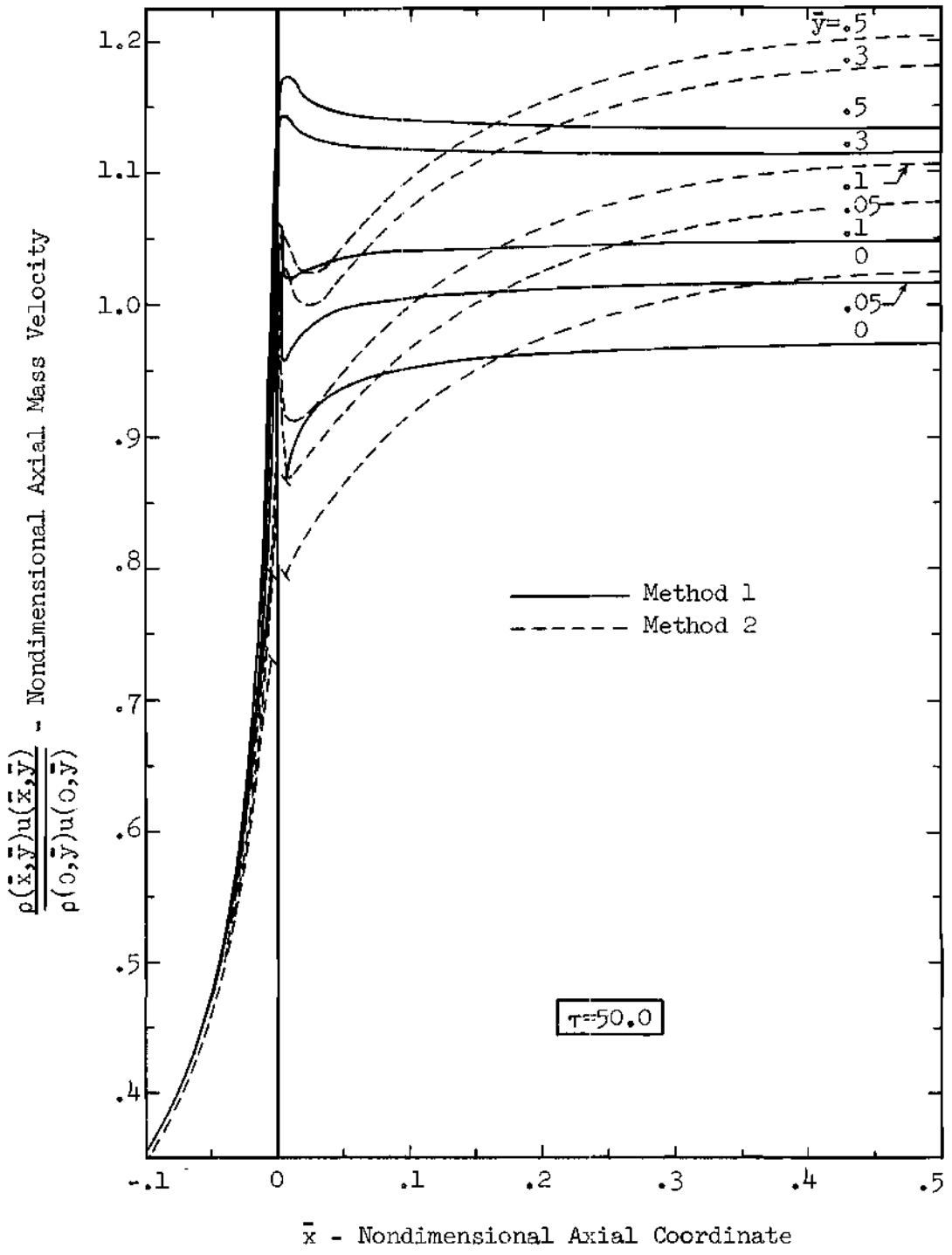

Figure 7. Nondimensional Axial Mass Velocity for Free Molecular Flow Through a Two Dimensional Channel with $\tau = 50$.

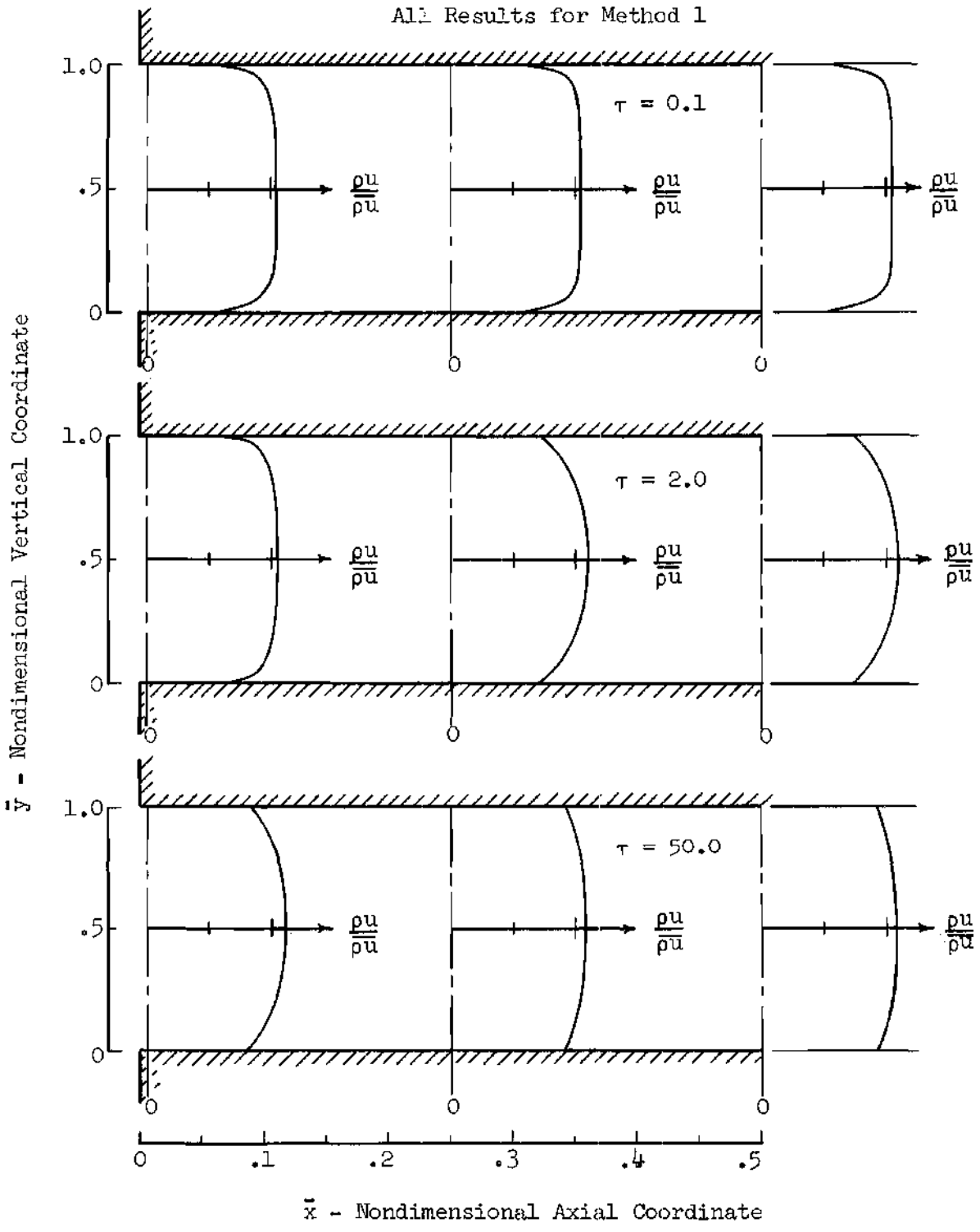

Figure 8. Nondimensional Axial Mass Velocity Profiles for Free Molecular Flow Through a Two Dimensional Channel for Three Points Along Channel and Length-to-Height Ratios of 0.1, 2.0, and 50.0.

comparison between Methods 1 and 3 for $\tau = 0.1$ was within approximately 1 per cent.

The vertical mass velocity component, as calculated by Methods 1 and 2, is presented in Figures 9 through 11 for values of τ of 0.1, 2.0, and 10.0, respectively. The results for $\tau = 50.0$ are not presented since the vertical mass velocity is essentially zero for $\bar{x} > 0.05$. For small τ the vertical velocity is always positive, as illustrated in Figure 9. However, as τ increases it can be seen that the maximum vertical mass velocity occurs just upstream of the inlet and that for a portion of the channel the vertical velocity becomes negative before finally vanishing at $\bar{x} = 0.5$. The comparison between Methods 1 and 2 is again excellent for $\tau = 0.1$ but becomes progressively worse for larger τ. In fact, Method 2 even predicts the wrong direction for the vertical mass velocity for large τ and $\bar{x}$ greater than approximately 0.075. Consequently, for intermediate and large values of τ it can be seen that the linear wall flux assumption leads to large errors in predicting the vertical mass velocity. Finally, although the results are not shown, a comparison between Methods 1 and 3 for $\tau = 0.1$ revealed that the results of Method 3 for $\bar{y} \geq 0.05$ were within 5 per cent. However, the results for $0 \leq \bar{y} < 0.05$ became progressively worse as the wall was approached.

Pressure and Temperature

The results for pressure, as calculated by Method 1, are presented in Figures 12 through 14 for $\tau = 0.1$, 2.0, and 50.0, respectively, $P_1/P_2 = 2.0$, $T_1/T_2 = 1.0$, and $T_w/T_1 = 0.25$, 1.0, and 4.0. The tank

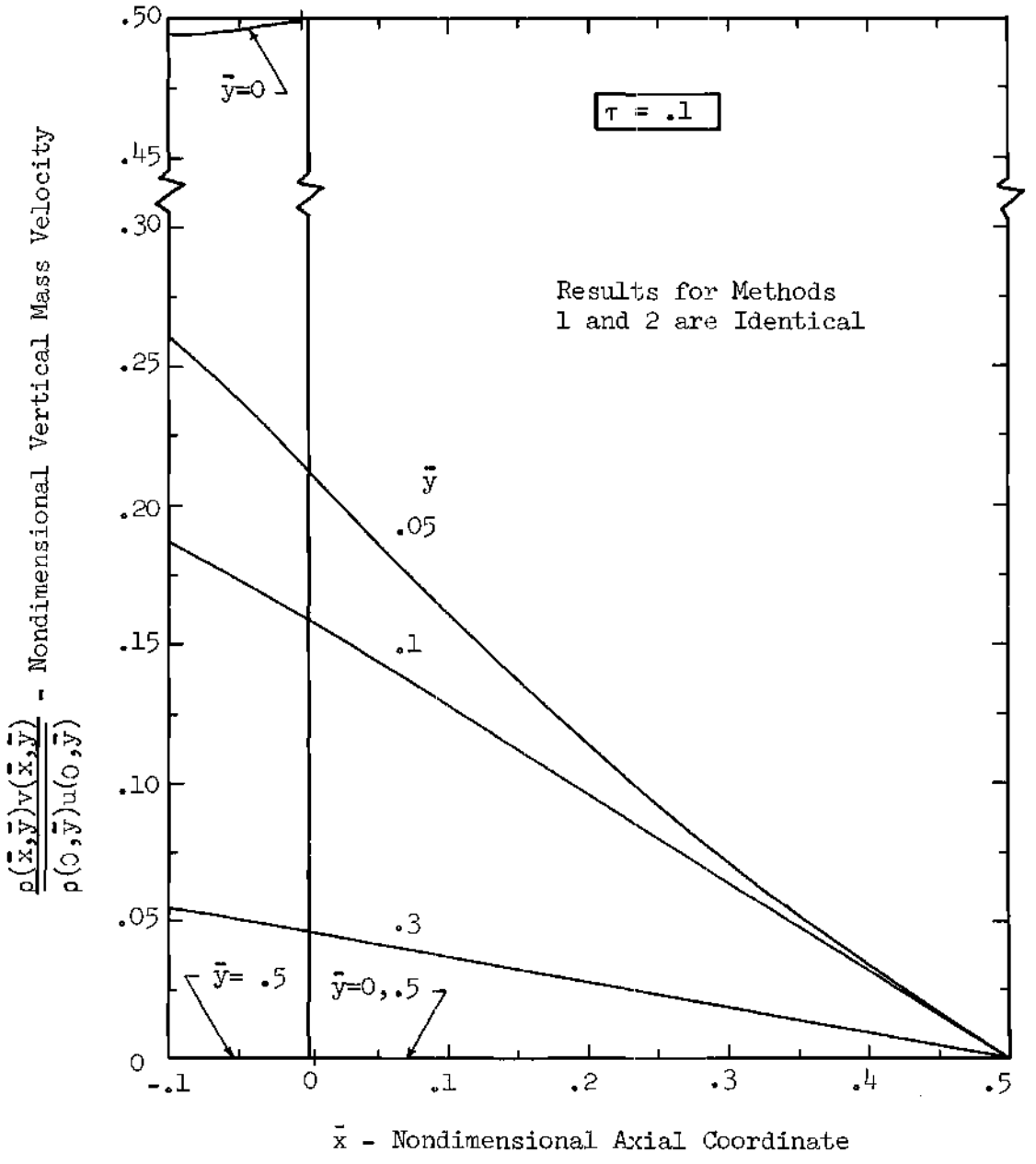

Figure 9. Nondimensional Vertical Mass Velocity for Free Molecular Flow Through a Two Dimensional Channel with $\tau = 0.1$.

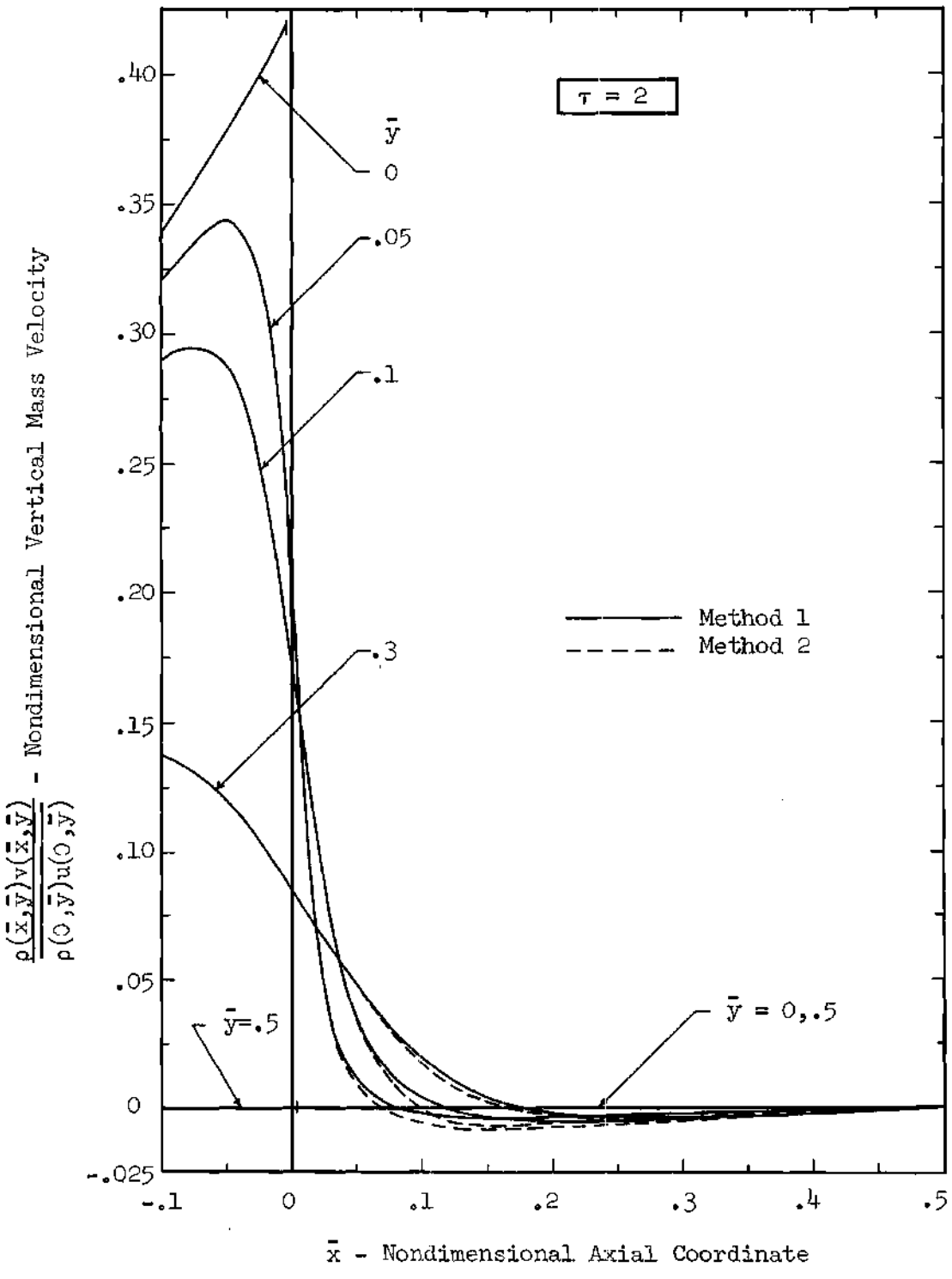

Figure 10. Nondimensional Vertical Mass Velocity for Free Molecular Flow Through a Two Dimensional Channel with $\tau = 2.0$.

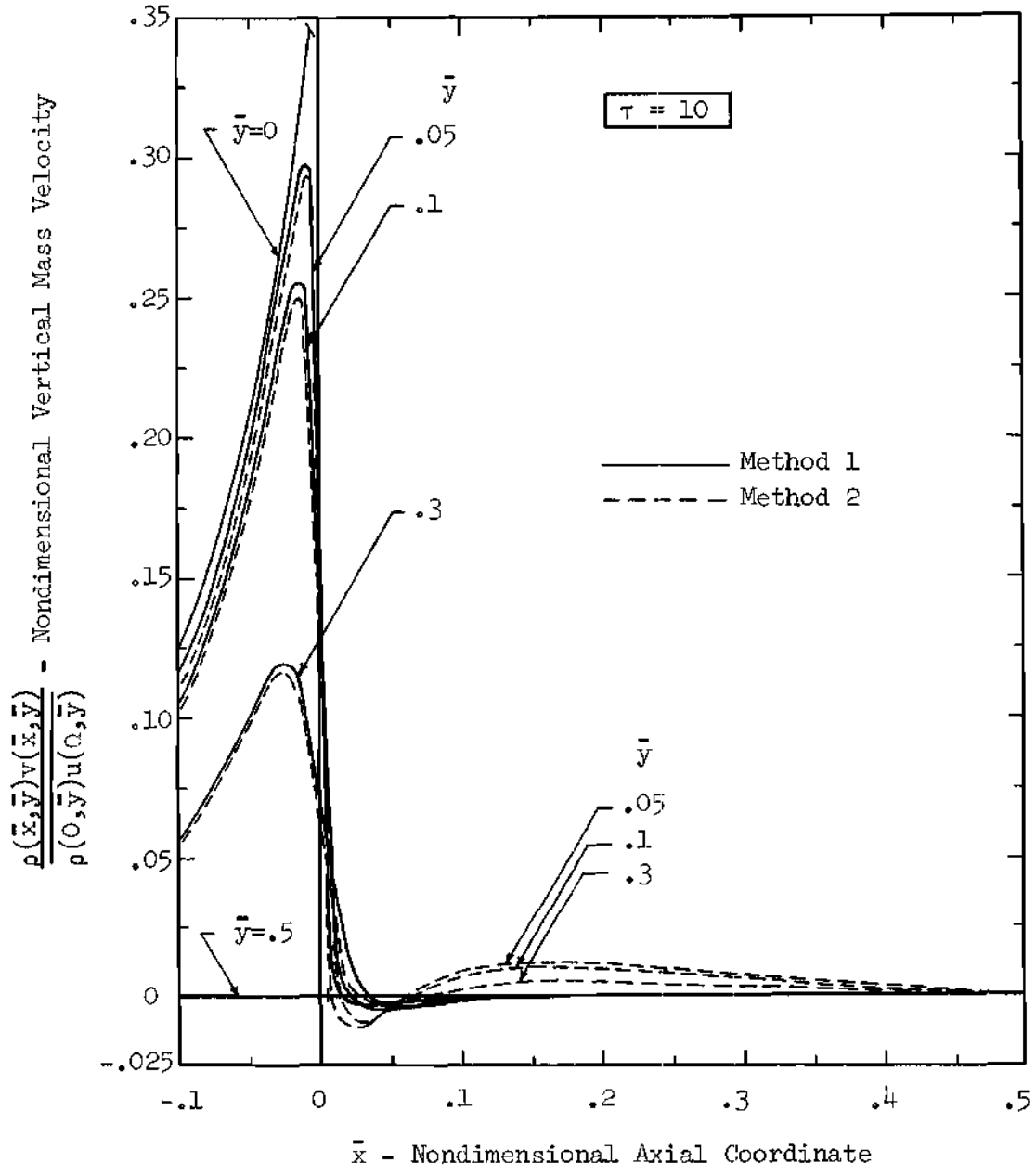

Figure 11. Nondimensional Vertical Mass Velocity for Free Molecular Flow Through a Two Dimensional Channel with τ = 10.0.

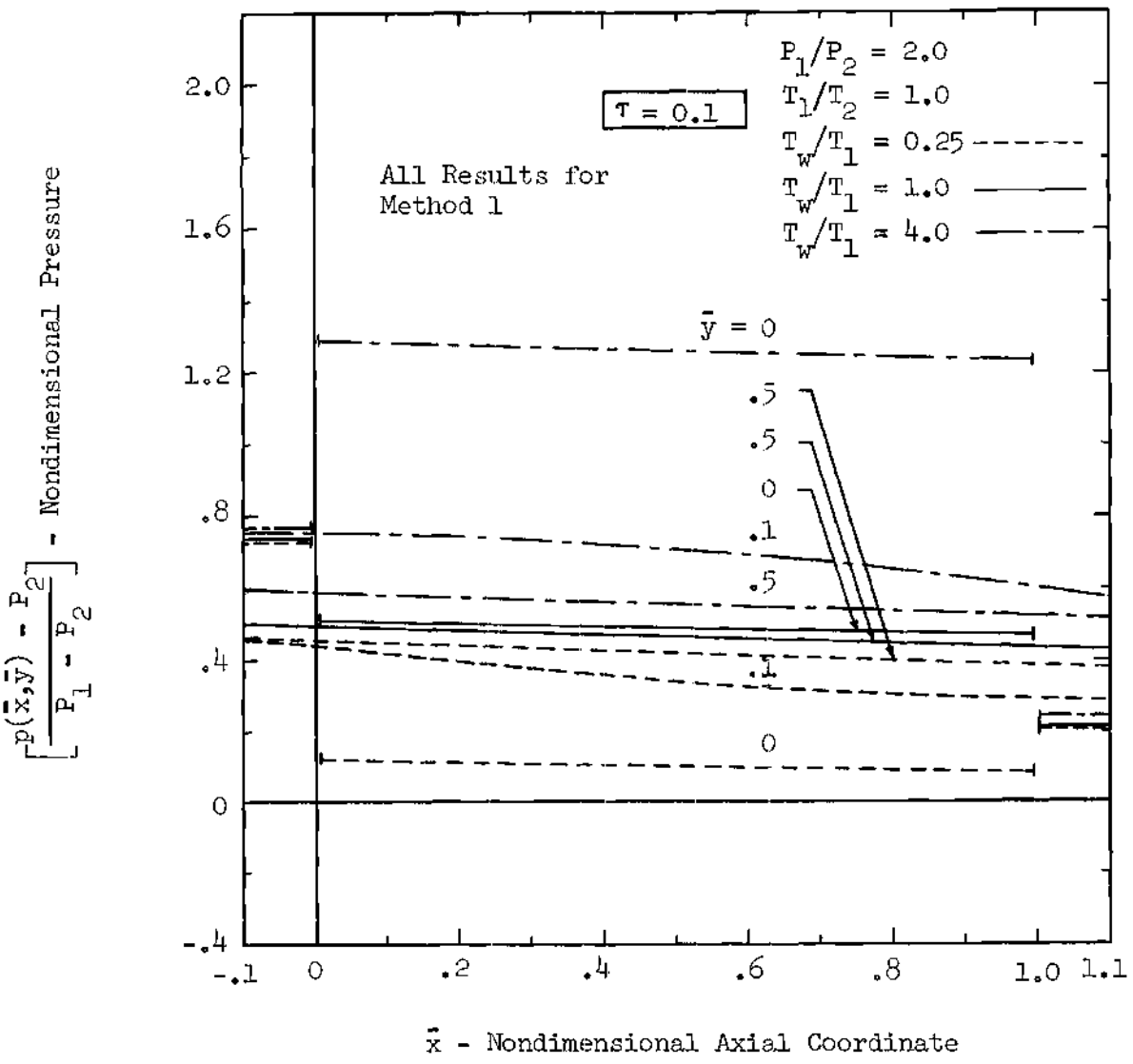

Figure 12. Nondimensional Pressure for Free Molecular Flow Through a Two Dimensional Channel for $\tau = 0.1$, $P_1/P_2 = 2.0$, $T_1/T_2 = 1.0$, and $T_w/T_1 = 0.25$, 1.0, 4.0.

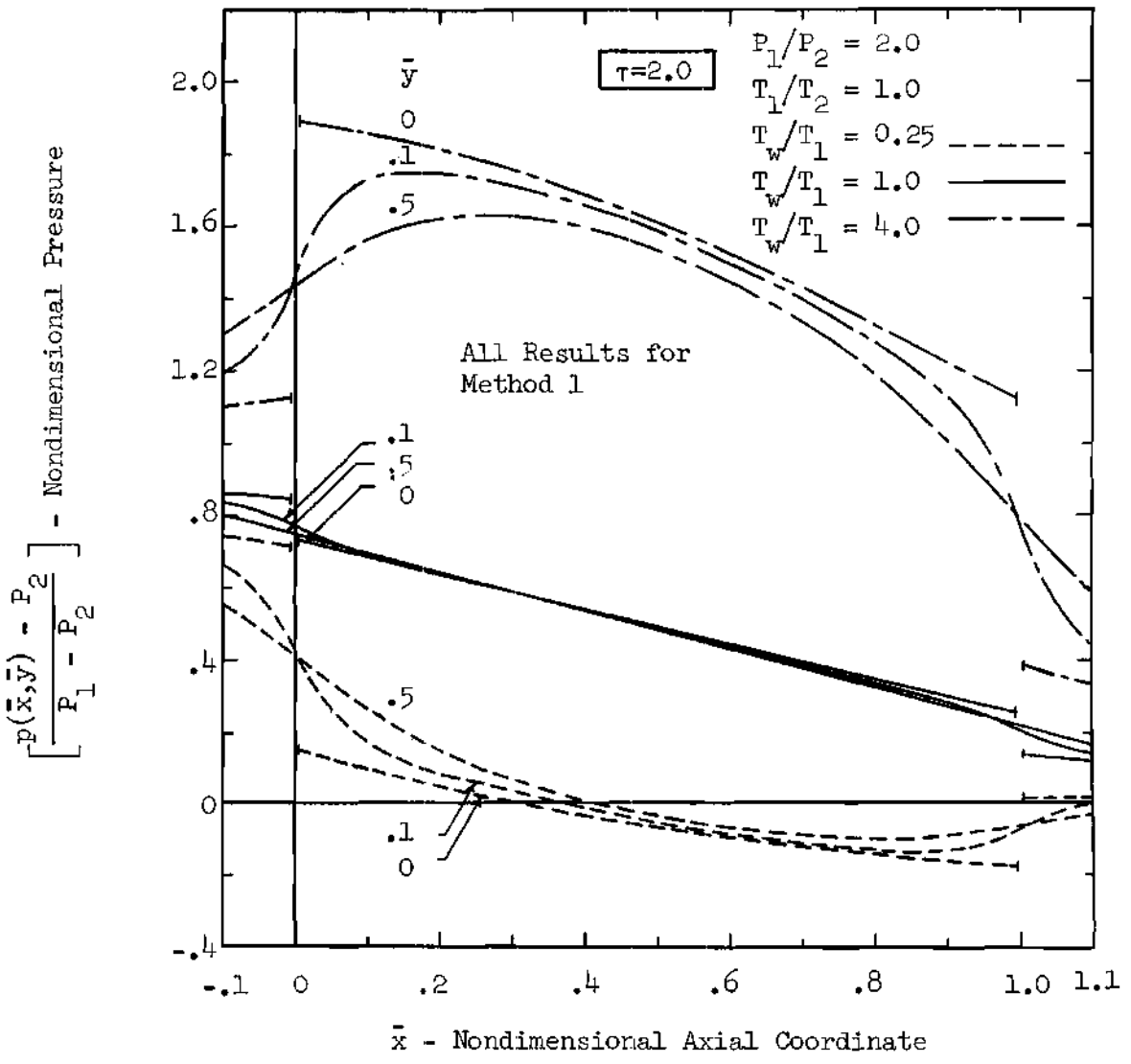

Figure 13. Nondimensional Pressure for Free Molecular Flow Through a Two Dimensional Channel for $\tau = 2.0$, $P_1/P_2 = 2.0$, $T_1/T_2 = 1.0$, and $T_w/T_1 = 0.25$, 1.0, 4.0.

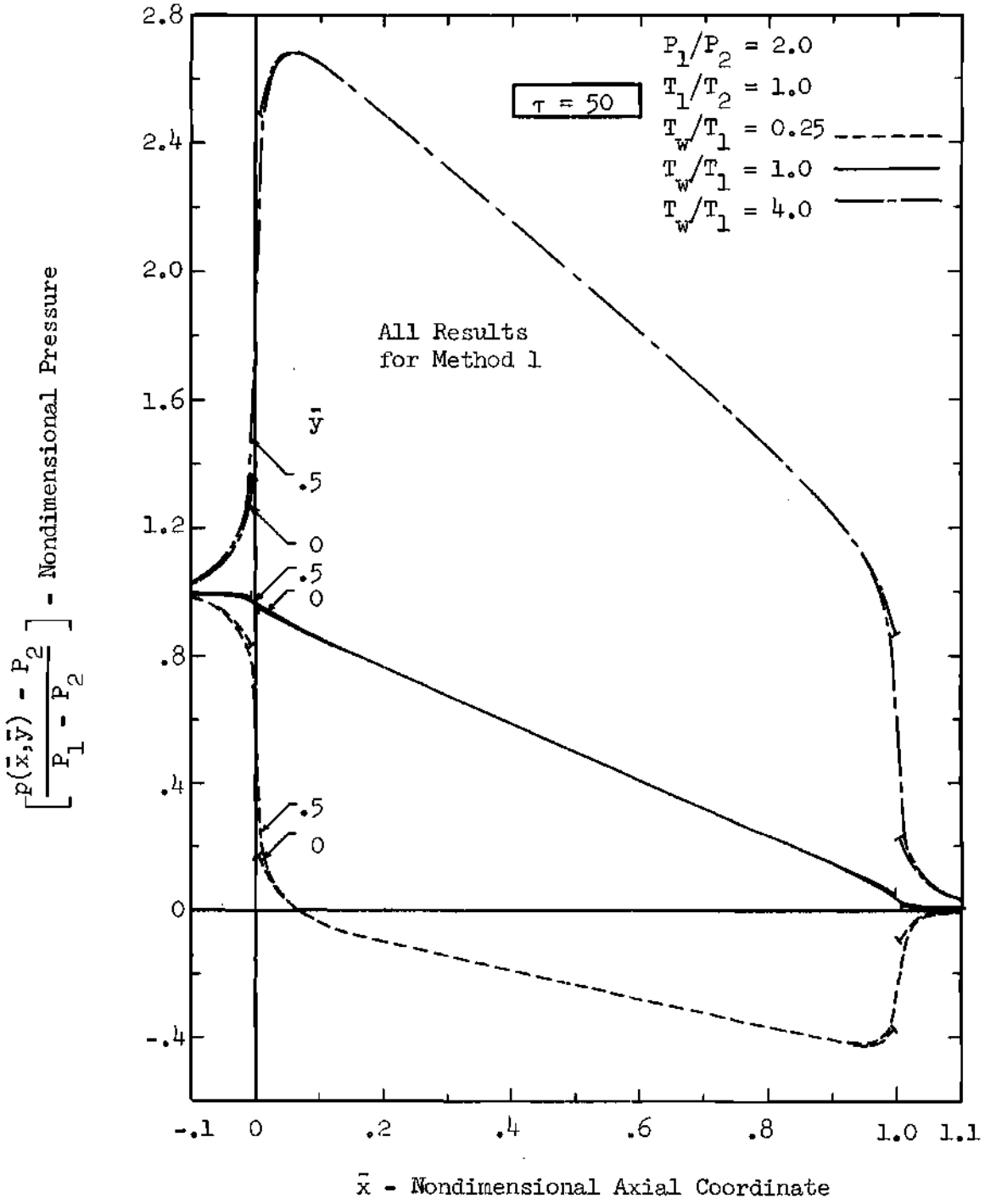

Figure 14. Nondimensional Pressure for Free Molecular Flow Through a Two Dimensional Channel for $\tau = 50.0$, $P_1/P_2 = 2.0$, $T_1/T_2 = 1.0$, and $T_w/T_1 = 0.25$, 1.0, 4.0.

temperatures have been taken as equal in order to illustrate the wall temperature effect. The pressure has been normalized so that the upstream and downstream limits are unity and zero, respectively. For small τ the pressure is essentially constant within the channel, as illustrated for $\tau = 0.1$ in Figure 12. For intermediate values of τ (e.g., $\tau = 2.0$) the pressure is essentially linear along the channel for points within the channel, but the hot and cold wall results exhibit a definite inlet and exit effect. There also exists a distinct pressure profile across the channel for the hot and cold wall cases, while the results for the isothermal case reveal an almost constant pressure across the channel. For large τ, as illustrated for $\tau = 50.0$, the pressure is essentially constant across the channel everywhere except near the inlet and exit for all three cases of hot, cold, and isothermal walls. However, for all three cases the variation along the channel is essentially linear with the magnitude of the results for each case being quite different. In conclusion, it is apparent that the assumptions of linear pressure variation along the channel and constant pressure across the channel are quite good for long channels.

The results for the temperature, as calculated by Method 1, are presented in Figures (15) through (17) for τ equal to 0.1, 2.0, and 50.0, respectively. The wall and tank properties are taken such that the ratios are the same as for the pressure results. Since the tank temperatures are equal, the results are normalized with the temperature of the tanks. Consequently, the upstream and downstream limits are unity. The axial variation for small τ, as illustrated in Figure 15

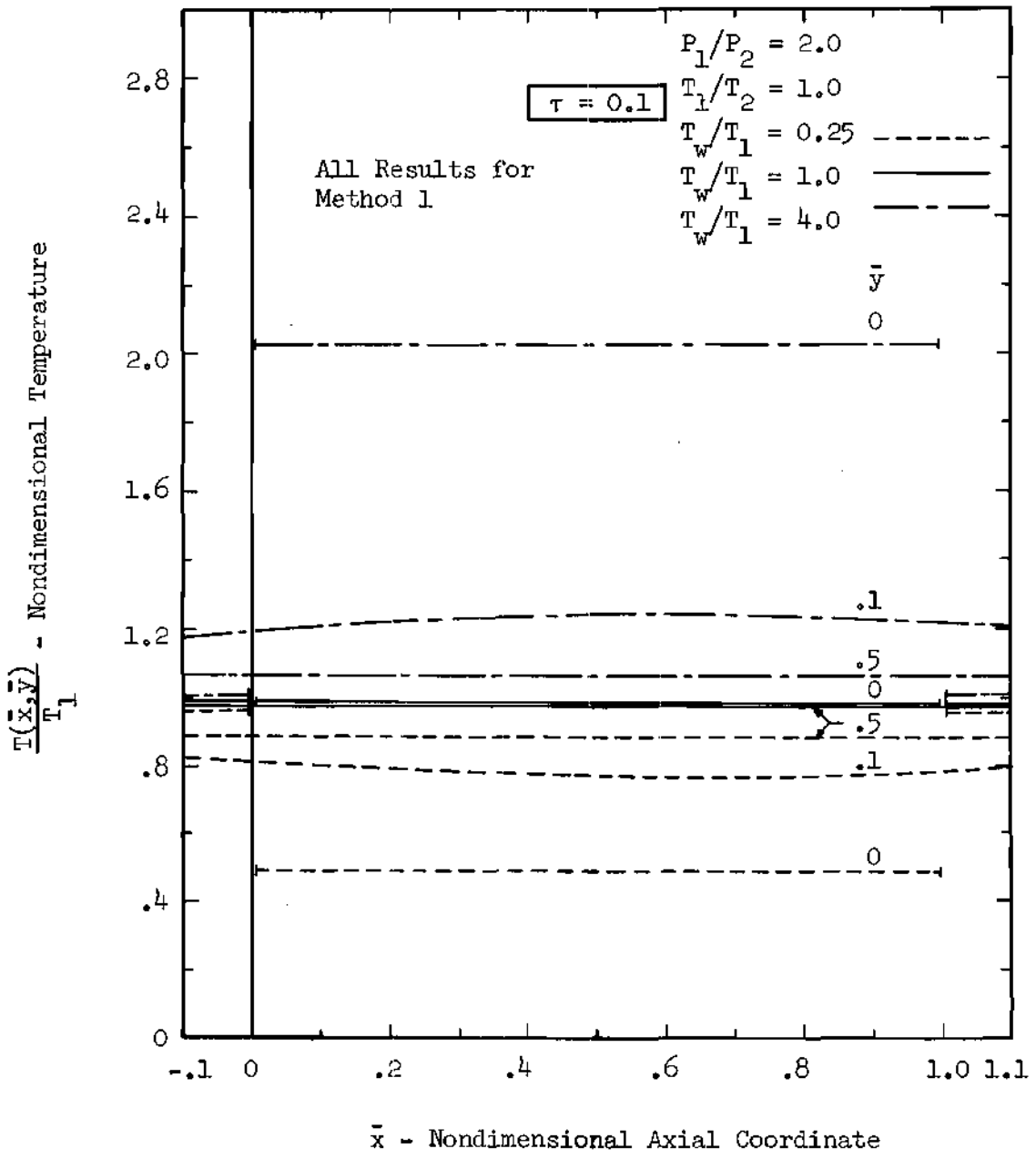

Figure 15. Nondimensional Temperature for Free Molecular Flow Through a Two Dimensional Channel for $\tau = 0.1$, $P_1/P_2 = 2.0$, $T_1/T_2 = 1.0$, and $T_w/T_1 = 0.25, 1.0, 4.0$.

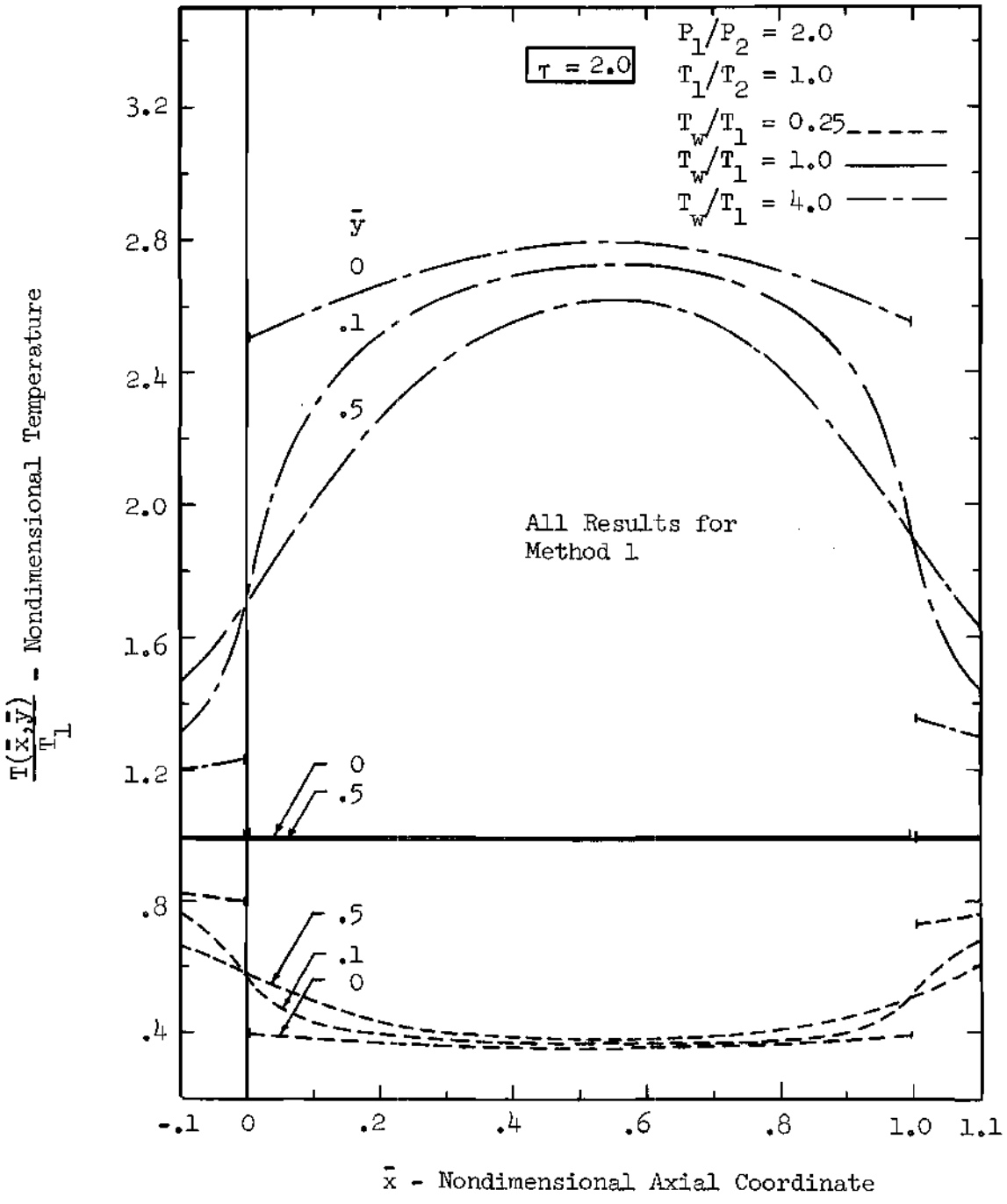

Figure 16. Nondimensional Temperature for Free Molecular Flow Through a Two Dimensional Channel for $\tau = 2.0$, $P_1/P_2 = 2.0$, $T_1/T_2 = 1.0$, and $T_w/T_1 = 0.25, 1.0, 4.0$.

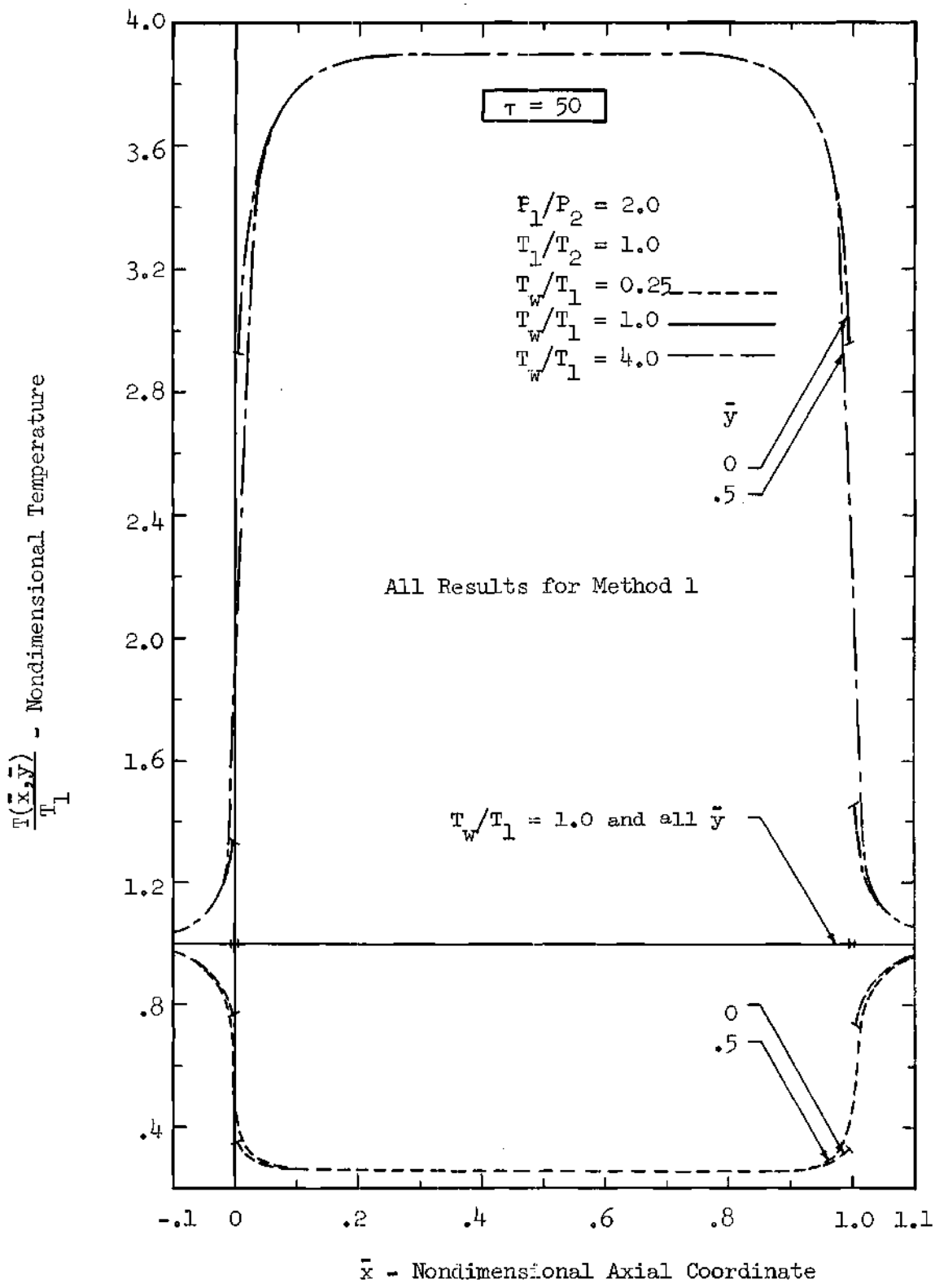

Figure 17. Nondimensional Temperature for Free Molecular Flow Through a Two Dimensional Channel for $\tau = 50.0$, $P_1/P_2 = 2.0$, $T_1/T_2 = 1.0$, $T_w/T_1 = 0.25, 1.0, 4.0$.

for $\tau = 0.1$, is again quite small for points within the channel. Since the channel is very short, the temperature of the gas at the wall is nowhere near the wall values. For a larger value of τ (e.g., $\tau = 2.0$ in Figure 16), the axial variation is quite pronounced for the non-isothermal cases, and the temperature of the gas at the wall is somewhat closer to the wall values than in the previous case. However, a large temperature jump at the wall still exists. For the case of $\tau = 50.0$ in Figure 17 the temperature of the gas becomes essentially constant along the channel everywhere except near the inlet and exit, and the temperature of the gas at the wall is very close to the wall values. However, a definite temperature jump still exists. This is as expected since there is a finite gas velocity at the wall in the axial direction for all values of τ. It should be noted that the isothermal results for $\tau = 50.0$ are constant at unity for all practical considerations. For smaller values of τ the variation is still quite small but the magnitude is slightly different from unity. Since for the isothermal case all temperatures at the boundaries are equal, the deviation of the temperature from unity can be attributed directly to the kinetic energy of the gas.

Although the results for the density are not presented, the density for the corresponding pressure and temperature at any point in the flow field, as presented in the preceding figures, can be obtained directly from the equation of state.

Although the results for Method 2 are not presented, a comparison was made with the results of Method 1 for $\tau = 0.1$, 2.0, 10.0, and 50.0,

$P_1/P_2 = 2.0$, $T_1/T_2 = 1.0$, and $T_w/T_1 = 0.25$, 1.0, and 4.0. The density and pressure were within one per cent for the isothermal case and within one and one-half per cent for the non-isothermal case. The temperature was essentially identical.

Results for density, pressure, and temperature were also obtained for a pressure ratio of 5.0. The results for Method 1 were qualitatively the same in that the variation for different values of τ was similar. However, the agreement between Methods 1 and 2 was not quite as good, indicating that the linear wall flux assumption becomes worse as the pressure ratio is increased.

Shear Stress

Results for the wall shear stress, as determined by Method 1, are presented in Figure 18 for $\tau = 0.1$, 2.0, and 50.0, $P_1/P_2 = 2.0$, $T_1/T_2 = 1.0$, and $T_w/T_1 = 0.25$, 1.0, and 4.0. The shear stress has been nondimensionalized with the upstream pressure. It can be seen that the wall shear stress depends quite strongly on τ and the wall temperature. For $\tau = 0.1$ the wall shear stress is essentially constant along the channel, but the magnitude is different for each wall temperature. As τ is increased the wall effect becomes significant and a large variation occurs for the hot and cold wall cases. For the case of a long channel (e.g., $\tau = 50.0$) the wall shear stress varies considerably near the inlet and exit but remains essentially constant over the major portion of the channel.

Although the results are not presented, the variation of the shear stress for $\bar{y}$ greater than zero was found to be quite similar to

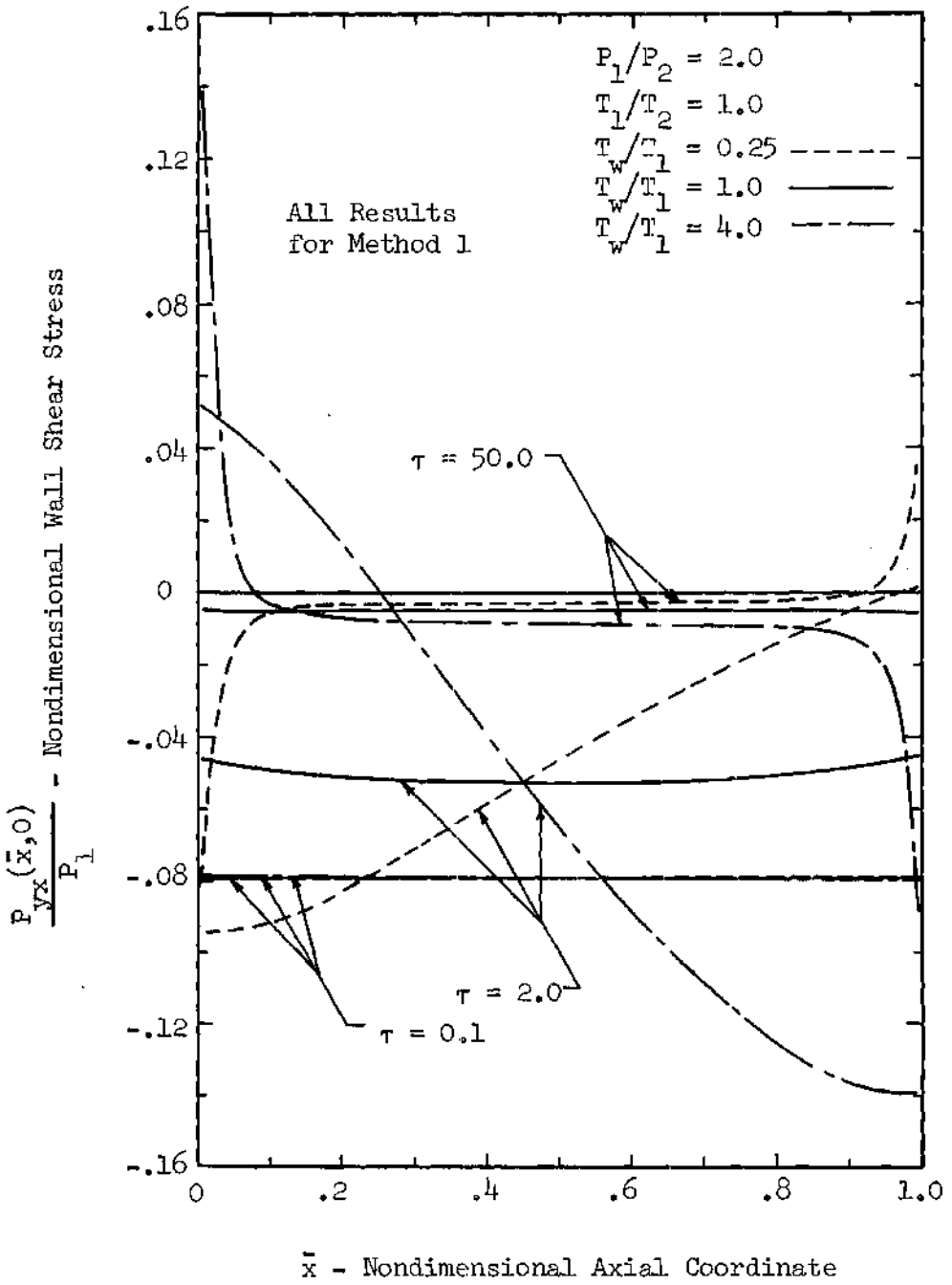

Figure 18. Comparison of Wall Shear Stress for Free Molecular Flow Through Two Dimensional Channels of τ = 0.1, 2.0, and 50.0 for P_1/P_2 = 2.0, T_1/T_2 = 1.0, and T_w/T_1 = 0.25, 1.0, and 4.0.

the wall variation. A comparison of the results for the shear stress and the vertical mass velocity for identical conditions indicated that the variation of the local shear stress is quite sensitive to the local vertical mass velocity. Therefore, a comparison of the results of Methods 1 and 2 is not expected to be as good as for the pressure, density, and temperature. Although the results of the comparison are not shown, this was found to be the case. Since the magnitude of the shear stress is small for points near the centerline (the shear stress vanishes at $\bar{y} = 0.5$ due to symmetry) and the results have been calculated to only four-place accuracy, a comparison based on percentage differences can be misleading. Therefore, the following discussion will be restricted to the wall shear stress values, which are normally the largest values in the channel. A comparison of the results of Methods 1 and 2 revealed the following:

(1) For $T_w/T_1 = 1.0$ (i.e., the isothermal case) the results were essentially identical for $\tau \leq 2.0$. For $\tau = 10.0$ and $\tau = 50.0$ the maximum percentage differences were six and sixteen, respectively.

(2) For $T_w/T_1 = 0.25$ and 4.0 the agreement was again excellent for $\tau \leq 2.0$. However, for $\tau = 10.0$ and $\tau = 50.0$ the results agreed in general within five and nine per cent, respectively, for the cold wall case and within seven and twelve per cent, respectively, for the hot wall case.

It should be noted that for $\tau = 50.0$ the magnitude of the shear stress nondimensionalized with the upstream pressure is of the order of 10^{-3}.

Since the accuracy attained in the calculations is of the order of 10^{-4}, the comparison based on percentage differences for this value of τ should not be taken as absolute, but rather as a relative comparison.

Heat Flux Components

Results for the heat transfer to the wall, as calculated by Method 1, are presented in Figure 19 for $\tau = 0.1$, 2.0, 10.0, and 50.0, $P_1/P_2 = 2.0$, $T_1/T_2 = 1.0$, and $T_w/T_1 = 0.25$, 1.0, and 4.0. The heat flux components have been nondimensionalized with the upstream equilibrium heat flux, $P_1\sqrt{2RT_1}$. Since there is a jump of $(P_{yx}(\bar{x},0)/P_1)\cdot(u(\bar{x},0)/\sqrt{2RT_1})$ in the $\bar{y}$-component of the heat flux vector at the wall this quantity must be added to $q_y(\bar{x},0)/P_1\sqrt{2RT_1}$ in order to determine the nondimensional heat transfer to the wall. For $\tau = 0.1$ the heat transfer to the wall is approximately constant along the channel. In contrast, for $\tau = 50.0$ the heat transfer is essentially zero over the major portion of the channel and varies rapidly near the inlet and exit. The heat transfer to the wall for the isothermal case is essentially zero for all values of τ.

Although the results are not presented, the variation of the $\bar{y}$-component of the heat flux vector for values of $\bar{y}$ not equal to zero is quite similar in that the heat flux component in the $\bar{y}$-direction varies quite rapidly in the inlet and exit regions. Due to the symmetry of the problem $q_y(\bar{x},\bar{y})$ vanishes at $\bar{y} = 0.5$. Following the same line of reasoning as discussed for the shear stress, only the wall values of the nondimensional heat flux component will be compared for Methods 1 and 2. Again, these results are not presented. For $T_w/T_1 = 1.0$ the $\bar{y}$-component

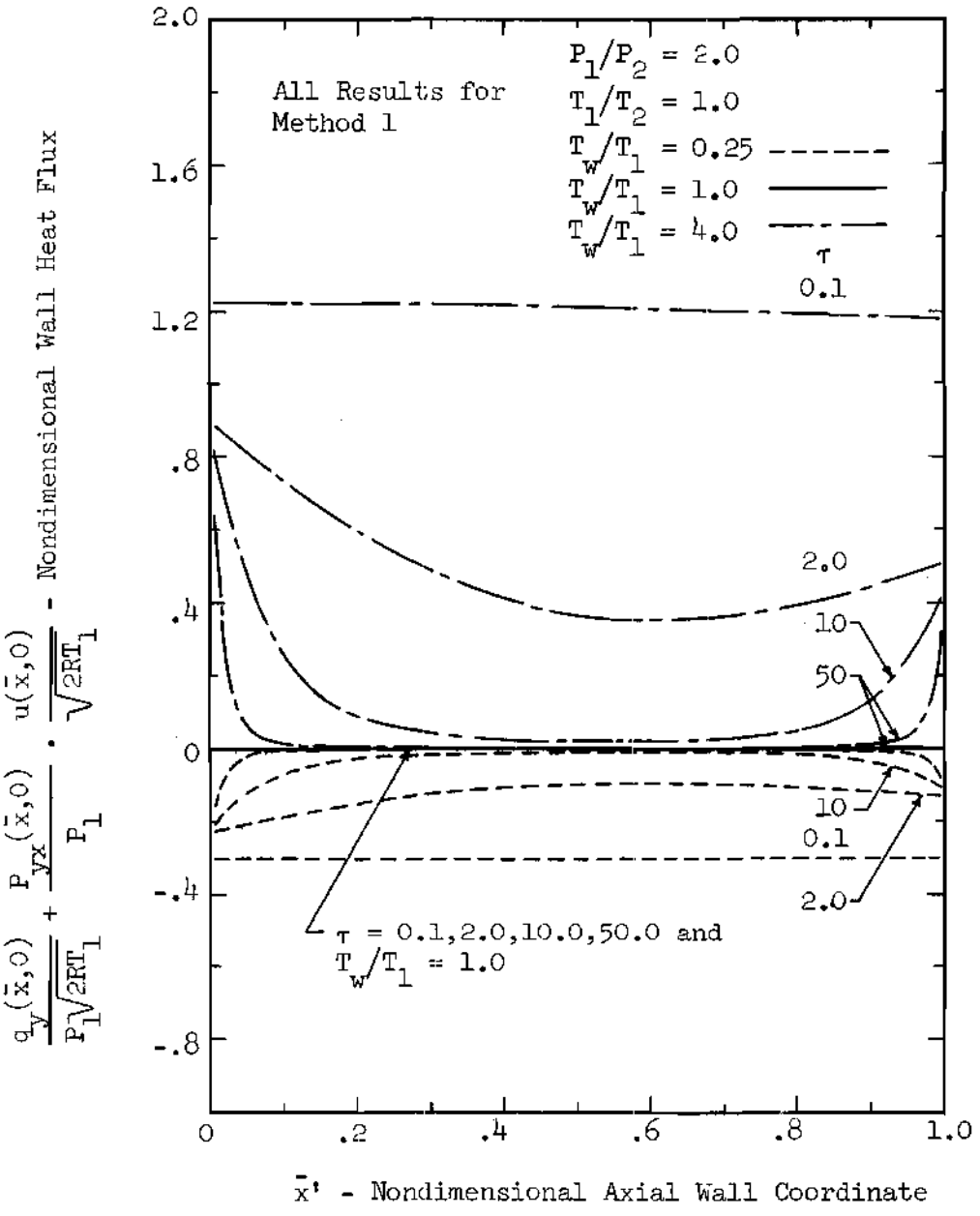

Figure 19. Comparison of Heat Flux to Wall for Free Molecular Flow Through Two Dimensional Channels of $\tau = 0.1$, 2.0, 10.0, and 50.0 for $P_1/P_2 = 2.0$, $T_1/T_2 = 1.0$, and $T_w/T_1 = 0.25$, 1.0, and 4.0.

of the heat flux vector is essentially zero for the moderate pressure ratio considered here. For the non-isothermal cases, a comparison of the results of Methods 1 and 2 revealed the following:

(1) For $T_W/T_1 = 0.25$ the comparison was excellent for $\tau \leq 2.0$, and for $\tau = 10.0$ and $\tau = 50.0$ the agreement was within one and two per cent, respectively.

(2) For $T_W/T_1 = 4.0$ the comparison was again excellent for $\tau \leq 2.0$, and for $\tau = 10.0$ and $\tau = 50.0$ the agreement was within two and five per cent, respectively.

The same comments concerning the comparison of the shear stress for $\tau = 50.0$ are applicable here for comparisons made at large values of τ.

Finally, results for the $\bar{x}$-component of the heat flux vector were obtained by Methods 1 and 2. Although the results are not presented, a comparison of the results of the two Methods was qualitatively the same as for the $\bar{y}$-component, but the magnitude of the differences was larger. As expected, the $\bar{x}$-component of the heat flux vector is essentially constant for small τ and for large τ varies rapidly at the inlet and exit before becoming essentially zero for the major portion of the channel.

Comparison of Average Mass Flow Rate With Experiment

It was pointed out in Chapter I that the only experimental data available for comparison with free molecular results is average mass flow rate measurements. Results for rectangular channels have been obtained for a large Knudsen number range by three different investigators: Gaede [9], Rasmussen [10], and Dong [14]. In all three

experiments the rectangular channel used was of such dimensions that the flow through the channel was assumed to be two dimensional for all practical considerations. However, the results of the experiments of Gaede [9] and Rasmussen [10] were reported in 1911 and 1937, respectively. Since vacuum technology was not nearly as advanced as at present, the accuracy of the results for large Knudsen numbers, or very low pressures, is somewhat in question. In addition, the geometries of the channels for both experiments were of such small dimensions that accurate geometrical measurements could not be performed. Since free molecular flow depends strongly on the geometry of the flow field, it was decided that the results of Dong [14], which were reported in 1956, would be used for a comparison between experiment and theory. It should be pointed out, however, that a final verification of the comparison with experiment should be based on measurements of local flow properties and not averaged results.

The apparatus of Dong's experiment consisted of two parallel steel plates, 0.324 cm. apart. The width of the channel was 22.86 cm. The inlet and exit were 127.00 cm. apart; however, the initial pressure tap and final pressure tap were 61.0 cm. apart, located 33.0 cm. from the inlet and exit, respectively. After the gas was treated and passed across two flowmeters it entered a header through a series of needle values. The header was constructed from 1/2 in. semi-circular steel plates. The gas entered perpendicular to the direction of flow, passed through a fine-mesh screen which distributed the gas, and proceeded to the test section through a slit in the flange. The dimensions of the

opening of the header at the inlet and exit of the channel were 2 in. by 10 in.

In order to compare with the theoretical results the pressures inside the headers must be known. Since these pressures were not monitored, it is necessary to make some assumptions concerning the pressure variation in order that a comparison between theory and experiment can be made. The length-to-height ratio for Dong's experiment is 400 and the system is essentially isothermal. Referring to Figure 14 it is apparent that the isothermal pressure variation for long channels is essentially linear over the entire channel length. Therefore, the difference in the inlet and exit pressures can be obtained by knowing the measured pressure difference in the center portion of the channel and assuming the pressure variation is linear. Based on this assumption the comparison with Dong's results for several gases is presented in Figure 20. The results are normalized using the theoretical free molecular value for the average mass flow rate of $\Lambda_{F.M.}(\tau) = 0.015$ based on a value of τ of 400. The value for $\Lambda_{F.M.}(\tau)$ was obtained from Figure 3. Expressed in the nondimensional form, $\Lambda(\tau)/\Lambda_{F.M.}(\tau)$, the results for different gases in the free molecular limit should be indistinguishable. However, for small values of the inverse Knudsen number there appears to be significant scatter in the results. It should be noted that the probable error of the experimental data for $\delta < 0.01$ is $\pm$ 10 per cent.

Although the comparison between the experimental values and the free molecular value of unity shown in Figure 20 is poor, it should be

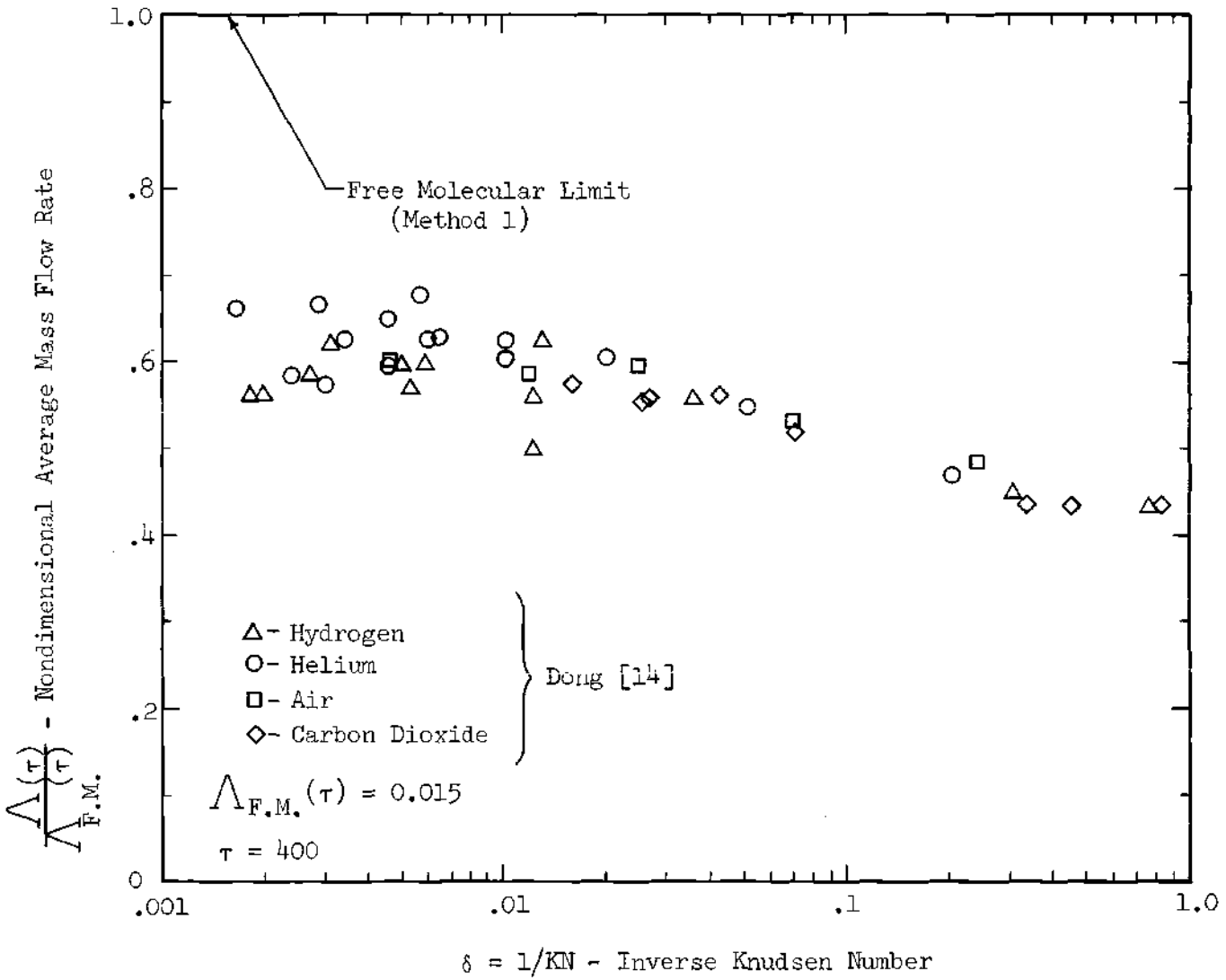

Figure 20. Comparison of Two Dimensional Theoretical Value for Free Molecular Average Flow Rate with Experimental Values Obtained from Dong [14] for the Flow of Several Gases Through a Rectangular Channel.

remembered that a number of assumptions has been made. For example, assuming a linear pressure variation from the inlet to the exit introduces errors which are difficult to estimate. Since the difference in header pressures used for non-dimensionalizing the experimental data is larger than the actual difference which is used for the theoretical values, the experimental values presented in Figure 20 are smaller than the true values. It is also questionable as to whether or not the equilibrium distribution functions were reached in the headers for large Knudsen numbers, and whether or not the headers are large enough to satisfy the infinite reservoir assumption of the theory. Finally, it is also questionable as to whether or not two dimensional free molecular flow is attained in the experiment since the inverse Knudsen number based on the width of the channel is approximately 100 times the inverse Knudsen number based on the height of the channel. Thus, for a comparison based on the width-inverse Knudsen number the experimental results are still in the transition flow regime. Consequently, the comparison between theory and experiment, as presented in Figure 20, should be construed as qualitative, and nothing more.

CHAPTER III

FREE MOLECULAR FLOW THROUGH A CIRCULAR TUBE OF ARBITRARY LENGTH

Statement of the Problem

The physical problem consists of a circular tube connecting two reservoirs which, respectively, contain gas in equilibrium at P_1, T_1 and P_2, T_2, as illustrated in Figure 21. The physical coordinates are now chosen such that the z-coordinate is coincident with the axis of the tube and the y-coordinate is taken as measured radially outward. The wall temperature is specified as constant at T_w. The reflection process is again taken as diffuse and the particles which encounter the tube walls are completely accommodated to the wall temperature. As in the two dimensional case, the mean free path is taken sufficiently large so that free molecular flow prevails. Therefore, once the distribution functions are known for all boundaries of the flow field the free molecular flow properties can readily be determined from their definitions.

Consider an arbitrary point embedded within the flow field as shown in Figure 21. The flow field is now divided into three regions by the surfaces $\sum_1$ and $\sum_2$. The corresponding surfaces of discontinuity in velocity space for the distribution functions are shown in Figure 22. It can be seen that the velocity space is similarly separated into three regions. By satisfying the boundary condition that there be no net

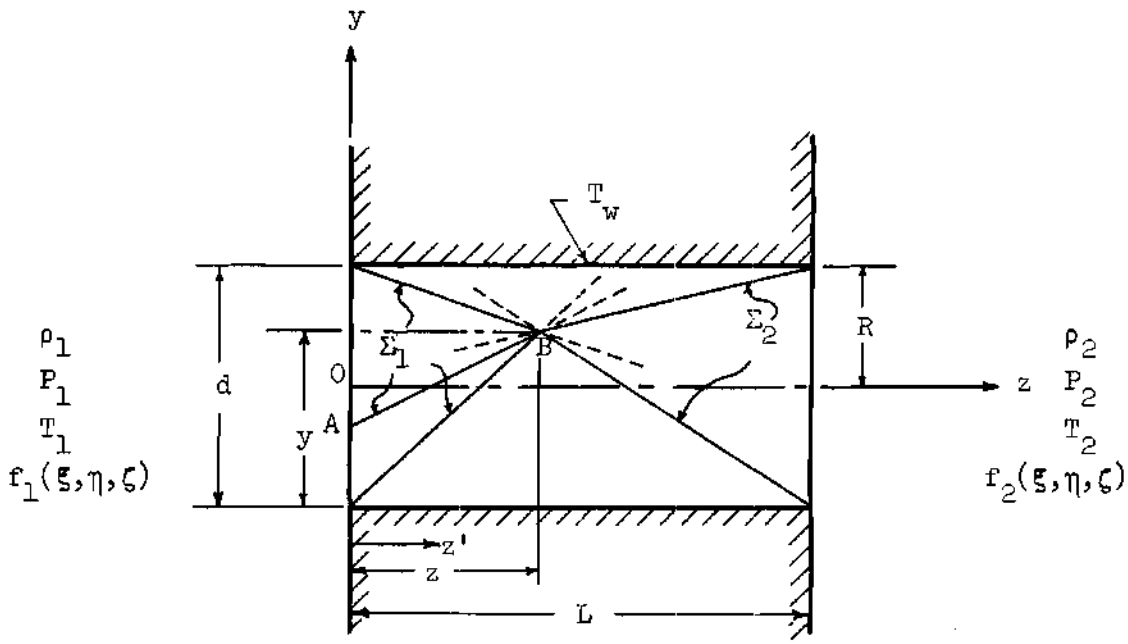

Sideview

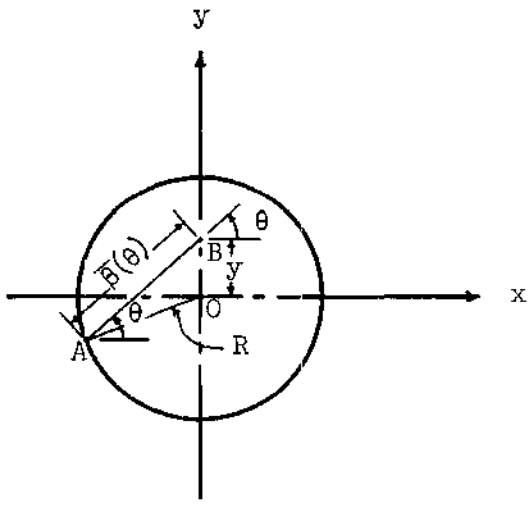

Endview

Figure 21. Geometry for Finite Length Circular Tube

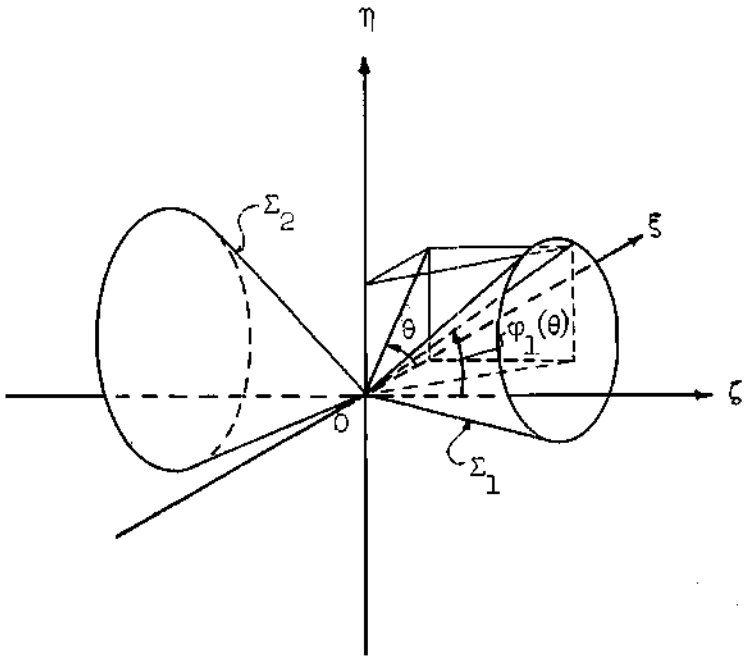

Velocity Space

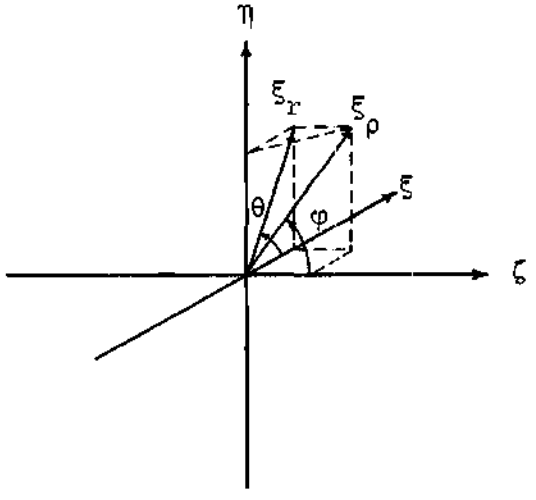

Spherical Velocity Coordinates

Figure 22. Velocity Space and Coordinate System for Circular Tube

flux of particles normal to the tube wall at the wall an integral equation for the wall flux can be obtained. Since the wall temperature is constant, the local wall density can be determined for all points along the tube. Consequently, the Maxwellian distribution functions are known for all boundaries of the flow field and the local flow properties can readily be obtained. The results obtained in this chapter, however, are valid only for the region defined by $0 \leq y \leq R$ and $-\infty < z < \infty$. The results for the other regions of the flow field can readily be obtained from the results presented here by eliminating the appropriate wall effects and changing the limits of integration over velocity space. However, the circular orifice results are valid for the entire flow field.

Just as in the other cases already considered, the wall distribution function varies with the wall coordinate. Since the wall coordinate can be expressed in terms of the physical coordinates specifying a point in the flow field and the angles θ and φ, which are the polar and azimuthal angles, respectively, for spherical velocity coordinates as shown in Figure 22, the wall distribution function depends on the velocity direction through the angles θ and φ as well as on the molecular velocity components. It is this point again which complicates the evaluation of free molecular flow properties for internal flow problems. It should be remembered that the wall density appearing in the wall distribution function is given by an integral equation for which the exact solution is not known.

General Formulation

In the following sections the distribution functions for the flow field are determined, the integral equation for the boundary condition is derived, the moments for density, velocity, pressure, etc. are determined in general by making no assumption regarding the wall density variation, and the general relation for the average mass flow rate is derived. The results for orifice flow are also presented as limiting cases by setting the length of the tube equal to zero.

Relations Between Physical and Velocity Coordinates

Consider the transformation equations for cylindrical and spherical coordinates as shown in Figure 22. The following relation can be written directly:

$$\frac{\zeta}{\xi_r} = \text{Cot } \varphi \tag{1}$$

where ζ is the z-component of molecular velocity and ξ_r is the total molecular velocity in the $\eta - \xi$ plane. For a particle leaving the tube wall at z' and passing through the point with coordinates y and z the following relation can be derived by equating the direction of the particle in physical space with the direction of the velocity vector:

$$\text{Cot } \varphi = \frac{\tau(\bar{z} - \bar{z}')}{\bar{\beta}\ (\theta)} \tag{2}$$

where τ is the length-to-radius ratio, L/R, $\bar{z}$ is the nondimensional z-coordinate, z/L, and $\bar{z}'$ is the nondimensional wall coordinate, z'/L. Equation (2) follows directly by using equation (1) and referring to Figures 21 and 22. The nondimensional distance $\bar{\beta}\ (\theta)$ is illustrated in

Figure 21. From geometrical considerations the following relation is readily obtained:

$$\bar{\beta}\ (\theta) = \bar{y}\ \mathrm{Sin}\ \theta + 1\ (1 - \bar{y}^2\ \mathrm{Cos}^2\ \theta)^{\frac{1}{2}} \tag{3}$$

where $\bar{y}$ is the nondimensional y-coordinate, y/d. It should be noted that the angle θ, as shown in Figure 21, is also the polar angle in velocity space, as illustrated in Figure 22.

The relations defining the surfaces of discontinuity for the distribution function, $\sum_1$ and $\sum_2$, can be obtained directly from equation (2) by setting $\bar{z}'$ equal to zero and unity, respectively. Denoting the limiting azimuthal angles for surfaces $\sum_1$ and $\sum_2$ by $\varphi_1(\theta)$ and $\varphi_2(\theta)$, respectively, for a fixed point in the flow field, the following relations are obtained from equation (2):

$$\mathrm{Cot}\ \varphi_1(\theta) = \frac{\tau\bar{z}}{\bar{\beta}(\theta)} \tag{4}$$

$$\mathrm{Cot}\ \varphi_2(\theta) = \frac{\tau(\bar{z} - 1)}{\bar{\beta}(\theta)} \tag{5}$$

Equations (4) and (5) will prove quite useful in defining the limits of integration for the evaluation of the flow properties.

Distribution Functions

The Maxwellian distribution functions for the three regions of velocity space, as shown in Figure 22, are as follows:

$$f_1(\xi,\eta,\zeta) = \frac{n_1}{(2\pi RT_1)^{3/2}} e^{-\frac{[\xi^2+\eta^2+\zeta^2]}{2RT_1}} \qquad \begin{cases} 0 \le \varphi < \varphi_1(\theta) \\ 0 \le \theta \le 2\pi \end{cases} \tag{6}$$

$$f_2(\xi,\eta,\zeta) = \frac{n_2}{(2\pi RT_2)^{3/2}} e^{-\frac{[\xi^2+\eta^2+\zeta^2]}{2RT_2}} \qquad \begin{cases} \varphi_2(\theta) < \varphi \le \pi \\ 0 \le \theta \le 2\pi \end{cases} \tag{7}$$

$$f_w(\bar{y},\bar{z},\xi,\eta,\zeta) = \frac{n_w(\bar{z}')}{(2\pi RT_w)^{3/2}} e^{-\frac{[\xi^2+\eta^2+\zeta^2]}{2RT_w}} \qquad \begin{cases} \varphi_1(\theta) < \varphi < \varphi_2(\theta) \\ 0 \le \theta \le 2\pi \end{cases} \tag{8}$$

where n_1 and n_2 are the number densities in the upstream and downstream tanks, respectively, and $n_w(\bar{z}')$ is the number density of the gas leaving the tube wall at $\bar{z}'$.

Boundary Condition

The boundary condition that there be no net flux of particles normal to the tube wall at the wall can be obtained by setting the radial component of mass velocity equal to zero at the tube wall. Introducing the definition for the radial mass velocity in terms of spherical velocity coordinates, the boundary condition can be expressed as follows for $0 \le \bar{z}' \le 1$:

$$\rho(\bar{y}=1,\bar{z}')v(\bar{y}=1,\bar{z}') \equiv m \int_0^\infty\int_0^{2\pi}\int_0^{\pi} f(\bar{y}=1,\bar{z}',\theta,\varphi,\xi_\rho)\xi_\rho^3 \operatorname{Sin}^2\varphi \operatorname{Sin}\theta \; d\varphi d\theta d\xi_\rho = 0 \tag{9}$$

where $\rho(\bar{y},\bar{z})$ is the local mass density, $v(\bar{y},\bar{z})$ is the radial component of average velocity, m is the molecular mass of a particle, and ξ_ρ is

the total molecular velocity, as illustrated in Figure 22. Substituting the distribution functions given by equations (6) through (8) into equation (9) and performing the necessary integrations the integral equation for the unknown wall flux can be derived. The details of the derivation are presented in Appendix C. By introducing the definition in equation (12) of Chapter II for the nondimensional wall flux for the circular tube and replacing $\bar{x}'$ with $\bar{z}'$, the integral equation for the boundary condition can be written as

$$g_w(\bar{z}') = F(\bar{z}') + \tau_d \int_0^1 g_w(\bar{z}'')K(\bar{z}', \bar{z}'')\, d\bar{z}'' \tag{10}$$

where

$$F(\bar{z}') = \frac{\tau_d^2\, \bar{z}'^2 + 0.5}{\sqrt{\tau_d^2\, \bar{z}'^2 + 1}} - \tau_d \bar{z}' \tag{11}$$

$$K(z', z'') = 1 - \left| \tau_d(\bar{z} - \bar{z}') \right| \left[\frac{2\, \tau_d^2(\bar{z}' - \bar{z}'')^2 + 3}{2[\tau_d^2(\bar{z}' - \bar{z}'')^2 + 1]^{3/2}} \right] \tag{12}$$

and τ_d is the length-to-diameter ratio, L/d, and is equal to $\tau/2$. It can be shown that the nondimensional wall flux has the following property:

$$g_w(\bar{z}') = 1 - g_w(1 - \bar{z}') \tag{13}$$

which is satisfied for all values of the parameter τ_d. Setting $\bar{z}'$ equal to 1/2 in equation (13) it is apparent that

$$g_w(\tfrac{1}{2}) = \frac{1}{2}$$

for all τ_d. Unfortunately, the exact solution of equation (10) for arbitrary τ_d is not known. However, it can be shown that the solutions for the special cases of $\tau_d = 0$ and $\tau_d = \infty$ are linear.

The relation between the wall density and the nondimensional wall flux will prove useful in the later text. Referring to equation (25) of Chapter II the following result can be written directly:

$$\rho_w(\theta,\varphi) = \left(\rho_1 \sqrt{\frac{T_1}{T_w}} - \rho_2 \sqrt{\frac{T_2}{T_w}} \right) g_w(\theta,\varphi) + \rho_2 \sqrt{\frac{T_2}{T_w}} \qquad (14)$$

The functional notation of equation (14) has been expressed in terms of the spherical velocity coordinates, θ and φ.

Moments for Arbitrary Wall Flux

Density. In terms of spherical velocity coordinates, as given in Figure 22, the density is defined as

$$\rho(\bar{y},\bar{z}) \equiv m \int_0^\infty \int_0^{2\pi} \int_0^{\pi} f(\bar{y},\bar{z},\theta,\varphi,\xi_\rho)\, \xi_\rho^{\,2} \operatorname{Sin} \varphi \, d\varphi d\theta d\xi_\rho \qquad (15)$$

Substituting equations (6) through (8) for the distribution functions into equation (15) and integrating over the appropriate regions of velocity space yield

$$\rho(\bar{y},\bar{z}) \equiv \frac{\rho_1}{(2\pi RT_1)^{3/2}} \int_0^{\infty} e^{-\frac{\xi_\rho^2}{2RT_1}} \xi_\rho^2 \, d\xi_\rho \int_0^{2\pi} d\theta \int_0^{\varphi_1(\theta)} \sin\varphi \, d\varphi + \tag{16}$$

$$\frac{\rho_2}{(2\pi RT_2)^{3/2}} \int_0^{\infty} e^{-\frac{\xi_\rho^2}{2RT_2}} \xi_\rho^2 \, d\xi_\rho \int_0^{2\pi} d\theta \int_{\varphi_2(\theta)}^{\pi} \sin\varphi \, d\varphi +$$

$$\frac{1}{(2\pi RT_w)^{3/2}} \int_0^{\infty} e^{-\frac{\xi_\rho^2}{2RT_w}} \xi_\rho^2 \, d\xi_\rho \int_0^{2\pi} d\theta \int_{\varphi_1(\theta)}^{\varphi_2(\theta)} \rho_w(\theta,\varphi) \sin\varphi \, d\varphi$$

where ρ_1 and ρ_2 are the mass densities in the upstream and downstream tanks, and the angles $\varphi_1(\theta)$ and $\varphi_2(\theta)$ are given by equations (4) and (5). Integrating over the angle φ and replacing the angles $\varphi_1(\theta)$ and $\varphi_2(\theta)$ with the expressions of equations (4) and (5), and introducing the integration formula given by equation (32) of Chapter II, the density can be expressed as

$$\rho(\bar{y},\bar{z}) = \frac{1}{2}\Big\{ \rho_1 \Big[1 - \frac{1}{2\pi} \int_0^{2\pi} \frac{\tau \bar{z} \, d\theta}{\sqrt{\tau^2 \bar{z}^2 + \bar{\beta}(\theta)^2}} \Big] + \rho_2 \Big[1 + \tag{17}$$

$$\frac{1}{2\pi} \int_0^{2\pi} \frac{\tau(\bar{z} - 1) \, d\theta}{\sqrt{\tau^2(\bar{z}-1)^2 + \bar{\beta}(\theta)^2}} \Big] + \frac{1}{2\pi} \int_0^{2\pi} d\theta \int_{\varphi_1(\theta)}^{\varphi_2(\theta)} \rho_w(\theta,\varphi) \sin\varphi \, d\varphi \Big\}$$

where $\bar{\beta}(\theta)$ is given by equation (3). Introducing equation (14) into equation (17) and rearranging give

$$\left[\frac{\rho(\bar{y},\bar{z}) - \rho_2}{\rho_1 - \rho_2}\right] = \frac{1}{2}\left\{1 - \frac{1}{2\pi(\rho_1 - \rho_2)}\left[\left(\rho_1 - \rho_2\sqrt{\frac{T_2}{T_w}}\right)\int_0^{2\pi} \frac{\tau\bar{z}\, d\theta}{\sqrt{\tau^2\bar{z}^2 + \bar{\beta}(\theta)^2}}\right.\right. \quad (18)$$

$$\rho_2\left(1 - \sqrt{\frac{T_2}{T_w}}\right)\int_0^{2\pi} \frac{\tau(\bar{z} - 1)\, d\theta}{\sqrt{\tau^2(\bar{z} - 1)^2 + \bar{\beta}(\theta)^2}} - \left(\rho_1\sqrt{\frac{T_1}{T_w}} - \rho_2\sqrt{\frac{T_2}{T_w}}\right) \cdot$$

$$\left.\left.\int_0^{2\pi} d\theta \int_{\varphi_1(\theta)}^{\varphi_2(\theta)} g_w(\theta,\varphi)\, \mathrm{Sin}\, \varphi\, d\varphi\right]\right\}$$

Consider the upstream and downstream limits of equation (18). For $\bar{z} = -\infty$ the angles $\varphi_1(\theta)$ and $\varphi_2(\theta)$ take on the value of π and $\rho(\bar{y},\bar{z})$ becomes ρ_1. Similarly, $\varphi_1(\theta)$ and $\varphi_2(\theta)$ are zero for $\bar{z} = +\infty$ and $\rho(\bar{y},\bar{z})$ becomes ρ_2.

For the case of an isothermal system, $T_1 = T_2 = T_w$, the following property can be derived from equation (18):

$$\left[\frac{\rho(\bar{y},\bar{z}) - \rho_2}{\rho_1 - \rho_2}\right] + \left[\frac{\rho(\bar{y}, 1 - \bar{z}) - \rho_2}{\rho_1 - \rho_2}\right] = 1 \quad (19)$$

Velocity Components. The z-component of velocity can be defined in terms of spherical coordinates as

$$\rho(\bar{y},\bar{z})w(\bar{y},\bar{z}) \equiv m \int_0^{\infty}\int_0^{2\pi}\int_0^{\pi} f(\bar{y},\bar{z},\theta,\varphi,\xi_\rho)\xi_\rho^{\,3}\,\mathrm{Cos}\,\varphi\,\mathrm{Sin}\,\varphi\,d\varphi d\theta d\xi_\rho \qquad (20)$$

Using equations (6) through (8) for the distribution functions, equation (20) can be expressed as

$$\rho(\bar{y},\bar{z})w(\bar{y},\bar{z}) = \frac{\rho_1}{(2\pi RT_1)^{3/2}} \int e^{-\frac{\xi_\rho^{\,2}}{2RT_1}} \xi_\rho^{\,3} d\xi_\rho \int_0^{2\pi} d\theta \int_0^{\varphi_1(\theta)} \mathrm{Cos}\,\varphi\,\mathrm{Sin}\,\varphi\,d\varphi + \qquad (21)$$

$$\frac{\rho_2}{(2\pi RT_2)^{3/2}} \int_0^{\infty} e^{-\frac{\xi_\rho^{\,2}}{2RT_2}} \xi_\rho^{\,3} d\xi_\rho \int_0^{2\pi} d\theta \int_{\varphi_2(\theta)}^{\pi} \mathrm{Cos}\,\varphi\,\mathrm{Sin}\,\varphi\,d\varphi +$$

$$\frac{1}{(2\pi RT_w)^{3/2}} \int_0^{\infty} e^{-\frac{\xi_\rho^{\,2}}{2RT_w}} \xi_\rho^{\,3} d\xi_\rho \int_0^{2\pi} d\theta \int_{\varphi_1(\theta)}^{\varphi_2(\theta)} \rho_w(\theta,\varphi)\,\mathrm{Cos}\,\varphi\,\mathrm{Sin}\,\varphi\,d\varphi$$

The integrations over φ and ξ_ρ can readily be performed. Introducing equation (14) for the wall density and making use of the definitions for the equilibrium fluxes in the upstream and downstream tanks, $\dot{m}_1$ and $\dot{m}_2$, the axial mass velocity given by equation (21) becomes

$$\frac{\rho(\bar{y},\bar{z})w(\bar{y},\bar{z})}{(\dot{m}_1 - \dot{m}_2)} = 1 - \frac{1}{2\pi}\left\{ \int_0^{2\pi} \frac{\tau^2 - \bar{z}^2\,d\theta}{[\tau^2\,\bar{z}^2 + \bar{\beta}(\theta)^2\,]} - \right. \qquad (22)$$

$$2\int_0^{2\pi} d\theta \int_{\varphi_1(\theta)}^{\varphi_2(\theta)} g_w(\theta,\varphi)\ \mathrm{Cos}\ \varphi\ \mathrm{Sin}\ \varphi\ d\varphi\Big\}$$

It can be shown that equation (22) contains the correct limits of zero for $\bar{z} = \pm \infty$.

The $\bar{y}$-component of velocity is similarly defined as

$$\rho(\bar{y},\bar{z})v(\bar{y},\bar{z}) \equiv m \int_0^{\infty}\int_0^{2\pi}\int_0^{\pi} f(\bar{y},\bar{z},\theta,\varphi,\xi_\rho)\ \xi_\rho^{\,3}\ \mathrm{Sin}^2\ \varphi\ \mathrm{Sin}\ \theta\ d\varphi d\theta d\xi_\rho \qquad (23)$$

Following the same procedure as outlined for the axial component of velocity yields

$$\frac{\rho(\bar{y},\bar{z})v(\bar{y},\bar{z})}{(\dot{m}_1 - \dot{m}_2)} = \frac{1}{2\pi}\Big\{\int_0^{2\pi} \mathrm{Sin}\ \theta\ \mathrm{Tan}^{-1}\left(\frac{\bar{\beta}(\theta)}{\tau\bar{z}}\right) d\theta - \qquad (24)$$

$$\int_0^{2\pi} \frac{\tau\bar{z}\bar{\beta}(\theta)\ \mathrm{Sin}\ \theta}{[\tau^2\bar{z}^2 + \bar{\beta}(\theta)^2]}\, d\theta + 2\int_0^{2\pi} \mathrm{Sin}\ \theta\ d\theta \int_{\varphi_1(\theta)}^{\varphi_2(\theta)} g_w(\theta,\varphi)\ \mathrm{Sin}^2\ \varphi\ d\varphi\Big\}$$

It can also be shown that equation (24) contains the appropriate upstream and downstream limits of zero.

The following two properties can be obtained readily from equations (22) and (24):

$$\frac{\rho(\bar{y},\bar{z})w(\bar{y},\bar{z})}{(\dot{m}_1 - \dot{m}_2)} = \frac{\rho(\bar{y},\ 1 - \bar{z})w(\bar{y},\ 1 - \bar{z})}{(\dot{m}_1 - \dot{m}_2)} \tag{25}$$

$$\frac{\rho(\bar{y},\bar{z})v(\bar{y},\bar{z})}{(\dot{m}_1 - \dot{m}_2)} = -\frac{\rho(\bar{y},\ 1 - \bar{z})v(\bar{y},\ 1 - \bar{z})}{(\dot{m}_1 - \dot{m}_2)} \tag{26}$$

Normal Pressure Components. The normal pressure components are defined as follows:

$$P_{zz}(\bar{y},\bar{z}) \equiv m \int_0^{\infty}\int_0^{2\pi}\int_0^{\pi} f(\bar{y},\bar{z},\theta,\varphi,\xi_\rho)\xi_\rho^4 \operatorname{Cos}^2\varphi \operatorname{Sin}\varphi\, d\varphi d\theta d\xi_\rho - \rho(\bar{y},\bar{z})w^2(\bar{y},\bar{z}) \tag{27}$$

$$P_{yy}(\bar{y},\bar{z}) \equiv m \int_0^{\infty}\int_0^{2\pi}\int_0^{\pi} f(\bar{y},\bar{z},\theta,\varphi,\xi_\rho)\xi_\rho^4 \operatorname{Sin}^3\varphi \operatorname{Sin}^2\theta\, d\varphi d\theta d\xi_\rho - \rho(\bar{y},\bar{z})v^2(\bar{y},\bar{z}) \tag{28}$$

$$P_{xx}(\bar{y},\bar{z}) \equiv m \int_0^{\infty}\int_0^{2\pi}\int_0^{\pi} f(\bar{y},\bar{z},\theta,\varphi,\xi_\rho)\ \xi_\rho^4 \operatorname{Sin}^3\varphi \operatorname{Cos}^2\theta\, d\varphi d\theta d\xi_\rho \tag{29}$$

Substituting equations (6) through (8) for the distribution functions, replacing the wall density using equation (14), and carrying out the necessary integrations yield the following:

$$\left[\frac{P_{zz}(\bar{y},\bar{z}) - P_2}{P_1 - P_2}\right] = \frac{1}{2}\left\{1 - \frac{1}{2\pi(P_1 - P_2)}\left[\left(P_1 - P_2\sqrt{\frac{T_w}{T_2}}\right)\cdot\right.\right. \tag{30}$$

$$\int_0^{2\pi} \frac{\tau^3 \bar{z}^3 \, d\theta}{[\tau^2 \bar{z}^2 + \bar{\beta}(\theta)^2]^{3/2}} - P_2 \left(1 - \sqrt{\frac{T_w}{T_2}}\right) \int_0^{2\pi} \frac{\tau^3 (\bar{z}-1)^3 \, d\theta}{[\tau^2 (\bar{z}-1)^2 + \bar{\beta}(\theta)^2]^{3/2}} -$$

$$3 \left(P_1 \sqrt{\frac{T_w}{T_1}} - P_2 \sqrt{\frac{T_w}{T_2}} \right) \int_0^{2\pi} d\theta \int_{\varphi_1(\theta)}^{\varphi_2(\theta)} g_w(\theta,\varphi) \cos^2 \varphi \sin \varphi \, d\varphi \Big] \Big\} -$$

$$\frac{\rho(\bar{y},\bar{z}) w^2(\bar{y},\bar{z})}{(P_1 - P_2)}$$

$$\left[\frac{P_{yy}(\bar{y},\bar{z}) - P_2}{P_1 - P_2} \right] = \frac{1}{2} \left\{ 1 + \frac{1}{2\pi(P_1 - P_2)} \left[\left(P_1 - P_2 \sqrt{\frac{T_w}{T_2}} \right) \int_0^{2\pi} \sin^2 \theta \cdot \right. \right. \quad (31)$$

$$\left[\frac{\tau^3 \bar{z}^3}{[\tau^2 \bar{z}^2 + \bar{\beta}(\theta)^2]^{3/2}} - \frac{3\tau\bar{z}}{\sqrt{\tau^2 \bar{z}^2 + \bar{\beta}(\theta)^2}} \right] d\theta - P_2 \left(1 - \sqrt{\frac{T_w}{T_2}} \right) \cdot$$

$$\int_0^{2\pi} \sin^2 \theta \left[\frac{\tau^3 (\bar{z}-1)^3}{[\tau^2 (\bar{z}-1)^2 + \bar{\beta}(\theta)]^{3/2}} - \frac{3\tau(\bar{z}-1)}{\sqrt{\tau^2 (\bar{z}-1)^2 + \bar{\beta}(\theta)^2}} \right] d\theta + 3 \left(P_1 \sqrt{\frac{T_w}{T_1}} - \right.$$

$$\left. \left. P_2 \sqrt{\frac{T_w}{T_2}} \right) \int_0^{2\pi} \sin^2 \theta \, d\theta \int_{\varphi_1(\theta)}^{\varphi_2(\theta)} g_w(\theta,\varphi) \sin^3 \varphi \, d\varphi \Big] \Big\} - \frac{\rho(\bar{y},\bar{z}) v^2(\bar{y},\bar{z})}{(P_1 - P_2)}$$

$$\left[\frac{P_{xx}(\bar{y},\bar{z})-P_2}{P_1-P_2}\right] = \frac{1}{2}\left\{1 + \frac{1}{2\pi(P_1-P_2)}\left[\left(P_1-P_2\sqrt{\frac{T_w}{T_2}}\right)\int_0^{2\pi}\cos^2\theta\left[\frac{\tau^3\bar{z}^3}{\left[\tau^2\bar{z}^2+\bar{\beta}(\theta)^2\right]^{3/2}} - \right.\right.\right. \quad (32)$$

$$\left.\frac{3\tau\bar{z}}{\sqrt{\tau^2\bar{z}^2+\bar{\beta}(\theta)^2}}\right] d\theta - P_2\left(1-\sqrt{\frac{T_w}{T_2}}\right)\int_0^{2\pi}\cos^2\theta\left[\frac{\tau^3(\bar{z}-1)^3}{\left[\tau^2(\bar{z}-1)^2+\bar{\beta}(\theta)^2\right]^{3/2}} -\right.$$

$$\left.\left.\frac{3\tau(\bar{z}-1)}{\sqrt{\tau^2(\bar{z}-1)^2+\bar{\beta}(\theta)^2}}\right] d\theta + 3\left(P_1\sqrt{\frac{T_w}{T_1}} - P_2\sqrt{\frac{T_w}{T_2}}\right)\int_0^{2\pi}\cos^2\theta\, d\theta \cdot \right.$$

$$\left.\int_{\varphi_1(\theta)}^{\varphi_2(\theta)} g_w(\theta,\varphi)\,\sin^3\varphi\, d\varphi\right]\Bigg\}$$

It can readily be shown that equations (30) through (32) contain the appropriate upstream and downstream limits of unity and zero, respectively.

Static or Thermodynamic Pressure. The static or thermodynamic pressure is defined as an average of the three normal pressure components; i.e.,

$$p(\bar{y},\bar{z}) \equiv \frac{1}{3}\left[P_{xx}(\bar{y},\bar{z}) + P_{yy}(\bar{y},\bar{z}) + P_{zz}(\bar{y},\bar{z})\right] \quad (33)$$

Substituting equations (30) through (32) into equation (33) and rearranging yield

$$\left[\frac{p(\bar{y},\bar{z}) - P_2}{P_1 - P_2}\right] = \frac{1}{2}\left\{1 - \frac{1}{2\pi(P_1-P_2)}\left[\left(P_1 - P_2\sqrt{\frac{T_w}{T_2}}\right)\int_0^{2\pi}\frac{\tau\bar{z}\, d\theta}{\sqrt{\tau^2\bar{z}^2 + \bar{\beta}(\theta)^2}} - \right.\right. \quad (34)$$

$$P_2\left(1 - \sqrt{\frac{T_w}{T_2}}\right)\int_0^{2\pi}\frac{\tau(\bar{z} - 1)\, d\theta}{\sqrt{\tau^2(\bar{z}-1)^2 + \bar{\beta}(\theta)^2}} - \left(P_1\sqrt{\frac{T_w}{T_1}} - P_2\sqrt{\frac{T_w}{T_2}}\right)\cdot$$

$$\left.\left.\int_0^{2\pi} d\theta \int_{\varphi_1(\theta)}^{\varphi_2(\theta)} g_w(\theta,\varphi)\,\mathrm{Sin}\,\varphi\, d\varphi\right]\right\} - \frac{\rho(\bar{y},\bar{z})[w^2(\bar{y},\bar{z}) + v^2(\bar{y},\bar{z})]}{3(P_1 - P_2)}$$

Since the normal pressure components contain the correct upstream and downstream limits, it is apparent that equation (34) also contains the correct limits.

Thermodynamic Temperature. The temperature distribution can be obtained directly from the equation of state. The temperature is expressed in nondimensional form by equation (50) of Chapter II. By substituting equations (18) and (34) in equation (50) of Chapter II the nondimensional temperature is obtained. Also shown following equation (50) of Chapter II is a particularly simple form for the temperature distribution for the case of an isothermal system. The same relation holds true for the circular tube when the coordinate $\bar{x}$ is replaced by $\bar{z}$.

Shear Stress Components. By definition, the $\bar{y}\bar{z}$-component of shear stress is given as

$$P_{yz}(\bar{y},\bar{z}) \equiv m \int_0^{\infty} \int_0^{2\pi} \int_0^{\pi} f_w(\bar{y},\bar{z},\theta,\varphi,\xi_\rho)\ \xi_\rho^4\ \mathrm{Sin}^2\ \varphi\ \mathrm{Cos}\ \varphi\ \mathrm{Sin}\ \theta\ d\varphi d\theta d\xi_\rho - \quad (35)$$

$$\rho(\bar{y},\bar{z})w(\bar{y},\bar{z})v(\bar{y},\bar{z})$$

Introducing equations (6) through (8) for the distribution functions and substituting equation (14) for the wall density yield upon integration

$$\frac{P_{yz}(\bar{y},\bar{z})}{P_1} = \frac{1}{4\pi} \left\{ \left(1 - \frac{P_2}{P_1}\sqrt{\frac{T_w}{T_2}}\right) \int_0^{2\pi} \frac{\mathrm{Sin}\ \theta\ \bar{\beta}(\theta)^3\, d\theta}{[\tau^2\,\bar{z}^2 + \bar{\beta}(\theta)^2]^{3/2}} - \frac{P_2}{P_1}\left(1 - \sqrt{\frac{T_w}{T_2}}\right) \cdot \right. \quad (36)$$

$$\int_0^{2\pi} \frac{\mathrm{Sin}\ \theta\ \ \bar{\beta}(\theta)^3\, d\theta}{[\tau^2(\bar{z}-1)^2 + \bar{\beta}(\theta)^2]^{3/2}} + 3\left(\sqrt{\frac{T_w}{T_1}} - \frac{P_2}{P_1}\sqrt{\frac{T_w}{T_2}}\right) \int_0^{2\pi} \mathrm{Sin}\ \theta\ d\theta \cdot$$

$$\left. \int_{\varphi_1(\theta)}^{\varphi_2(\theta)} g_w(\theta,\varphi)\ \mathrm{Sin}^2\ \varphi\ \mathrm{Cos}\ \varphi\ d\varphi \right\} - \frac{\rho(\bar{y},\bar{z})w(\bar{y},\bar{z})v(\bar{y},\bar{z})}{P_1}$$

It can be shown that for $\bar{z} = \pm \infty$ the shear stress given by equation (36) has the appropriate limits of zero. The $\bar{z}\bar{y}$-component of shear stress is identical to the $\bar{y}\bar{z}$-component. The other shear stress components are zero everywhere in the flow field.

Heat Flux Components. The heat flux components are defined as follows in terms of spherical velocity coordinates:

$$q_z(\bar{y},\bar{z}) = -\left\{ \frac{3}{2} p(\bar{y},\bar{z})w(\bar{y},\bar{z}) + P_{zz}(\bar{y},\bar{z})w(\bar{y},\bar{z}) + P_{yz}(\bar{y},\bar{z})v(\bar{y},\bar{z}) + \right. \tag{37}$$

$$\left. \frac{1}{2} \rho(\bar{y},\bar{z})w(\bar{y},\bar{z}) \left[w^2(\bar{y},\bar{z}) + v^2(\bar{y},\bar{z}) \right] \right\} + \frac{m}{2} \left[\int_0^\infty \int_0^{2\pi} \int_0^{\pi} f(\bar{y},\bar{z},\theta,\varphi,\xi_\rho) \cdot \right.$$

$$\xi_\rho^5 \sin^4\varphi \cos^3\theta \, d\varphi d\theta d\xi_\rho + \int_0^\infty \int_0^{2\pi} \int_0^{\pi} f(\bar{y},\bar{z},\theta,\varphi,\xi_\rho)\xi_\rho^5 \sin^4\varphi \cos\theta \sin^2\theta \, d\varphi d\theta d\xi_\rho +$$

$$\left. \int_0^\infty \int_0^{2\pi} \int_0^{\pi} f(\bar{y},\bar{z},\theta,\varphi,\xi_\rho)\xi_\rho^5 \sin^2\varphi \cos^2\varphi \cos\theta \, d\varphi d\theta d\xi_\rho \right]$$

$$q_y(\bar{y},\bar{z}) = -\left\{ \frac{3}{2} p(\bar{y},\bar{z})v(\bar{y},\bar{z}) + P_{yy}(\bar{y},\bar{z})v(\bar{y},\bar{z}) + P_{yz}(\bar{y},\bar{z})w(\bar{y},\bar{z}) + \right. \tag{38}$$

$$\left. \frac{1}{2} \rho(\bar{y},\bar{z})v(\bar{y},\bar{z}) \left[w^2(\bar{y},\bar{z}) + v^2(\bar{y},\bar{z}) \right] \right\} + \frac{m}{2} \left[\int_0^\infty \int_0^{2\pi} \int_0^{\pi} f(\bar{y},\bar{z},\theta,\varphi,\xi_\rho) \cdot \right.$$

$$\xi_\rho^5 \sin^4\varphi \cos^2\theta \sin\theta \, d\varphi d\theta d\xi_r + \int_0^\infty \int_0^{2\pi} \int_0^{\pi} f(\bar{y},\bar{z},\theta,\varphi,\xi_\rho)\xi_\rho^5 \sin^4\varphi \cdot$$

$$\left. \sin^3\theta \, d\varphi d\theta d\xi_\rho + \int_0^\infty \int_0^{2\pi} \int_0^{\pi} f(\bar{y},\bar{z},\theta,\varphi,\xi_\rho)\xi_\rho^5 \sin^2\varphi \cos^2\varphi \sin\theta \, d\varphi d\theta d\xi_\rho \right]$$

Introducing equations (6) through (8) into equations (37) and (38), replacing the wall density with equation (14), and performing the necessary integrations yield

$$q_z(\bar{y},\bar{z}) = -\left\{ \frac{3}{2} p(\bar{y},\bar{z})w(\bar{y},\bar{z}) + P_{zz}(\bar{y},\bar{z})w(\bar{y},\bar{z}) + P_{yz}(\bar{y},\bar{z})v(\bar{y},\bar{z}) + \frac{1}{2}\rho(\bar{y},\bar{z}) \cdot \right. \quad (39)$$

$$\left. w(\bar{y},\bar{z})\left[w^2(\bar{y},\bar{z}) + v^2(\bar{y},\bar{z})\right]\right\} + \frac{1}{2\pi^{3/2}}\left\{\left[\rho_1(2RT_1)^{3/2} - \rho_2(2RT_2)^{3/2}\frac{T_w}{T_2}\right]\cdot\right.$$

$$\int_0^{2\pi} \text{Cos}\ \theta\left[\frac{\varphi_1(\theta)}{2} - \frac{\text{Sin}\ 2\varphi_1(\theta)}{4}\right]d\theta - \rho_2(2RT_2)^{3/2}\left[1 - \frac{T_w}{T_2}\right]\int_0^{2\pi} \text{Cos}\ \theta\left[\frac{\varphi_2(\theta)}{2} - \right.$$

$$\left.\left.\frac{\text{Sin}\ 2\varphi_2(\theta)}{4}\right]d\theta + \left[\rho_1(2RT_1)^{3/2}\frac{T_w}{T_1} - \rho_2(2RT_2)^{3/2}\frac{T_w}{T_2}\right]\int_0^{2\pi} \text{Cos}\ \theta\, d\theta \int_{\varphi_1(\theta)}^{\varphi_2(\theta)} g_w(\theta,\varphi)\text{Sin}^2\varphi\, d\varphi\right\}$$

$$q_y(\bar{y},\bar{z}) = -\left\{\frac{3}{2} p(\bar{y},\bar{z})v(\bar{y},\bar{z}) + P_{yy}(\bar{y},\bar{z})v(\bar{y},\bar{z}) + P_{yz}(\bar{y},\bar{z})w(\bar{y},\bar{z}) + \frac{1}{2}\rho(\bar{y},\bar{z}) \cdot \right. \quad (40)$$

$$\left. v(\bar{y},\bar{z})\cdot\left[w^2(\bar{y},\bar{z}) + v^2(\bar{y},\bar{z})\right]\right\} + \frac{1}{2\pi^{3/2}}\left\{\left[\rho_1(2RT_1)^{3/2} - \rho_2(2RT_2)^{3/2}\frac{T_w}{T_2}\right]\cdot\right.$$

$$\int_0^{2\pi} \text{Sin}\,\theta \left[\frac{\varphi_1(\theta)}{2} - \frac{\text{Sin}\,2\varphi_1(\theta)}{4} \right] d\theta - \rho_2(2RT_2)^{3/2} \left[1 - \frac{T_w}{T_2} \right] \int_0^{2\pi} \text{Sin}\,\theta \left[\frac{\varphi_2(\theta)}{2} - \right.$$

$$\left. \frac{\text{Sin}\,2\varphi_2(\theta)}{4} \right] d\theta + \left[\rho_1(2RT_1)^{3/2} \frac{T_w}{T_1} - \rho_2(2RT_2)^{3/2} \frac{T_w}{T_2} \right] \int_0^{2\pi} \text{Sin}\theta\, d\theta \int_{\varphi_1(\theta)}^{\varphi_2(\theta)} g_w(\theta,\varphi) \text{Sin}^2\varphi\, d\varphi \Bigg\}$$

Again it can be shown that equations (39) and (40) contain the appropriate upstream and downstream limits of zero.

Orifice Limit

The results for orifice flow for $\bar{y} \leq 1$ can be obtained directly from equations (15) through (40) by setting the length of the channel equal to zero. However, for $\bar{y} > 1$ the limits of integration are different and the results cannot be obtained from equations (15) through (40).

Consider the flow through a circular orifice. For a point located at $\bar{y} > 1$ the geometry of the flow field and the surfaces of discontinuity for the distribution functions in velocity space are illustrated in Figure 23. The following parameters will prove useful:

$$\theta_1 = \text{Tan}^{-1} \left(\sqrt{\bar{y}^2 - 1} \right) \tag{41}$$

$$\theta_2 = \pi + \text{Tan}^{-1} \left(- \sqrt{\bar{y}^2 - 1} \right) \tag{42}$$

$$\bar{\beta}_1(\theta) = \bar{y}\,\text{Sin}\,\theta - \sqrt{1 - \bar{y}^2 \text{Cos}^2\,\theta} \tag{43}$$

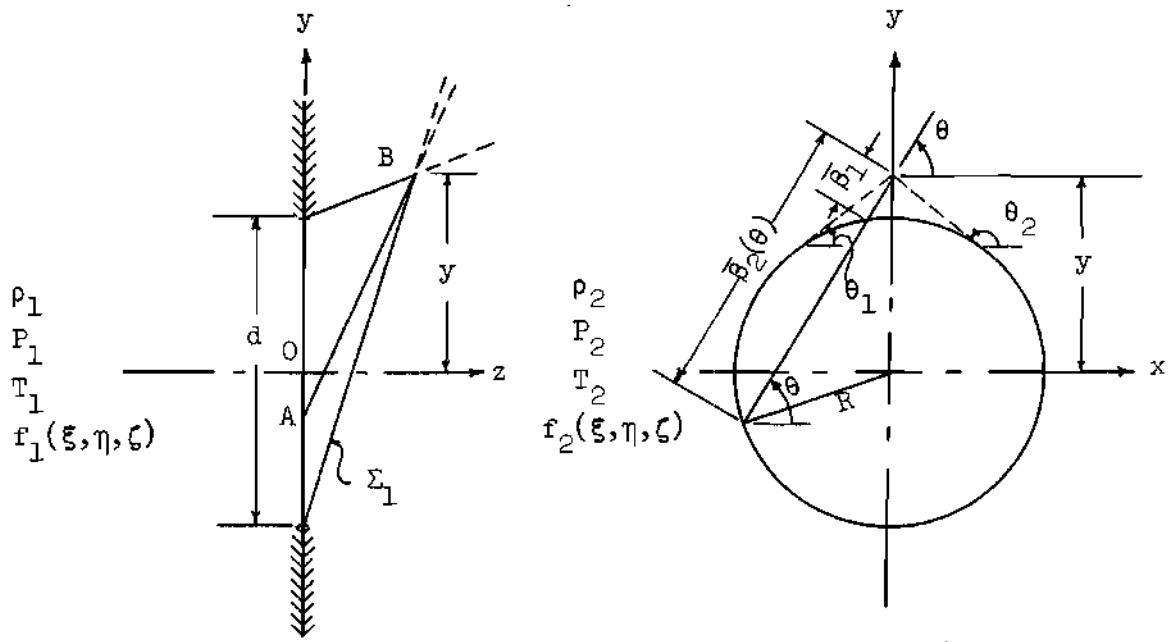

Circular Orifice Geometry

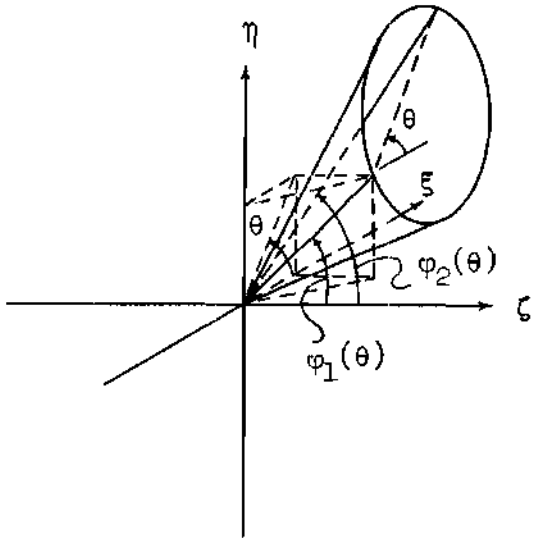

Velocity Space for Orifice

Figure 23. Geometry and Velocity Space for Circular Orifice

$$\bar{\beta}_2(\theta) = \bar{y}\ \mathrm{Sin}\ \theta + \sqrt{1 - \bar{y}^2\ \mathrm{Cos}^2\ \theta} \qquad (44)$$

Since for a given value of θ there are two values of the angle φ, as can be seen readily from Figure 23, it is apparent that the integration for each moment must be performed again in order to obtain the results for $\bar{y} > 1$. As an example consider the density variation for a circular orifice. For $\bar{y} \leq 1$ and all $\bar{z}$ the result can be obtained directly from equation (18) by setting the length of the tube equal to zero. Noting that $\varphi_1(\theta) = \varphi_2(\theta)$ the density becomes

$$\left[\frac{\rho(\bar{y},\bar{z}) - \rho_2}{\rho_1 - \rho_2}\right] = \frac{1}{2}\left\{1 - \frac{1}{2\pi}\int_0^{2\pi} \frac{\bar{z}_r\ d\ \theta}{\sqrt{\bar{z}_r^{\,2} + \bar{\beta}(\theta)^2}}\right\} \quad \bar{y} \leq 1 \text{ and all } \bar{z}_r \qquad (45)$$

where $\bar{z}_r$ is the z-coordinate nondimensionalized with the radius of the tube, R. In order to obtain the results for $\bar{y} > 1$ the integration over velocity space must be performed using the new limits as shown in Figure 23. Referring to equation (16) and simplifying to the case of orifice flow, and changing the limits of integration to correspond to the limits shown in Figure 23 the following is obtained:

$$\rho(\bar{y},\bar{z}_r) = \frac{\rho_1}{(2\pi RT_1)^{3/2}}\int_0^{\infty} e^{-\frac{\xi_\rho^{\,2}}{2RT_1}}\xi_\rho^{\,2}\,d\,\xi_\rho \int_{\theta_1}^{\theta_2} d\theta \int_{\varphi_1'(\theta)}^{\varphi_2'(\theta)} \mathrm{Sin}\ \varphi\ d\varphi + \frac{\rho_2}{(2\pi RT_2)^{3/2}} \cdot (46)$$

$$\int_0^{\infty} e^{-\frac{\xi_\rho^2}{2RT_2}} \xi_\rho^2 d\xi_\rho \left[\int_0^{\theta_1} d\theta \int_0^{\pi} \text{Sin}\,\varphi\, d\varphi + \int_{\theta_2}^{\pi} d\theta \int_0^{\pi} \text{Sin}\,\varphi\, d\varphi + \int_{\theta_1}^{\theta_2} d\theta \int_0^{\varphi'_1(\theta)} \text{Sin}\,\varphi\, d\varphi + \right.$$

$$\left. \int_{\theta_1}^{\theta_2} d\theta \int_{\varphi'_2(\theta)}^{\pi} \text{Sin}\,\varphi\, d\varphi + \int_{\pi}^{2\pi} d\theta \int_0^{\pi} \text{Sin}\,\varphi\, d\varphi \right]$$

for $\bar{z}_r \geq 0$, and

$$\rho(\bar{y},\bar{z}_r) = \frac{\rho_2}{(2\pi RT_2)^{3/2}} \int_0^{\infty} e^{-\frac{\xi_\rho^2}{2RT_2}} \xi_\rho^2 d\xi_\rho \int_{\theta_1}^{\theta_2} d\theta \int_{\varphi'_2(\theta)}^{\varphi'_1(\theta)} \text{Sin}\,\varphi\, d\varphi + \frac{\rho_2}{(2\pi RT_1)^{3/2}} \cdot \quad (47)$$

$$\int_0^{\infty} e^{-\frac{\xi_\rho^2}{2RT_1}} \xi_\rho^2 d\xi_\rho \left[\int_0^{\theta_1} d\theta \int_0^{\pi} \text{Sin}\,\varphi\, d\varphi + \int_{\theta_1}^{\theta_2} d\theta \int_{\varphi'_1(\theta)}^{\pi} \text{Sin}\,\varphi\, d\varphi + \int_{\theta_2}^{\pi} d\theta \int_0^{\pi} \text{Sin}\,\varphi\, d\varphi + \right.$$

$$\left. \int_{\pi}^{2\pi} d\theta \int_0^{\pi} \text{Sin}\,\varphi\, d\varphi - \int_{\theta_1}^{\theta_2} d\theta \int_0^{\varphi'_2(\theta)} \text{Sin}\,\varphi\, d\varphi \right]$$

for $\bar{z}_r \leq 0$. The angles $\varphi'_1(\theta)$ and $\varphi'_2(\theta)$ are given by

$$\text{Tan}\,\varphi'_1(\theta) = \frac{\bar{\beta}_1(\theta)}{\bar{z}_r} \quad (48)$$

$$\text{Tan}\,\varphi'_2(\theta) = \frac{\bar{\beta}_2(\theta)}{\bar{z}_r} \quad (49)$$

where $\bar{\beta}_1(\theta)$ and $\bar{\beta}_2(\theta)$ are given by equations (43) and (44), and the angles θ_1 and θ_2 are given by equations (41) and (42). Performing the integrations in equations (46) and (47) gives

$$\left[\frac{\rho(\bar{y},\bar{z}_r)-\rho_2}{\rho_1-\rho_2}\right] = \frac{1}{4\pi}\int_{\theta_1}^{\theta_2}\left[\frac{\bar{z}_r}{\sqrt{\bar{z}_r^2+\bar{\beta}_1(\theta)^2}} - \frac{\bar{z}_r}{\sqrt{\bar{z}_r^2+\bar{\beta}_2(\theta)^2}}\right]d\theta \quad \bar{y}\geq 1 \text{ and } \bar{z}_r \geq 0 \tag{50}$$

and

$$\left[\frac{\rho(\bar{y},\bar{z}_r)-\rho_2}{\rho_1-\rho_2}\right] = 1 + \frac{1}{4\pi}\int_{\theta_1}^{\theta_2}\left[\frac{\bar{z}_r}{\sqrt{\bar{z}_r^2+\bar{\beta}(\theta)^2}} - \frac{\bar{z}_r}{\sqrt{\bar{z}_r^2+\bar{\beta}_2(\theta)^2}}\right]d\theta \quad \bar{y}\geq 1 \text{ and } \bar{z}_r \leq 0 \tag{51}$$

In a similar manner the results for the velocity components for circular orifice flow can be obtained. For $\bar{y} < 1$ the results can be obtained directly from equations (22) and (24) by setting $\varphi_1(\theta)$ equal to $\varphi_2(\theta)$. Thus,

$$\frac{\rho(\bar{y},\bar{z}_r)w(\bar{y},\bar{z}_r)}{(\dot{m}_1-\dot{m}_2)} = 1 - \frac{1}{2\pi}\int_0^{2\pi}\frac{\bar{z}_r^2\,d\theta}{[\bar{z}_r^2+\bar{\beta}(\theta)^2]} \tag{52}$$

$$\frac{\rho(\bar{y},\bar{z}_r)v(\bar{y},\bar{z}_r)}{(\dot{m}_1-\dot{m}_2)} = \frac{1}{2\pi}\left\{\int_0^{2\pi}\text{Sin }\theta\ \text{Tan}^{-1}\left(\frac{\bar{\beta}(\theta)}{\bar{z}_r}\right)d\theta - \int_0^{2\pi}\frac{\bar{z}_r\bar{\beta}(\theta)\ \text{Sin }\theta\ d\theta}{[\bar{z}_r^2+\bar{\beta}(\theta)^2]}\right\} \tag{53}$$

for $\bar{y}\leq 1$ and all $\bar{z}_r$. For $\bar{y}\geq 1$ and all $\bar{z}_r$ the results are

$$\frac{\rho(\bar{y},\bar{z}_r)w(\bar{y},\bar{z}_r)}{(\dot{m}_1 - \dot{m}_2)} = \frac{1}{2\pi}\int_{\theta_1}^{\theta_2} \left\{ \cos^2 \varphi'_1(\theta) - \cos^2 \varphi'_2(\theta) \right\} d\theta \qquad (54)$$

$$\frac{\rho(\bar{y},\bar{z}_r)v(\bar{y},\bar{z}_r)}{(\dot{m}_1 - \dot{m}_2)} = \frac{1}{\pi}\int_{\theta_1}^{\theta_2} \sin\theta \left\{ \frac{[\varphi'_2(\theta) - \varphi'_1(\theta)]}{2} - \frac{[\sin 2\varphi'_2(\theta) - \sin 2\varphi'_1(\theta)]}{4} \right\} d\theta \qquad (55)$$

It has been shown that the results for the density and velocity components, as given by equations (45) and (50) through (55), are identical to the results given by Narasimha [21] and Willis [33] for free molecular flow through a circular orifice.

The results for circular orifice flow for the other moments can be obtained in a similar manner as outlined for the lower moments.

Average Mass Flow Rate

The average mass flow rate is obtained by averaging the local axial mass velocity over the height of the channel. Introduce the following definitions:

$$\Lambda(\bar{z},\tau_d) \equiv \frac{\overline{\rho(\bar{y},\bar{z})w(\bar{y},\bar{z})}}{(\dot{m}_1 - \dot{m}_2)} \equiv 2\int_0^1 \frac{\rho(\bar{y},\bar{z})w(\bar{y},\bar{z})}{(\dot{m}_1 - \dot{m}_2)}\, \bar{y}\, d\bar{y} \qquad (56)$$

Just as in the cases of the rectangular and two dimensional channels, the average mass flow rate must be independent of the axial coordinate, $\bar{z}$. This is necessary in order to satisfy the conservation of mass principle.

Substituting equation (22) into equation (56) and simplifying yield

$$\Lambda(\bar{z},\tau_d)=1 - \frac{1}{\pi}\int_0^1 \bar{y}\left[\int_0^{2\pi}\frac{\tau^2\bar{z}^2\, d\theta}{[\tau^2\bar{z}^2+\beta(\theta)^2]} - 2\int_0^{2\pi} d\theta \int_{\varphi_1(\theta)}^{\varphi_2(\theta)} g_w(\theta,\varphi)\cos\varphi \sin\varphi\, d\varphi\right] d\bar{y} \quad (57)$$

Equation (57) is the general expression for the average mass flow passing through the tube. Following the normal procedure by evaluating equation (57) at $\bar{z} = 0$ and replacing $\Lambda(0,\tau_d)$ with $\Lambda(\tau_d)$, equation (57) reduces to

$$\Lambda(\tau_d) = 1 + \frac{2}{\pi}\int_0^1 \bar{y}\, d\bar{y} \int_0^{2\pi} d\theta \int_{\varphi_1^o(\theta)}^{\varphi_2^o(\theta)} g_w(\theta,\varphi)\cos\varphi \sin\varphi\, d\varphi \quad (58)$$

where $\varphi_1^o(\theta)$ and $\varphi_2^o(\theta)$ denote the angles $\varphi_1(\theta)$ and $\varphi_2(\theta)$, given by equations (4) and (5), evaluated at $\bar{z} = 0$. Equation (58) represents the general expression for the average mass flow rate through circular tubes for arbitrary wall flux variation. It is interesting to note that when the wall contribution of equation (58) is removed $\Lambda(\tau_d)$ takes on the value of unity, which corresponds to orifice flow.

It should be noted that the variable of integration, φ, of equation (58) can be replaced with the wall coordinate, $\bar{z}'$, by introducing equation (2). Since no simplification results, as for the rectangular and two dimensional channels, this operation has not been performed here.

Solution Technique for Linear Wall Flux Segments

Discussion

In order to determine expressions for the flow properties, which were presented in general form in the first part of this chapter, it is necessary to make some assumption regarding the wall flux variation. A convenient representation is again given by a series of linear segments for the wall flux. The constants required for this representation are obtained from the solution of the integral equation for the boundary condition. The results presented here are not given solely in terms of analytical expressions, as was possible for the two dimensional case, since the integrations with respect to the velocity polar angle could not be performed analytically. The accuracy which can be attained with the present development depends on the number of linear wall flux segments taken, the accuracy with which the integral equation for the boundary condition can be solved, and the accuracy of the numerical integration with respect to the polar velocity angle. As will be seen in the following development, a desired degree of accuracy can be specified and the final results obtained accordingly.

In the following sections a polynomial solution of the integral equation for the boundary condition is presented, the results for the moments for arbitrary wall flux, which were presented in the first part of this chapter, are expressed in terms of single integrals by integrating the wall contribution for the assumption of linear wall flux segments, and the expression for the average mass flow rate based on the assumption of linear wall flux segments is given. It should be noted

that the results for a constant or linear wall flux over the entire channel length can be obtained directly from the following results by setting the appropriate terms equal to zero.

Polynomial Solution for Boundary Condition

In order to evaluate the flow properties it is necessary to determine the wall flux variation. The nondimensional wall flux is obtained from the Fredholm integral equation of the second kind given by equation (10). Since the exact solution of this integral equation is not known, a polynomial solution is obtained. The method used to solve equation (10) is the same as that used for the two dimensional case of Chapter II. The comments made there concerning the difficulties of obtaining an accurate solution are also appropriate here. It should be noted, however, that the kernel, given by equation (12), for the circular tube integral equation is continuous but has discontinuous derivatives at $\bar{z}' = \bar{z}''$. It will be seen that this causes no difficulties in obtaining an accurate solution using the collocation method.

In order to obtain accurate results by the collocation method it is necessary to choose functions to represent $g_w(\bar{z}')$ which satisfy all the properties of the solution of equation (10) and are integrable when weighted by the kernel. Such an approximation is contained in the series

$$g_w(\bar{z}') = \frac{1}{2} + \sum_{k=1}^{M} B_{2k-1}(\tau_d)\, \varphi_{2k-1}(\bar{z}') \qquad (59)$$

where

$$\varphi_{2k-1}(\bar{z}') = (\bar{z}' - \frac{1}{2})^{2k-1} \tag{60}$$

and the coefficients, $B_{2k-1}(\tau_d)$, are functions of τ_d and can be obtained by satisfying the integral equation at discrete points over the interval $0 \leq \bar{z}' < 1/2$.

By substituting equation (59) into equation (10) the following equation is obtained:

$$\sum_{k=1}^{M} B_{2k-1}(\tau_d) \left\{ \varphi_{2k-1}(\bar{z}') - \left[\Phi^{+}_{2k-1}(\tau_d,\bar{z}') + \Phi^{-}_{2k-1}(\tau_d,\bar{z}') \right] \right\} = \tag{61}$$

$$F(\bar{z}') + \left[\Phi^{+}_{-1}(\tau_d,\bar{z}') + \Phi^{-}_{-1}(\tau_d,\bar{z}') \right] - \frac{1}{2}$$

where the following definitions have been introduced:

$$\Phi^{+}_{2k-1}(\tau_d,\bar{z}') \equiv \tau_d \int_0^{(1-\bar{z}')} \left[\xi + (\bar{z}' - \tfrac{1}{2}) \right]^{2k-1} K^{+}(\xi)\, d\xi \tag{62}$$

$$\Phi^{-}_{2k-1}(\tau_d,\bar{z}') \equiv \tau_d \int_{-\bar{z}'}^{0} \left[\xi + (\bar{z}' - \tfrac{1}{2}) \right]^{2k-1} K^{-}(\xi)\, d\xi \tag{63}$$

$$\Phi^{+}_{-1}(\tau_d,\bar{z}') \equiv \frac{\tau_d}{2} \int_0^{(1-\bar{z}')} K^{+}(\xi)\, d\xi \tag{64}$$

$$\bar{\Phi}_{-1}(\tau_d,\bar{z}') \equiv \frac{\tau_d}{2}\int_{-\bar{z}'}^{0} \bar{K}(\xi)\, d\xi \tag{65}$$

The variable of integration, ξ, is given by

$$\xi = \bar{z}'' - \bar{z}' \tag{66}$$

and the functions $K^{+}(\xi)$ and $K^{-}(\xi)$ are obtained from the kernel of equation (12) by introducing the transformation of equation (66), removing the absolute value signs, and defining the kernel for $\xi \geq 0$ as $\overset{+}{K}(\xi)$ and for $\xi \leq 0$ as $\bar{K}(\xi)$. Thus,

$$\overset{+}{K}(\xi) = 1 - \frac{\tau_d\xi}{\sqrt{\tau_d^2\xi^2 + 1}} - \frac{\tau_d\xi}{2[\tau_d^2\xi^2 + 1]^{3/2}} \qquad \xi \geq 0 \tag{67}$$

$$\bar{K}(\xi) = 1 + \frac{\tau_d\xi}{\sqrt{\tau_d^2\xi^2 + 1}} + \frac{\tau_d\xi}{2[\tau_d^2\xi^2 + 1]^{3/2}} \qquad \xi \leq 0 \tag{68}$$

The coefficients, $B_{2k-1}(\tau_d)$, can be obtained from equation (61) by evaluating the equation at M points in the interval $0 \leq \bar{z}' < 1/2$.

In order to obtain accurate results using the collocation method it is necessary to evaluate the integrals of equations (62) through (65) analytically. The details of the integrations are presented in Appendix C. The results are:

$$\Phi^{+}_{-1}(\tau_d,\bar{z}') = \frac{1}{2}\left\{\tau_d(1-\bar{z}') - \sqrt{\tau_d^2(1-\bar{z}')^2+1} + \frac{1}{2}\left[1 + \frac{1}{\sqrt{\tau_d^2(1-\bar{z}')^2+1}}\right]\right\} \quad (69)$$

$$\Phi^{-}_{-1}(\tau_d,\bar{z}') = \frac{1}{2}\left\{\tau_d\bar{z}' - \sqrt{\tau_d^2\bar{z}'^2+1} + \frac{1}{2}\left[1 + \frac{1}{\sqrt{\tau_d^2\bar{z}'^2+1}}\right]\right\} \quad (70)$$

$$\Phi^{+}_{2k-1}(\tau_d,\bar{z}') = \sum_{i=0}^{2k-1}\binom{2k-1}{i}(\bar{z}' - \frac{1}{2})^i \; A^{+}_{2k-1-i}(\tau_d,\bar{z}') \quad k \geq 1 \quad (71)$$

$$\Phi^{-}_{2k-1}(\tau_d,\bar{z}') = \sum_{i=0}^{2k-1}\binom{2k-1}{i}(\bar{z}' - \frac{1}{2})^i \; A^{-}_{2k-1-i}(\tau_d,\bar{z}') \; k \geq 1 \quad (72)$$

where

$$A^{+}_{2k-1-i}(\tau_d,\bar{z}') = \frac{\tau_d(1-\bar{z}')^{2k-i}}{(2k-i)} - C^{+}_{2k-1}(\tau_d,\bar{z}') - \frac{1}{2}B^{+}_{2k-i}(\tau_d,\bar{z}') \quad (2k-1-i)\geq 0 \quad (73)$$

$$A^{-}_{2k-1-i}(\tau_d,\bar{z}') = -\frac{\tau_d(-\bar{z}')^{2k-i}}{(2k-i)} + C^{-}_{2k-i}(\tau_d,\bar{z}') + \frac{1}{2}B^{-}_{2k-i}(\tau_d,\bar{z}') \quad (2k-1-i)\geq 0 \quad (74)$$

and

$$B^{+}_{2k-i}(\tau_d,\bar{z}') = \frac{1}{(2k-2-i)}\left[\frac{(1-\bar{z}')^{2k-1-i}}{\sqrt{\tau_d^2(1-\bar{z}')^2+1}} - \frac{(2k-1-i)}{\tau_d^2}B^{+}_{2k-2-i}(\tau_d,\bar{z}')\right] \quad (2k-i)\geq 3 \quad (75)$$

$$B^{-}_{2k-i}(\tau_d,\bar{z}') = \frac{-1}{(2k-2-i)}\left[\frac{(-\bar{z}')^{2k-1-i}}{\sqrt{\tau_d^2\bar{z}'^2+1}} + \frac{(2k-1-i)}{\tau_d^2}B^{-}_{2k-2-i}(\tau_d,\bar{z}')\right] \quad (2k-i)\geq 3 \quad (76)$$

$$C^{+}_{2k-i}(\tau_d,\bar{z}') = \frac{1}{(2k-i)}\left\{(1-\bar{z}')\sqrt{\tau_d^{2(2k-1-i)}(1-\bar{z}')^2+1} - \frac{(2k-1-i)}{\tau_d^2} C^{+}_{2k-2-i}(\tau_d,\bar{z}')\right\}(2k-i)\geq 3 \quad (77)$$

$$C^{-}_{2k-i}(\tau_d,\bar{z}') = \frac{-1}{(2k-i)}\left\{(-\bar{z}')\sqrt{\tau_d^{2(2k-1-i)}\bar{z}'^2+1} + \frac{(2k-1-i)}{\tau_d^2} C^{-}_{2k-2-i}(\tau_d,\bar{z}')\right\}(2k-i)\geq 3 \quad (78)$$

$$B^{+}_{1}(\tau_d,\bar{z}') = \left[\, 1 - \frac{1}{\sqrt{\tau_d^2(1-\bar{z}')^2+1}} \,\right] \quad (79)$$

$$B^{-}_{1}(\tau_d,\bar{z}') = \left[\, \frac{1}{\sqrt{\tau_d^2\bar{z}'^2+1}} - 1 \,\right] \quad (80)$$

$$B^{+}_{2}(\tau_d,\bar{z}') = \left[\, \frac{1}{\tau_d} \mathrm{LN}\left|\tau_d(1-\bar{z}') + \sqrt{\tau_d^2(1-\bar{z}')^2+1}\,\right| - \frac{(1-\bar{z}')}{\sqrt{\tau_d^2(1-\bar{z}')^2+1}} \,\right] \quad (81)$$

$$B^{-}_{2}(\tau_d,\bar{z}') = -\left[\, \frac{1}{\tau_d} \mathrm{LN}\left|\sqrt{\tau_d^2\bar{z}'^2+1} - \tau_d\bar{z}'\,\right| + \frac{\bar{z}'}{\sqrt{\tau_d^2\bar{z}'^2+1}} \,\right] \quad (82)$$

$$C^{+}_{1}(\tau_d,\bar{z}') = \left[\sqrt{\tau_d^2(1-\bar{z}')^2+1} - 1\,\right] \quad (83)$$

$$C_1^-(\tau_d,\bar{z}') = \left[\, 1 - \sqrt{\tau_d^2\bar{z}'^2 + 1}\,\right] \tag{84}$$

$$C_2^+(\tau_d,\bar{z}') = \frac{1}{2}\left[(1-\bar{z}')\sqrt{\tau_d^2(1-\bar{z}')^2+1} - \frac{1}{\tau_d}\,LN\left|\tau_d(1-\bar{z}')+\sqrt{\tau_d^2(1-\bar{z}')^2+1}\,\right|\right] \tag{85}$$

$$C_2^-(\tau_d,\bar{z}') = \frac{1}{2}\left[\bar{z}'\sqrt{\tau_d^2\bar{z}'^2+1} + \frac{1}{\tau_d}\,LN\left|\sqrt{\tau_d^2\bar{z}'^2+1} - \tau_d\bar{z}'\right|\right] \tag{86}$$

and $\binom{2k-1}{i}$ is the binomial coefficient. The procedure for obtaining an accurate solution for the nondimensional wall flux is identical to that outlined for the two dimensional case. Once the coefficients, $B_{2k-1}(\tau_d)$, have been obtained to some desired degree of accuracy, the polynomial solution is known from equations (59) and (60). As pointed out for the two dimensional case, it is necessary to solve a M x M system for the unknown coefficients, $B_{2k-1}(\tau_d)$, for each value of τ_d. For the case of a linear wall flux assumption the single coefficient, $B_1(\tau_d)$, can be expressed explicitly in terms of τ_d. The result for $B_1(\tau_d)$ is given by equation (C-71) of Appendix C.

Having determined the polynomial solution for the nondimensional wall flux, it is now necessary to express these results in terms of functions which are readily integrable. Since we have already chosen to represent the wall flux as a series of linear segments, the nondimensional wall flux for each section can be expressed as

$$g_w(\bar{z}') = a_i(\tau_d)\bar{z}' + b_i(\tau_d) \qquad \bar{z}'_i \le \bar{z}' \le \bar{z}'_{i+1} \tag{87}$$

where

$$a_i(\tau_d) = \frac{[g_{w_i}(\tau_d) - g_{w_{i+1}}(\tau_d)]}{[\bar{z}'_i - \bar{z}'_{i+1}]} \tag{88}$$

$$b_i(\tau_d) = \frac{[g_{w_{i+1}}(\tau_d)\bar{z}'_i - g_{w_i}(\tau_d)\bar{z}'_{i+1}]}{[\bar{z}'_i - \bar{z}'_{i+1}]} \tag{89}$$

and $g_{w_i}(\tau_d)$ denotes the value of the nondimensional wall flux at $\bar{z}'_i$. It will prove helpful in the subsequent work to express $g_w(\bar{z}')$ in terms of the velocity coordinates, θ and φ. Substituting equation (2) for $\bar{z}'$ into equation (87) gives

$$g_w(\theta,\varphi) = A_i(\bar{z},\tau_d) - B_i(\tau_d)\bar{\beta}(\theta)\,\mathrm{Cot}\,\varphi \qquad \varphi_i(\theta) \le \varphi \le \varphi_{i+1}(\theta) \tag{90}$$

where

$$A_i(\bar{z},\tau_d) \equiv a_i(\tau_d)\bar{z} + b_i(\tau_d) \tag{91}$$

$$B_i(\tau_d) \equiv \frac{a_i(\tau_d)}{2\tau_d} \tag{92}$$

$$\mathrm{Tan}\,\varphi_i(\theta) = \frac{\bar{\beta}(\theta)}{\tau(\bar{z} - \bar{z}'_i)} \tag{93}$$

Note that $\varphi_0(\theta) = \varphi_1(\theta)$ and $\varphi_{N+1}(\theta) = \varphi_2(\theta)$, where $\varphi_1(\theta)$ and $\varphi_2(\theta)$ are given by equations (4) and (5), and N is the number of linear wall flux segments.

Moments for Linear Wall Flux Segments

In the following sections the wall contribution for each of the moments is determined by using linear wall flux segments and analytically integrating with respect to the azimuthal angle, φ, to obtain the contribution for each segment. The total wall contribution for each moment is then determined by summing up the contributions of all the wall flux segments.

Density. The density is given by equation (18) for arbitrary wall flux variation. Introducing equation (90) for the nondimensional wall flux and performing the necessary integrations for each segment, the integral for the wall contribution can be expressed as

$$\int_0^{2\pi} d\theta \int_{\varphi_1(\theta)}^{\varphi_2(\theta)} g_w(\theta,\varphi)\ \mathrm{Sin}\ \varphi\ d\varphi = \sum_{i=0}^{N} \int_0^{2\pi} d\theta \int_{\varphi_i(\theta)}^{\varphi_{i+1}(\theta)} g_w(\theta,\varphi)\ \mathrm{Sin}\ \varphi\ d\varphi = \tag{94}$$

$$\sum_{i=0}^{N} \left[A_i(z,\tau_d) \int_0^{2\pi} [\mathrm{Cos}\ \varphi_i(\theta) - \mathrm{Cos}\ \varphi_{i+1}(\theta)]\, d\theta - B_i(\tau_d) \int_0^{2\pi} \bar{\beta}(\theta) [\mathrm{Sin}\ \varphi_{i+1}(\theta) - \mathrm{Sin}\ \varphi_i(\theta)]\, d\theta \right]$$

Replacing the double integral of equation (18) with the expression in equation (94) yields the final form for the local density.

Velocity Components. The integrals for the wall contribution of the velocity components, as presented in equations (22) and (24) for arbitrary wall flux variation, can be evaluated by substituting equation (90) for the nondimensional wall flux and performing the necessary integrations for each segment. The results can be expressed as follows:

$$\int_0^{2\pi} d\theta \int_{\varphi_1(\theta)}^{\varphi_2(\theta)} g_w(\theta,\varphi)\cos\varphi \sin\varphi \, d\varphi = \sum_{i=0}^{N} \int_0^{2\pi} d\theta \int_{\varphi_i(\theta)}^{\varphi_{i+1}(\theta)} g_w(\theta,\varphi)\cos\varphi \sin\varphi \, d\varphi = \tag{95}$$

$$\sum_{i=0}^{N} \Big[\frac{1}{2} A_i(\bar{z},\tau_d) \int_0^{2\pi} [\cos^2 \varphi_i(\theta) - \cos^2 \varphi_{i+1}(\theta)]d\theta - \frac{1}{4} B_i(\tau_d) \cdot$$

$$\int_0^{2\pi} \bar{\beta}(\theta) \, [2(\varphi_{i+1}(\theta) - \varphi_i(\theta)) + (\sin 2\varphi_{i+1}(\theta) - \sin 2\varphi_i(\theta)) \,] \, d\theta \Big]$$

$$\int_0^{2\pi} \sin\theta \, d\theta \int_{\varphi_1(\theta)}^{\varphi_2(\theta)} g_w(\theta,\varphi)\sin^2\varphi \, d\varphi = \sum_{i=0}^{N} \int_0^{2\pi} \sin\theta \, d\theta \int_{\varphi_i(\theta)}^{\varphi_{i+1}(\theta)} g_w(\theta,\varphi)\sin^2\varphi \, d\varphi = \tag{96}$$

$$\sum_{i=0}^{N} \Big[\frac{1}{4} A_i(\bar{z},\tau_d) \int_0^{2\pi} \sin\theta \, [2(\varphi_{i+1}(\theta) - \varphi_i(\theta)) - (\sin 2\varphi_{i+1}(\theta) -$$

$$\sin 2\varphi_i(\theta)) \,] d\theta - \frac{1}{2} B_i(\tau_d) \int_0^{2\pi} \sin\theta \, \bar{\beta}(\theta)[\cos^2\varphi_i(\theta) - \cos^2\varphi_i(\theta)]d\theta \Big]$$

$$\sum_{i=0}^{N}\Big[\frac{1}{3}A_i(\bar{z},\tau_d)\int_0^{2\pi}\mathrm{Sin}^2\theta\,[3(\mathrm{Cos}\,\varphi_i(\theta)-\mathrm{Cos}\,\varphi_{i+1}(\theta))+\mathrm{Cos}^3\varphi_{i+1}(\theta)-$$

$$\mathrm{Cos}^3\varphi_i(\theta)]\,d\theta-\frac{1}{3}B_i(\tau_d)\int_0^{2\pi}\mathrm{Sin}^2\theta\,\bar{\beta}(\theta)[\mathrm{Sin}^3\varphi_{i+1}(\theta)-\mathrm{Sin}^3\varphi_i(\theta)]\,d\theta\Big]$$

$$\int_0^{2\pi}\mathrm{Cos}^2\theta\,d\theta\int_{\varphi_1(\theta)}^{\varphi_2(\theta)}g_w(\theta,\varphi)\mathrm{Sin}^3\varphi\,d\varphi=\sum_{i=0}^{N}\int_0^{2\pi}\mathrm{Cos}^2\theta\,d\theta\int_{\varphi_i(\theta)}^{\varphi_{i+1}(\theta)}g_w(\theta,\varphi)\mathrm{Sin}^3\varphi\,d\varphi= \quad (99)$$

$$\sum_{i=0}^{N}\Big[\frac{1}{3}A_i(\bar{z},\tau_d)\int_0^{2\pi}\mathrm{Cos}^2\theta\,[3(\mathrm{Cos}\,\varphi_i(\theta)-\mathrm{Cos}\,\varphi_{i+1}(\theta))+\mathrm{Cos}^3\varphi_{i+1}(\theta)-$$

$$\mathrm{Cos}^3\varphi_i(\theta)]\,d\theta-\frac{1}{3}B_i(\tau_d)\int_0^{2\pi}\mathrm{Cos}^2\theta\,\bar{\beta}(\theta)[\mathrm{Sin}^3\varphi_{i+1}(\theta)-\mathrm{Sin}^3\varphi_i(\theta)]d\theta\Big]$$

The final expressions for the normal pressure components are obtained by substituting the appropriate integrals of equations (97) through (99) for the double integrals of equations (30) and (32).

Thermodynamic Pressure and Temperature. The general expressions for the thermodynamic pressure for arbitrary wall flux variation is given by equation (34). The wall contribution of the pressure, as represented by the double integral of equation (34), is identical to

the corresponding contribution for the density, which is given by equation (94). Therefore, the final expression for the pressure is obtained by combining the double integral of equation (94) with equation (34). The corresponding expression for the temperature is obtained by combining the equation of state with the final expressions for the density and pressure.

Shear Stress Components. The general expression for the shear stress is given by equation (36) for arbitrary wall flux variation. Substituting equation (90) for the wall flux variation over each segment of the tube wall into the double integral of equation (36) and performing the integration with respect to the azimuthal angle, φ, yield the following:

$$\int_0^{2\pi} \mathrm{Sin}\ \varphi\ d\varphi \int_{\varphi_1(\theta)}^{\varphi_2(\theta)} g_w(\theta,\varphi)\mathrm{Sin}^2\varphi\ \mathrm{Cos}\ \varphi\ d\varphi = \sum_{i=0}^{N} \int_0^{2\pi} \mathrm{Sin}\ \theta\ d\theta \int_{\varphi_i(\theta)}^{\varphi_{i+1}(\theta)} g_w(\theta,\varphi)\mathrm{Sin}^2\varphi\ \mathrm{Cos}\ \varphi\ d\varphi = (100)$$

$$\sum_{i=0}^{N} \Bigg[\frac{1}{3} A_i(\bar{z},\tau_d) \int_0^{2\pi} \mathrm{Sin}\ \theta\ [\mathrm{Sin}^3\varphi_{i+1}(\theta) - \mathrm{Sin}^3\varphi_i(\theta)]\ d\theta - \frac{1}{3} B_i(\tau_d) \cdot$$

$$\int_0^{2\pi} \mathrm{Sin}\ \theta\ \bar{\beta}(\theta)\ [\mathrm{Cos}^3\varphi_i(\theta) - \mathrm{Cos}^3\varphi_{i+1}(\theta)]\ d\theta \Bigg]$$

Substituting the result of equation (100) for the double integral of equation (36) yields the final expression for the shear stress.

Heat Flux Components. The heat flux components are expressed in general for arbitrary wall flux variation by equations (39) and (40). The wall contribution for the $\bar{y}$-component of the heat flux vector consists of the same double integral which appeared in the $\bar{y}$-component of the velocity. The expression for this integral is given by equation (96). The wall contribution for the $\bar{x}$-component of the heat flux vector can be written directly from equation (96) by comparing the double integrals of equations (39) and (40). The result is

$$\int_0^{2\pi} \mathrm{Cos}\ \theta\, d\theta \int_{\varphi_1(\theta)}^{\varphi_2(\theta)} g_w(\theta,\varphi)\mathrm{Sin}^2\ \varphi\, d\varphi = \sum_{i=0}^{N} \int_0^{2\pi} \mathrm{Cos}\ \theta\, d\theta \int_{\varphi_i(\theta)}^{\varphi_{i+1}(\theta)} g_w(\theta,\varphi)\mathrm{Sin}^2\ \varphi\, d\varphi = \quad (101)$$

$$\sum_{i=0}^{N} \Bigg[\frac{1}{4} A_i(\bar{z},\tau_d) \int_0^{2\pi} \mathrm{Cos}\ \theta\, [2(\varphi_{i+1}(\theta) - \varphi_i(\theta)) - (\mathrm{Sin}\ 2\varphi_{i+1}(\theta) -$$

$$\mathrm{Sin}\ 2\varphi_i(\theta))]\, d\theta - \frac{1}{2} B_i(\tau_d) \int_0^{2\pi} \mathrm{Cos}\ \theta\, \bar{\beta}(\theta)[\mathrm{Cos}^2\ \varphi_i(\theta) - \mathrm{Cos}^2\ \varphi_{i+1}(\theta)]d\theta \Bigg]$$

The final expressions for the heat flux components are obtained by replacing the double integrals of equations (39) and (40) with the appropriate expressions from equations (96) and (101).

Average Mass Flow Rate

The average mass flow rate for the assumption of linear wall flux segments can be obtained directly from the general formulation given by

equation (58). Noting that the double integral for the angles θ and φ is identical to the double integral of equation (95) when the latter is evaluated at $\bar{z} = 0$, the average mass flow rate can be obtained by combining equations (58) and (95). The final result is expressed in terms of integrals for the polar angle, θ, and the normal coordinate, $\bar{y}$, which must be evaluated numerically.

Moments for Constant or Linear Wall Flux Over Entire Channel Length

The expressions for a constant or linear wall flux over the entire tube length can be obtained as special cases of the results presented above for linear wall flux segments by following the procedure outlined in Chapter II for the two dimensional case. It should be noted, however, that completely analytical expressions are not obtained for the circular tube as in the case for the two dimensional channel since the polar angle integration could not be performed analytically. Therefore, the only advantage of these approximate solutions is that the results for the integration with respect to the azimuthal angle, φ, for the wall contribution can be represented by a single expression instead of a series, as presented for the case of linear wall flux segments. In order to determine the exact range of τ for which these approximate solutions are applicable, it is necessary to compare the results of the approximate solutions with the results of the accurate solution for linear wall flux segments. This comparison will be made in a subsequent section.

Computational Procedures

Nondimensional Wall Flux

The nondimensional wall flux can be determined by the series approximation of equation (59) once the coefficients, $B_{2k-1}(\tau_d)$, are known. The procedure used to determine these coefficients is identical to that used for the two dimensional channel and presented in Chapter II. The tolerance for the computations was taken to be 10^{-4} for $\tau_d \leq 30$ and 10^{-3} for $\tau_d > 30$. For the tolerance of 10^{-4}, the number of terms, M, for the polynomial varied from one for small τ_d to a maximum of ten for $\tau_d \approx 30$. For the tolerance of 10^{-3}, M varied from one for small τ_d to five for $\tau_d \approx 30$, and then dropped to one for τ_d greater than approximately 100.

Local and Average Flow Properties

The local and average flow properties for the case of linear wall flux segments have been expressed in terms of a series of integrals, which represents the wall contribution, and a single expression in terms of an integral, which represents the contribution of the two reservoirs. The accuracy of the final results depends on the accuracy with which the wall contribution and the integrals are evaluated. Having specified some desired degree of accuracy consistent with the accuracy of the nondimensional wall flux results, the wall contribution of the flow properties can be evaluated by the procedure outlined in Chapter II for the two dimensional case. However, a numerical integration with respect to the polar angle, θ, must be performed for each wall flux segment. Since the results of the numerical integration

can be obtained to any desired degree of accuracy, the procedure for obtaining the wall contribution is essentially the same. The flow property is then determined by combining the value obtained for the wall contribution with the value obtained for the contribution of the reservoirs. It should be noted that the latter quantity is obtained by numerically integrating with respect to the polar angle, θ.

The approximate expressions for the cases of a constant or linear wall flux over the entire channel length can be evaluated directly by numerically integrating with respect to the polar angle, since the wall contribution consists of a single expression.

The tolerance for all local and average flow property calculations of this work was taken as 10^{-3}.

Results

The presentation of the circular tube results will be quite similar to that given for the two dimensional channel in Chapter II. The same key for reference to the different results (i.e., linear wall flux segments and linear or constant wall flux over the entire tube length) is used here. However, the inlet value of the nondimensional wall flux, $g_{w_0}(\tau_d)$, required for Method 2 is now determined from equations (C-71) and (C-72), and not from the polynomial expression used in Method 1. Again all numerical calculations were performed using a Burroughs B5500 digital computer.

Nondimensional Wall Flux

The results for the nondimensional wall flux for various values of τ_d are presented in Figure 24. For $\tau_d \geq 50$ the results are

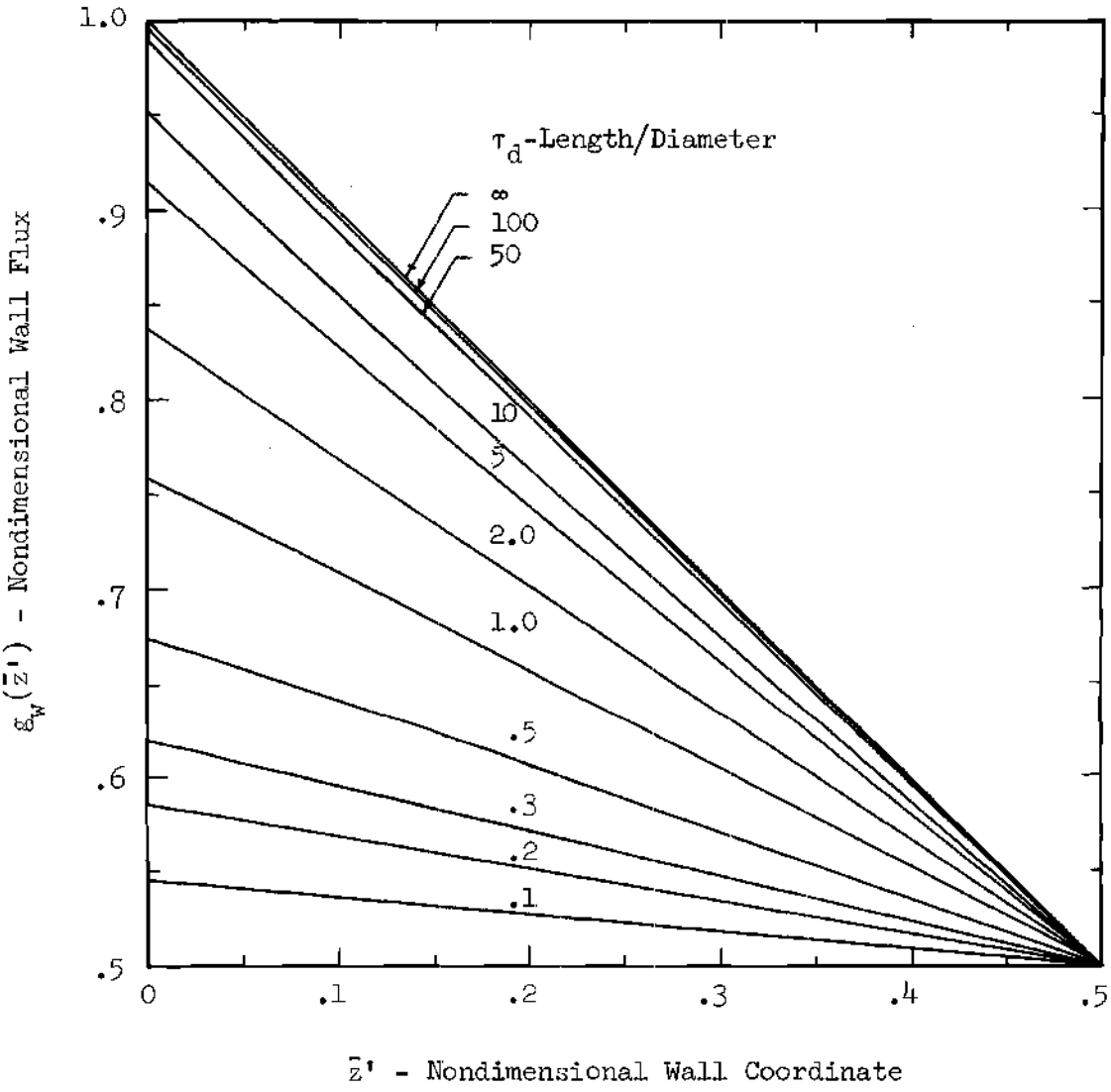

Figure 24. Nondimensional Wall Flux for Free Molecular Flow Through Circular Tubes for Various Values of τ_d.

essentially linear over the entire tube length. Thus the approach to the linear solution for infinite τ_d is quite rapid, as illustrated by the results for the case of $\tau_d = 10^2$. Although the results for $\tau_d = 10^3$ are not presented, the results were almost identical to the infinite τ_d solution. This is in contrast to the results obtained for the two dimensional case where the approach to the linear solution for infinite τ_d is quite slow. Although the results are not shown, a comparison of the results presented in Figure 24 with the results obtained for a linear wall flux over the entire tube length, with the inlet value of the wall flux given by equation (C-72) of Appendix C, showed that the results were identical to three-place accuracy for $\tau_d \geq 200$, and for $80 \leq \tau_d < 200$ the results agreed within 1×10^{-3}.

Results for the circular tube wall flux have been reported by several sources for limited ranges of τ_d. Sparrow, Jonsson, and Lundgren [20] have reported graphical results for $0 \leq \tau_d \leq 24$. Reynolds and Richley [26] have tabulated their results to three significant figures for $\tau_d \leq 8$. Both sources used a successive approximation scheme for solving the integral equation for the wall flux. The disadvantages of this method were discussed in Chapter II. For the larger values of τ_d the results of Reynolds and Richley [26] do not satisfy the property that $g_w(1/2) = 1/2$ for all τ_d. Therefore, their results for the larger values of τ_d are not exact to three significant figures. Taking this into account the results obtained here agreed with the results of both sources to the accuracy attainable from their results. For $\tau_d > 24$ there are no results available with which to compare.

Average Mass Flow Rate

The results for Method 1 are presented in Figure 25 for τ_d ranging from 10^{-3} to 10^{3}. As expected the average mass flow rate through a circular tube is less than the corresponding average mass flow rate through a two dimensional channel, as can readily be seen by comparing Figures 3 and 25. In particular, even for very small τ_d the effect of restricting the flow in all directions can readily be seen to be significant in comparison to the two dimensional results, and the approach to the orifice results is much slower than for the two dimensional case. This effect is illustrated best by comparing the results of Method 3 with the results of Method 1 for the two dimensional channel and circular tube. Referring to Figure 25, it can be seen that for $\tau_d = 1.0$ the circular tube results of Method 3 are in error by thirteen per cent. For the two dimensional channel the agreement between the two methods is within three per cent for the same value of τ_d. Since the effects of the wall are much smaller for the two dimensional channel, the approximate results for a constant wall flux are accurate over a larger range of length-to-height ratio. Also shown in the inset of Figure 25 is a comparison of Methods 1 and 2 with Knudsen's long tube formula. It can be seen that Method 2 coincides with the results of Method 1 for $\tau_d > 50$, and the results for the long tube formula of Knudsen appear to be approaching the results of Method 1 for large τ_d. For $\tau_d > 100$ a direct comparison of the results of Method 1 with the results of Knudsen's formula showed that the differences between the two results to three-place accuracy are diminishing. Since the results

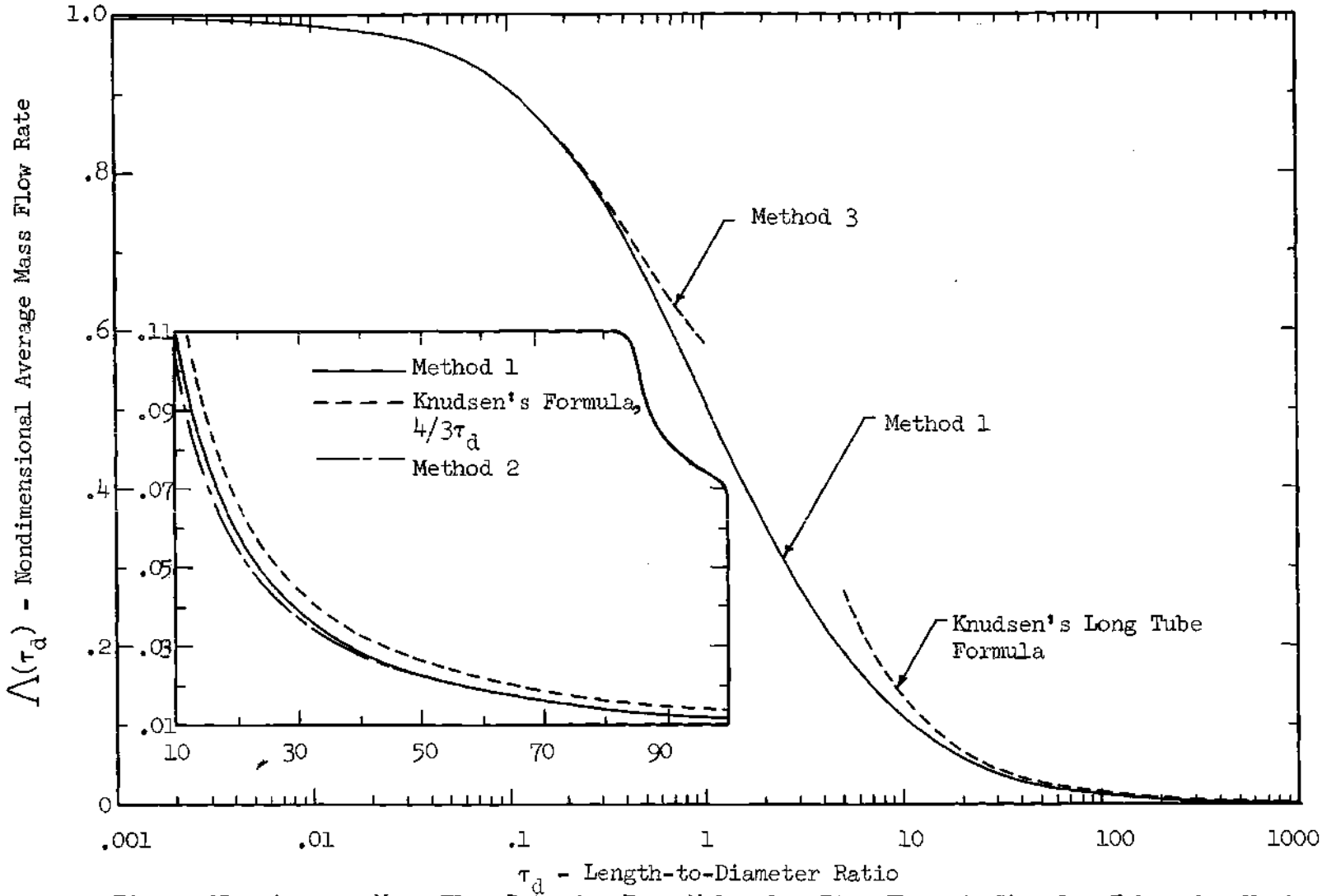

Figure 25. Average Mass Flow Rate for Free Molecular Flow Through Circular Tubes for Various Values of τ_d, and Comparison of Results for Three Different Methods for Large τ_d.

of Method 1 have been obtained to only three-place accuracy, due to the limited accuracy of the wall flux results, this is the only comparison which could be made. Although the results for Method 2 are not presented for the entire range of τ_d, the results agreed within one per cent for τ_d less than approximately 3.5 and greater than approximately 75. The maximum difference in per cent was about five and occurred for τ_d approximately equal to 20.

The most accurate results to date for the average flow rate through circular tubes have been reported by Demarcus [13] for $0 \leq \tau_d \leq 10$. He establishes upper bounds for the values of $\Lambda(\tau_d)$. The results of Method 1 to three-place accuracy were always equal to or less than the corresponding values of Demarcus. Demarcus also proves rigorously that in the limit of very large τ_d the long tube formula of Knudsen is indeed correct. In proving this result Demarcus presents the upper and lower bounds of the average flow rate in terms of series, the leading term in each series being Knudsen's formula and the second terms being negative correction terms. By defining the upper and lower bounds for $\Lambda(\tau_d)$ for large τ_d as the first two terms in each of these series and evaluating these expressions for several large values of τ_d, it is found that the results of Method 1 fall between these two limits for $\tau_d \leq 100$. For $\tau_d > 100$, $\Lambda(\tau_d)$ is needed to four-place accuracy in order to determine whether or not the results of Method 1 fall between the two limits. However, the upper and lower limits and the results of Method 1 all agree to three-place accuracy. Regardless of the results of a comparison for $\tau_d > 100$, it is evident that for $\tau_d \leq 100$ correction

terms are needed for Knudsen's formula in order to bring the results into agreement with Method 1. For example, for $\tau_d = 50$ the upper limit is approximately 0.0258, the lower limit is approximately 0.0231, and the Knudsen value is 0.0267. The result for Method 1 is approximately 0.0233. Note that the lower limit falls very close to the result of Method 1.

The results of Clausing [8] have not been presented here. However, a comparison with the results of Method 1 and Demarcus' results showed that Clausing's results are consistently high. Although Clausing's results are for a linear wall flux over the entire tube length, his solution differs from that presented here for Method 2 in that Clausing modified the linear wall flux so that $\Lambda(\tau_d)$ contained Knudsen's limit for tubes of reasonable length.

Velocity Components

The velocity components have been expressed in universal form by dividing by the average mass flow rate as defined in equation (56). Due to the symmetric and anti-symmetric properties, as illustrated in equations (25) and (26), the results are presented for only half of the channel length.

The results of Methods 1 and 2 for the axial velocity component for $\tau_d = 0.1$, 2.0, 10.0, and 50.0 are presented in Figures 26 through 29, respectively. It should be noted that the results for the singular point, $(\bar{z},\bar{y}) = (0,1)$, are not presented.

The results for Methods 1 and 2 for $\tau_d = 0.1$ and $\tau_d = 2.0$ for the axial velocity component are identical for all practical considerations,

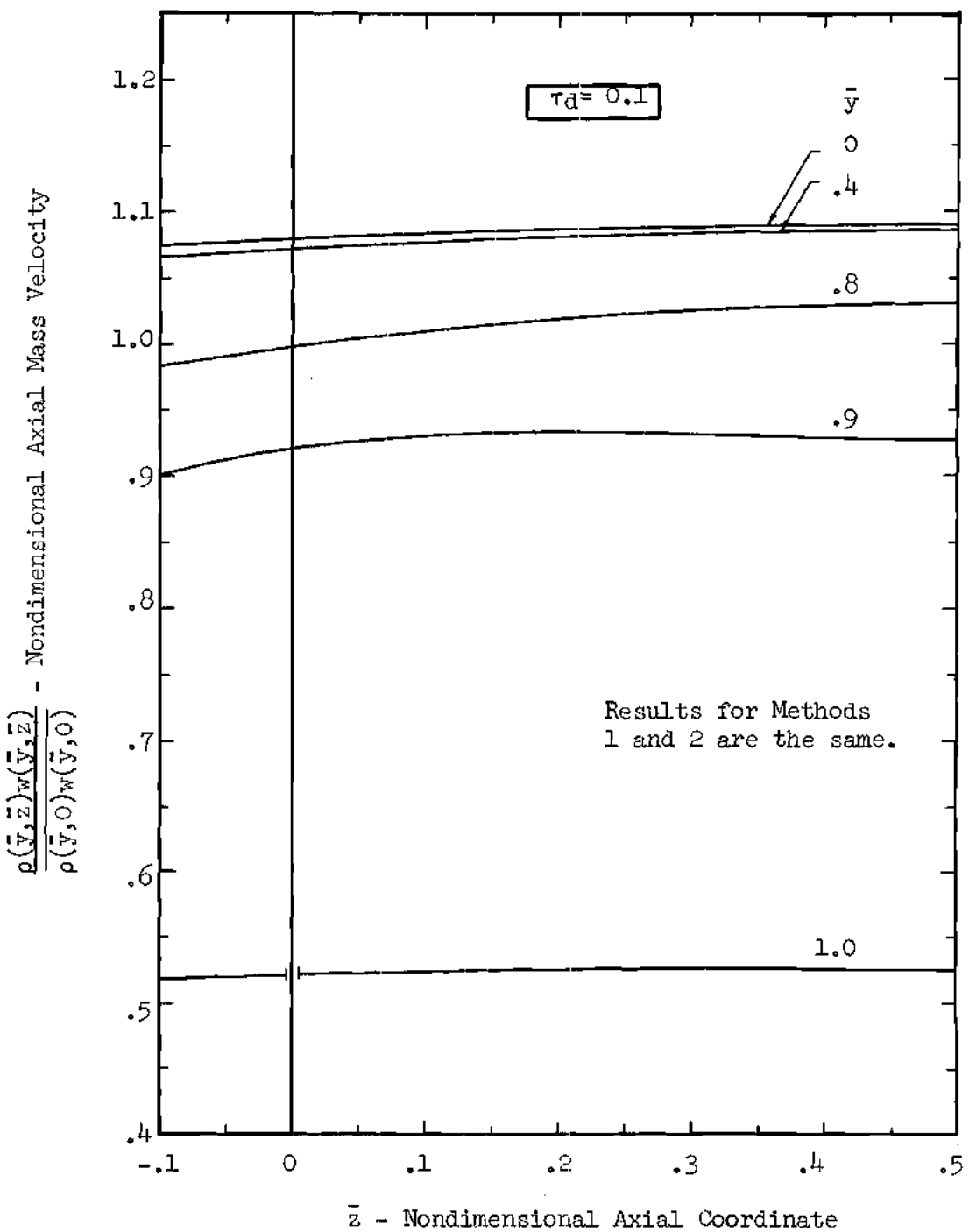

Figure 26. Nondimensional Axial Mass Velocity for Free Molecular Flow Through a Circular Tube with $\tau_d = 0.1$.

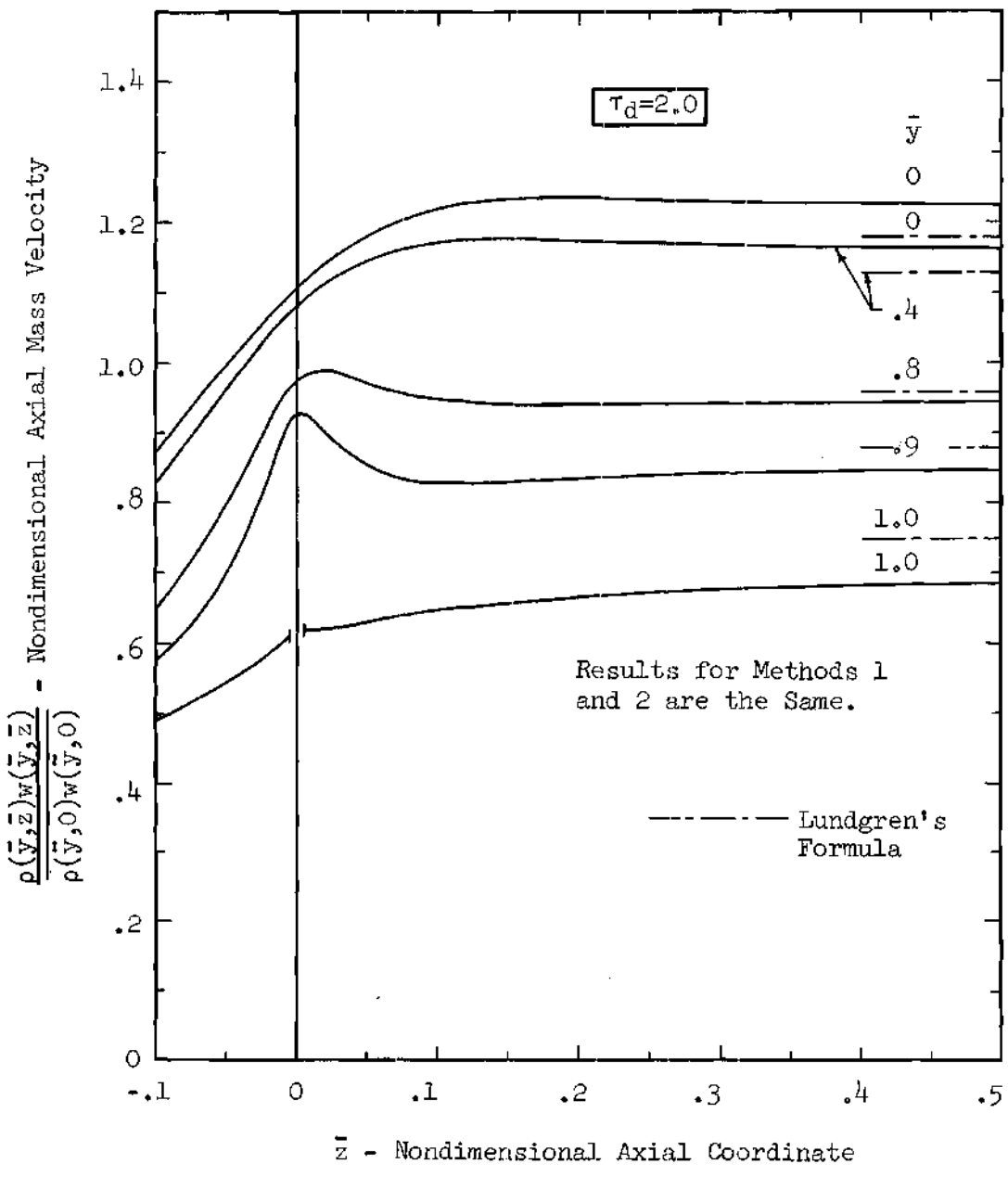

Figure 27. Nondimensional Axial Mass Velocity for Free Molecular Flow Through a Circular Tube with $\tau_d = 2.0$.

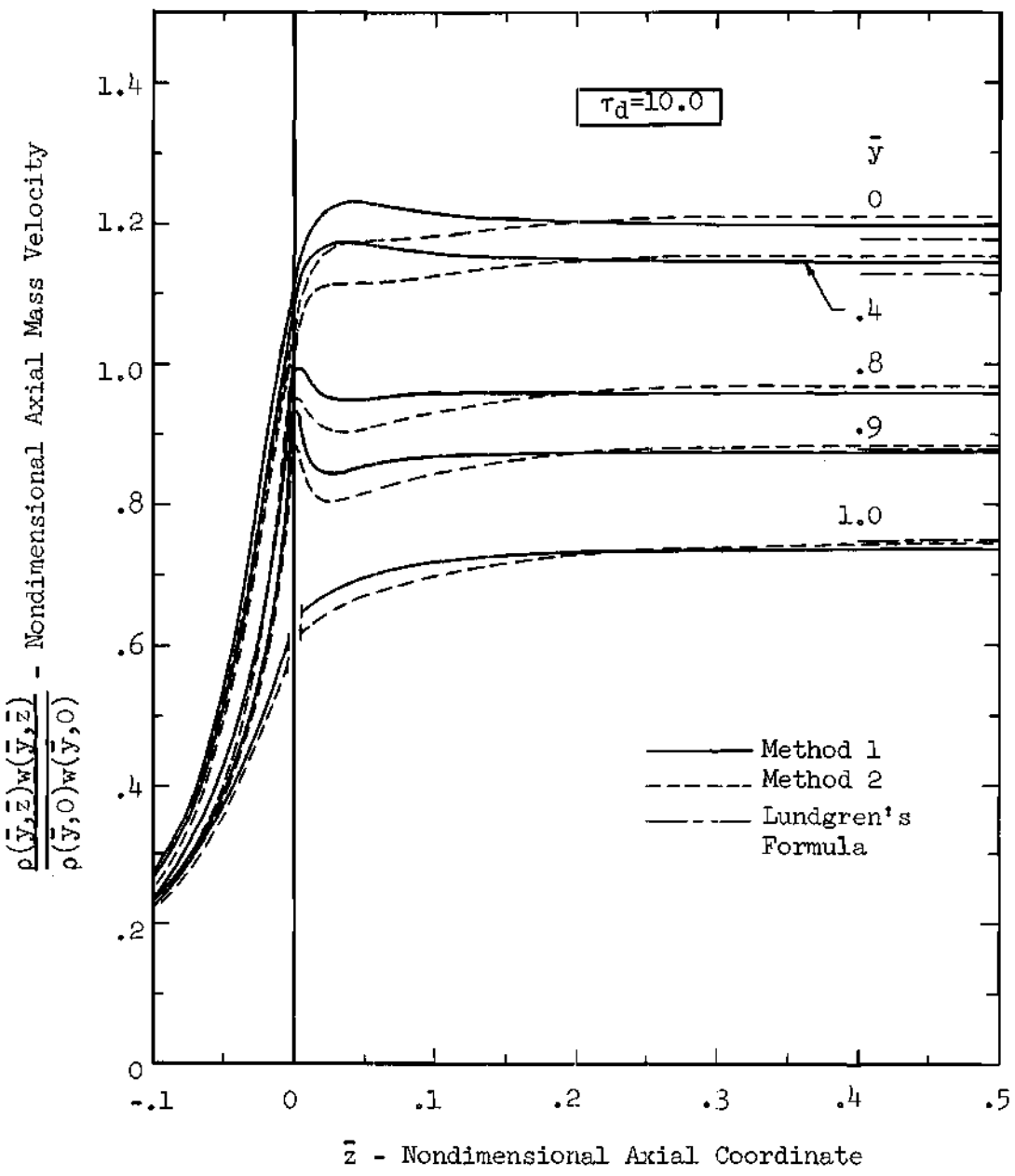

Figure 28. Nondimensional Axial Mass Velocity for Free Molecular Flow Through a Circular Tube with τ_d = 10.0.

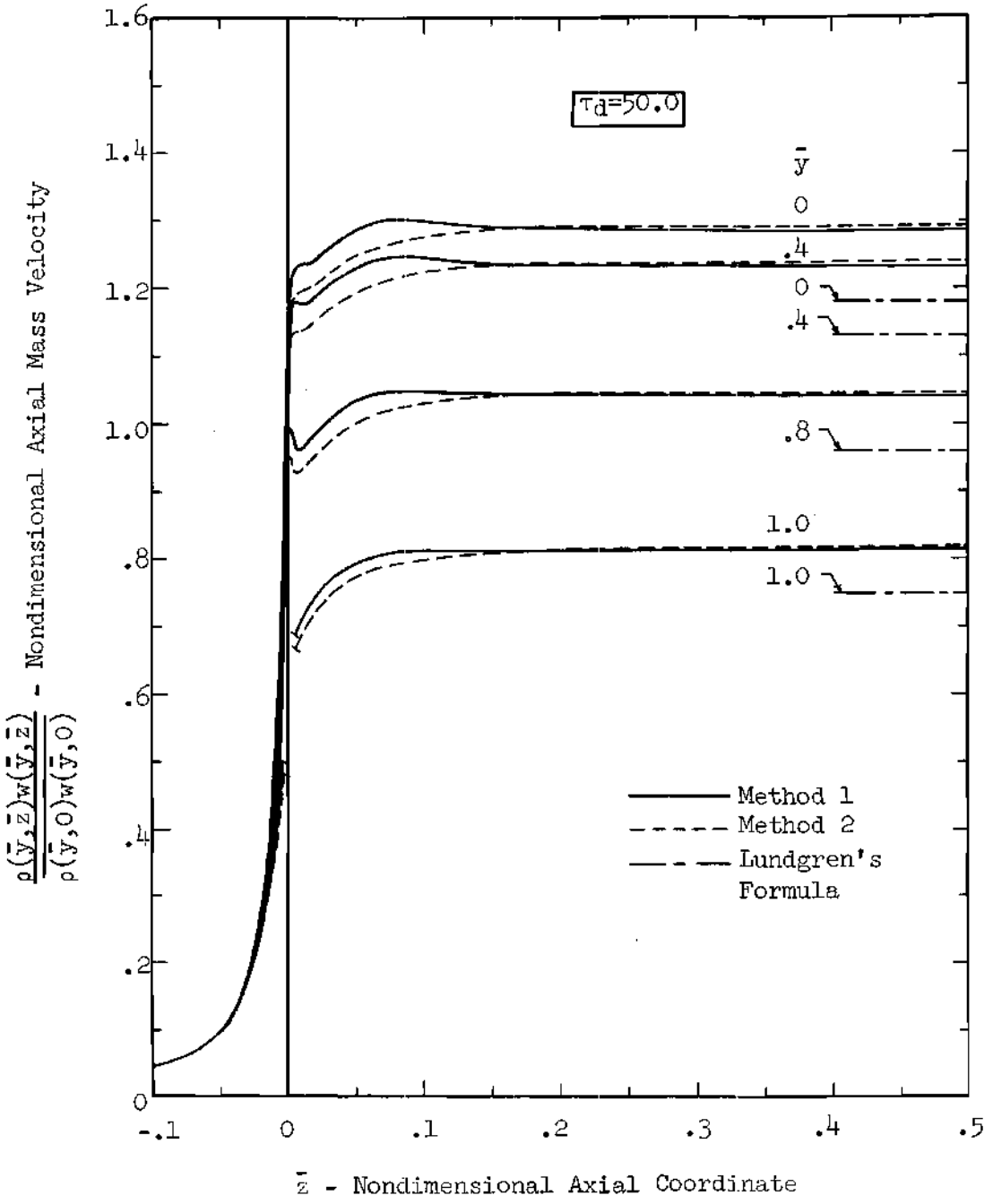

Figure 29. Nondimensional Axial Mass Velocity for Free Molecular Flow Through a Circular Tube with τ_d = 50.0.

as illustrated in Figures 26 and 27. For $\tau_d = 10$ the results of Method 2 are in fair agreement with the results of Method 1 everywhere except in the inlet region. For $\tau_d = 50$ the results of Method 2 for the axial velocity component are in better agreement with the results of Method 1 than for the case of $\tau_d = 10$, as can be seen by referring to Figures 28 and 29. It might be noted that this is not surprising in view of the close agreement between the correct nondimensional wall flux and that predicted by a linear wall flux over the entire tube length for $\tau_d \geq 50$.

The results of Method 1 for the axial velocity component for $\tau_d = 10$ were compared with the graphical results of Sparrow and Haji-Sheikh [28]. The results were in good agreement. Sparrow and Haji-Sheikh compare their results for $\tau_d = 10$ with a formula for doubly infinite tubes as derived by Lundgren and reported in the same work. This formula, written in terms of the universal velocity notation as used in Figures 26 through 29, is simply $3\ E(\bar{y})/4$, where $E(\bar{y})$ is the complete elliptic integral of the second kind. The results for this formula appear in Figures 27 through 29 for $\tau_d = 2.0$, 10.0, and 50.0, respectively. Although fair agreement is obtained with the results of Method 1 for $\tau_d = 10$, the comparison is worse for smaller and larger values of τ_d. Based on this comparison it is apparent that the validity of this long tube formula is questionable.

The results for Methods 1 and 2 for the vertical velocity component for $\tau_d = 0.1$, 2.0, and 10.0 are presented in Figures 30 through 32, respectively. It can be seen that for all practical considerations the results of Methods 1 and 2 are identical for $\tau_d = 0.1$ and $\tau_d = 2.0$. For

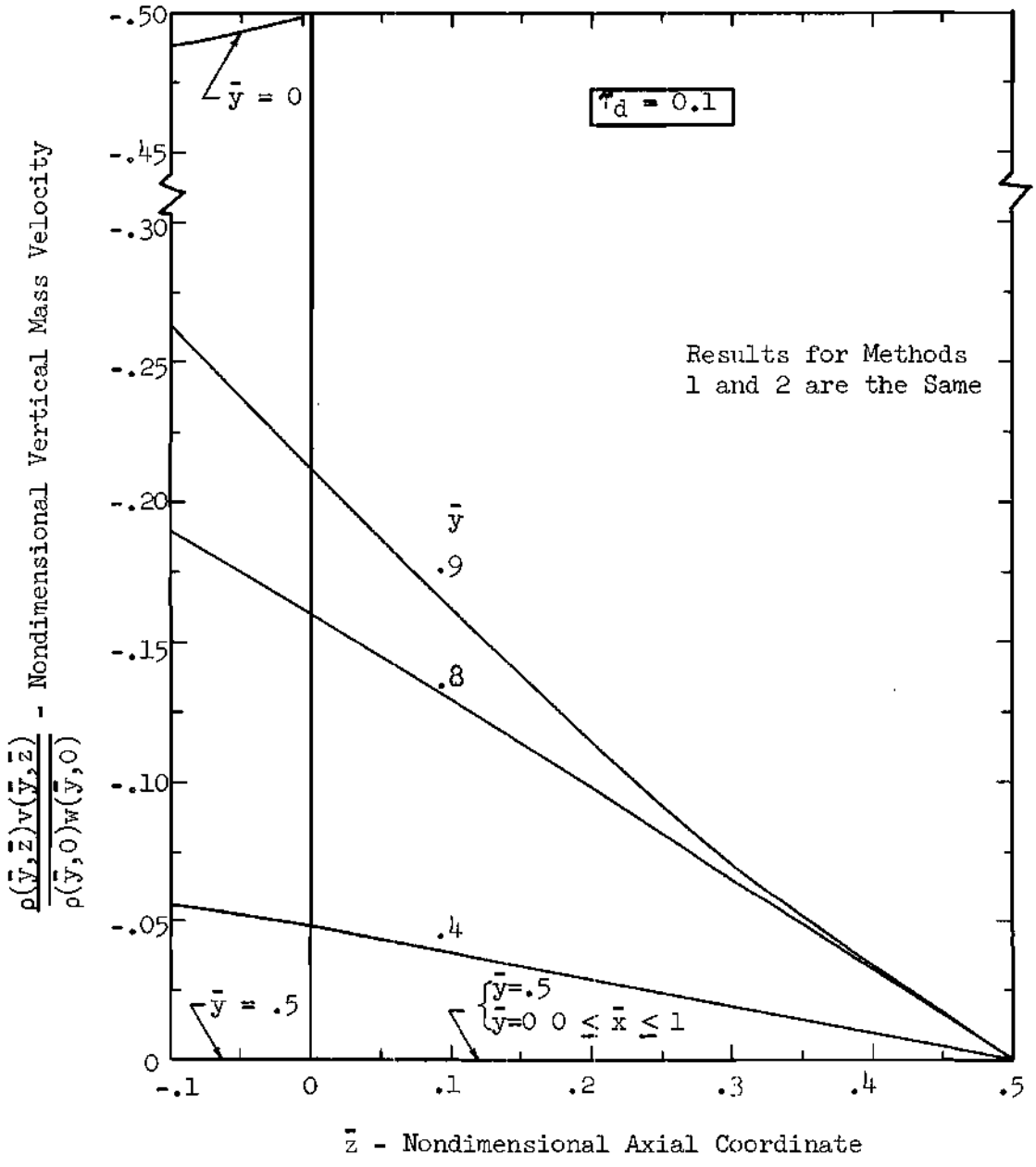

Figure 30. Nondimensional Vertical Mass Velocity for Free Molecular Flow Through a Circular Tube with $\tau_d = 0.1$.

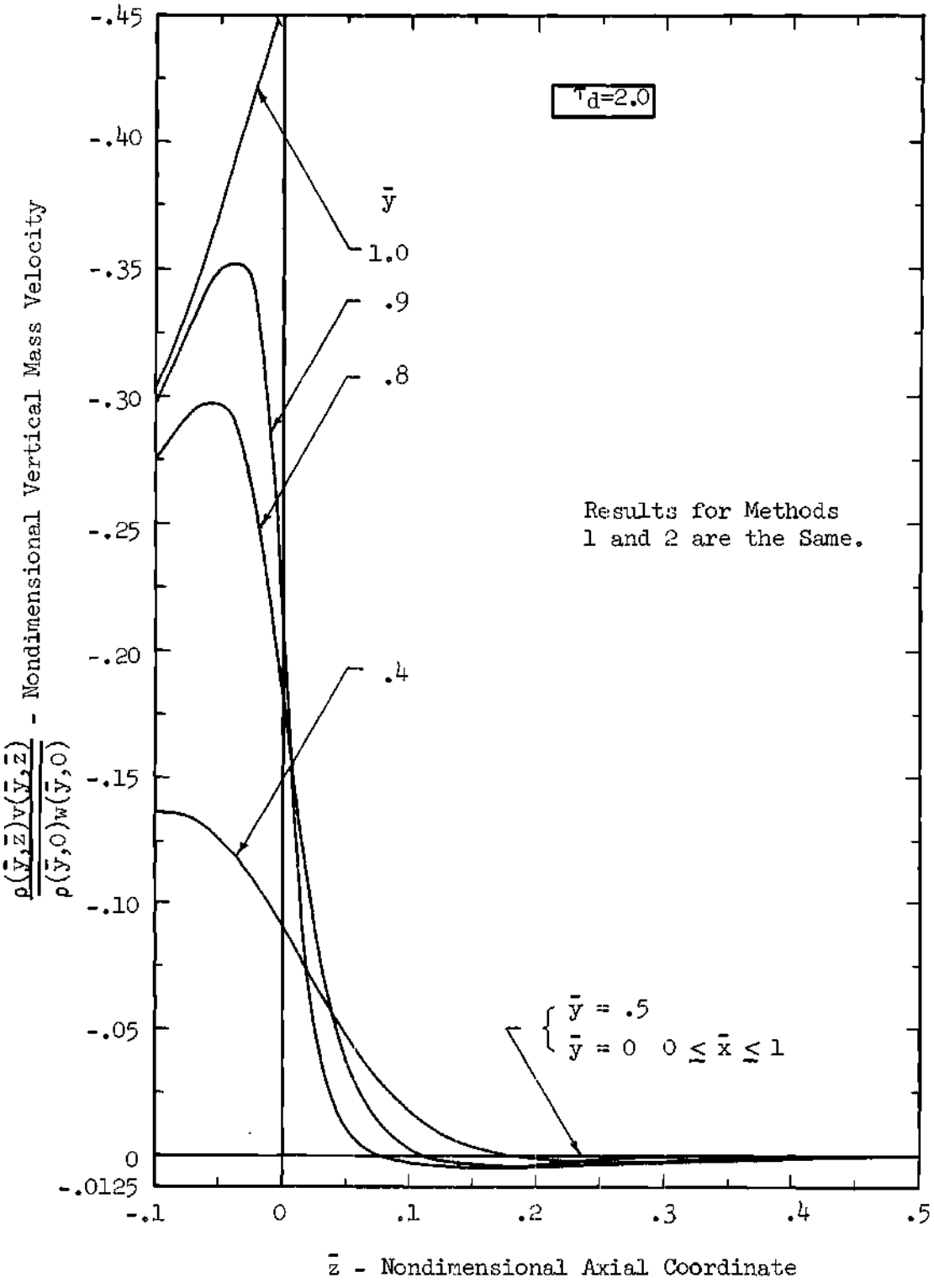

Figure 31. Nondimensional Vertical Mass Velocity for Free Molecular Flow Through a Circular Tube with $\tau_d = 2.0$.

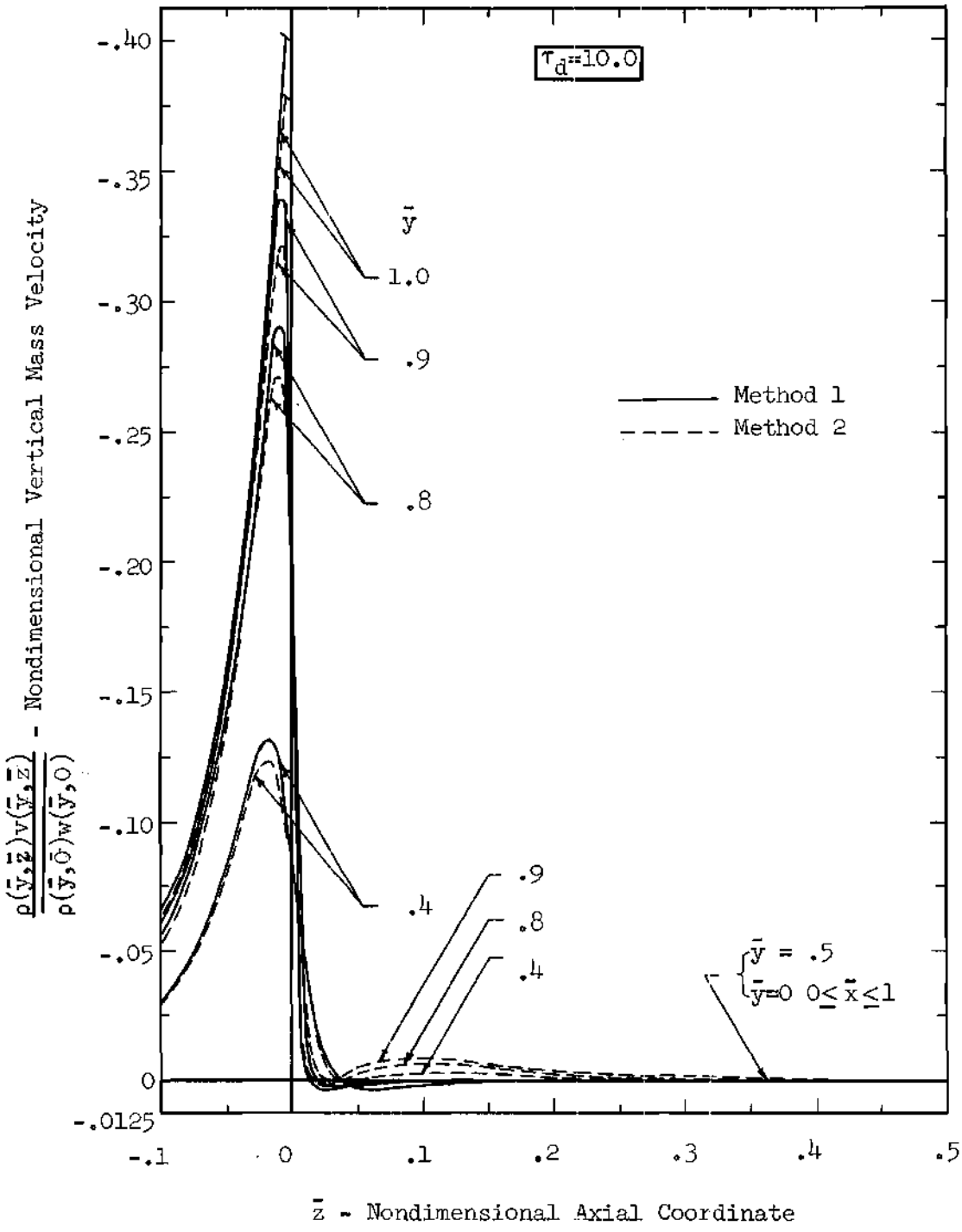

Figure 32. Nondimensional Vertical Mass Velocity for Free Molecular Flow Through a Circular Tube with τ_d = 10.0.

$\tau_d = 10.0$ the results of the vertical velocity component, as predicted by Methods 1 and 2, are in fair agreement for points outside the tube but do not even predict the same direction for $\bar{z}$ greater than approximately 0.05. Although the results for the vertical component for $\tau_d = 50$ are not presented, the agreement between Methods 1 and 2 was quite good for the entire flow field. This indicates that the linear wall flux assumption is quite good for τ_d less than approximately five and greater than approximately fifty, since it has been successful in describing the flux normal to the walls for these ranges of τ_d.

Pressure and Temperature

The results for pressure, as calculated by Method 1, are presented in Figures 33 through 35 for $\tau_d = 0.1$, 2.0, and 50.0, respectively, $P_1/P_2 = 2.0$, $T_1/T_2 = 1.0$, and $T_w/T_1 = 0.25$, 1.0, and 4.0. The tank temperatures have been taken as equal in order to illustrate the wall temperature effect. The pressure has been normalized so that the upstream and downstream limits are unity and zero, respectively. In general, the effects of the wall temperature and the length-to-diameter ratio are the same as discussed for the two dimensional case of Chapter II. It might be noted that the assumption of a linear pressure variation along the tube and constant pressure across the tube for large τ_d, as utilized by many earlier investigators, is quite good, as illustrated in Figure 35 for $\tau_d = 50.0$.

The results for the temperature, as calculated by Method 1, are presented in Figures 36 through 38 for the same conditions as for the pressure. Since the tank temperatures have been taken as equal, the

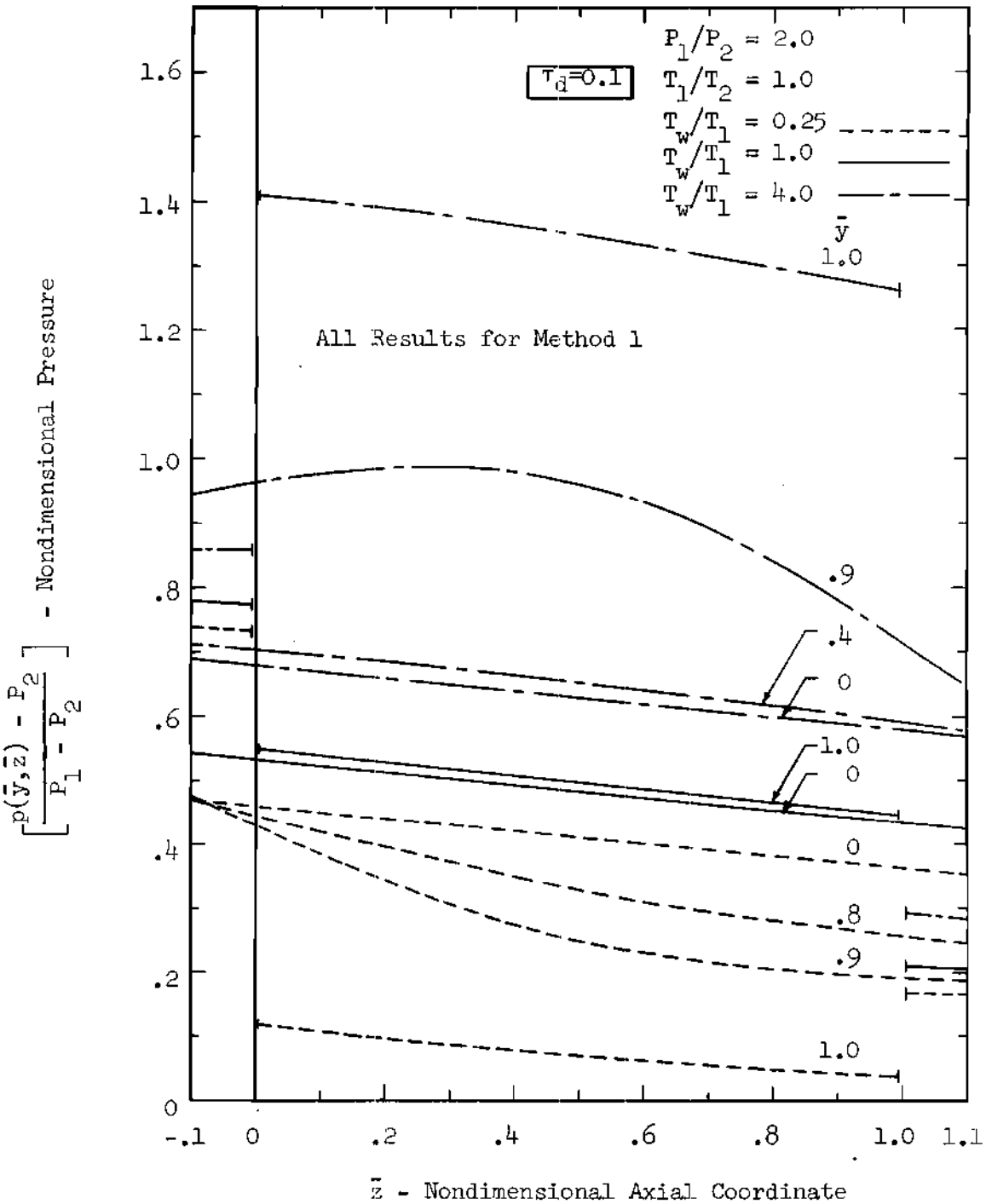

Figure 33. Nondimensional Pressure for Free Molecular Flow Through a Circular Tube for τ_d = 0.1, P_1/P_2 = 2.0, T_1/T_2 = 1.0, and T_w/T_1 = 0.25, 1.0, 4.0.

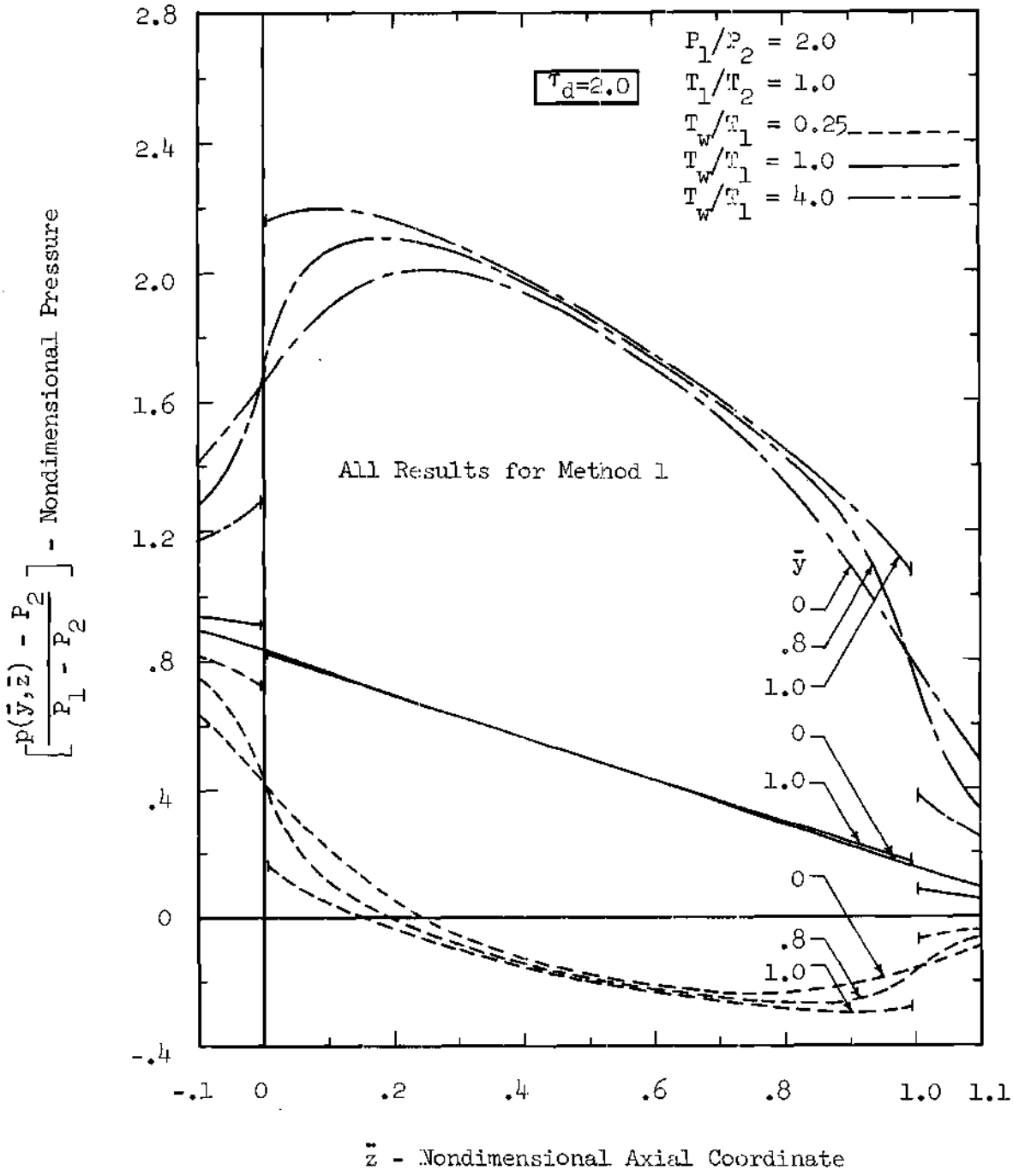

Figure 34. Nondimensional Pressure for Free Molecular Flow Through a Circular Tube for $\bar{\tau}_d$ = 2.0, P_1/P_2 = 2.0, T_1/T_2 = 1.0, and T_w/T_1 = 0.25, 1.0, 4.0.

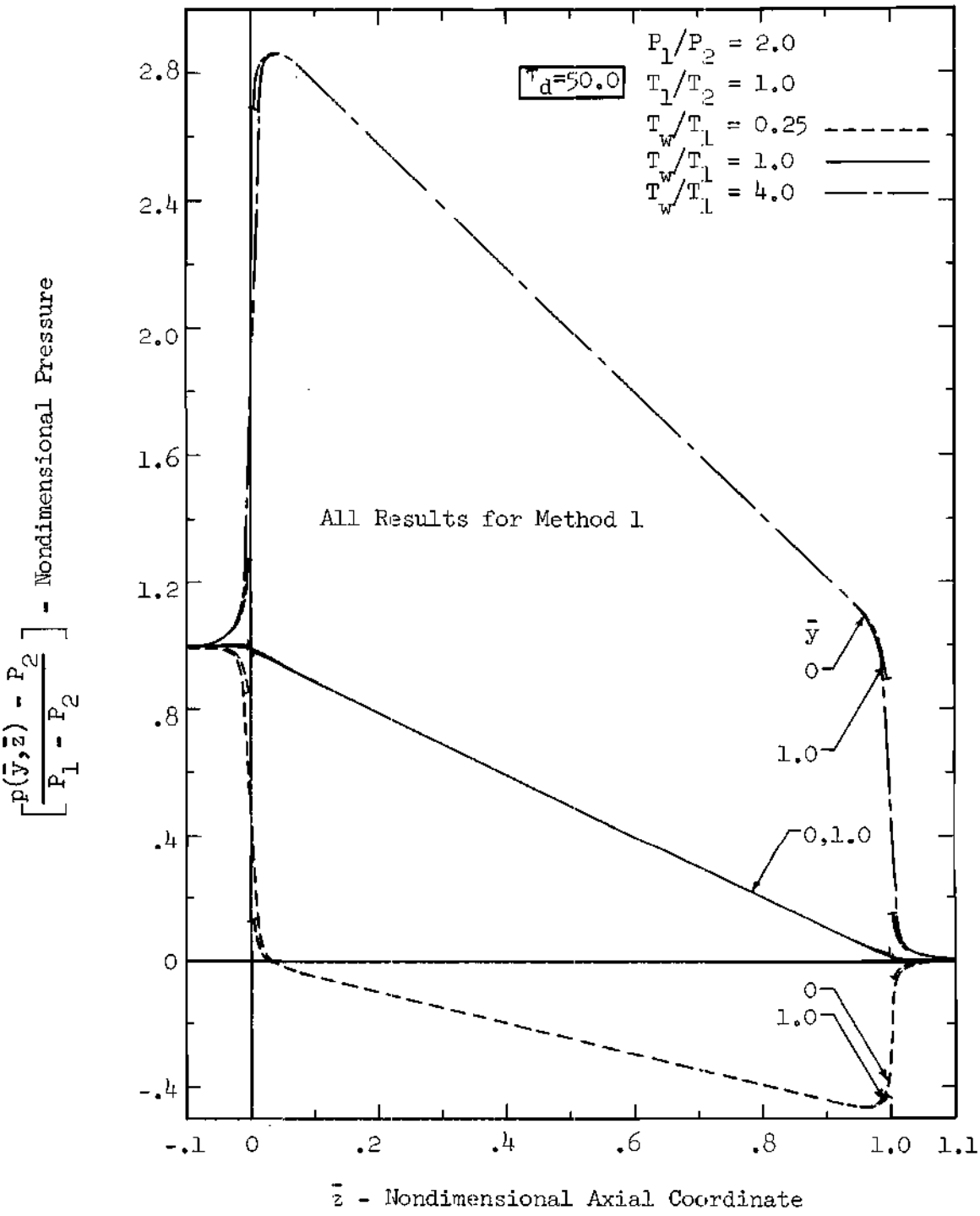

Figure 35. Nondimensional Pressure for Free Molecular Flow Through a Circular Tube for τ_d = 50.0, P_1/P_2 = 2.0, T_1/T_2 = 1.0, and T_w/T_1 = 0.25, 1.0, 4.0.

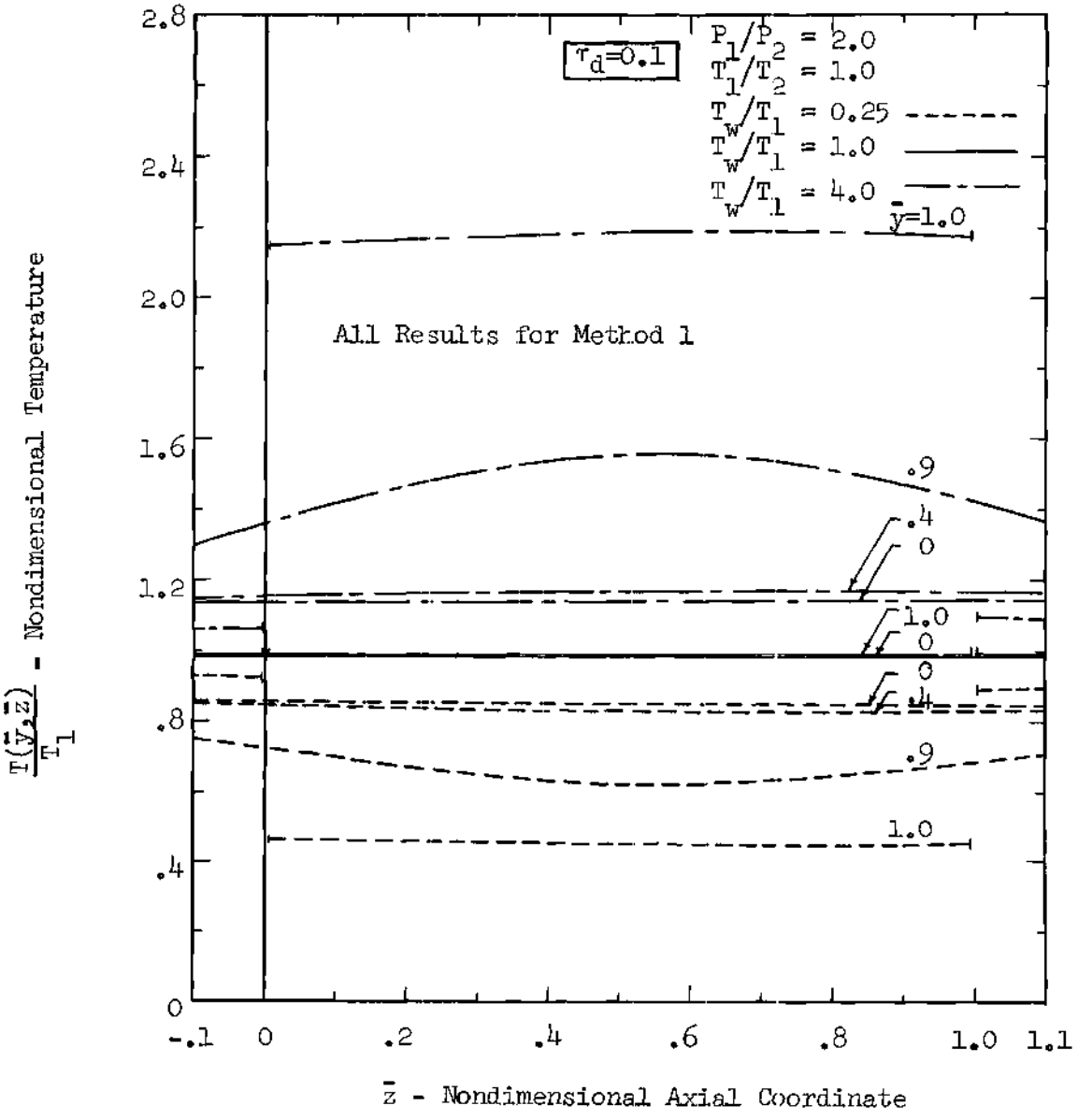

Figure 36. Nondimensional Temperature for Free Molecular Flow Through a Circular Tube for τ_d = 0.1, P_1/P_2 = 2.0, T_1/T_2 = 1.0, and T_w/T_1 = 0.25, 1.0, 4.0.

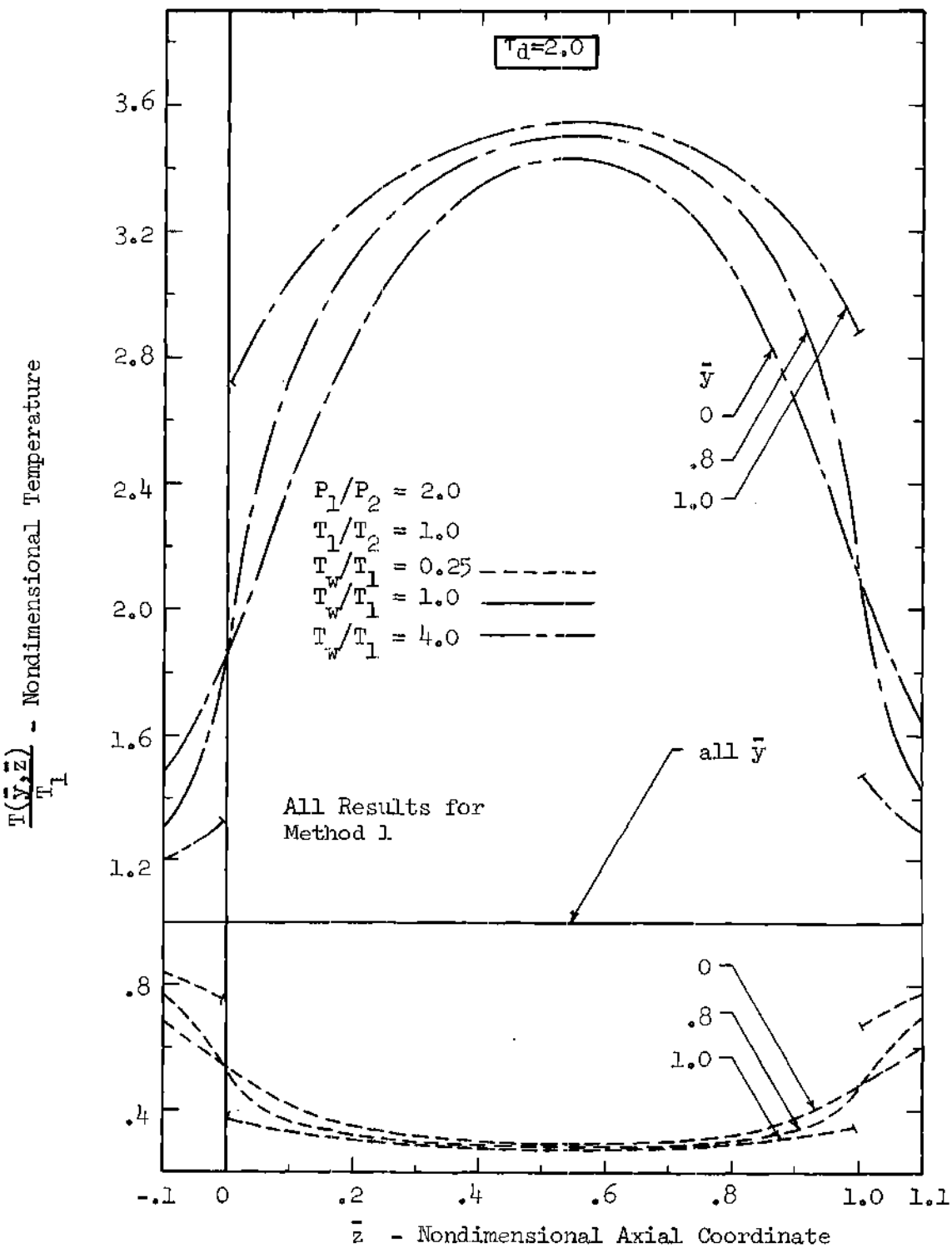

Figure 37. Nondimensional Temperature for Free Molecular Flow Through a Circular Tube for τ_d = 2.0, P_1/P_2 = 2.0, T_1/T_2 = 1.0, and T_w/T_1 = 0.25, 1.0, 4.0.

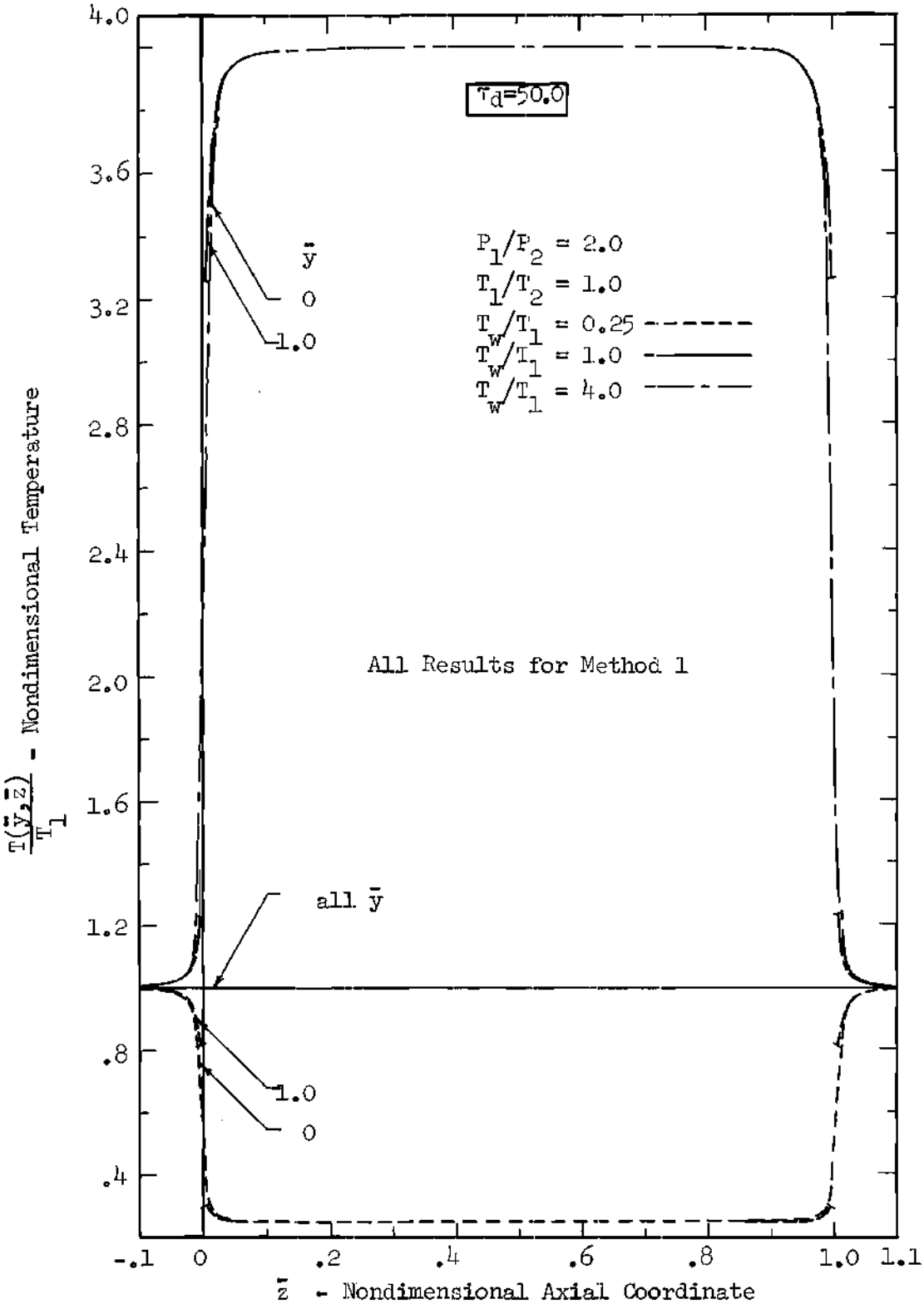

Figure 38. Nondimensional Temperature for Free Molecular Flow Through a Circular Tube for τ_d = 50.0, P_1/P_2 = 2.0, T_1/T_2 = 1.0, and T_w/T_1 = 0.25,1.0,4.0.

temperature is normalized with the common tank temperature. Thus, both upstream and downstream limits are unity. Again, the effects of wall temperature and length-to-diameter ratio are qualitatively the same as discussed for the two dimensional case of Chapter II. It might be noted that as expected a definite temperature jump occurs at the tube wall for all cases.

Although the results for Method 2 are not presented, a comparison with the results of Method 1 revealed that excellent results can be obtained for the density, pressure, and temperature for a linear wall flux over the entire channel length. The agreement was within one per cent for length-to-diameter ratios of 0.1, 2.0, 10.0, and 50.0. The largest discrepencies occurred for $\tau_d = 10.0$. As in the two dimensional case, the temperature results were essentially identical.

Shear Stress

Results for the wall shear stress, as determined by Method 1, are presented in Figure 39 for $\tau_d = 0.1$, 2.0, and 50.0, $P_1/P_2 = 2.0$, $T_1/T_2 = 1.0$, and $T_w/T_1 = 0.25$, 1.0, and 4.0. The shear stress has been nondimensionalized with the upstream pressure. The dependency of the shear stress on wall temperature is quite strong. For small τ_d the wall shear stress is essentially constant. For very large τ_d the wall shear stress is again essentially constant for the major portion of the tube, but near the inlet and exit the variation is quite large.

As pointed out for the two dimensional case, the shear stress is very sensitive to the variation of the vertical velocity. Therefore, the shear stress results of Method 2 are not expected to be in as good

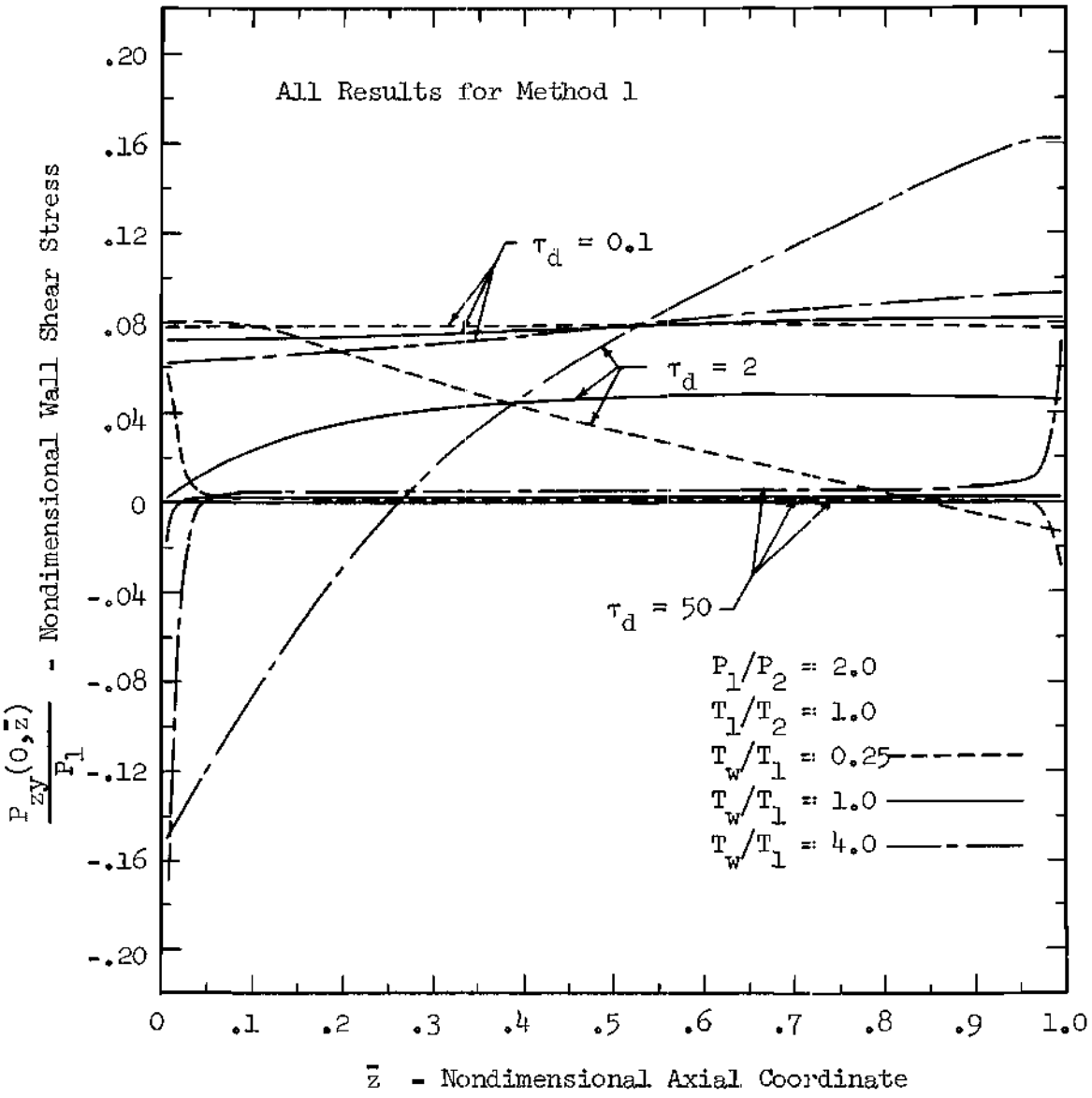

Figure 39. Comparison of Wall Shear Stress for Free Molecular Flow Through Circular Tubes of τ_d = 0.1, 2.0, and 50.0 for P_1/P_2 = 2.0, T_1/T_2 = 1.0, T_w/T_1 = 0.25, 1.0, and 4.0.

agreement with the results of Method 1 as for the pressure and temperature. Although the results of Method 2 are not presented, a comparison with the results of Method 1 for the wall shear stress showed that the differences were largest for the case of $\tau_d = 10$. The maximum difference in per cent for $T_w/T_1 = 0.25$, 1.0, and 4.0 was approximately five.

Comparison with Experiment

An immense volume of results has been obtained for the measured average flow rate through circular tubes for conditions approaching free molecular conditions. As discussed in Chapter II, the experimental results of Dong [14] have been chosen for a comparison between theory and experiment. Again it should be pointed out, however, that a final verification of the comparison with experiment should be based on measurements of local flow properties and not averaged results.

The apparatus of Dong's experiment for the rectangular channel was discussed in Chapter II. The physical set-up is essentially the same except that now a circular tube of 3.64 cm.-radius and 10.5 ft-length is inserted in place of the rectangular channel. The pressure was again monitored at two points a distance of 5.005 ft. apart in the center of the tube. In order to compare with experiment the pressure was assumed to vary linearly over the entire tube length. Since $\tau_d = 44$ for these results, a comparison with Figure 35 for $\tau_d = 50.0$ offers justification for this assumption. Nondimensionalizing the experimentally measured average flow rates with the theoretical free molecular

limit of Figure 25, $\Lambda_{F.M.}(\tau_d) = 0.027$, the results are presented in Figure 40 for a large range of δ, the inverse Knudsen number. The comparison with the experimental values, which appear to have reached a constant value for δ slightly less than unity, is very good.

Comparison of the local flux for flow at large Knudsen numbers downstream of short circular tubes as predicted by the free molecular theory and measured in experiments has been made by Gadamer [24] and Cook and Richley [25]. These works have already been discussed in Chapter I, and the comparison of the experimental and free-molecular results is fair, in general, even for upstream Knudsen numbers which are normally considered well in the transition region. It is precisely this type of comparison which is needed for more general problems in order to establish the range of validity of the free molecular solutions for internal flow problems.

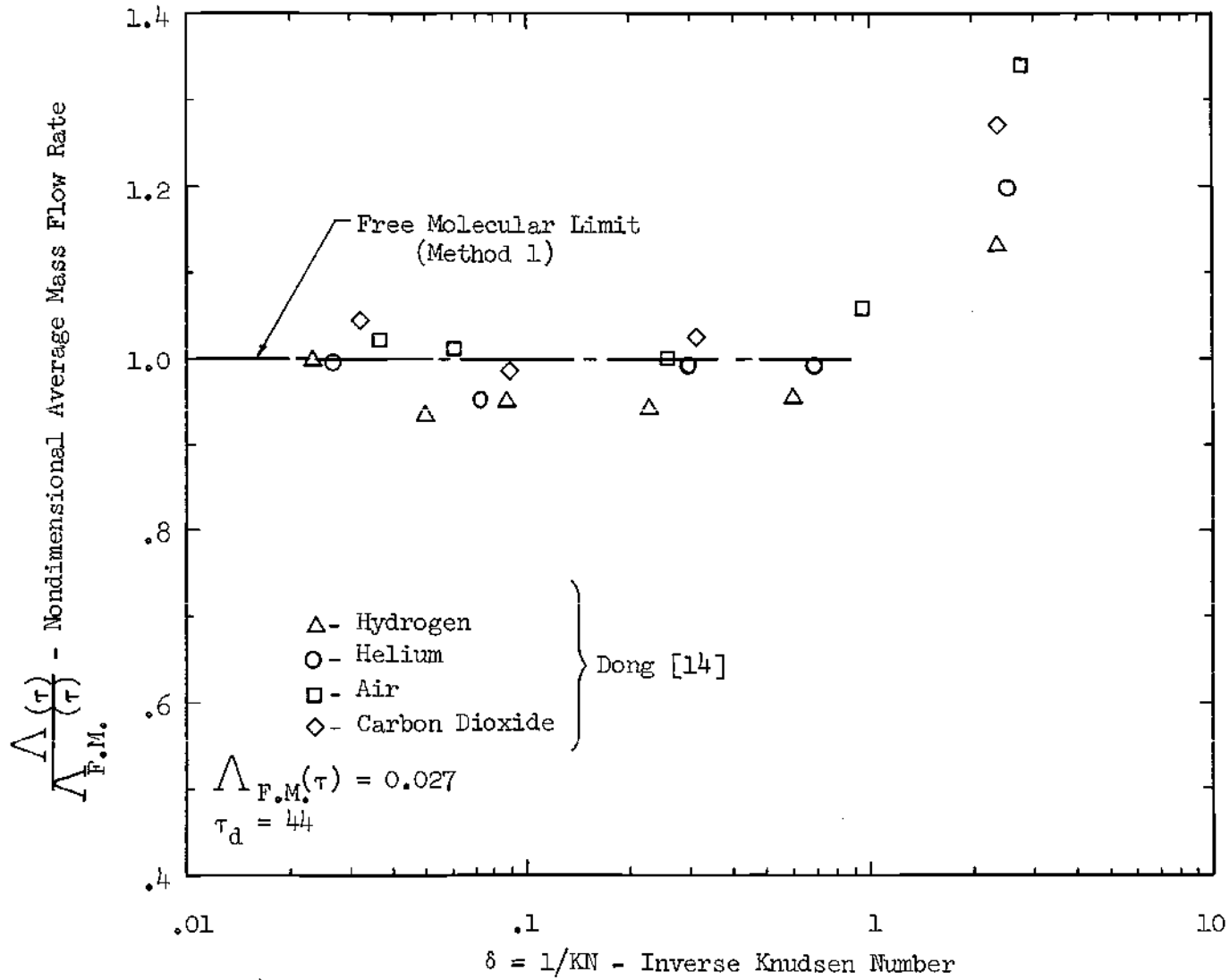

Figure 40. Comparison of Circular Tube Theoretical Value for Free Molecular Average Flow Rate with Experimental Data from Dong [14] for the Flow of Several Gases Through a Circular Tube.

CHAPTER IV

NEARLY-FREE MOLECULAR FLOW THROUGH A TWO DIMENSIONAL SLIT FOR ARBITRARY PRESSURE RATIO

In this chapter the iterative method of Willis [4] is used to determine the local and average mass flow rates for nearly-free molecular flow through a two dimensional slit for arbitrary pressure ratio. As discussed in Chapter I, the free molecular solution is required in order to determine the results for the nearly-free molecular problem via the iterative method. For the problem considered here, the free molecular solution was obtained as a special case from the general solution presented in Chapter II for the two dimensional channel.

Statement of the Problem

The physical problem consists of the flow of gas between two reservoirs which, respectively, contain gas in equilibrium at P_1, T_1 and P_2, T_2, as shown in Figure 41. The opening between the two reservoirs is in the form of a two dimensional slit and the walls separating the two reservoirs are of infinitesimal thickness. For all practical considerations the thickness of the walls is assumed zero; their only purpose is the separation of the two reservoirs. Although the reservoirs are assumed infinite, for all practical purposes they may be finite so long as their dimensions are very large in comparison to the slit height. The walls of each individual reservoir are assumed to be diffuse reflectors and at the same temperature as the gas in that reservoir.

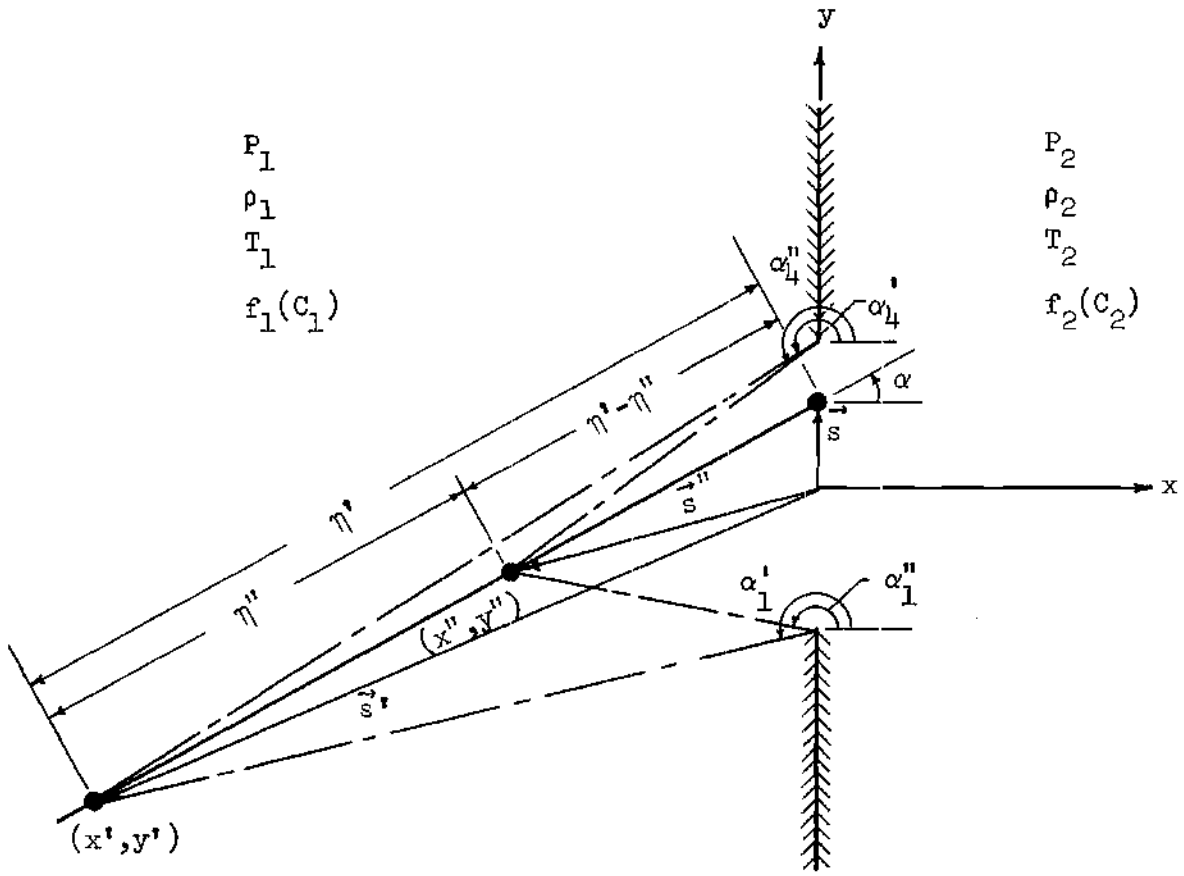

Two Dimensional Slit

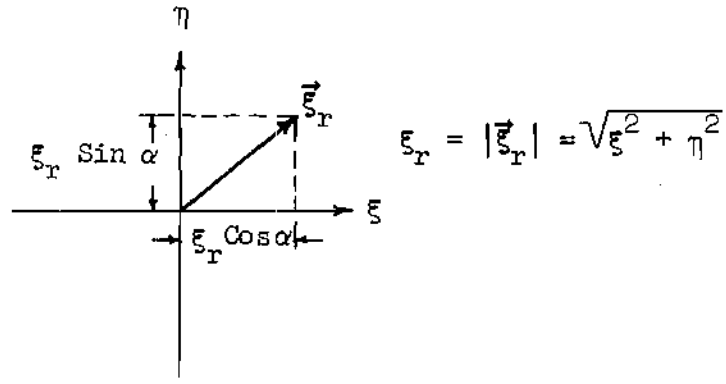

Velocity Coordinate System

Figure 41. Schematic of the Two Dimensional Slit and Illustration of Velocity Coordinate System.

The velocity distribution function in each reservoir is assumed to be the Maxwellian distribution function corresponding to the appropriate reservoir densities and temperatures. However, forthe purpose of the theoretical analysis the gas is assumed to have these equilibrium distribution functions at infinity.

The analysis presented in this chapter is specifically designed for the mean free path of the gas approximately equal to or larger than the slit height. Since this is the only finite physical dimension appearing in the problem, it is apparent that the Knudsen number for this problem should bebased on the slit height.

Formulation of Problem

In the following sections the boundary conditions are presented, the iterative form of the Boltzmann equation used for this analysis is derived, and the corresponding forms for the local and average mass flow rates are determined for points in the plane of the slit for an isothermal system (i.e., $T_1 = T_2$).

Boundary Conditions

As discussed in the preceding section, the boundary conditions for the velocity distribution function are specified as Maxwellian. The corresponding densities and temperatures required for these equilibrium distribution functions are taken as the reservoir densities and temperatures. Thus, the equilibrium distribution functions for the boundary conditions are simply

$$f(\eta' = \infty, \alpha, \xi, \eta, \zeta) = f_1(\xi, \eta, \zeta) \equiv \frac{n_1}{(2\pi RT_1)^{3/2}} e^{-\frac{[\xi^2+\eta^2+\zeta^2]}{2RT_1}} \quad -\frac{\pi}{2} \leq \alpha \leq \frac{\pi}{2} \quad (1)$$

$$f(\eta' = \infty, \alpha, \xi, \eta, \zeta) = f_2(\xi, \eta, \zeta) \equiv \frac{n_2}{(2\pi RT_2)^{3/2}} e^{-\frac{[\xi^2+\eta^2+\zeta^2]}{2RT_2}} \quad \frac{\pi}{2} \leq \alpha \leq \frac{3\pi}{2} \quad (2)$$

where η' and α denote polar coordinates with origin at x = 0 and y, as shown in Figure 41, $f(\eta', \alpha, \xi, \eta, \zeta)$ is the velocity distribution function at the point η', α, and $f_1(\xi, \eta, \zeta)$ and $f_2(\xi, \eta, \zeta)$ are the Maxwellian distribution functions. The velocity components are again taken as ξ, η, and ζ in the x,y,and z directions, respectively, and n_1 and n_2 denote the number densities in the upstream and downstream tanks, respectively. The gas constant is given by R.

Referring to Figure 41 it is apparent that for points in the plane of the slit the velocity space is divided into two half-spaces. The effects of the upstream chamber on flow properties in the plane of the slit are confined to the half-space given by $-\frac{\pi}{2} \leq \alpha \leq \frac{\pi}{2}$, while the effects of the downstream chamber are confined to the half-space given by $\frac{\pi}{2} \leq \alpha \leq \frac{3\pi}{2}$.

Iterative Form of the Boltzmann Equation

The Boltzmann equation for steady state conditions with no external forces can be written in the following form for the two dimensional case if the total collision cross section is finite:

$$\vec{\xi}_r \cdot \frac{\partial f}{\partial \vec{s}} = - fD(f,\vec{\xi}_r) + P(f,\vec{\xi}_r) \tag{3}$$

where $f(\vec{s},\vec{\xi}_r)$ has been replaced with f for simplicity and represents the local distribution function, $\vec{s}$ is the spatial coordinate, $\vec{\xi}_r$ is the molecular velocity in the ξ - η plane, $P(f,\vec{\xi}_r)$ represents the production of molecules of velocity $\vec{\xi}_r$ due to collisions, and $fD(f,\vec{\xi}_r)$ represents the loss of molecules of this class due to collisions. The iterative scheme as proposed by Willis [4] is derived from equation (3). As represented by Willis the scheme is given by

$$\vec{\xi}_r \cdot \frac{\partial f^{(n+1)}}{\partial \vec{s}} = - f^{(n+1)} D(f^{(n)},\vec{\xi}_r) + P(f^{(n)},\vec{\xi}_r) \tag{4}$$

Thus, given the n-th iteration for the distribution function, the (n + 1)-th iteration can be obtained by solving the differential equation given by equation (4). For large Knudsen numbers (i.e., nearly-free molecular flow) the obvious choice of $f^{(n)}$ is the free molecular solution, which will be denoted by $f^{(o)}$ and referred to as the zero-th iteration.

Consider the solution of equation (4) for the (n + 1)-th iteration. By integrating along a path which coincides with the particle velocity direction, equation (4) can be expressed as a first order differential equation in $f^{(n+1)}$ with ξ_r, the magnitude of the molecular velocity in the ξ - η plane, as a parameter. Note that it has been

assumed that $f^{(n)}$ is specified and therefore $D(f^{(n)}, \vec{\xi}_r)$ and $P(f^{(n)}, \vec{\xi}_r)$ are known. Introducing an integrating factor the formal solution of equation (4) for $f^{(1)}$ becomes

$$f^{(1)}(\vec{s},\vec{\xi}_r) = f(\vec{s}_o,\vec{\xi}_r) + \int_{\vec{s}_o}^{\vec{s}} \frac{ds'}{\xi_r} \Big[P^{(o)}(\vec{s}') - f(\vec{s}_o,\vec{\xi}_r) D^{(o)}(\vec{s}') \Big] e^{-\int_{\vec{s}'}^{\vec{s}} \frac{D^{(o)}(\vec{s}'')}{\xi_r} ds''} \tag{5}$$

where ds' and ds" are differential quantities measured along the line specified by the angle α, and $P^{(o)}(\vec{s}')$ and $D^{(o)}(\vec{s}')$ are shorthand notation for $P(f^{(o)}, \vec{\xi}_r)$ and $D(f^{(o)}, \vec{\xi}_r)$, respectively. The vectors $\vec{s}$, $\vec{s}'$, and $\vec{s}''$ are as shown in Figure 41, and $f(\vec{s}_o, \vec{\xi}_r)$ is the distribution function at the boundary point $\vec{s}_o$.

The calculation of $P^{(o)}(\vec{s}')$ and $D^{(o)}(\vec{s}')$ can be greatly simplified by replacing the Maxwell-Boltzmann collisional operator by the simple statistical operator suggested by Bhatnager, Gross, and Krook [38]. This model will be referred to as the B-G-K model in the following text. For this model $D^{(o)}(f,\vec{\xi}_r)$ and $P^{(o)}(f,\vec{\xi}_r)$ are given by the simple expressions

$$D^{(o)}(f,\vec{\xi}_r) = \nu n^o \tag{6}$$

$$P^{(o)}(f,\vec{\xi}_r) = \nu n^{o2} \left| \frac{h^o}{\pi} \right|^{3/2} e^{-h^o[\vec{\xi}_r - \vec{w}^o]^2} \tag{7}$$

where $h^o = (2RT^o)^{-1}$, ν is a constant, and n^o, $\vec{w}^o$, and T^o are the local number density, macroscopic velocity, and temperature, respectively. For the nearly-free molecular problem considered here, n^o, $\vec{w}^o$, and T^o are given by the free molecular solutions of Chapter II.

Introduce the following definitions:

$$N_i^o \equiv \frac{n^o}{n_i} \quad , \qquad B^o{}_i \equiv \frac{h^o}{h_i} \quad , \qquad \vec{c}_i \equiv h_i^{\frac{1}{2}} \vec{\xi}_r \quad , \tag{8}$$

$$c^2{}_i \equiv h_i \xi^2{}_r \quad , \qquad C^2{}_i = h_i [\xi^2{}_r + \zeta^2] \quad ,$$

and

$$\vec{W}_i^o \equiv h_i^{\frac{1}{2}} \vec{w}^o \quad , \qquad \delta_i \equiv \nu n_i h_i^{\frac{1}{2}} \frac{d}{2} \quad , \qquad h_i^{-\frac{1}{2}} \equiv \sqrt{2RT_i} \quad , \tag{9}$$

$$\eta' \equiv \frac{|\vec{s} - \vec{s}'|}{d} \quad , \qquad \eta'' \equiv \frac{|\vec{s}' - \vec{s}''|}{d}$$

where the subscript i is either 1 or 2 denoting the upstream and downstream tanks, respectively. The parameter δ_i is the inverse Knudsen number based on one-half the slit width. Substituting equations (6) through (9) into equation (5) and applying equation (5) for each of the boundary conditions given by equations (1) and (2), the following form for the first iteration of the distribution function is obtained:

$$f_i^{(1)}(\bar{y},\alpha,C_i) = f_i(C_i)\left\{1 - 2\,\delta_i \int_{\infty}^{0} \frac{d\eta'}{c_i} N^{\circ}_i(\eta',\alpha)\left[N^{\circ}_i(\eta',\alpha)B^{\circ}_i(\eta',\alpha)\right]^{3/2} \cdot \right. \quad (10)$$

$$\left. e^{-B^{\circ}_i(\eta',\alpha)[\vec{c}_i - \vec{W}^{\circ}_i(\eta',\alpha)]^2 + C^2_i} - 1\right] e^{-2\,\delta_i \int_0^{\eta'} \frac{N^{\circ}_i(\eta'',\alpha)}{c_i}\, d\eta''}\Bigg\}$$

where $i = 1$ for $-\frac{\pi}{2} \leq \alpha \leq \frac{\pi}{2}$ and $i = 2$ for $\frac{\pi}{2} \leq \alpha \leq \frac{3\pi}{2}$. It should be noted that the functions $N^{\circ}_i(\eta',\alpha)$, $B^{\circ}_i(\eta',\alpha)$ and $\vec{W}^{\circ}_i(\eta',\alpha)$ depend on the nondimensional spatial variable $\bar{y}$, but the dependency has been omitted for simplicity in writing the equation. There is no dependency on x since only points in the plane of the slit are considered. The equilibrium distribution functions for the boundary conditions, as given by equations (1) and (2), are denoted by $f_i(C_i)$ for $i = 1$ and $i = 2$, respectively. Equation (10) can be expressed in terms of the Reynolds number by introducing the Chapman-Enskog viscosity based on the B-G-K model into the definition of Reynolds number, and simplifying the resulting expression by introducing δ_i of equation (9). The constant ν appearing in the definition of δ_i is obtained by the method used by Narasimha [21]. This method consists of equating the number of collisions per unit volume per unit time as obtained for the Maxwellian distribution function to the same quantity as predicted by the B-G-K model. Thus, the Reynolds number can be expressed as

$$Re_i = 2\sqrt{2}\,\delta_i \quad (11)$$

and equation (10) in terms of Reynolds number becomes

$$f_i^{(1)}(\bar{y},\alpha,C_i) = f_i(C_i)\left\{1 + \frac{Re_i}{\sqrt{2}}\int_0^{\infty}\frac{d\eta'}{c_i}\, N^{\circ}{}_i(\eta',\alpha)\left[N^{\circ}{}_i(\eta',\alpha)B^{\circ}{}_i(\eta',\alpha)\right]^{3/2}\cdot(12)\right.$$

$$\left. e^{-B^{\circ}{}_i(\eta',\alpha)[\vec{c}_i - \vec{W}^{\circ}{}_i(\eta',\alpha)]^2 + C^2{}_i} - 1\right] e^{-\frac{Re_i}{\sqrt{2}}\int_0^{\eta'}\frac{N^{\circ}{}_i(\eta'',\alpha)}{c_i}\,d\eta''}\right\}$$

Since moments of equation (12) are of interest, a further simplification can be made by integrating the molecular velocity component in the z-direction over the full range (i.e., $-\infty$ to $+\infty$). Defining

$$F_i^{(1)}(\bar{y},\alpha,c_i) \equiv \frac{1}{\sqrt{\pi}}\int_{-\infty}^{\infty} f^{(1)}{}_i(\bar{y},\alpha,C_i)h^{\frac{1}{2}}{}_i\, d\zeta \qquad (13)$$

$$F_i(c_i) \equiv \frac{n_i}{(2\pi RT_i)^{3/2}}\, e^{-C^2{}_i} \qquad (14)$$

and noting that

$$\int_{-\infty}^{\infty} e^{-ax^2}\, dx = \sqrt{\frac{\pi}{a}} \qquad (15)$$

then equation (12) can be written as follows:

$$F_i^{(1)}(\bar{y},\alpha,c_i) = F_i(c_i)\left\{1 + \frac{Re_i}{\sqrt{2}}\int_0^{\infty}\frac{d\eta'}{c_i}\,N_i^{o}(\eta',\alpha)\left[N^{o}{}_i(\eta',\alpha)B^{o}{}_i(\eta',\alpha)\cdot\right.\right. \quad (16)$$

$$\left.\left. e^{-B_i^{o}(\eta',\alpha)[c_i^2-2c_i\cdot\vec{W}_i^{o}(\eta',\alpha)+W_i^{o}(\eta',\alpha)^2]} + c^2{}_{i-1}\right]e - \frac{Re_i}{\sqrt{2}}\int_0^{\eta'}\frac{N_i^{o}(\eta'',\alpha)}{c_i}\,d\eta''\right\}$$

Equation (16) can now be applied directly to determine the local mass flow rate from the appropriate moment.

Local and Average Mass Flow Rate

The local flow rate can be expressed as follows from its definition:

$$\dot{m}^{(1)}(\bar{y}) \equiv n^{(1)}(o,\bar{y})u^{(1)}(o,\bar{y}) \equiv \int_{-\infty}^{\infty}\int\int \xi f^{(1)}(\bar{y},\xi,\eta,\zeta)\,d\xi d\eta d\zeta = \sqrt{\pi}\int_{-\infty}^{\infty}\int \xi F^{(1)}(\bar{y},\xi,\eta)d\xi d\eta \quad (17)$$

where $f^{(1)}(\bar{y},\xi,\eta,\zeta)$ and $F^{(1)}(\bar{y},\xi,\eta)$ with no subscript denote the complete first iteration, which consists of $f_i^{(1)}(\bar{y},\alpha,C_i)$ or $F_i^{(1)}(\bar{y},\alpha,c_i)$ for $i = 1$ and $i = 2$. Thus, in cylindrical velocity coordinates, as illustrated in Figure 41, the local flow rate becomes

$$\dot{m}^{(1)}(\bar{y}) = \sqrt{\pi}\left[h_1^{-2}\int_0^{\infty}\int_{-\frac{\pi}{2}}^{\frac{\pi}{2}} F_1^{(1)}(\bar{y},\alpha,c_1)c_1^{2}\,\mathrm{Cos}\,\alpha\,d\alpha dc_1 + \right. \quad (18)$$

$$h_2^{-2} \int_0^{\infty} \int_{\frac{\pi}{2}}^{\frac{3\pi}{2}} F_2^{(1)}(\bar{y},\alpha,c_2) c_2^2 \cos\alpha \, d\alpha dc_2 \Big]$$

Introducing the definitions,

$$\dot{m}_1^{(1)}(\bar{y}) \equiv \sqrt{\pi}\, h_1^{-2} \int_0^{\infty} \int_{-\frac{\pi}{2}}^{\frac{\pi}{2}} F_1^{(1)}(\bar{y},\alpha,c_1) c_1^2 \cos\alpha \, d\alpha dc_1 \qquad (19)$$

and

$$\dot{m}_2^{(1)}(\bar{y}) \equiv \sqrt{\pi}\, h_2^{-2} \int_0^{\infty} \int_{\frac{\pi}{2}}^{\frac{3\pi}{2}} F_2^{(1)}(\bar{y},\alpha,c_2) c_2^2 \cos\alpha \, d\alpha dc_2 \qquad (20)$$

equation (18) for the local flow rate becomes

$$\dot{m}^{(1)}(\bar{y}) = \dot{m}_1^{(1)}(\bar{y}) + \dot{m}_2^{(1)}(\bar{y}) \qquad (21)$$

Consider the evaluation of $\dot{m}_1^{(1)}(\bar{y})$. Substituting equation (16) for i = 1 into equation (19) and performing the necessary integrations the following form of $\dot{m}_1^{(1)}(\bar{y})$ is obtained:

$$\dot{m}_1^{(1)}(\bar{y}) = \dot{m}_1^{f.m.} \Big\{ 1 + \frac{2Re_1}{\sqrt{2\pi}} \int_0^{\infty} d\eta' \int_{-\frac{\pi}{2}}^{\frac{\pi}{2}} \cos\alpha \, N_1^{\circ}(\eta',\alpha) d\alpha \Big[N_I^{\circ}(\eta',\alpha) B_1^{\circ}(\eta',\alpha) \cdot \qquad (22)$$

$$\int_0^\infty e^{-B^\circ_1(\eta',\alpha)[c_1^2 - 2\vec{c}_1 \cdot \vec{W}_1^\circ(\eta',\alpha) + \vec{W}_1^\circ(\eta',\alpha)^2]} \cdot e^{-\frac{Re_1}{\sqrt{2}} \int_0^{\eta'} \frac{N^\circ_1(\eta'',\alpha)}{c_i} d\eta''} \cdot$$

$$c_1 dc_1 - \int_0^\infty e^{-c_1^2} e^{-\frac{Re_1}{\sqrt{2}} \int_0^{\eta'} \frac{N^\circ_1(\eta'',\alpha)}{c_1} d\eta''} c_1 dc_1 \Big] \Big\}$$

where $\dot{m}_1^{f.m.}$ represents the local flow rate under free molecular conditions and is given by $n_1/2\sqrt{\pi}\, h_1^{1/2}$. Introduce the following definitions:

$$\bar{c}_1 \equiv \sqrt{B^\circ_1(\eta',\alpha)}\; c_1 \tag{23}$$

$$b_1 \equiv \sqrt{B^\circ_1(\eta',\alpha)} \left[U^\circ_1(\eta',\alpha) \operatorname{Cos} \alpha + V^\circ_1(\eta',\alpha) \operatorname{Sin} \alpha \right] \tag{24}$$

$$a_1 \equiv \frac{Re_1 \sqrt{B^\circ_1(\eta',\alpha)}}{\sqrt{2}} \int_0^{\eta'} N^\circ_1(\eta'',\alpha) d\eta'' \tag{25}$$

$$a_2 \equiv \frac{Re_1}{\sqrt{2}} \int_0^{\eta'} N^\circ_1(\eta'',\alpha) d\eta'' \tag{26}$$

where $U_1^\circ(\eta',\alpha)$ and $V_1^\circ(\eta',\alpha)$ are the nondimensional x and y components of the velocity vector $\vec{W}_1{}^\circ(\eta',\alpha)$. Equation (22) for $\dot{m}_1^{(1)}(\bar{y})$ can now be written as

$$\dot{m}_1^{(1)}(\vec{y}) = \dot{m}_1^{f.m.} \left\{ 1 + \frac{2Re_1}{\sqrt{2\pi}} \int_0^\infty d\eta' \int_{-\frac{\pi}{2}}^{\frac{\pi}{2}} \operatorname{Cos} \alpha\, N^\circ_1(\eta',\alpha) d\alpha \left[N^\circ_1(\eta',\alpha) \cdot \right. \right. \tag{27}$$

$$e^{-B^{\circ}_1(\eta',\alpha)[U^{\circ}_1(\eta',\alpha)^2 + V^{\circ}_1(\eta',\alpha)^2]} \cdot \int_0^{\infty} e^{\left[-\bar{c}_1^{\,2} + 2b_1\bar{c}_1 - \frac{a_1}{\bar{c}_1}\right]} \bar{c}_1 d\bar{c}_1$$

$$- \int_0^{\infty} e^{\left[-c_1^{\,2} - \frac{a_2}{c_1}\right]} c_1 dc_1 \Big] \Big\}$$

Finally, defining the following,

$$G_1(\eta',\alpha) \equiv \int_0^{\infty} \bar{c}_1 \, e^{-\left[\bar{c}_1^{\,2} - 2\, b_1\bar{c}_1 + \frac{a_1}{\bar{c}_1}\right]} d\bar{c}_1 \tag{28}$$

$$G_2(\eta',\alpha) \equiv \int_0^{\infty} c_1 e^{-\left[c_1^{\,2} + \frac{a_2}{c_1}\right]} dc_1 \tag{29}$$

$$H_1(\bar{y},\eta',\alpha) \equiv N^{\circ}_1(\eta',\alpha)\Big[N^{\circ}_1(\eta',\alpha)G_1(\eta',\alpha)e^{-B^{\circ}_1(\eta',\alpha)[U^{\circ}_1(\eta',\alpha)^2+V^{\circ}_1(\eta',\alpha)^2]} \tag{30}$$

$$- G_2(\eta',\alpha) \Big]$$

the local flow rate of equation (27) can be written in the following final form:

$$\dot{m}_1^{(1)}(\bar{y}) = \dot{m}_1^{f.m.} \left[1 + \frac{2Re_1}{\sqrt{2\pi}} \int_{-\frac{\pi}{2}}^{\frac{\pi}{2}} \text{Cos } \alpha \, d\alpha \int_0^{\infty} H_1(\bar{y},\eta',\alpha) d\eta' \right] \tag{31}$$

The corresponding expression for $\dot{m}_2^{(1)}(\bar{y})$ can be obtained directly from the results of $\dot{m}_1^{(1)}(\bar{y})$ for the isothermal case. Thus, since $T_1 = T_2$

$$Re_2 = \left(\frac{P_2}{P_1} \right) Re_1 \tag{32}$$

and

$$N^{\circ}{}_2(\eta',\alpha) = \left(\frac{P_1}{P_2} \right) N^{\circ}{}_1(\eta',\alpha) \tag{33}$$

It is apparent that equations (23) through (26) and equations (28) and (29) are identical to the corresponding expressions written in terms of the downstream properties. Following the same procedure as outlined above for obtaining $\dot{m}_1^{(1)}(\bar{y})$, the contribution to the local flow rate given by equation (20) can be expressed as follows:

$$\dot{m}_2^{(1)}(\bar{y}) = - \dot{m}_2^{f.m.} \left[1 - \frac{2Re_1}{\sqrt{2\pi}} \int_{\frac{\pi}{2}}^{\frac{3\pi}{2}} \text{Cos } \alpha \, d\alpha \int_0^{\infty} H_2(\bar{y},\eta',\alpha) d\eta' \right] \tag{34}$$

where

$$H_2(\bar{y},\eta',\alpha) \equiv N_1^{\circ}(\eta',\alpha) \left[\frac{P_2}{P_1} \cdot N_1^{\circ}(\eta',\alpha) G_1(\eta',\alpha) e^{-B_1^{\circ}(\eta',\alpha)[U_1^{\circ}(\eta',\alpha)^2 + V^{\circ}{}_1(\eta',\alpha)^2]} - G_2(\eta',\alpha) \right] \tag{35}$$

and $\dot{m}_2^{f.m.}$ is the free-molecular local flow rate and is given by $n_2/2\sqrt{\pi}\, h_2^{1/2}$.

Once equations (31) and (34) have been evaluated for a given pressure ratio and Reynolds number for specified points across the slit, the total local flow rate at each of these points can be obtained directly from equation (21). The average mass flow rate through the slit is then obtained from the following definition:

$$\overline{\dot{m}^{(1)}(\bar{y})} \equiv \int_0^1 \dot{m}^{(1)}(\bar{y})\, d\bar{y} = 2\int_0^{1/2} \dot{m}^{(1)}(\bar{y})\, d\bar{y} \qquad (36)$$

Free Molecular Results

Before any results can be obtained, however, the free molecular solution for flow through a two dimensional slit is needed. This solution can be obtained directly from the results of Chapter II. For the isothermal case the results for the nondimensional density, temperature, and velocity components can be written as follows:

$$N_1^{\circ}(\eta',\alpha) = \left(1 - \frac{P_2}{P_1}\right)\left[1 - \frac{(\alpha_4 - \alpha_1)}{2\pi}\right] + \frac{P_2}{P_1} \quad \text{for } \frac{\pi}{2} \le \alpha_4 \le 2\pi \qquad (37)$$

$$N_1^{\circ}(\eta',\alpha) = \left(1 - \frac{P_2}{P_1}\right)\left[-\frac{(\alpha_4 - \alpha_1)}{2\pi}\right] + \frac{P_2}{P_1} \quad \text{for } 0 \le \alpha_4 \le \frac{\pi}{2} \qquad (38)$$

$$N_1^{\circ}(\eta',\alpha)U_1^{\circ}(\eta',\alpha) = \frac{1}{4\sqrt{\pi}}\left(1 - \frac{P_2}{P_1}\right)[\text{Sin } \alpha_1 - \text{Sin } \alpha_4] \qquad (39)$$

$$N_1^{\circ}(\eta',\alpha)V_1^{\circ}(\eta',\alpha) = \frac{1}{4\sqrt{\pi}}\left(1 - \frac{P_2}{P_1}\right)[\text{Cos } \alpha_4 - \text{Cos } \alpha_1] \qquad (40)$$

$$B_1^o(\eta',\alpha) = \left\{ 1 - \frac{2}{3}\left[U_1^o(\eta',\alpha)^2 + V_1^o(\eta',\alpha)^2\right] \right\}^{-1} \tag{41}$$

The angles, α_1 and α_4, are, in general, functions of $\bar{y}$, η', and α. From Figure 41 it can be seen that the following relations are applicable:

$$\text{Tan } \alpha_1(\bar{y},\eta',\alpha) = \frac{\eta' \text{ Sin } \alpha - (\bar{y} + \frac{1}{2})}{\eta' \text{ Cos } \alpha} \tag{42}$$

$$\text{Tan } \alpha_4(\bar{y},\eta',\alpha) = \frac{\eta' \text{ Sin } \alpha - (\bar{y} - \frac{1}{2})}{\eta' \text{ Cos } \alpha} \tag{43}$$

The corresponding expressions for the angles specifying the point x", y", as shown in Figure 41, are

$$\text{Tan } \alpha_1(\bar{y},\eta'',\eta',\alpha) = \frac{(\eta' - \eta'') \text{ Sin } \alpha - (\bar{y} + \frac{1}{2})}{(\eta' - \eta'') \text{ Cos } \alpha} \tag{44}$$

$$\text{Tan } \alpha_4(\bar{y},\eta'',\eta',\alpha) = \frac{(\eta' - \eta'') \text{ Sin } \alpha - (\bar{y} - \frac{1}{2})}{(\eta' - \eta'') \text{ Cos } \alpha} \tag{45}$$

Computational Procedures

In order to determine the local mass flow rate, as given by equation (21), it is necessary to evaluate the integrals of equations (31) and (34). The integrands of these integrals are expressed in terms of the integrals $G_1(\eta', \alpha)$ and $G_2(\eta',\alpha)$, as given by equations (28) and (29).

The parameters b_1 and b_2 appearing in the functions $G_1(\eta',\alpha)$ and $G_2(\eta',\alpha)$ are in turn defined in terms of an integral over the density. In the following sections the methods used to evaluate these integrals, as well as the integrals for η' and α, are presented.

Evaluation of the Integrating Factor

Introducing equations (37) and (38) into the integrals of equations (25) and (26) and making use of equations (44) and (45) for the angles, the integral of of the integrating factor can be expressed as follows:

$$\int_0^{\eta'} N_1^o(\eta'',\alpha)d\eta'' = \left(1 - \frac{P_2}{P_1}\right)\left\{\eta' - \frac{1}{2\pi}\left[E(\eta',\alpha) - D(\eta',\alpha)\right]\right\} + \frac{P_2}{P_1}\eta' \quad (46)$$

for $-\frac{\pi}{2} \leq \alpha \leq \frac{\pi}{2}$,

$$\int_0^{\eta'} N_1^o(\eta'',\alpha)d\eta'' = \left(1 - \frac{P_2}{P_1}\right)\left\{ - \frac{1}{2\pi}\left[E(\eta',\alpha) - D(\eta',\alpha)\right]\right\} + \frac{P_2}{P_1}\eta' \quad (47)$$

for $\frac{\pi}{2} \leq \alpha \leq \frac{3\pi}{2}$, and

$$E(\eta',\alpha) \equiv \int_0^{\eta'} \text{Tan}^{-1}\left[\frac{(\eta' - \eta'')\ \text{Sin}\ \alpha - (\bar{y} - \frac{1}{2})}{(\eta' - \eta'')\ \text{Cos}\ \alpha}\right]d\eta'' \quad (48)$$

$$D(\eta',\alpha) \equiv \int_0^{\eta'} \text{Tan}^{-1}\left[\frac{(\eta' - \eta'')\text{Sin}\ \alpha - (\bar{y} + \frac{1}{2})}{(\eta' - \eta'')\ \text{Cos}\ \alpha}\right]d\eta'' \quad (49)$$

Performing the straightforward but rather tedious integrations of equations (48) and (49), the following expressions for $E(\eta', \alpha)$ and $D(\eta', \alpha)$ are obtained:

$$E(\eta', \alpha) = \frac{(\bar{y} - \frac{1}{2})}{2} \left\{ \cos\alpha \left[\mathrm{LN}\left|(\bar{y} - \tfrac{1}{2})^2\right| - \mathrm{LN}\left|[\eta' \sin\alpha - (\bar{y} - \tfrac{1}{2})]^2 + \eta'^2 \cos^2\alpha\right| \right] - 2 \sin\alpha \left[\tan^{-1}(\tan\alpha) + \tan^{-1}\left(\frac{\eta' - (\bar{y} - \frac{1}{2})\sin\alpha}{(\bar{y} - \frac{1}{2})\cos\alpha} \right) \right] \right\} + \eta' \tan^{-1}\left(\frac{\eta' \sin\alpha - (\bar{y} - \frac{1}{2})}{\eta' \cos\alpha} \right) \tag{50}$$

$$D(\eta', \alpha) = \frac{(\bar{y} + \frac{1}{2})}{2} \left\{ \cos\alpha \left[\mathrm{LN}\left|(\bar{y} + \tfrac{1}{2})^2\right| - \mathrm{LN}\left|[\eta' \sin\alpha - (\bar{y} + \tfrac{1}{2})]^2 + \eta'^2 \cos^2\alpha\right| \right] - 2 \sin\alpha \left[\tan^{-1}(\tan\alpha) + \tan^{-1}\left(\frac{\eta' - (\bar{y} + \frac{1}{2})\sin\alpha}{(\bar{y} + \frac{1}{2})\cos\alpha} \right) \right] \right\} + \eta' \tan^{-1}\left(\frac{\eta' \sin\alpha - (\bar{y} + \frac{1}{2})}{\eta' \cos\alpha} \right) \tag{51}$$

All arctangents appearing in equations (50) and (51) are principal-valued arctangents.

Evaluation of the Integral $\int_0^\infty x^n e^{-\left[bx - \frac{a}{x} - x^2\right]} dx$

The only integral appearing in equations (31) and (34) which offers more than routine difficulties is of the form given by the following definition:

$$I_n(a,b) \equiv \int_0^\infty x^n e^{\left[bx - \frac{a}{x} - x^2\right]} dx \tag{52}$$

Comparing equations (28) and (29) with equation (52) it can be seen that

$$G_1(\eta',\alpha) = I_1(a_1,b_1) \tag{53}$$

$$G_2(\eta',\alpha) = I_1(a_2,0) \tag{54}$$

For the case when $b = 0$ and $a \geq 0$ the integral of equation (52) can be evaluated with an error of less than $\pm 2 \times 10^{-6}$ by using the expressions given by Willis [39]. These were derived from the results of Abramowitz [40]. However, when $b \neq 0$ and $a \geq 0$ the integral is difficult to evaluate in general. Following the procedure outlined by Willis [41] and expanding the term e^{bx} in a Taylor series about zero, interchanging the summation and integration, and introducing the results for the case when $b = 0$, the following expression is obtained for $a \geq 0$ and $b \neq 0$:

$$I_n(a,b) = \sum_{r=0}^{\infty} \frac{b^r}{r!} F_{(n+r)}(a) \tag{55}$$

where

$$F_s(a) \equiv I_s(a,o) = \int_0^{\infty} x^s e^{\left[-\frac{a}{x} - x^2\right]} dx \tag{56}$$

Equation (55) was used to evaluate $I_n(a,b)$ for $0 \leq a \leq 20$ and $-2 \leq b \leq 2$, and the results were compared with the numerical results of Chahine and Narasimha [42] for n = 0, 1, and 2. The latter results are reported to be accurate to better than eight places. The comparison revealed the following:

(1) For $-1 < b < 1$ the results were in agreement within $\pm 2 \times 10^{-6}$ for all three values of n.

(2) For $-1.5 \leq b \leq -1.0$ the maximum error was $\pm 8 \times 10^{-6}$ for n = 0, 1, and 2.

(3) For $1.0 \leq b \leq 1.5$ the maximum errors were $+ 9 \times 10^{-6}$ for n = 0, $+ 2 \times 10^{-5}$ for n = 1, and $+ 4 \times 10^{-5}$ for n = 2.

(4) For $-2.0 \leq b < -1.5$ the maximum errors were $+ 3 \times 10^{-6}$ for n = 0, -5×10^{-6} for n = 1, and $+ 9 \times 10^{-6}$ for n = 2.

(5) For $1.5 < b < 2.0$ the maximum errors were $+ 1.5 \times 10^{-5}$ for n = 0, $+ 4 \times 10^{-5}$ for n = 1, and $+ 1 \times 10^{-4}$ for n = 2.

It should be noted that these maximum errors occurred only for a limited range of a and in general the results for the other values of a were still within $\pm$ 2 x 10^{-6}. It can also be seen that for the larger values of b the series of equation (55) is subject to round-off, and that the round-off affects the results for a positive b more than for an equal negative b.

For the problem considered here the range of b was $-2.0 < b < 1.2$. Therefore, the scheme discussed in the last paragraph was used to provide accurate results for the integral of equation (28).

Evaluation of Other Integrals

The integrations with respect to η' and α can be performed by numerical quadrature. It is convenient to use the Gauss-Laguerre quadrature for the η' integration and the regular Gauss quadrature for the integration with respect to α. In order to determine the number of points required to obtain accurate results by the numerical quadrature, the integrals of equations (31) and (34) were evaluated for pressure ratios of 2, 100, and infinity and upstream Reynolds numbers of 0.05, 1.0, and 6.4. The number of points taken for each quadrature was varied for each of these conditions and the numerical results compared. Based on this comparison the results for the integrals are considered accurate to within one-tenth of a per cent for all combinations of pressure ratios and Reynolds numbers considered herein.

The integrands of equations (31) and (34) were evaluated for a number of cases and the results plotted. It was found that the integrand, in general, for a given angle α had a peak which occurred

for small η' and then asymptotically approached zero for large η'. For small Reynolds numbers (i.e., close to free molecular conditions) it was found that the contribution of the integrand for large η' was quite significant, whereas for larger Reynolds numbers this contribution became insignificant. The contribution for small η' was always significant. Therefore, the integration with respect to η' was divided into two parts. For each pressure ratio and Reynolds number the range of η' within which the peaks of the integrand always fell was determined. A regular Gauss quadrature was used for this range and a Gauss-Laguerre quadrature was used to evaluate the remaining contribution of the integrand. Finally, the average flow rate was evaluated by applying a Simpson integration over the five points across half of the slit.

Results

Local and Average Mass Flow Rate

The results for the local mass flow rate are presented in Figures 42 through 44 for pressure ratios of 2, 100, and infinity and Reynolds numbers ranging from zero to 6.4. The local flow rate is nondimensionalized with the constant free molecular flow rate, $(\dot{m}_1^{f.m.}-\dot{m}_2^{f.m.})$, and is presented for only one-half of the slit. For very small Reynolds numbers the local flow rate is almost constant across the entire slit. For larger Reynolds numbers the local flow rate is still essentially constant near the center of the slit, but near the edge of the slit the local flow rate drops off rapidly. This drop in the local flow rate near the edge of the slit illustrates the shielding effect of the slit walls. The results for infinite pressure ratio, as

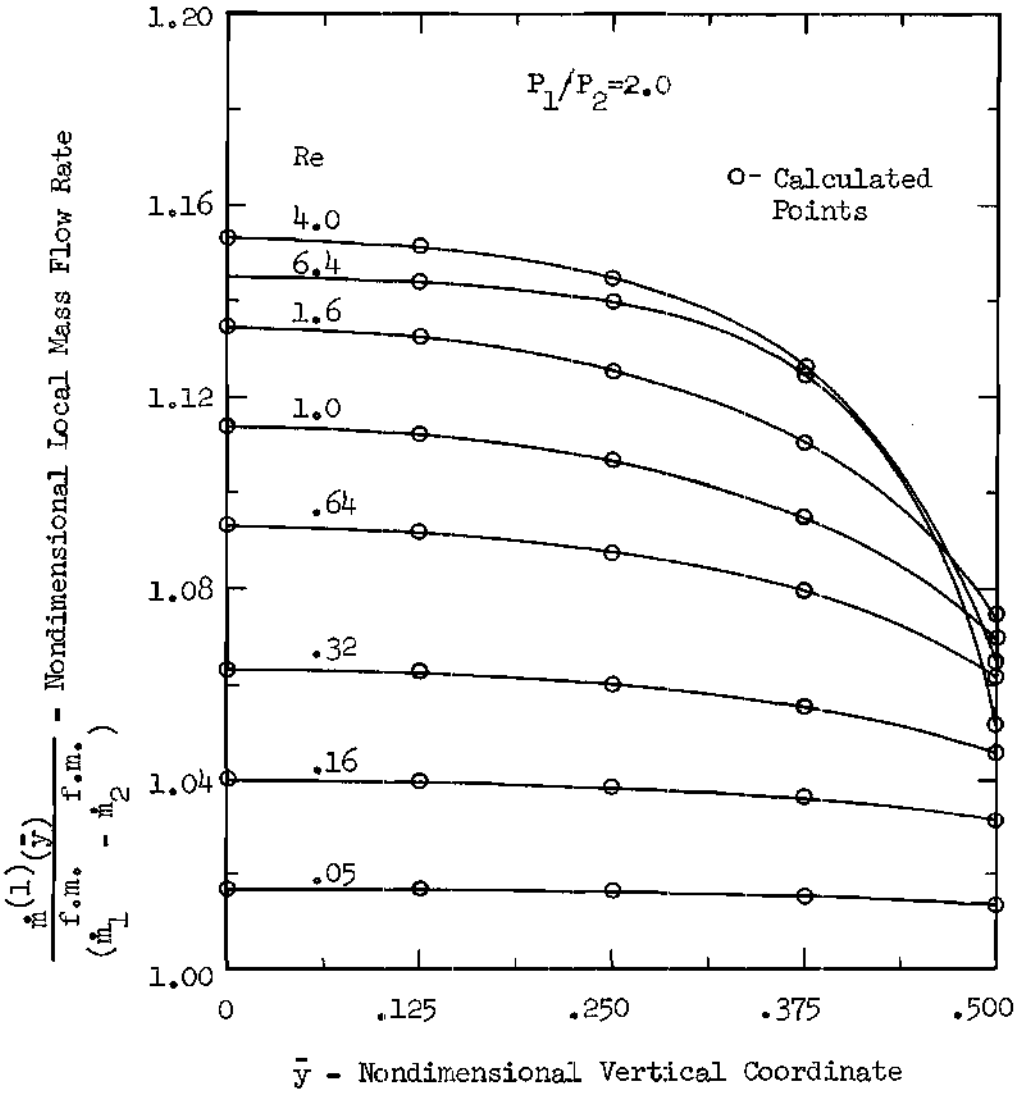

Figure 42. Nondimensional Local Mass Flow Rate for Several Points Across a Slit for Various Reynolds Numbers and a Pressure Ratio of 2.0.

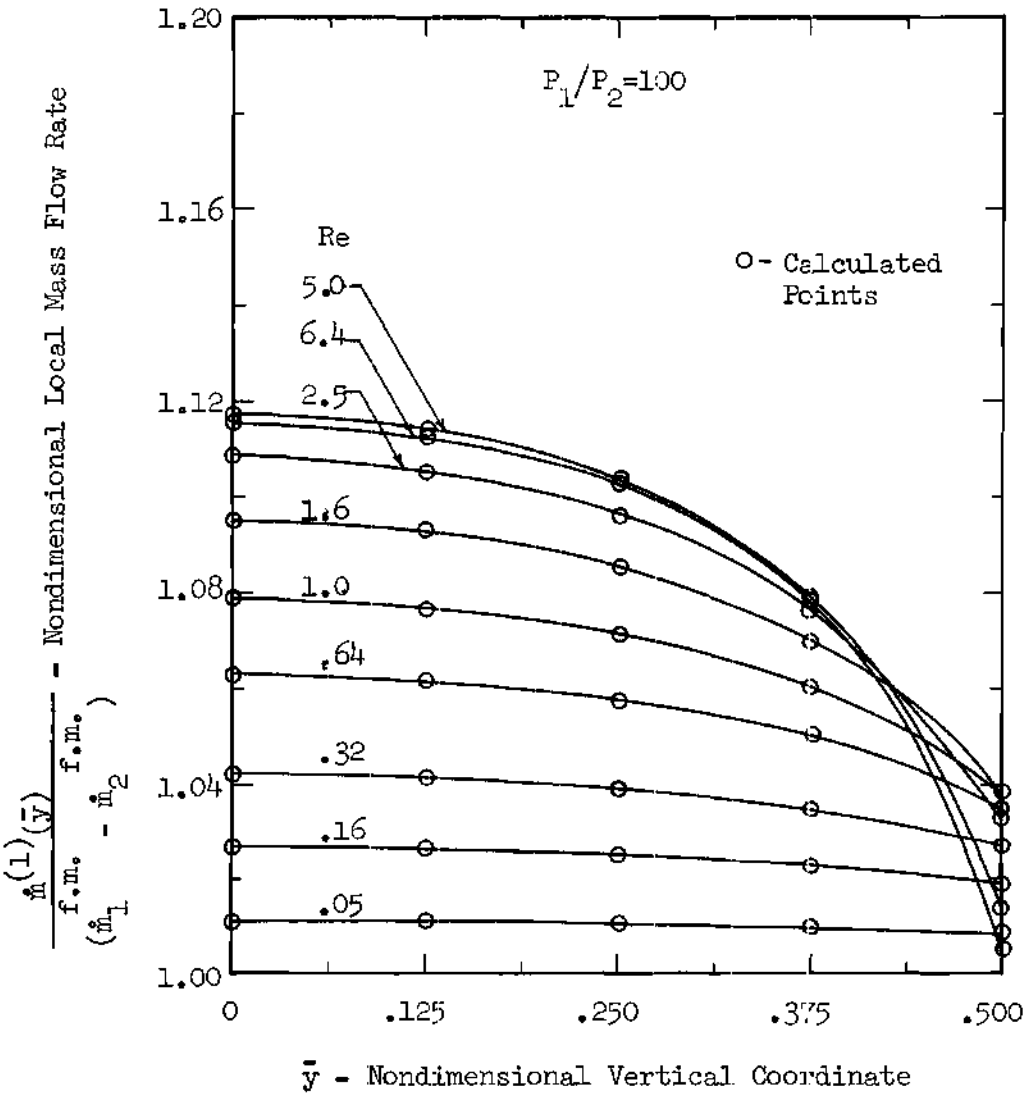

Figure 43. Nondimensional Local Mass Flow Rate for Several Points Across a Slit for Various Reynolds Numbers and a Pressure Ratio of 100.

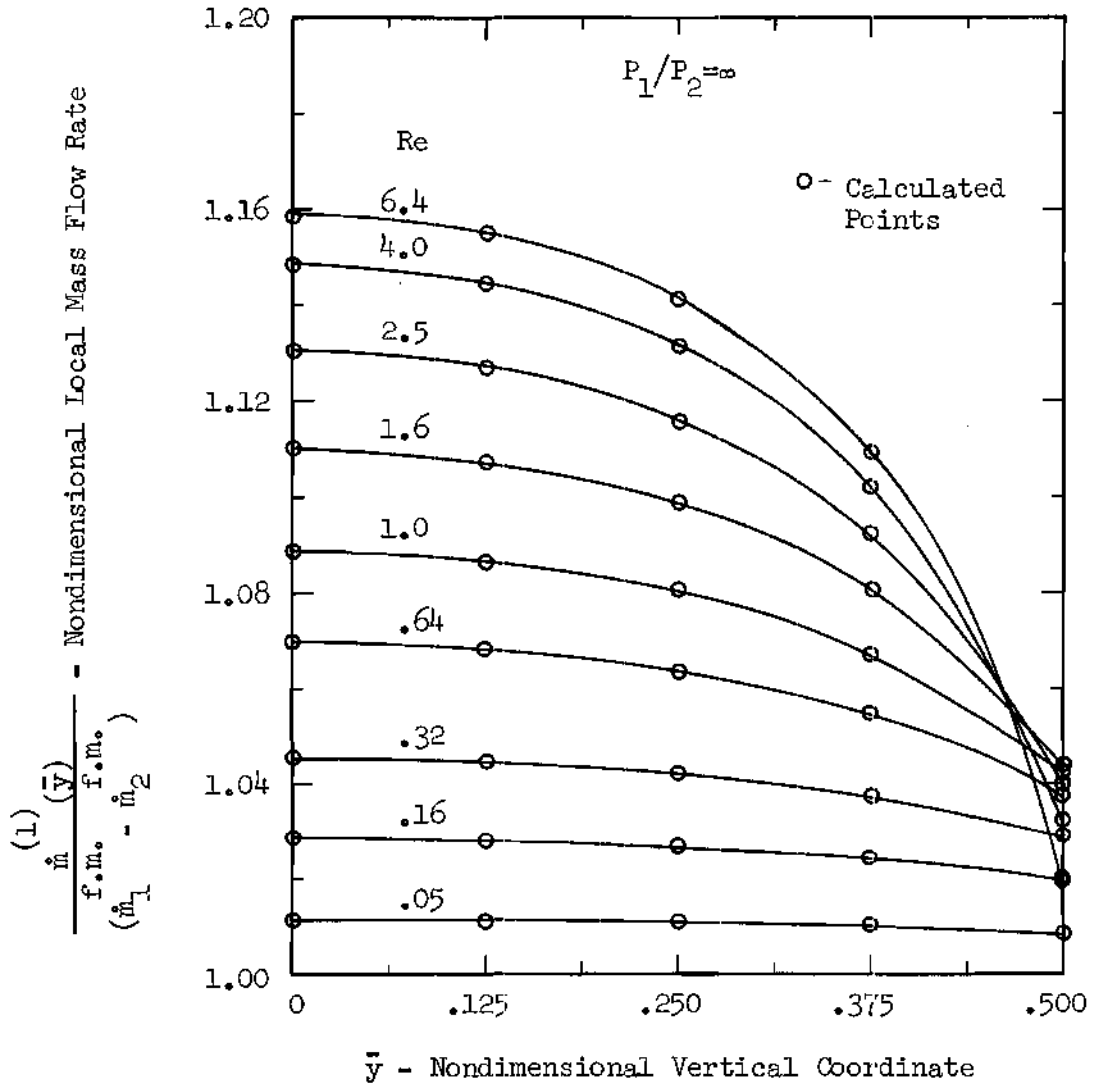

Figure 44. Nondimensional Local Mass Flow Rate for Several Points Across a Slit for Various Reynolds Numbers and an Infinite Pressure Ratio.

shown in Figure 44, were compared with the graphical results of Willis [33]. The agreement was good everywhere except at the edge of the slit, where the results differed by as much as approximately 15 per cent for a Reynolds number of 6.4. For the smaller Reynolds numbers of 3.2, 1.6, 0.64, and 0.32 the results differed by 4.3, 4.0, 2.0, and 2.2 per cent, respectively. It should be noted, however, that the integrating factor was analytically evaluated for the results reported herein and the numerical quadrature was considered more accurate than that used by Willis.

The average flow rate is presented in Figures 45 and 46. The results were nondimensionalized with the upstream free molecular value. In Figure 45 the nondimensional average flow rate is plotted against the Reynolds number for pressure ratios of 2.0, 100, and infinity. The intercept for Reynolds number of zero is the free molecular value. It is apparent that the average flow rate increases with Reynolds number. For the finite pressure ratios a slight maximum occurred for a Reynolds number of approximately 4.5. However, the iterative method is specifically designed for small Reynolds numbers (i.e., large Knudsen numbers). Therefore, the slight maximum is considered to be caused by the inadequacy of the first iterative solution to describe the correct results for large Reynolds numbers.

The nondimensional average flow rate is plotted against the pressure ratio for Reynolds numbers of 0, 0.05, 1.0, and 6.4 in Figure 46. It is interesting to note that the average flow rate increases quite rapidly for small pressure ratios and then increases quite slowly

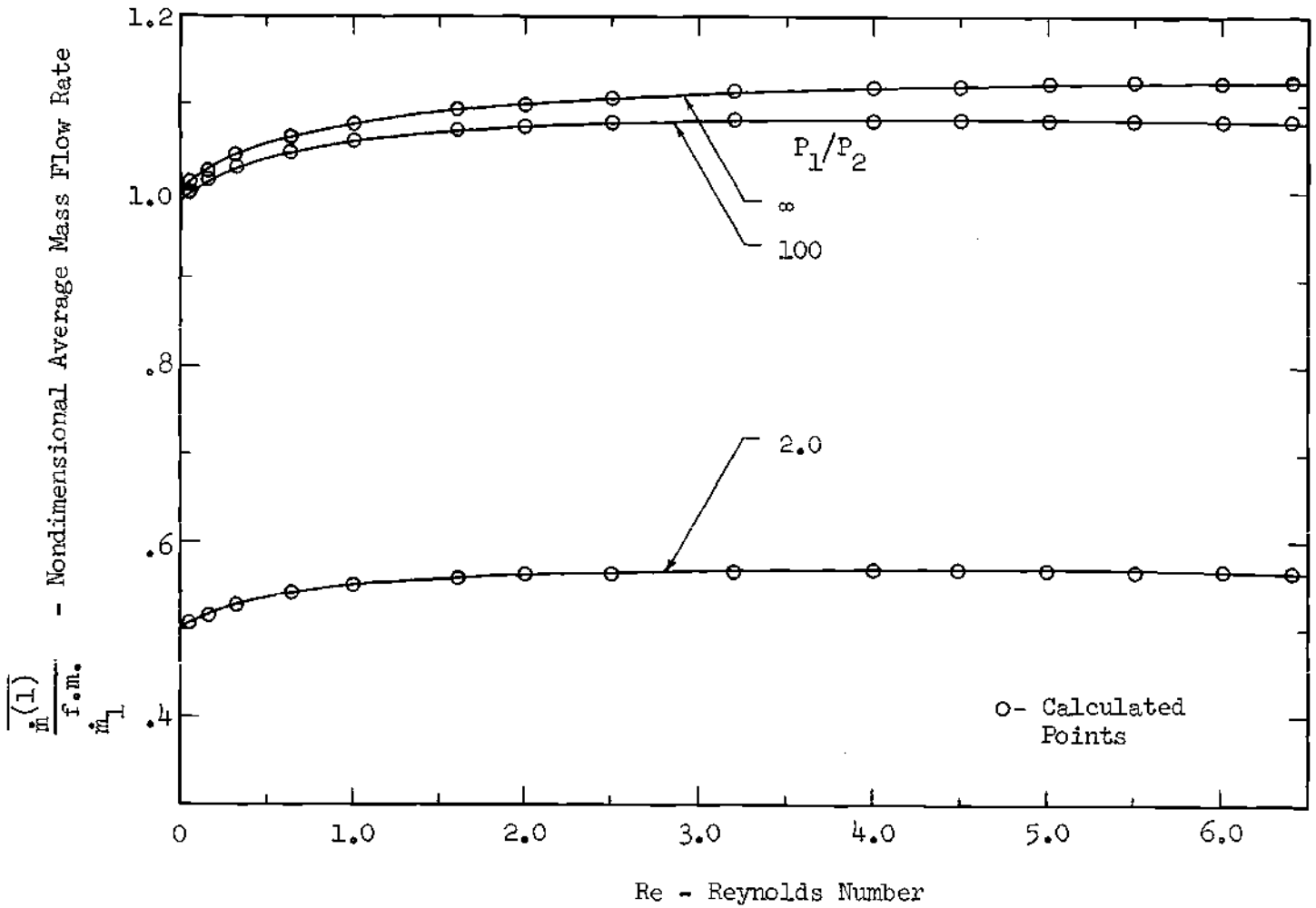

Figure 45. Nondimensional Average Mass Flow Rate versus Reynolds Number for Pressure Ratios of 2.0, 100, and Infinity.

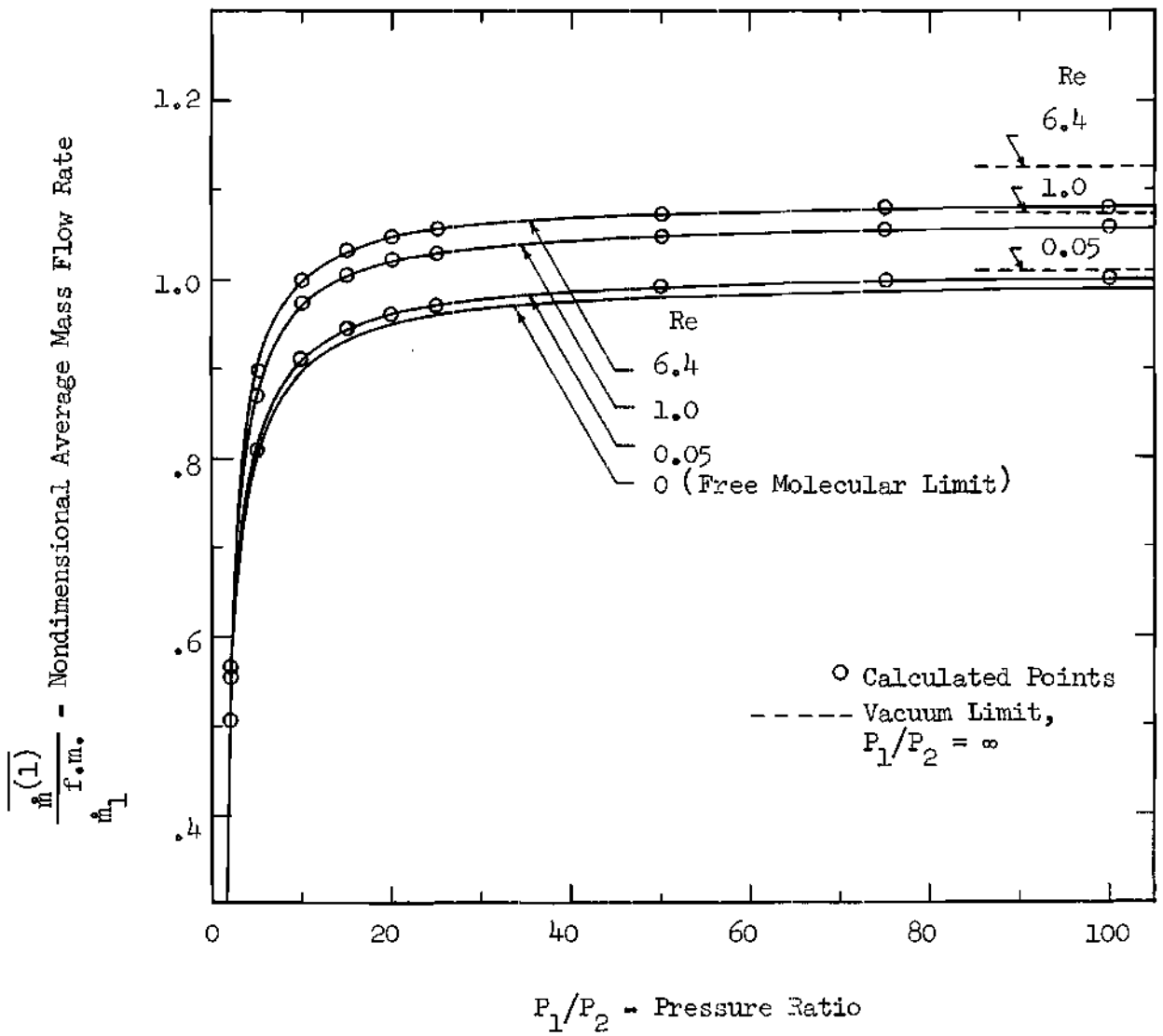

Figure 46. Nondimensional Average Mass Flow Rate versus the Pressure Ratio for Reynolds Numbers of 0.05, 1.0, and 6.4.

for large pressure ratios. It should be noted also that the maximum average flow rates for an infinite pressure ratio are also shown for each Reynolds number. The rate of approach to this maximum value as the Reynolds number is increased can be seen to be slow. The nondimensional average mass flow rate for an infinite Reynolds number has been calculated by Frankl [43] for a specific heat ratio of 1.4. He obtains a value of 1.46. Note that this value is significantly higher than the nearly-free molecular values presented in Figures 45 and 46.

CHAPTER V

DISCUSSION AND CONCLUSIONS

Several free molecular internal flow problems have been formulated and solved by the method presented herein. This method consists of determining the velocity distribution function for all boundaries of the flow field and obtaining the macroscopic moments directly from the corresponding definitions. The integral equations for the boundary conditions were solved by the collocation method for arbitrary length-to-height ratios. The usefulness of this approach was illustrated by obtaining the complete free molecular solutions for a two dimensional channel and circular tube of arbitrary length-to-height ratio. The corresponding problem for free molecular flow through a rectangular channel was also formulated for a few of the lower moments. In addition, the local and average mass flow rates for nearly-free molecular flow through a two dimensional slit for arbitrary pressure ratios were obtained by the Willis iterative method. The free molecular solution needed for this iterative method was obtained as a special case of the solution for the two dimensional channel.

The results of the investigation may be summarized in the following conclusions:

1. The method presented herein can be used to formulate the general problem of obtaining the local and average flow properties for free molecular flow through internal flow geometries, as illustrated for

the cases of a two dimensional channel, a rectangular channel, and a circular tube.

2. Accurate numerical results for both local and average flow properties for free molecular internal flow problems can be obtained by using the collocation method to solve the integral equations for the wall flux. This method is a great improvement over all previous methods if the approximating functions weighted by the kernel can be analytically integrated.

3. The free molecular results obtained by previous investigators for the rectangular orifice, two dimensional channel, circular tube, and corresponding slit and orifice flows can be obtained as special cases of the general results presented herein, which are valid for arbitrary length-to-height ratios.

4. The results for a linear wall flux over the entire channel length are in worse agreement with the results for linear wall flux segments for intermediate values of length-to-height ratios. The limits of this range depend on the particular flow property of interest, the geometry considered, and the accuracy desired. For all practical purposes the linear wall flux solutions are good approximations for length-to-height ratios outside this intermediate range. For the circular tube case, the linear wall flux solutions for some of the flow properties are very accurate for the entire range of length-to-diameter ratios. Finally, the solutions for a constant wall flux over the entire channel length are accurate for only small length-to-height ratios.

5. The well-known long-channel and long-tube formulas of Clausing

and Knudsen, respectively, for the average mass flow rate yield accurate results for sufficiently large length-to-height ratios.

6. The theoretical free-molecular values of average mass flow rate, as determined for the case of linear wall flux segments, agree quite well with the experimental values for the flow of a rarefied gas through a circular tube, even for inverse Knudsen numbers as large as one. The corresponding theoretical free-molecular average mass flow rates for a two dimensional channel do not agree well with the measured values for a rectangular channel whose width-to-height ratio is very large, even in the limit of very small inverse Knudsen numbers.

7. The backflow contribution for nearly-free molecular flow through a two dimensional slit is strongly dependent on the pressure ratio for small pressure ratios, but for large pressure ratios the Reynolds number effect is predominant.

8. The nearly-free molecular flow rate through a two dimensional slit is larger than the corresponding free molecular value for all pressure ratios considered, and the magnitude of the difference continually increases with increasing Reynolds numbers.

APPENDIX A

FREE MOLECULAR FLOW THROUGH A RECTANGULAR CHANNEL OF ARBITRARY LENGTH

Statement of the Problem

Consider a rectangular channel connecting two reservoirs which, respectively, contain gas in equilibrium at P_1, T_1 and P_2, T_2, as depicted in Figure A-1. The wall temperature is constant at T_w for all walls. All the assumptions concerning the reflection properties at the channel walls and the distribution functions for the boundaries of the flow field are the same as those presented in Chapter II for the two dimensional channel. The addition of the two side walls, however, greatly complicates the problem in that the flow field is three dimensional and is divided into six regions, as shown in Figure A-1 for the arbitrary point specified by the coordinates x, y, and z. The corresponding velocity space, illustrating the surfaces of discontinuity for the distribution functions, is similarly divided into six regions. In addition, the condition that the net flux normal to the channel walls at the walls be zero provides four boundary conditions. Satisfying these boundary conditions yields two integral equations, in terms of the nondimensional wall fluxes, which must be solved simultaneously. The corresponding wall densities may then be obtained. Since the wall temperature is given and the reflection properties have been specified, the wall distribution functions can

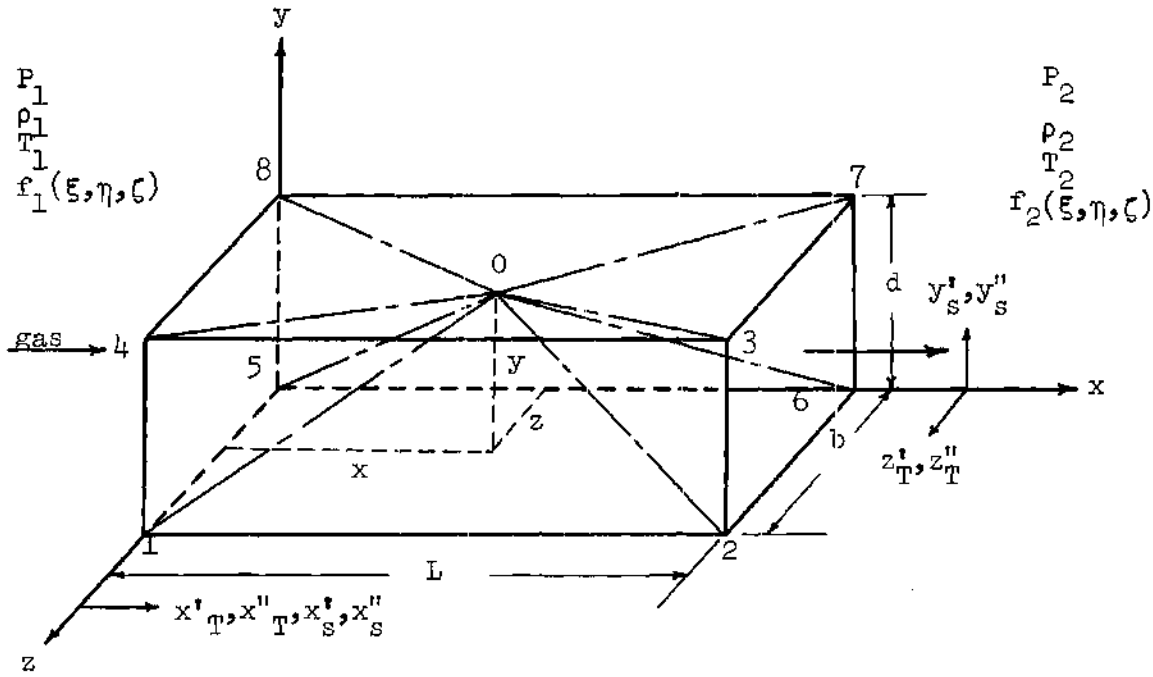

Rectangular Channel

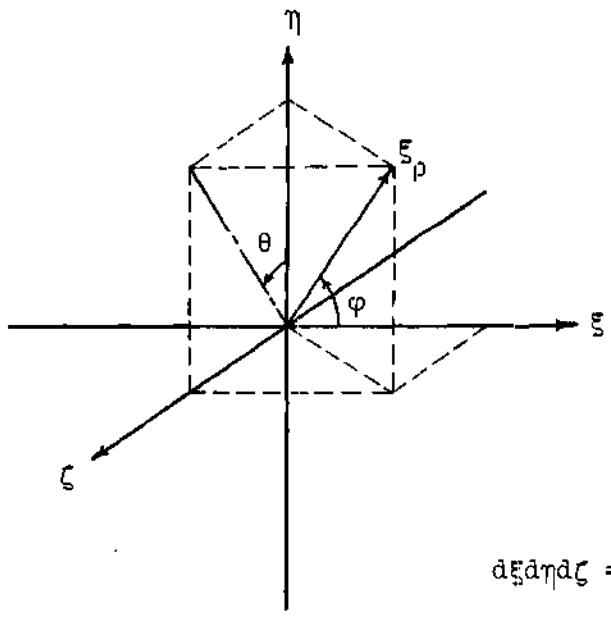

$$\xi = \xi_\rho \text{ Cos } \theta$$
$$\zeta = \xi_\rho \text{ Sin } \varphi \text{ Sin } \theta$$
$$\eta = \xi_\rho \text{ Sin } \varphi \text{ Cos } \theta$$
$$d\xi d\eta d\zeta = \xi_\rho^2 \text{ Sin } \varphi \, d\theta d\varphi d\xi_\rho$$

Velocity Coordinate System

Figure A-1. Schematic of Rectangular Channel Illustrating the Division of Physical Space for a General Point (x,y,z) and Illustration of Velocity Coordinate System.

readily be obtained. The procedure for obtaining the local flow properties is identical to that followed in Chapter II for the two dimensional channel. The solutions obtained in this chapter, however, are valid only for the region within $0 \leq z \leq b$, $0 \leq y \leq d$, $-\infty < x < \infty$. The results for the other regions of the flow field can readily be obtained from the results presented here by eliminating the appropriate wall effects and changing the limits of integration over velocity space. It should be noted that the rectangular orifice results are also subject to the limits specified above.

Since the number densities for all four walls are functions of the corresponding wall coordinates, the wall distribution functions also vary with the wall coordinates. By making use of the relation coupling the velocity coordinates and physical coordinates for free molecular flow, the wall coordinates for each wall can be expressed in terms of the physical coordinates of a point within the flow field and the angles θ and φ, which are the polar and azimuthal angles, respectively, for spherical velocity coordinates as shown in Figure A-1. Consequently, the wall distribution functions vary with θ and φ. It is essentially this point which makes evaluation of free molecular flow properties for variable wall densities quite difficult. It should also be noted that the wall densities must be obtained from the simultaneous solution of two integral equations, the integral parts of which consist of double integrations.

In the following sections the distribution functions for the flow field are determined, the moments for the density and the velocity

components are determined in general by making no assumptions regarding the variation of the wall densities, the general relation for the average mass flow rate is derived, and the integral equations for the boundary conditions are derived. The results for rectangular orifice flow can be obtained as limiting cases by setting the length of the channel equal to zero. It should be noted that only the lower order moments have been presented due to the fact that the results are very lengthy. However, the higher order moments can readily be determined by making use of the procedure outlined in this Appendix for the lower order moments.

General Formulation

Relations Between Physical and Velocity Coordinates

Consider the transformation equations for spherical and rectangular velocity coordinates, as shown in Figure A-1. The following relations can be written directly:

$$\frac{\eta}{\xi} = \text{Tan } \varphi \text{ Cos } \theta \tag{A-1}$$

$$\frac{\zeta}{\eta} = \text{Tan } \theta \tag{A-2}$$

$$\frac{\zeta}{\xi} = \text{Tan } \varphi \text{ Sin } \theta \tag{A-3}$$

Since there are no gas-gas collisions occurring, functional relations between the angles in velocity space and the physical coordinates can

be obtained by setting the direction of a particle in physical space equal to the direction of the corresponding velocity vector in velocity space. For example, for particles leaving the lower wall,

$$\frac{\eta}{\xi} = \frac{\bar{y}}{\tau_d(\bar{x}-\bar{x}'_T)}$$

$$\frac{\eta}{\zeta} = \frac{\tau_b\bar{y}}{\tau_d(\bar{z}-\bar{z}'_T)}$$

where τ_d is the length-to-height ratio, L/d, τ_b is the length-to-width ratio, L/b, and $\bar{x}$,$\bar{y}$, and $\bar{z}$ are the physical coordinates, x,y, and z, nondimensionalized with L, d, and b, respectively. The lower wall coordinates are denoted by $\bar{x}'_T$ and $\bar{z}'_T$. The molecular velocities in the x,y, and z directions are again defined as ξ, η, and ζ, respectively. Similar results can be written for particles leaving the other channel walls and passing through the point (x,y,z) in the flow field. When these results are combined with equations (A-1) through (A-3), the following equations are deduced:

$$\text{Tan } \varphi \text{ Cos } \theta = \frac{\bar{y}}{\tau_d(\bar{x}-\bar{x}'_T)} \qquad \text{(Lower Wall)} \quad \text{(A-4)}$$

$$\text{Cot } \theta = \frac{\tau_b\bar{y}}{\tau_d(\bar{z}-\bar{z}'_T)} \qquad \text{(Lower Wall)} \quad \text{(A-5)}$$

$$\text{Tan } \varphi \text{ Cos } \theta = \frac{(\bar{y}-1)}{\tau_d(\bar{x}-\bar{x}''_T)} \qquad \text{(Upper Wall)} \qquad \text{(A-6)}$$

$$\text{Cot } \theta = \frac{\tau_b(\bar{y}-1)}{\tau_d(\bar{z}-\bar{z}''_T)} \qquad \text{(Upper Wall)} \qquad \text{(A-7)}$$

$$\text{Tan } \varphi \text{ Sin } \theta = \frac{\bar{z}}{\tau_b(\bar{x}-\bar{x}'_s)} \qquad \text{(Rear Side Wall)} \qquad \text{(A-8)}$$

$$\text{Tan } \theta = \frac{\tau_d\bar{z}}{\tau_b(\bar{y}-\bar{y}'_s)} \qquad \text{(Rear Side Wall)} \qquad \text{(A-9)}$$

$$\text{Tan } \varphi \text{ Sin } \theta = \frac{(\bar{z}-1)}{\tau_b(\bar{x}-\bar{x}''_s)} \qquad \text{(Front Side Wall)} \qquad \text{(A-10)}$$

$$\text{Tan } \theta = \frac{\tau_d(\bar{z}-1)}{\tau_b(\bar{y}-\bar{y}''_s)} \qquad \text{(Front Side Wall)} \qquad \text{(A-11)}$$

where $\bar{x}''_T$ and $\bar{z}''_T$ are the upper wall coordinates, and $\bar{x}'_s$, $\bar{y}'_s$, $\bar{x}''_s$, $\bar{y}''_s$ are the rear and front side wall coordinates, respectively. Equations (A-4) through (A-11) are the general functional relations connecting the physical and velocity coordinates for a particle which leaves one of the channel walls and passes through the point (x,y,z) in the flow field.

The relations for the surfaces of discontinuity for the distribution functions can be obtained from equations (A-4) through (A-11) by setting the wall coordinates equal to unity or zero, whichever is applicable. For example, referring to Figure A-1 and setting $\bar{x}'_T$ in equation (A-4) equal to zero, it can be seen that the azimuthal angle in velocity space for the plane 105 can be written in terms of the polar angle θ and the coordinates of the point as

$$\operatorname{Tan} \varphi_{105}(\theta) = \frac{\bar{y}}{\tau_d \bar{x} \operatorname{Cos} \theta} \tag{A-12}$$

Similarly, from equations (A-6), (A-8), and (A-10)

$$\operatorname{Tan} \varphi_{401}(\theta) = \frac{(\bar{z}-1)}{\tau_b \bar{x} \operatorname{Sin} \theta} \tag{A-13}$$

$$\operatorname{Tan} \varphi_{804}(\theta) = \frac{(\bar{y}-1)}{\tau_d \bar{x} \operatorname{Cos} \theta} \tag{A-14}$$

$$\operatorname{Tan} \varphi_{508}(\theta) = \frac{\bar{z}}{\tau_b \bar{x} \operatorname{Sin} \theta} \tag{A-15}$$

$$\operatorname{Tan} \varphi_{206}(\theta) = \frac{\bar{y}}{\tau_d (\bar{x}-1) \operatorname{Cos} \theta} \tag{A-16}$$

$$\operatorname{Tan} \varphi_{302}(\theta) = \frac{(\bar{z}-1)}{\tau_b (\bar{x}-1) \operatorname{Sin} \theta} \tag{A-17}$$

$$\text{Tan } \varphi_{706}(\theta) = \frac{\bar{z}}{\tau_b(\bar{x}-1)\text{Sin } \theta} \tag{A-18}$$

$$\text{Tan } \varphi_{703}(\theta) = \frac{(\bar{y}-1)}{\tau_d(\bar{x}-1)\text{Cos } \theta} \tag{A-19}$$

In order to obtain the corresponding limits for the polar angle θ, equations (A-5), (A-7), (A-9), and (A-11) are evaluated for the appropriate values of the wall coordinates, which can be obtained by referring to the y z-plane of Figure A-2. Thus,

$$\text{Tan } \alpha_{506} = \frac{\tau_d \bar{z}}{\tau_b \bar{y}} \tag{A-20}$$

$$\text{Tan } \alpha_{102} = \frac{\tau_d(\bar{z}-1)}{\tau_b \bar{y}} \tag{A-21}$$

$$\text{Tan } \alpha_{807} = \frac{\tau_d \bar{z}}{\tau_b(\bar{y}-1)} \tag{A-22}$$

$$\text{Tan } \alpha_{403} = \frac{\tau_d(\bar{z}-1)}{\tau_b(\bar{y}-1)} \tag{A-23}$$

The limiting angles shown in the y x-plane and in the x z-plane of Figure A-2 will prove useful in the subsequent analysis. Thus, referring to Figure A-2, the following relations can be written directly:

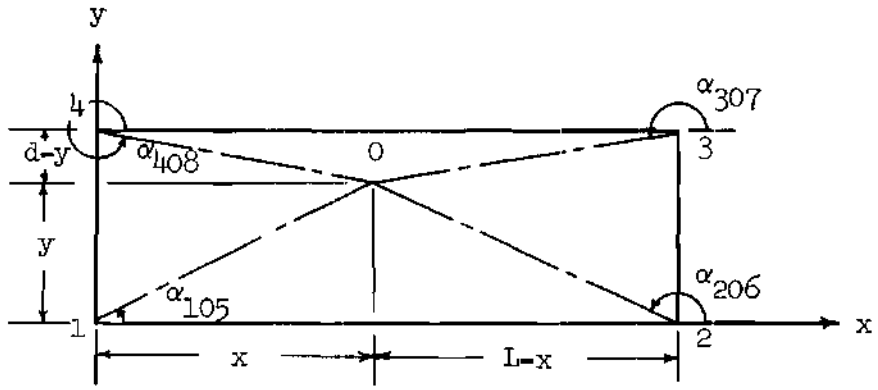

y-x Plane

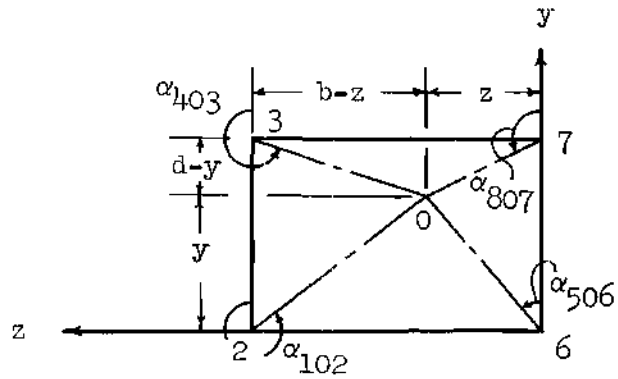

y-z Plane

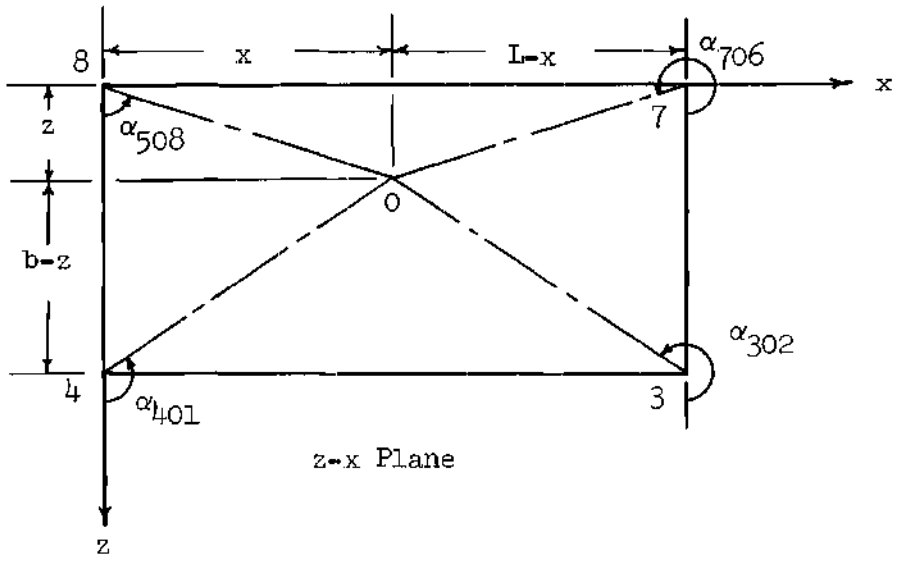

z-x Plane

Figure A-2. Side, Top, and End Views of the Rectangular Channel Illustrating the Separation of the Flow Field for a General Point (x,y,z).

$$\underset{105}{\text{Tan } \alpha} = \frac{\bar{y}}{\tau_d \bar{x}} \tag{A-24}$$

$$\underset{206}{\text{Tan } \alpha} = \frac{\bar{y}}{\tau_d (\bar{x}-1)} \tag{A-25}$$

$$\underset{307}{\text{Tan } \alpha} = \frac{(\bar{y}-1)}{\tau_d (\bar{x}-1)} \tag{A-26}$$

$$\underset{408}{\text{Tan } \alpha} = \frac{(\bar{y}-1)}{\tau_d \bar{x}} \tag{A-27}$$

$$\underset{508}{\text{Tan } \alpha} = \frac{\tau_b \bar{x}}{\bar{z}} \tag{A-28}$$

$$\underset{401}{\text{Tan } \alpha} = \frac{\tau_b \bar{x}}{(\bar{z}-1)} \tag{A-29}$$

$$\underset{302}{\text{Tan } \alpha} = \frac{\tau_b (\bar{x}-1)}{(\bar{z}-1)} \tag{A-30}$$

$$\underset{706}{\text{Tan } \alpha} = \frac{\tau_b (\bar{x}-1)}{\bar{z}} \tag{A-31}$$

Distribution Functions

Before defining the distribution functions it is convenient to define the regions of physical and velocity space for which each distribution function is valid. The planes separating these regions are the surfaces of discontinuity for the distribution functions. The relations between the physical and velocity coordinates derived in the last section can be used to specify these regions as follows:

Region Ω_1: $0 \leq \varphi < \varphi_{105}(\theta)$ for $\alpha_{102} < \theta \leq 2\pi$ and $0 \leq \theta < \alpha_{506}$

$0 \leq \varphi < \varphi_{508}(\theta)$ for $\alpha_{506} < \theta < \alpha_{807}$

$0 \leq \varphi < \varphi_{804}(\theta)$ for $\alpha_{807} < \theta < \alpha_{403}$

$0 \leq \varphi < \varphi_{401}(\theta)$ for $\alpha_{403} < \theta < \alpha_{102}$

Region Ω_2: $\varphi_{206}(\theta) < \varphi \leq \pi$ for $\alpha_{102} < \theta \leq 2\pi$ and $0 \leq \theta < \alpha_{506}$

$\varphi_{706}(\theta) < \varphi \leq \pi$ for $\alpha_{506} < \theta < \alpha_{807}$

$\varphi_{703}(\theta) < \varphi \leq \pi$ for $\alpha_{807} < \theta < \alpha_{403}$

$\varphi_{302}(\theta) < \varphi \leq \pi$ for $\alpha_{403} < \theta < \alpha_{102}$

Region Ω_{w_s}: $\varphi_{508}(\theta) < \varphi < \varphi_{706}(\theta)$ for $\alpha_{506} < \theta < \alpha_{807}$

$\varphi_{401}(\theta) < \varphi < \varphi_{302}(\theta)$ for $\alpha_{403} < \theta < \alpha_{102}$

Region Ω_{w_T}: $\varphi_{804}(\theta) < \varphi < \varphi_{703}(\theta)$ for $\alpha_{807} < \theta < \alpha_{403}$

$\varphi_{105}(\theta) < \varphi < \varphi_{206}(\theta)$ for $\alpha_{102} < \theta \leq 2\pi$ and $0 \leq \theta < \alpha_{506}$

The distribution functions can now be defined as follows:

$$f_1(\xi,\eta,\zeta) \equiv \frac{n_1}{(2\pi RT_1)^{3/2}} e^{-\frac{[\xi^2+\eta^2+\zeta^2]}{2RT_1}} \qquad \text{Region } \Omega_1 \qquad \text{(A-32)}$$

$$f_2(\xi,\eta,\zeta) \equiv \frac{n_2}{(2\pi RT_2)^{3/2}} e^{-\frac{[\xi^2+\eta^2+\zeta^2]}{2RT_2}} \qquad \text{Region } \Omega_2 \qquad \text{(A-33)}$$

$$f_{w_s}(\bar{x},\bar{y},\bar{z},\xi,\eta,\zeta) \equiv \frac{n_{w_s}(\bar{x}_s,\bar{y}_s)}{(2\pi RT_w)^{3/2}} e^{-\frac{[\xi^2+\eta^2+\zeta^2]}{2RT_w}} \qquad \text{Region } \Omega_{w_s} \qquad \text{(A-34)}$$

$$f_{w_T}(\bar{x},\bar{y},\bar{z},\xi,\eta,\zeta) \equiv \frac{n_{w_T}(\bar{x}_T,\bar{z}_T)}{(2\pi RT_w)^{3/2}} e^{-\frac{[\xi^2+\eta^2+\zeta^2]}{2RT_w}} \qquad \text{Region } \Omega_{w_T} \qquad \text{(A-35)}$$

where $n_{w_s}(\bar{x}_s,\bar{y}_s)$ is the number density for the side walls, $n_{w_T}(\bar{x}_T,\bar{z}_T)$ is the number density for the upper and lower walls, and each of the unprimed wall coordinates, $\bar{x}_s$, $\bar{x}_T$, etc. denotes the primed wall coordinates, $\bar{x}'_s$, $\bar{x}''_s$, $\bar{x}'_T$, $\bar{x}''_T$, etc.

Boundary Conditions

The boundary conditions that there be no net flux of particles normal to the channel walls can be expressed as follows by introducing the average mass velocities and setting these quantities equal to zero at the walls:

$$\rho(\bar{x},\bar{y}=\tfrac{1}{0},\bar{z})v(\bar{x},\bar{y}=\tfrac{1}{0},\bar{z}) \equiv m\int_{-\infty}^{\infty}\int_{-\infty}^{\infty}\int_{-\infty}^{\infty} f'(\bar{x},\bar{y}=\tfrac{1}{0},\bar{z},\xi,\eta,\zeta)\eta d\xi d\eta d\zeta = 0 \quad \text{(A-36)}$$

$$\rho(\bar{x},\bar{y},\bar{z}=\tfrac{1}{0})w(\bar{x},\bar{y},\bar{z}=\tfrac{1}{0}) \equiv m\int_{-\infty}^{\infty}\int_{-\infty}^{\infty}\int_{-\infty}^{\infty} f(\bar{x},\bar{y},\bar{z}=\tfrac{1}{0},\xi,\eta,\zeta)\zeta d\xi d\eta d\zeta = 0 \quad \text{(A-37)}$$

where $\rho(\bar{x},\bar{y},\bar{z})$ is the local density and m is the molecular mass of the particle. By introducing equations (A-32) through (A-35) for the distribution functions into equations (A-36) and (A-37), integrating over the appropriate regions of velocity space using spherical velocity coordinates as shown in Figure A-1, and introducing the nondimensional wall fluxes defined as

$$g_{w_s}(\bar{x}_s,\bar{y}_s) \equiv \frac{\dot{m}_{w_s}(\bar{x}_s,\bar{y}_s) - \dot{m}_2}{\dot{m}_1 - \dot{m}_2} \quad \text{(A-38)}$$

$$g_{w_T}(\bar{x}_T,\bar{z}_T) \equiv \frac{\dot{m}_{w_T}(\bar{x}_T,\bar{z}_T) - \dot{m}_2}{\dot{m}_1 - \dot{m}_2} \quad \text{(A-39)}$$

where

$$\dot{m}_{w_s}(\bar{x}_s,\bar{y}_s) = \frac{m.n_{w_s}(\bar{x}_s,\bar{y}_s)\cdot\sqrt{2\pi RT_w}}{2\pi} \tag{A-40}$$

$$\dot{m}_{w_T}(\bar{x}_T,\bar{z}_T) = \frac{m.n_{w_T}(\bar{x}_T,\bar{z}_T)\cdot\sqrt{2\pi RT_w}}{2\pi} \tag{A-41}$$

and $\dot{m}_1$ and $\dot{m}_2$ are the equilibrium fluxes of the tanks given by equations (14) and (15) of Chapter II, the following integral equations are obtained for the boundary conditions:

$$g_{w_T}(\bar{x}_T,\bar{z}_T) = G_{w_T}(\bar{x}_T,\bar{z}_T) + \frac{1}{\pi}\left[\int_0^{11}\int_0^{11} g_{w_T}(\bar{x}'_T,\bar{z}'_T)K'_{w_T}(\bar{x}_T,\bar{x}'_T,\bar{z}_T,\bar{z}'_T)d\bar{x}'_T d\bar{z}'_T\right. \tag{A-42}$$

$$+\int_0^{11}\int_0^{11} g_{w_s}(\bar{x}'_s,\bar{y}'_s)K'_{w_s}(\bar{x}_T,\bar{x}'_s,\bar{y}'_s,\bar{z}_T)\,d\bar{x}'_s d\bar{y}'_s +$$

$$\left.\int_0^{11}\int_0^{11} g_{w_s}(\bar{x}''_s,\bar{y}''_s)K''_{w_s}(\bar{x}_T,\bar{x}''_s,\bar{y}''_s,\bar{z}_T)d\bar{x}''_s d\bar{y}''_s\right]$$

$$g_{w_s}(\bar{x}_s,\bar{y}_s) = G_{w_s}(\bar{x}_s,\bar{y}_s) + \frac{1}{\pi}\left[\int_0^{11}\int_0^{11} g_{w_s}(\bar{x}'_s,\bar{y}'_s)K'_{w_s}(\bar{x}_s,\bar{x}'_s,\bar{y}_s,\bar{y}'_s)d\bar{x}'_s d\bar{y}'_s + \right. \tag{A-43}$$

$$\int_0^{11}\int_0^{11} g_{w_T}(\bar{x}'_T,\bar{z}'_T)K'_{w_T}(\bar{x}_s,\bar{x}'_T,\bar{y}_s,\bar{z}'_T)d\bar{x}'_T d\bar{z}'_T +$$

$$\left.\int_0^{11}\int_0^{11} g_{w_T}(\bar{x}''_T,\bar{z}''_T)K''_{w_T}(\bar{x}_s,\bar{x}''_T,\bar{y}_s,\bar{z}''_T)d\bar{x}''_T d\bar{z}''_T\right]$$

where

$$G_{w_T}(\bar{x}_T,\bar{z}_T) = \frac{1}{2\pi}\left[\frac{\tau_d\bar{x}_T}{\sqrt{1+\tau_d^2\bar{x}_T^2}}\left[\mathrm{Tan}^{-1}\left(\frac{\tau_d(\bar{z}_T-1)}{\tau_b\sqrt{1+\tau_d^2\bar{x}_T^2}}\right)-\right.\right. \tag{A-44}$$

$$\left.\left.\mathrm{Tan}^{-1}\left(\frac{\tau_d\bar{z}_T}{\tau_b\sqrt{1+\tau_d^2\bar{x}_T^2}}\right)\right]+\mathrm{Tan}^{-1}\left(\frac{\bar{z}_T}{\tau_b\bar{x}_T}\right)-\mathrm{Tan}^{-1}\left(\frac{\bar{z}_T-1}{\tau_b\bar{x}_T}\right)\right]$$

$$G_{w_s}(\bar{x}_s,\bar{y}_s) = \frac{1}{2\pi}\left[\frac{\tau_b\bar{x}_s}{\sqrt{1+\tau_b^2\bar{x}_s^2}}\left[\mathrm{Tan}^{-1}\left(\frac{\tau_b(\bar{y}_s-1)}{\tau_d\sqrt{1+\tau_b^2\bar{x}_s^2}}\right)-\right.\right. \tag{A-45}$$

$$\left.\left.\mathrm{Tan}^{-1}\left(\frac{\tau_b\bar{y}_s}{\tau_d\sqrt{1+\tau_b^2\bar{x}_s^2}}\right)\right]+\mathrm{Tan}^{-1}\left(\frac{\bar{y}_s}{\tau_d\bar{x}_s}\right)-\mathrm{Tan}^{-1}\left(\frac{\bar{y}_s-1}{\tau_d\bar{x}_s}\right)\right]$$

$$K'_{w_T}(\bar{x}_T,\bar{x}'_T,\bar{z}_T,\bar{z}'_T) = \frac{\tau_d^2\tau_b^3}{\left[\tau_b^2+\tau_d^2(\bar{z}_T-\bar{z}'_T)^2+\tau_d^2\tau_b^2(\bar{x}_T-\bar{x}'_T)^2\right]^2} \tag{A-46}$$

$$K'_{w_T}(\bar{x}_s,\bar{x}'_T,\bar{y}_s,\bar{z}'_T) = \frac{\tau_d^3\tau_b^2\bar{y}_s(1-\bar{z}'_T)}{\left[\tau_b^2\bar{y}_s^2+\tau_d^2(1-\bar{z}'_T)^2+\tau_d^2\tau_b^2(\bar{x}_s-\bar{x}'_T)^2\right]^2} \tag{A-47}$$

$$K'_{w_s}(\bar{x}_T,\bar{x}'_s,\bar{y}'_s,\bar{z}_T) = \frac{\tau_d^2\tau_b^3\bar{z}_T(1-\bar{y}'_s)}{\left[\tau_d^2\bar{z}_T^2+\tau_b^2(1-\bar{y}'_s)^2+\tau_d^2\tau_b^2(\bar{x}_T-\bar{x}'_s)^2\right]^2} \tag{A-48}$$

$$K'_{w_s}(\bar{x}_s,\bar{x}'_s,\bar{y}_s,\bar{y}'_s) = \frac{\tau_d^{\,3}\tau_b^{\,2}}{[\tau_d^{\,2} + \tau_b^{\,2}(\bar{y}_s - \bar{y}'_s)^2 + \tau_d^{\,2}\tau_b^{\,2}(\bar{x}_s - \bar{x}'_s)^2]^2} \quad \text{(A-49)}$$

$$K''_{w_s}(\bar{x}_T,\bar{x}''_s,\bar{y}''_s,\bar{z}_T) = \frac{\tau_d^{\,2}\tau_b^{\,3}(1 - \bar{z}_T)(1-\bar{y}''_s)}{[\tau_d^{\,2}(\bar{z}_T-1)^2 + \tau_b^{\,2}(1 - \bar{y}''_s)^2 + \tau_d^{\,2}\tau_b^{\,2}(\bar{x}_T-\bar{x}''_s)^2]^2} \quad \text{(A-50)}$$

$$K''_{w_T}(\bar{x}_s,\bar{x}''_T,\bar{y}_s,\bar{z}''_T) = \frac{\tau_d^{\,3}\tau_b^{\,2}(1 - \bar{y}_s)(1 - \bar{z}''_T)}{[\tau_b^{\,2}(\bar{y}_s-1)^2 + \tau_d^{\,2}(1-\bar{z}''_T)^2 + \tau_d^{\,2}\tau_b^{\,2}(\bar{x}_s-\bar{x}''_T)^2]^2} \quad \text{(A-51)}$$

The details of the derivation of equations (A-42) and (A-43) are presented in Appendix D.

It has been shown that the nondimensional wall fluxes possess symmetric properties as follows:

$$g_{w_s}(\bar{x}_s,\bar{y}_s) = g_{w_s}(\bar{x}_s,\ 1 - \bar{y}_s) \quad \text{(A-52)}$$

$$g_{w_T}(\bar{x}_T,\bar{z}_T) = g_{w_T}(\bar{x}_T,1 - \bar{z}_T) \quad \text{(A-53)}$$

It has also been shown that for the limits of $\tau_b = 0$ and τ_d finite, or vice versa, equations (A-42) and (A-43) reduce to the corresponding two dimensional result given by equation (16) of Chapter II. It is also expected that the nondimensional wall flux is anti-symmetric with respect to the axial coordinate about the midpoint of the channel; however, this has not been proven.

Moments for Arbitrary Wall Flux

Density. By definition, in terms of spherical coordinates, the density can be written as

$$\rho(\bar{x},\bar{y},\bar{z}) \equiv m \int_0^{\infty} \int_0^{2\pi} \int_0^{\pi} f(\bar{x},\bar{y},\bar{z},\xi_\rho,\theta,\varphi)\xi_\rho^{\,2} \operatorname{Sin}\varphi \, d\varphi d\theta \xi_\rho \qquad \text{(A-54)}$$

Substituting equations (A-32) through (A-35) into equation (A-54) yields

$$\rho(\bar{x},\bar{y},\bar{z}) = \frac{\rho_1}{(2\pi RT_1)^{3/2}} \int_0^{\infty} e^{-\frac{\xi_\rho^{\,2}}{2RT_1}} \xi_\rho^{\,2} \, d\xi_\rho \left[\int_0^{\alpha_{506}} d\theta \int_0^{\varphi_{105}(\theta)} \operatorname{Sin}\varphi \, d\varphi + \right. \qquad \text{(A-55)}$$

$$\int_{\alpha_{506}}^{\alpha_{807}} d\theta \int_0^{\varphi_{508}(\theta)} \operatorname{Sin}\varphi d\varphi + \int_{\alpha_{807}}^{\alpha_{403}} d\theta \int_0^{\varphi_{804}(\theta)} \operatorname{Sin}\varphi d\varphi + \int_{\alpha_{403}}^{\alpha_{102}} d\theta \int_0^{\varphi_{401}(\theta)} \operatorname{Sin}\varphi d\varphi +$$

$$\left. \int_{\alpha_{102}}^{2\pi} d\theta \int_0^{\varphi_{105}(\theta)} \operatorname{Sin}\varphi d\varphi \right] + \frac{\rho_2}{(2\pi RT_2)^{3/2}} \int_0^{\infty} e^{-\frac{\xi_\rho^{\,2}}{2RT_2}} \xi_\rho^{\,2} d\xi_\rho \left[\int_0^{\alpha_{506}} d\theta \int_{\varphi_{206}(\theta)}^{\pi} \operatorname{Sin}\varphi d\varphi + \right.$$

$$\int_{\alpha_{506}}^{\alpha_{807}} d\theta \int_{\varphi_{706}(\theta)}^{\pi} \operatorname{Sin}\varphi d\varphi + \int_{\alpha_{807}}^{\alpha_{403}} d\theta \int_{\varphi_{703}(\theta)}^{\pi} \operatorname{Sin}\varphi d\varphi + \int_{\alpha_{403}}^{\alpha_{102}} d\theta \int_{\varphi_{302}(\theta)}^{\pi} \operatorname{Sin}\varphi d\varphi +$$

$$\int_{\alpha_{102}}^{2\pi} d\theta \int_{\varphi_{206}(\theta)}^{\pi} \text{Sin}\,\varphi\, d\varphi \Bigg] + \frac{1}{(2\pi RT_w)^{3/2}} \int_0^{\infty} e^{-\frac{\xi_\rho^2}{2RT_w}} \xi_\rho^2 d\xi_\rho \Bigg[\int_{\alpha_{506}}^{\alpha_{807}} d\theta \int_{\varphi_{508}(\theta)}^{\varphi_{706}(\theta)} \rho_{w_s}(\theta,\varphi)\, \text{Sin}\,\varphi\, d\varphi +$$

$$\int_{\alpha_{403}}^{\alpha_{102}} d\theta \int_{\varphi_{401}(\theta)}^{\varphi_{302}(\theta)} \rho_{w_s}(\theta,\varphi)\, \text{Sin}\,\varphi\, d\varphi + \int_{\alpha_{807}}^{\alpha_{403}} d\theta \int_{\varphi_{804}(\theta)}^{\varphi_{703}(\theta)} \rho_{w_T}(\theta,\varphi)\, \text{Sin}\,\varphi\, d\varphi +$$

$$\int_{\alpha_{102}}^{2\pi} d\theta \int_{\varphi_{105}(\theta)}^{\varphi_{206}(\theta)} \rho_{w_T}(\theta,\varphi)\, \text{Sin}\,\varphi\, d\varphi + \int_0^{\alpha_{506}} d\theta \int_{\varphi_{105}(\theta)}^{\varphi_{206}(\theta)} \rho_{w_T}(\theta,\varphi)\, \text{Sin}\,\varphi\, d\varphi \Bigg]$$

where ρ_1 and ρ_2 are the mass densities in the upstream and downstream tanks, respectively, and $\rho_{w_s}(\theta,\varphi)$ and $\rho_{w_T}(\theta,\varphi)$ are the mass densities of the channel walls. Equations (A-38) through (A-41) can be combined to give the following expression for the wall mass densities in terms of the nondimensional wall fluxes:

$$\rho_{w_{s,T}}(\theta,\varphi) = \left(\rho_1 \sqrt{\frac{T_1}{T_w}} - \rho_2 \sqrt{\frac{T_2}{T_w}} \right) g_{w_{s,T}}(\theta,\varphi) + \rho_2 \sqrt{\frac{T_2}{T_w}} \qquad \text{(A-56)}$$

The following integrals will prove useful:

$$\int \frac{a\ \text{Sin}\ \theta\ d\theta}{\sqrt{b^2 + a^2\ \text{Sin}^2\ \theta}} = \text{Sin}^{-1}\left[\frac{a\ \text{Cos}\ \theta}{\sqrt{a^2 + b^2}} \right] \qquad \text{(A-57)}$$

$$\int \frac{a\ \text{Cos}\ \theta\ d\theta}{\sqrt{b^2 + a^2\ \text{Cos}^2\ \theta}} = \text{Sin}^{-1}\left[\frac{a\ \text{Sin}\ \theta}{\sqrt{a^2 + b^2}} \right] \qquad \text{(A-58)}$$

Substituting equation (A-56) in equation (A-55), integrating over the angle φ and expressing the results in terms of the angle θ by using equations (A-12) through (A-19), and performing the remaining integrations by using equations (A-57), (A-58), and equation (32) of Chapter II yield upon rearrangement

$$\left[\frac{\rho(\bar{x},\bar{y},\bar{z})-\rho_2}{\rho_1-\rho_2}\right] = \frac{1}{2}\left\{1 - \frac{1}{2\pi(\rho_1-\rho_2)}\left[\left(\rho_1-\rho_2\sqrt{\frac{T_2}{T_w}}\right)\left(\sin^{-1}(\cos\alpha_{105}\ \sin\alpha_{506}) + \right.\right.\right. \tag{A-59}$$

$$\sin^{-1}(\sin\alpha_{508}\cos\alpha_{807}) - \sin^{-1}(\sin\alpha_{508}\cos\alpha_{506}) -$$

$$\sin^{-1}(\sin\alpha_{401}\cos\alpha_{102}) + \sin^{-1}(\sin\alpha_{401}\cos\alpha_{403}) -$$

$$\sin^{-1}(\cos\alpha_{408}\sin\alpha_{403}) + \sin^{-1}(\cos\alpha_{408}\sin\alpha_{807}) -$$

$$\left.\sin^{-1}(\cos\alpha_{105}\sin\alpha_{102})\right) - \rho_2\left(1-\sqrt{\frac{T_2}{T_w}}\right)\left(\sin^{-1}(\cos\alpha_{206}\sin\alpha_{506}) -\right.$$

$$\sin^{-1}(\cos\alpha_{307}\sin\alpha_{403}) + \sin^{-1}(\cos\alpha_{307}\sin\alpha_{807}) +$$

$$\sin^{-1}(\sin\alpha_{706}\cos\alpha_{807}) - \sin^{-1}(\sin\alpha_{706}\cos\alpha_{506}) -$$

$$\sin^{-1}(\sin\alpha_{302}\cos\alpha_{102}) + \sin^{-1}(\sin\alpha_{302}\cos\alpha_{403}) -$$

$$\left.\left.\left.\sin^{-1}(\cos\alpha_{206}\sin\alpha_{102})\right) - \left(\rho_1\sqrt{\frac{T_1}{T_w}} - \rho_2\sqrt{\frac{T_2}{T_w}}\right)\right].$$

$$\int_{\alpha_{506}}^{\alpha_{807}} d\theta \int_{\varphi_{508}(\theta)}^{\varphi_{706}(\theta)} g_{w_s}(\theta,\varphi)\,\mathrm{Sin}\,\varphi\,d\varphi + \int_{\alpha_{403}}^{\alpha_{102}} d\theta \int_{\varphi_{401}(\theta)}^{\varphi_{302}(\theta)} g_{w_s}(\theta,\varphi)\,\mathrm{Sin}\,\varphi\,d\varphi +$$

$$\int_{\alpha_{807}}^{\alpha_{403}} d\theta \int_{\varphi_{804}(\theta)}^{\varphi_{703}(\theta)} g_{w_T}(\theta,\varphi)\,\mathrm{Sin}\,\varphi\,d\varphi + \int_{\alpha_{102}}^{2\pi} d\theta \int_{\varphi_{105}(\theta)}^{\varphi_{206}(\theta)} g_{w_T}(\theta,\varphi)\,\mathrm{Sin}\,\varphi\,d\varphi +$$

$$\left.\int_{0}^{\alpha_{506}} d\theta \int_{\varphi_{105}(\theta)}^{\varphi_{206}(\theta)} g_{w_T}(\theta,\varphi)\,\mathrm{Sin}\,\varphi\,d\varphi \right]\Bigg\}$$

It should be noted that equations (A-24) through (A-31) have been used in order to express equation (A-59) solely in terms of the geometrical angles specifying the point in the flow field.

Equation (A-59) is the general expression for the local density for free molecular flow through rectangular channels. Once the wall flux variation has been determined for each wall, the integrals of equation (A-59) can be evaluated. For an isothermal system, $T_1 = T_2 = T_w$, the density variation is anti-symmetric with respect to the axial coordinate and satisfies the following relation:

$$\left[\frac{\rho(\bar{x},\bar{y},\bar{z}) - \rho_2}{\rho_1 - \rho_2}\right] + \left[\frac{\rho(1-\bar{x},\bar{y},\bar{z}) - \rho_2}{\rho_1 - \rho_2}\right] = 1 \qquad \text{(A-60)}$$

Consider now the rectangular orifice limit. Setting L equal to

zero and holding b and d fixed, it can be seen by referring to equations (A-12) through (A-31) and Figures A-1 and A-2 that the following relations hold: $\varphi_{206}(\theta) = \varphi_{105}(\theta)$, $\varphi_{703}(\theta) = \varphi_{804}(\theta)$, $\varphi_{706}(\theta) = \varphi_{508}(\theta)$, $\varphi_{302}(\theta) = \varphi_{401}(\theta)$, $\alpha_{206} = \alpha_{105}$, $\alpha_{307} = \alpha_{403}$, $\alpha_{302} = \alpha_{401}$, and $\alpha_{706} = 2\pi + \alpha_{508}$. Substituting these expressions into equation (A-59) yields the local density for a rectangular orifice. It can be shown that the resulting orifice limit reduces to the expression for the local density for rectangular orifice flow as derived independently by Howard [22] and Gustafson and Kiel [23] for a vacuum downstream. It can also be shown that equation (A-59) reduces to the corresponding two dimensional limit, as given by equation (26) of Chapter II, by setting τ_b equal to zero for finite L and simplifying.

$\bar{x}$-Component of Velocity. By definition, in terms of spherical coordinates,

$$\rho(\bar{x},\bar{y},\bar{z})u(\bar{x},\bar{y},\bar{z}) \equiv m \int_0^{\infty}\int_0^{2\pi}\int_0^{\pi} f(\bar{x},\bar{y},\bar{z},\xi_\rho,\theta,\varphi)\xi_\rho^{\,3} \operatorname{Sin}\varphi \operatorname{Cos}\varphi \, d\varphi d\theta \xi_\rho \quad \text{(A-61)}$$

Substituting the distribution functions from equations (A-32) through (A-35) into equation (A-61) yields

$$\rho(\bar{x},\bar{y},\bar{z})u(\bar{x},\bar{y},\bar{z}) = \frac{\rho_1}{(2\pi RT_1)^{3/2}} \int_0^{\infty} e^{-\frac{\xi_\rho^{\,2}}{2RT_1}} \xi_\rho^3 d\xi_\rho \left[\int_0^{\alpha_{506}} d\theta \int_0^{\varphi_{105}(\theta)} \operatorname{Sin}\varphi \operatorname{Cos}\varphi \, d\varphi \right. \quad \text{(A-62)}$$

$$+ \int_{\alpha_{506}}^{\alpha_{807}} d\theta \int_0^{\varphi_{508}(\theta)} \operatorname{Sin}\varphi \operatorname{Cos}\varphi \, d\varphi + \int_{\alpha_{807}}^{\alpha_{403}} d\theta \int_0^{\varphi_{804}(\theta)} \operatorname{Sin}\varphi \operatorname{Cos}\varphi \, d\varphi + \int_{\alpha_{403}}^{\alpha_{102}} d\theta \int_0^{\varphi_{401}(\theta)} \operatorname{Sin}\varphi \operatorname{Cos}\varphi \, d\varphi +$$

$$\int_{\alpha_{102}}^{2\pi} d\theta \int_{0}^{\varphi_{105}(\theta)} \text{Sin } \varphi \text{ Cos } \varphi \, d\varphi \Bigg] + \frac{\rho_2}{(2\pi RT_2)^{3/2}} \int_0^\infty e^{-\frac{\xi_\rho^2}{2RT_2}} \xi_\rho^3 \xi_\rho \Bigg[\int_0^{\alpha_{506}} d\theta \int_{\varphi_{206}(\theta)}^{\pi} \text{Sin } \varphi \text{ Cos } \varphi d\varphi +$$

$$\int_{\alpha_{506}}^{\alpha_{807}} d\theta \int_{\varphi_{705}(\theta)}^{\pi} \text{Sin } \varphi \text{ Cos } \varphi \, d\varphi + \int_{\alpha_{807}}^{\alpha_{403}} d\theta \int_{\varphi_{703}(\theta)}^{\pi} \text{Sin } \varphi \text{ Cos } \varphi \, d\varphi + \int_{\alpha_{403}}^{\alpha_{102}} d\theta \int_{\varphi_{302}(\theta)}^{\pi} \text{Sin } \varphi \text{ Cos } \varphi \, d\varphi +$$

$$\int_{\alpha_{102}}^{2\pi} d\theta \int_{\varphi_{206}(\theta)}^{\pi} \text{Sin } \varphi \text{ Cos } \varphi \, d\varphi \Bigg] + \frac{1}{(2\pi RT_w)^{3/2}} \int_0^\infty e^{-\frac{\xi_\rho^2}{2RT_w}} \xi_\rho^3 d\xi_\rho \Bigg[\int_{\alpha_{506}}^{\alpha_{807}} d\theta \int_{\varphi_{508}(\theta)}^{\varphi_{706}(\theta)} \rho_{w_s}(\theta,\varphi) \text{Sin } \varphi \text{ Cos } \varphi \, d\varphi$$

$$+ \int_{\alpha_{403}}^{\alpha_{102}} d\theta \int_{\varphi_{401}(\theta)}^{\varphi_{302}(\theta)} \rho_{w_s}(\theta,\varphi) \text{Sin } \varphi \text{ Cos } \varphi \, d\varphi + \int_{\alpha_{807}}^{\alpha_{403}} d\theta \int_{\varphi_{804}(\theta)}^{\varphi_{703}(\theta)} \rho_{w_T}(\theta,\varphi) \text{ Sin } \varphi \text{ Cos } \varphi \, d\varphi +$$

$$\int_{\alpha_{102}}^{2\pi} d\theta \int_{\varphi_{105}(\theta)}^{\varphi_{206}(\theta)} \rho_{w_T}(\theta,\varphi) \text{Sin } \varphi \text{ Cos } \varphi \, d\omega + \int_0^{\alpha_{506}} d\theta \int_{\varphi_{105}(\theta)}^{\varphi_{206}(\theta)} \rho_{w_T}(\theta,\varphi) \text{ Sin } \varphi \text{ Cos } \varphi \, d\varphi \Bigg]$$

The following integral formulas will prove useful:

$$\int_0^\infty e^{-ax^2} x^3 dx = \frac{1}{2\pi^2} \left(\frac{\pi}{a} \right)^2 \qquad \text{(A-63)}$$

$$\int \frac{a^2\, d\beta}{[a^2 + b^2 \sin^2 \beta]} = \frac{a}{\sqrt{a^2 + b^2}} \tan^{-1}\left[\frac{\sqrt{a^2 + b^2}\, \tan \beta}{a} \right] \qquad \text{(A-64)}$$

$$\int \frac{a^2\, d\beta}{[a^2 + b^2 \cos^2 \beta]} = \frac{a}{\sqrt{a^2 + b^2}} \tan^{-1}\left[\frac{a \tan \beta}{\sqrt{a^2 + b^2}} \right] \qquad \text{(A-65)}$$

Substituting equation (A-56) into equation (A-62), integrating over the angle φ and expressing the result in terms of θ by using equations (A-12) through (A-19), and performing the remaining integrations by using equations (A-63) through (A-65) yield upon rearrangement

$$\frac{\rho(\bar{x},\bar{y},\bar{z})u(\bar{x},\bar{y},\bar{z})}{(\dot{m}_1 - \dot{m}_2)} = \frac{1}{2\pi}\Bigg[\sin \alpha_{105} \left[\tan^{-1}(\sin \alpha_{105} \tan \alpha_{506}) - \tan^{-1}(\sin \alpha_{105} \tan \alpha_{102}) \right] + \cos \alpha_{508} \left[\tan^{-1}(\sec \alpha_{508} \tan \alpha_{807}) - \tan^{-1}(\sec \alpha_{508} \tan \alpha_{506}) \right] + \sin \alpha_{408} \left[\tan^{-1}(\sin \alpha_{408} \tan \alpha_{403}) - \tan^{-1}(\sin \alpha_{408} \tan \alpha_{807}) \right] + \cos \alpha_{401} \left[\tan^{-1}(\sec \alpha_{401} \tan \alpha_{102}) - \tan^{-1}(\sec \alpha_{401} \tan \alpha_{403}) \right] + 2\Bigg[\int_{\alpha_{506}}^{\alpha_{807}} d\theta \int_{\varphi_{508}(\theta)}^{\varphi_{706}(\theta)} g_{w_s}(\theta,\varphi) \sin \varphi \cos \varphi\, d\varphi \qquad \text{(A-66)}$$

$$+\int_{\alpha_{402}}^{\alpha_{102}} d\theta \int_{\varphi_{401}(\theta)}^{\varphi_{302}(\theta)} g_{w_s}(\theta,\varphi)\,\mathrm{Sin}\,\varphi\,\mathrm{Cos}\,\varphi\,d\varphi + \int_{\alpha_{807}}^{\alpha_{403}} d\theta \int_{\varphi_{804}(\theta)}^{\varphi_{703}(\theta)} g_{w_T}(\theta,\varphi)\mathrm{Sin}\,\varphi\,\mathrm{Cos}\,\varphi\,d\varphi +$$

$$\left.\int_{\alpha_{102}}^{2\pi} d\theta \int_{\varphi_{105}(\theta)}^{\varphi_{206}(\theta)} g_{w_T}(\theta,\varphi)\,\mathrm{Sin}\,\varphi\,\mathrm{Cos}\,\varphi\,d\varphi + \int_{0}^{\alpha_{506}} d\theta \int_{\varphi_{105}(\theta)}^{\varphi_{206}(\theta)} g_{w_T}(\theta,\varphi)\mathrm{Sin}\,\varphi\,\mathrm{Cos}\,\varphi\,d\varphi\right]\Bigg]$$

where equations (A-24) through (A-31) have been used in order to express equation (A-66) in terms of the angles specifying the point in the flow field.

It can be shown that the axial velocity component given by equation (A-66) satisfies the following property:

$$\rho(\bar{x},\bar{y},\bar{z})u(\bar{x},\bar{y},\bar{z}) = \rho(1-\bar{x},\bar{y},\bar{z})\,u(1-\bar{x},\bar{y},\bar{z}) \qquad \text{(A-67)}$$

The results for a rectangular orifice can be obtained by following the procedure outlined for the density. Similarly, the two dimensional limit of equation (A-66) can be shown to be identical to the corresponding expression given by equation (33) of Chapter II by following the same procedure as outlined for obtaining the two dimensional limit for the density.

<u>$\bar{y}$-Component of Velocity</u>. The definition for the $\bar{y}$-component of velocity can be written in terms of spherical coordinates as follows:

$$\rho(\bar{x},\bar{y},\bar{z})v(\bar{x},\bar{y},\bar{z}) \equiv m \int_0^{\infty}\int_0^{2\pi}\int_0^{\pi} f(\bar{x},\bar{y},\bar{z},\xi_\rho,\theta,\varphi)\ \xi_\rho^{\,3}\ \mathrm{Sin}^2\ \varphi\ \mathrm{Cos}\ \theta\ d\varphi d\theta d\xi_\rho \quad \text{(A-68)}$$

Substituting equations (A-32) through (A-35) into equation (A-68) and expanding yield an expression similar to that of equation (A-62). In order to perform the integrations, the following integral formulas are introduced:

$$\int \frac{\mathrm{Cos}^2\ \theta\ d\theta}{[a^2 + b^2\ \mathrm{Cos}^2\ \theta]} = \frac{1}{b^2}\left[\theta - \frac{a}{\sqrt{a^2 + b^2}}\ \mathrm{Tan}^{-1}\left(\frac{a\ \mathrm{Tan}\ \theta}{\sqrt{a^2 + b^2}}\right)\right] \quad \text{(A-69)}$$

$$\int \frac{\mathrm{Cos}\ \theta\ \mathrm{Sin}\ \theta\ d\theta}{[a^2 + b^2\ \mathrm{Sin}^2\ \theta]} = \frac{1}{2b^2} \cdot \mathrm{LN}\ |\ a^2 + b^2\ \mathrm{Sin}^2\ \theta\ | \quad \text{(A-70)}$$

$$\int \mathrm{Tan}^{-1}(a\ \mathrm{Csc}\ \theta)\ \mathrm{Cos}\ \theta\ d\theta = \mathrm{Sin}\ \theta\ \mathrm{Tan}^{-1}\left(\frac{a}{\mathrm{Sin}\ \theta}\right) + \frac{a}{2} \cdot \mathrm{LN}\left|\frac{\mathrm{Sin}^2\ \theta + a^2}{a^2}\right| \quad \text{(A-71)}$$

$$\int \mathrm{Tan}^{-1}(a\ \mathrm{Sec}\ \theta)\mathrm{Cos}\ \theta\ d\theta = \mathrm{Sin}\ \theta\ \mathrm{Tan}^{-1}(a\ \mathrm{Sec}\ \theta) + a\theta - \quad \text{(A-72)}$$

$$\sqrt{a^2 + 1}\ \cdot\ \mathrm{Tan}^{-1}\left(\frac{a\ \mathrm{Tan}\ \theta}{\sqrt{a^2 + 1}}\right)$$

Performing the necessary integrations and simplifying yield

$$\frac{\rho(\bar{x},\bar{y},\bar{z})v(\bar{x},\bar{y},\bar{z})}{(\dot{m}_1 - \dot{m}_2)} = \frac{1}{2\pi}\left\{\underset{105}{\text{Cos}\alpha}\left[\text{Tan}^{-1}(\underset{105}{\text{Sin}\alpha}\ \underset{102}{\text{Tan}\alpha}) - \text{Tan}^{-1}(\underset{105}{\text{Sin}\alpha}\ \underset{506}{\text{Tan}\alpha})\right] + \right. \quad \text{(A-73)}$$

$$\underset{408}{\text{Cos}\alpha}\left[\text{Tan}^{-1}(\underset{408}{\text{Sin}\alpha}\ \underset{807}{\text{Tan}\alpha}) - \text{Tan}^{-1}(\underset{408}{\text{Sin}\alpha}\ \underset{403}{\text{Tan}\alpha})\right] +$$

$$2\left[\int_{\underset{506}{\alpha}}^{\underset{807}{\alpha}} \text{Cos}\,\theta\, d\theta \int_{\underset{508}{\varphi(\theta)}}^{\underset{706}{\varphi(\theta)}} g_{w_s}(\theta,\varphi)\text{Sin}^2\,\varphi d\varphi + \int_{\underset{403}{\alpha}}^{\underset{102}{\alpha}} \text{Cos}\,\theta d\theta \int_{\underset{401}{\varphi(\theta)}}^{\underset{302}{\varphi(\theta)}} g_{w_s}(\theta,\varphi)\,\text{Sin}^2\,\varphi d\varphi + \right.$$

$$\int_{\underset{807}{\alpha'}}^{\underset{403}{\alpha}} \text{Cos}\,\theta d\theta \int_{\underset{304}{\varphi(\theta)}}^{\underset{703}{\varphi(\theta)}} g_{w_T}(\theta,\varphi)\text{Sin}^2\,\varphi d\varphi + \int_{\underset{102}{\alpha'}}^{2\pi} \text{Cos}\,\theta d\theta \int_{\underset{105}{\varphi(\theta)}}^{\underset{206}{\varphi(\theta)}} g_{w_T}(\theta,\varphi)\,\text{Sin}^2\,\varphi d\varphi +$$

$$\left.\left.\int_{\underset{0}{\alpha'}}^{\underset{506}{\alpha}} \text{Cos}\,\theta d\theta \int_{\underset{105}{\varphi(\theta)}}^{\underset{206}{\varphi(\theta)}} g_{w_T}(\theta,\varphi)\text{Sin}^2\,\varphi d\varphi \right]\right\}$$

Equations (A-24) through (A-31) have been used again to write equation (A-73) in terms of the angles specifying the point in the flow field.

It can be shown that equation (A-73) satisfies the following property:

$$\rho(\bar{x},\bar{y},\bar{z})v(\bar{x},\bar{y},\bar{z}) = - \rho(1-\bar{x},\bar{y},\bar{z})v(1-\bar{x},\bar{y},\bar{z}) \qquad \text{(A-74)}$$

The results for a rectangular orifice can be obtained directly from equation (A-73) by following the procedure outlined for the other moments. Likewise, the two dimensional limit of equation (A-73) can be shown to be identical to the corresponding expression given by equation (36) of Chapter II.

$\bar{z}$-Component of Velocity. In terms of spherical coordinates the $\bar{z}$-component of velocity is defined as follows:

$$\rho(\bar{x},\bar{y},\bar{z})w(\bar{x},\bar{y},\bar{z}) \equiv m\int_0^{\infty}\int_0^{2\pi}\int_0^{\pi} f(\bar{x},\bar{y},\bar{z},\xi_\rho,\theta,\varphi)\xi_\rho^3 \operatorname{Sin}^2\varphi \operatorname{Sin}\theta \, d\varphi d\theta d\xi_\rho \qquad \text{(A-75)}$$

Comparing equations (A-68) and (A-75) it is apparent that the only difference is interchanging of the sine and cosine of the angle θ. Consequently, when equations (A-32) through (A-35) are introduced into equation (A-75), all the integrations, with the exception of the integration with respect to the angle θ, will be the same as before. In order to carry out the integrations with respect to θ the following integral formulas are needed:

$$\int \frac{\operatorname{Sin}^2\theta \, d\theta}{[a^2 + b^2 \operatorname{Sin}^2\theta]} = \frac{1}{b^2}\left\{ \theta - \frac{a}{\sqrt{a^2 + b^2}} \operatorname{Tan}^{-1}\left(\frac{\sqrt{a^2 + b^2}\operatorname{Tan}\theta}{a} \right) \right\} \qquad \text{(A-76)}$$

$$\int \frac{\cos\theta \sin\theta \, d\theta}{[a^2 + b^2 \cos^2\theta]} = \frac{-1}{2b^2} \text{ LN } | a^2 + b^2 \cos^2\theta | \qquad \text{(A-77)}$$

$$\int \text{Tan}^{-1}(a \sec\theta)\sin\theta \, d\theta = -\cos\theta \, \text{Tan}^{-1}(a \sec\theta) - \frac{a}{2} \text{ LN} \left| \frac{a^2 \cos^2\theta}{a^2} \right| \qquad \text{(A-78)}$$

$$\int \text{Tan}^{-1}(a \csc\theta)\sin\theta \, d\theta = -\cos\theta \, \text{Tan}^{-1}(a \csc\theta) + a\theta - \qquad \text{(A-79)}$$

$$\sqrt{a^2 + 1} \quad \text{Tan}^{-1}\left(\frac{\sqrt{a^2 + 1} \ \text{Tan}\,\theta}{a} \right)$$

Following the same procedure as used in determining the other two velocity components the general expression for the $\bar{z}$-component of velocity becomes:

$$\frac{\rho(\bar{x},\bar{y},\bar{z})w(\bar{x},\bar{y},\bar{z})}{(\dot{m}_1 - \dot{m}_2)} = \frac{1}{2\pi} \left\{ \underset{508}{\text{Sin}\alpha} \left[\text{Tan}^{-1}(\underset{508}{\text{Sec}\alpha} \ \underset{506}{\text{Tan}\alpha}) - \text{Tan}^{-1}(\underset{508}{\text{Sec}\alpha} \ \underset{807}{\text{Tan}\alpha}) \right] + \qquad \text{(A-80)} \right.$$

$$\underset{401}{\text{Sin}\alpha} \left[\text{Tan}^{-1}(\underset{401}{\text{Sec}\alpha} \ \underset{403}{\text{Tan}\alpha}) - \text{Tan}^{-1}(\underset{401}{\text{Sec}\alpha} \ \underset{102}{\text{Tan}\alpha}) \right] +$$

$$2\left[\int_{506}^{\alpha} \sin\theta \, d\theta \int_{\varphi_{508}(\theta)}^{\varphi_{706}(\theta)} g_{w_s}(\theta,\varphi)\sin^2\varphi \, d\varphi + \int_{403}^{\alpha} \sin\theta \, d\theta \int_{\varphi_{401}(\theta)}^{\varphi_{302}(\theta)} g_{w_s}(\theta,\varphi)\sin^2\varphi \, d\varphi + \right.$$

$$\int_{\alpha_{807}}^{\alpha_{403}} \mathrm{Sin}\,\theta d\theta \int_{\varphi_{804}(\theta)}^{\varphi_{703}(\theta)} g_{w_T}(\theta,\varphi)\mathrm{Sin}^2\,\varphi d\varphi + \int_{\alpha_{102}}^{2\pi} \mathrm{Sin}\,\theta d\theta \int_{\varphi_{105}(\theta)}^{\varphi_{206}(\theta)} g_{w_T}(\theta,\omega)\mathrm{Sin}^2\,\varphi d\varphi +$$

$$\int_{0}^{\alpha_{506}} \mathrm{Sin}\,\theta d\theta \int_{\varphi_{105}(\theta)}^{\varphi_{206}(\theta)} g_{w_T}(\theta,\varphi)\mathrm{Sin}^2\,\varphi d\varphi \Big] \Big\}$$

Again following the procedure as outlined for the other two velocity components the rectangular orifice limit can be obtained directly from equation (A-80). Similarly, the two dimensional limit of equation (A-80), which is $\rho(\bar{x},\bar{y},\bar{z})\cdot w(\bar{x},\bar{y},\bar{z}) = 0$, can be deduced by following the procedure outlined to determine the two dimensional limits of the other velocity components. Finally, the $\bar{z}$-component of velocity satisfies the anti-symmetric property given by

$$\rho(\bar{x},\bar{y},\bar{z})w(\bar{x},\bar{y},\bar{z}) = -\rho(1-\bar{x},\bar{y},\bar{z})w(1-\bar{x},\bar{y},\bar{z}) \qquad \text{(A-81)}$$

Average Mass Flow Rate

The nondimensional average mass flow rate crossing the channel at $\bar{x}$ is defined as follows:

$$\Lambda(\bar{x},\tau_d,\tau_b) \equiv \frac{\overline{\rho(\bar{x},\bar{y},\bar{z})u(\bar{x},\bar{y},\bar{z})}}{(\dot{m}_1 - \dot{m}_2)} = \int_0^1\int_0^1 \frac{\rho(\bar{x},\bar{y},\bar{z})u(\bar{x},\bar{y},\bar{z})}{(\dot{m}_1 - \dot{m}_2)}\, d\bar{y}d\bar{z} \qquad \text{(A-82)}$$

Introduce the following definitions:

$$A(\bar{x},\tau_d,\tau_b) \equiv \int_0^1 \int_0^1 \frac{\bar{y}}{\sqrt{\bar{y}^2 + \tau_d^2\bar{x}^2}} \operatorname{Tan}^{-1}\left(\frac{\tau_d\bar{z}}{\tau_b\sqrt{\bar{y}^2 + \tau_d^2\bar{x}^2}}\right) d\bar{y}d\bar{z} \qquad \text{(A-83)}$$

$$B(\bar{x},\tau_d,\tau_b) \equiv \int_0^1 \int_0^1 \frac{\bar{z}}{\sqrt{\bar{z}^2 + \tau_b^2\bar{x}^2}} \operatorname{Tan}^{-1}\left(\frac{\tau_b\bar{y}}{\tau_d\sqrt{\bar{z}^2 + \tau_b^2\bar{x}^2}}\right) d\bar{y}d\bar{z} \qquad \text{(A-84)}$$

When equation (A-66) is substituted into equation (A-82) and the resulting integrals, with the exception of the wall contribution, expressed in terms of the coordinates $\bar{x},\bar{y}$, and $\bar{z}$, the following result is obtained:

$$\Lambda(\bar{x},\tau_d,\tau_b) = \frac{2}{\pi}\Big\{ A(\bar{x},\tau_d,\tau_b) + B(\bar{x},\tau_d,\tau_b) + \qquad \text{(A-85)}$$

$$\frac{1}{2}\Big[\int_0^1 d\bar{y} \int_0^1 d\bar{z} \int_{\alpha_{506}}^{\alpha_{807}} d\theta \int_{\varphi_{508}(\theta)}^{\varphi_{706}(\theta)} g_{w_s}(\theta,\varphi)\, \text{Sin}\, \varphi\, \text{Cos}\, \varphi\, d\varphi +$$

$$\int_0^1 d\bar{y} \int_0^1 d\bar{z} \int_{\alpha_{403}}^{\alpha_{102}} d\theta \int_{\varphi(\theta)_{401}}^{\varphi_{302}(\theta)} g_{w_s}(\theta,\varphi)\text{Sin}\, \varphi\, \text{Cos}\, \varphi\, d\varphi + \int_0^1 d\bar{y}\int_0^1 d\bar{z}\int_{\alpha_{807}}^{\alpha_{403}} d\theta \int_{\varphi_{804}(\theta)}^{\varphi_{703}(\theta)} g_{w_T}(\theta,\varphi)\text{Sin}\varphi\, \text{Cos}\, \varphi\, d\varphi +$$

$$\int_0^1 d\bar{y} \int_0^1 d\bar{z} \left[\int_0^{2\pi} d\theta \int_{\varphi(\theta)_{105}}^{\varphi(\theta)_{206}} g_{w_T}(\theta,\varphi) \operatorname{Sin}\varphi \operatorname{Cos}\varphi d\varphi + \int_0^{\alpha_{506}} d\theta \int_{\varphi(\theta)_{105}}^{\varphi(\theta)_{206}} g_{w_T}(\theta,\varphi) \operatorname{Sin}\varphi \operatorname{Cos}\varphi d\varphi \right] \Bigg\}$$

In order to perform the integrations with respect to $\bar{y}$ and $\bar{z}$ in the wall contribution, it is necessary to transform from the velocity coordinates θ and φ to the wall coordinates. Equations (A-4) through (A-11) are the necessary transformation equations. By applying the appropriate transformation equations for each integral of equation (A-85), the following relations are deduced:

$$\operatorname{Sin}\varphi \operatorname{Cos}\varphi \, d\varphi d\theta = H'_{w_s}(\bar{x}'_s, \bar{x}, \bar{y}'_s, \bar{y}, \bar{z}) \, d\bar{x}'_s d\bar{y}'_s \tag{A-86}$$

$$\operatorname{Sin}\varphi \operatorname{Cos}\varphi \, d\varphi d\theta = - H''_{w_s}(\bar{x}''_s, \bar{x}, \bar{y}''_s, \bar{y}, \bar{z}) \, d\bar{x}''_s d\bar{y}''_s \tag{A-87}$$

$$\operatorname{Sin}\varphi \operatorname{Cos}\varphi \, d\varphi d\theta = - H'_{w_T}(\bar{x}'_T, \bar{x}, \bar{y}, \bar{z}'_T, \bar{z}) \, d\bar{x}'_T d\bar{z}'_T \tag{A-88}$$

$$\operatorname{Sin}\varphi \operatorname{Cos}\varphi \, d\varphi d\theta = H''_{w_T}(\bar{x}''_T, \bar{x}, \bar{y}, \bar{z}''_T, \bar{z}) \, d\bar{x}''_T d\bar{z}''_T \tag{A-89}$$

where

$$H'_{w_s}(\bar{x}'_s, \bar{x}, \bar{y}'_s, \bar{y}, \bar{z}) \equiv \frac{\tau_b^3 \tau_d^3 \bar{z} \, (\bar{x} - \bar{x}'_s)}{[\tau_d^2 \bar{z}^2 + \tau_b^2 (\bar{y} - \bar{y}'_s)^2 + \tau_b^2 \tau_d^2 (\bar{x} - \bar{x}'_s)^2]^2} \tag{A-90}$$

$$H''_{w_s}(\bar{x}''_s,\bar{x},\bar{y}''_s,\bar{y},\bar{z}) \equiv \frac{\tau_b^3\tau_d^3(1-\bar{z})(\bar{x}-\bar{x}''_s)}{[\tau_d^2(\bar{z}-1)^2 + \tau_b^2(\bar{y}-\bar{y}''_s)^2 + \tau_b^2\tau_d^2(\bar{x}-\bar{x}''_s)^2]^2} \qquad (A\text{-}91)$$

$$H'_{w_T}(\bar{x}'_T,\bar{x},\bar{y},\bar{z}'_T,\bar{z}) \equiv \frac{\tau_b^3\tau_d^3\bar{y}\,(\bar{x}-\bar{x}'_T)}{[\tau_b^2\bar{y}^2 + \tau_d^2(\bar{z}-\bar{z}'_T)^2 + \tau_b^2\tau_d^2(\bar{x}-\bar{x}'_T)^2]^2} \qquad (A\text{-}92)$$

$$H''_{w_T}(\bar{x}''_T,\bar{x},\bar{y},\bar{z}''_T,\bar{z}) \equiv \frac{\tau_b^3\tau_d^3(1-\bar{y})(\bar{x}-\bar{x}''_T)}{[\tau_b^2(\bar{y}-1)^2 + \tau_d^2(\bar{z}-\bar{z}''_T)^2 + \tau_b^2\tau_d^2(\bar{x}-\bar{x}''_T)^2]^2} \qquad (A\text{-}93)$$

and the primes have the same meaning as for the wall coordinates. Introducing the following definitions,

$$C(\bar{x},\tau_d,\tau_b) \equiv \int_0^1\int_0^1\int_0^1\int_0^1 g_{w_T}(\bar{x}'_T,\bar{z}'_T)H'_{w_T}(\bar{x}'_T,\bar{x},\bar{y},\bar{z}'_T,\bar{z})\,d\bar{x}'_T d\bar{z}'_T d\bar{y} d\bar{z} \qquad (A\text{-}94)$$

and

$$D(\bar{x},\tau_d,\tau_b) \equiv \int_0^1\int_0^1\int_0^1\int_0^1 g_{w_s}(\bar{x}'_s,\bar{y}'_s)H'_{w_s}(\bar{x}'_s,\bar{x},\bar{y}'_s,\bar{y},\bar{z})\,d\bar{x}'_s d\bar{y}'_s d\bar{y} d\bar{z} \qquad (A\text{-}95)$$

and noting that all the integrals for the wall contributions in equation (A-85) can be expressed in terms of the definitions in equations (A-94) and (A-95), the following form for the average mass flow rate is obtained from equation (A-85):

$$\Lambda(\bar{x},\tau_d,\tau_b) = \frac{2}{\pi}\left\{A(\bar{x},\tau_d,\tau_b) + B(\bar{x},\tau_d,\tau_b) + C(\bar{x},\tau_d,\tau_b) + D(\bar{x},\tau_d,\tau_b)\right\} \quad \text{(A-96)}$$

The task of determining the average mass flow rate has been reduced to that of evaluating the functions appearing on the right-hand side of equation (A-96) from the definitions in equations (A-83), (A-84), (A-94), and (A-95). After straightforward but rather tedious integrations the following results are obtained:

$$A(x,\tau_d,\tau_b) = \sqrt{1+\tau_d^2\bar{x}^2}\ \mathrm{Tan}^{-1}\left(\frac{\tau_d}{\tau_b\sqrt{1+\tau_d^2\bar{x}^2}}\right) - \tau_d\bar{x}\ \mathrm{Tan}^{-1}\left(\frac{1}{\tau_b\bar{x}}\right) + \frac{1}{4}\left\{\frac{\tau_d}{\tau_b}\cdot \right. \quad \text{(A-97)}$$

$$\left[2\mathrm{LN}\left|\tau_d^2 + \tau_b^2(1+\tau_d^2\bar{x}^2)\right| - \mathrm{LN}\left|1+\tau_b^2\bar{x}^2\right| - \mathrm{LN}\left|\tau_b^2+\tau_d^2\right.\right.\cdot$$

$$\left.\left.(1+\tau_b^2\bar{x}^2)\right| - \mathrm{LN}\left|\tau_d^2\right|\right] + \frac{\tau_b}{\tau_d}\left[\mathrm{LN}\left|1+\tau_d^2\bar{x}^2\right| + \mathrm{LN}\left|\tau_b^2\right| -\right.$$

$$\left.\mathrm{LN}\left|\tau_b^2+\tau_d^2(1+\tau_b^2\bar{x}^2)\right|\right] + \tau_d\tau_b\bar{x}^2\left[\mathrm{LN}\left|1+\tau_b^2\bar{x}^2\right| -\right.$$

$$\left.\left.\mathrm{LN}\left|\tau_b^2+\tau_d^2(1+\tau_b^2\bar{x}^2)\right| + \mathrm{LN}\left|1+\tau_d^2\bar{x}^2\right| - \mathrm{LN}\left|\bar{x}^2\right|\right]\right\}$$

$$C(\bar{x},\tau_d,\tau_b) = \int_0^1 \int_0^1 g_{w_T}(\bar{x}'_T,\bar{z}'_T) F'_{w_T}(\bar{x},\bar{x}'_T,\bar{z}'_T,\tau_d,\tau_b)\, d\bar{x}'_T d\bar{z}'_T \qquad \text{(A-98)}$$

where

$$F'_{w_T}(\bar{x},\bar{x}'_T,\bar{z}'_T,\tau_d,\tau_b) \equiv \frac{\tau_d^2(\bar{x}-\bar{x}'_T)}{2}\left\{ \frac{1}{\tau_d|\bar{x}-\bar{x}'_T|}\left[\mathrm{Tan}^{-1}\left(\frac{1-\bar{z}'_T}{\tau_b|\bar{x}-\bar{x}'_T|}\right) + \right.\right. \qquad \text{(A-99)}$$

$$\left. \mathrm{Tan}^{-1}\left(\frac{\bar{z}'_T}{\tau_b|\bar{x}-\bar{x}'_T|}\right)\right] - \frac{1}{\sqrt{1+\tau_d^2(\bar{x}-\bar{x}'_T)^2}}\left[\mathrm{Tan}^{-1}\left(\frac{\tau_d(1-\bar{z}'_T)}{\tau_b\sqrt{1+\tau_d^2(\bar{x}-\bar{x}'_T)^2}}\right) + \right.$$

$$\left.\left. \mathrm{Tan}^{-1}\left(\frac{\tau_d\bar{z}'_T}{\tau_b\sqrt{1+\tau_d^2(\bar{x}-\bar{x}'_T)^2}}\right)\right]\right\}$$

and

$$D(\bar{x},\tau_d,\tau_b) = \int_0^1 \int_0^1 g_{w_s}(\bar{x}'_s,\bar{y}'_s) F'_{w_s}(\bar{x},\bar{x}'_s,\bar{y}'_s,\tau_d,\tau_b)\, d\bar{x}'_s d\bar{y}'_s \qquad \text{(A-100)}$$

The expressions for $B(\bar{x},\tau_d,\tau_b)$ and $F'_{w_s}(\bar{x},\bar{x}'_s,\bar{y}'_s,\tau_d,\tau_b)$ can be obtained from equations (A-97) and (A-99) by interchanging the variables and parameters. Thus,

$$B(\bar{x},\tau_d,\tau_b) = A(\bar{x},\tau_b,\tau_d) \qquad \text{(A-101)}$$

$$F'_{w_s}(\bar{x},\bar{x}'_s,\bar{y}'_s,\tau_d,\tau_b) = F'_{w_T}(\bar{x},\bar{x}'_s,\bar{y}'_s,\tau_b,\tau_d) \qquad \text{(A-102)}$$

Combining equations (A-96) through (A-101) and simplifying the resulting expression yield:

$$\Lambda(\bar{x},\tau_d,\tau_b) = \frac{2}{\pi}\left\{\sqrt{1+\tau_d^2\bar{x}^2}\ \mathrm{Tan}^{-1}\left(\frac{\tau_d}{\tau_b\sqrt{1+\tau_d^2\bar{x}^2}}\right) - \tau_d\bar{x}\ \mathrm{Tan}^{-1}\left(\frac{1}{\tau_b\bar{x}}\right) + \right. \qquad \text{(A-103)}$$

$$\sqrt{1+\tau_b^2\bar{x}^2}\ \ \mathrm{Tan}^{-1}\left(\frac{\tau_b}{\tau_d\sqrt{1+\tau_b^2\bar{x}^2}}\right) - \tau_b\bar{x}\ \mathrm{Tan}^{-1}\left(\frac{1}{\tau_d\bar{x}}\right) + \frac{\tau_b\tau_d\bar{x}^2}{2} \cdot$$

$$\left[\ \mathrm{LN}\left|1+\tau_b^2\bar{x}^2\right| + \mathrm{LN}\left|1+\tau_d^2\bar{x}^2\right| - \mathrm{LN}\left|\tau_d^2+\tau_b^2(1+\tau_d^2\bar{x}^2)\right| - \mathrm{LN}\left|\bar{x}^2\right|\right] +$$

$$\int_0^1\int_0^1 g_{w_T}(\bar{x}'_T,\bar{z}'_T)F'_{w_T}(\bar{x},\bar{x}'_T,\bar{z}'_T,\tau_d,\tau_b)d\bar{x}'_T d\bar{z}'_T +$$

$$\left.\int_0^1\int_0^1 g_{w_s}(\bar{x}'_s,\bar{y}'_s)F'_{w_s}(\bar{x},\bar{x}'_s,\bar{y}'_s,\tau_d,\tau_b)d\bar{x}'_s d\bar{y}'_s\ \right\}$$

Consider the two dimensional limit of $\Lambda(\bar{x},\tau_d,\tau_b)$. Setting $\tau_b = 0$ in equation (A-103), performing the necessary integrations, and simplifying

the resulting expression, it can be shown that equation (A-103) reduces to equation (65) of Chapter II. It should be noted that the same argument, as presented for the two dimensional case, concerning the independence of the average mass flow rate on the axial coordinate is also applicable here. Thus, in order to determine the average mass flow rate passing through the channel, equation (103) can be evaluated for any $\bar{x}$ in the range $0 \leq \bar{x} \leq 1$. Following the normal procedure and evaluating equation (103) at $\bar{x} = 0$ yields

$$\Lambda(\tau_d,\tau_b) = 1 - \frac{2}{\pi}\left\{ \int_0^1\int_0^1 g_{w_T}(\bar{x}_T',\bar{z}_T')F_{w_T}(\bar{x}_T',\bar{z}_T',\tau_d,\tau_b)d\bar{x}_T'd\bar{z}_T' + \right. \tag{A-104}$$

$$\left. \int_0^1\int_0^1 g_{w_s}(\bar{x}_s',\bar{y}_s')F_{w_s}(\bar{x}_s',\bar{y}_s',\tau_d,\tau_b)d\bar{x}_s'd\bar{y}_s' \right\}$$

where

$$F_{w_T}(\bar{x}_T',\bar{z}_T',\tau_d,\tau_b) \equiv F'_{w_T}(0,\bar{x}_T',\bar{z}_T',\tau_d,\tau_b) \tag{A-105}$$

$$F_{w_s}(\bar{x}_s',\bar{y}_s',\tau_d,\tau_b) \equiv F'_{w_s}(0,\bar{x}_s',\bar{y}_s',\tau_d,\tau_b) \tag{A-106}$$

Again setting $\tau_b = 0$ it can be shown that equation (A-104) reduces to the two dimensional limit given by equation (69) of Chapter II.

APPENDIX B

DERIVATION AND APPROXIMATE SOLUTION OF INTEGRAL EQUATION REPRESENTING BOUNDARY CONDITION FOR FREE MOLECULAR FLOW THROUGH TWO DIMENSIONAL CHANNELS

Derivation of Integral Equation

The boundary condition for free molecular flow through two dimensional channels of finite length is given by equation (11) of Chapter II as

$$\int_{-\infty}^{\infty}\int\int \eta \cdot f(\bar{x}, \bar{y} = \begin{matrix}0\\1\end{matrix}, \xi, \eta, \zeta)\, d\xi d\eta d\zeta = 0 \qquad \text{(B-1)}$$

Rewrite equation (B-1) as separate integrals over positive and negative values of η. Introducing equations (1) through (4) of Chapter II for the distribution functions and noting that for a point on the upper wall the angles $\alpha_3(\bar{x},\bar{y})$ and $\alpha_4(\bar{x},\bar{y})$ take on the values of π and 2π, respectively, equation (B-1) can be written as follows for $\bar{y} = 1$:

$$\frac{n_U(\bar{x}'')}{(2\pi RT_U)^{3/2}} \int_{-\infty}^{\infty}\int_{-\infty}^{0}\int_{-\infty}^{\infty} \eta \cdot e^{-\frac{[\xi^2+\eta^2+\zeta^2]}{2RT_U}}\, d\xi d\eta d\zeta + \qquad \text{(B-2)}$$

$$\frac{n_1}{(2\pi RT_1)^{3/2}} \int_{-\infty}^{\infty}\int_{0}^{\infty}\int_{\tau\bar{x}\eta}^{\infty} \eta \cdot e^{-\frac{[\xi^2+\eta^2+\zeta^2]}{2RT_1}}\, d\xi d\eta d\zeta +$$

$$\frac{1}{(2\pi RT_L)^{3/2}} \int_{-\infty}^{\infty}\int_{0}^{\infty}\int_{\tau(1-\bar{x})\eta}^{\tau\bar{x}\eta} n_L(\bar{x}')\eta . e^{-\frac{[\xi^2+\eta^2+\zeta^2]}{2RT_L}} d\xi d\eta d\zeta +$$

$$\frac{n_2}{(2\pi RT_2)^{3/2}} \int_{-\infty}^{\infty}\int_{0}^{\infty}\int_{-\infty}^{\tau(1-\bar{x})\eta} \eta . e^{-\frac{[\xi^2+\eta^2+\zeta^2]}{2RT_2}} d\xi d\eta d\zeta = 0$$

It should be noted that the upper wall density function has been taken outside the integration but the lower wall density function has been kept inside. The reason is obvious when one remembers that the point in the flow field under observation is that located at $\bar{y} = 1$ and $\bar{x} = \bar{x}''$. Since the upper wall density varies only with $\bar{x}''$, $n_U(\bar{x}'')$ is a constant for the particular point and can therefore be taken outside the integral. However, it can be seen from equation (9) of Chapter II that $\bar{x}'$ is a function of the molecular velocities and correspondingly the lower wall density must be kept inside the integral.

Introducing cylindrical velocity coordinates defined as

$$\xi_r \equiv \sqrt{\xi^2 + \eta^2} \tag{B-3}$$

$$\text{Tan } \alpha \equiv \frac{\eta}{\xi}$$

and noting from equation (9) of Chapter II that the variable $\bar{x}'$ can be replaced by the polar angle α, then equation (B-2) becomes

$$\frac{n_U(\bar{x}'')}{(2\pi RT_U)^{3/2}}\int_{-\infty}^{\infty} e^{-\frac{\zeta^2}{2RT_U}}\,d\zeta \int_0^{\infty} e^{-\frac{\xi_r^2}{2RT_U}}\,\xi_r^2 d\xi_r \int_{\pi}^{2\pi} \mathrm{Sin}\,\alpha\,d\alpha + \qquad \text{(B-4)}$$

$$\frac{n_1}{(2\pi RT_1)^{3/2}}\int_{-\infty}^{\infty} e^{-\frac{\zeta^2}{2RT_1}}\,d\zeta \int_0^{\infty} e^{-\frac{\xi_r^2}{2RT_1}}\,\xi_r^2 d\xi_r \int_0^{\alpha_{1_d}} \mathrm{Sin}\,\alpha\,d\alpha +$$

$$\frac{1}{(2\pi RT_L)^{3/2}}\int_{-\infty}^{\infty} e^{-\frac{\zeta^2}{2RT_L}}\,d\zeta \int_0^{\infty} e^{-\frac{\xi_r^2}{2RT_L}}\,\xi_r^2 d\xi_r \int_{\alpha_{1_d}}^{\alpha_{2_d}} n_L(\alpha)\mathrm{Sin}\,\alpha\,d\alpha +$$

$$\frac{n_2}{(2\pi RT_2)^{3/2}}\int_{-\infty}^{\infty} e^{-\frac{\zeta^2}{2RT_2}}\,d\zeta \int_0^{\infty} e^{-\frac{\xi_r^2}{2RT_2}}\,\xi_r^2 d\xi_r \int_{\alpha_{2_d}}^{\pi} \mathrm{Sin}\,\alpha\,d\,\alpha = 0$$

where the angles α_{1_d} and α_{2_d} are the angles $\alpha_1(\bar{x},\bar{y})$ and $\alpha_2(\bar{x},\bar{y})$ evaluated at $\bar{y} = 1$. Making use of the following integrals,

$$\int_{-\infty}^{\infty} e^{-ax^2}\,dx = \sqrt{\frac{\pi}{a}} \qquad \text{(E-5)}$$

and

$$\int_0^{\infty} e^{-ax^2}\,x^2\,dx = \frac{1}{4\pi}\left(\frac{\pi}{a}\right)^{3/2}$$

equation (B-4) reduces to

$$- \frac{n_U(\bar{x}")\sqrt{2\pi RT_U}}{2\pi} + \frac{n_1\sqrt{2\pi RT_1}}{4\pi} \left(1 - \cos \alpha_{1_d} \right) + \frac{\sqrt{2\pi RT_L}}{4\pi} \cdot \tag{B-6}$$

$$\int_{\alpha_{1_d}}^{\alpha_{2_d}} n_L(\alpha) \sin \alpha \, d\alpha + \frac{n_2\sqrt{2\pi RT_2}}{4\pi} \left(1 + \cos \alpha_{2_d} \right) = 0$$

Define:

$$\dot{m}_L(\alpha) \equiv \frac{n_L(\alpha)\sqrt{2\pi RT_L}}{2\pi} \tag{B-7}$$

$$\dot{m}_U(\bar{x}") \equiv \frac{n_U(\bar{x}")\sqrt{2\pi RT_U}}{2\pi}$$

$$\dot{m}_1 \equiv \frac{n_1\sqrt{2\pi RT_1}}{2\pi}$$

$$\dot{m}_2 \equiv \frac{n_2\sqrt{2\pi RT_2}}{2\pi}$$

and note that $\dot{m}_1$ and $\dot{m}_2$ are the mass fluxes from the left and right reservoirs, respectively, into the channel. Equation (B-6) can now be written as

$$\dot{m}_U(\bar{x}") = \frac{\left(1 - \cos \alpha_{1_d}\right)}{2} \dot{m}_1 + \frac{\left(1 + \cos \alpha_{2_d}\right)}{2} \dot{m}_2 + \tag{B-8}$$

$$\frac{1}{2} \int_{\alpha_{1_d}}^{\alpha_{2_d}} \dot{m}_L(\alpha) \sin \alpha \, d\alpha$$

In a similar manner the boundary condition for $\bar{y} = 0$ reduces to

$$\dot{m}_L(\bar{x}') = \frac{(1 - \text{Cos } \alpha_{4_0})}{2} \dot{m}_1 + \frac{(1 + \text{Cos } \alpha_{3_0})}{2} \dot{m}_2 + \frac{1}{2} \int_{\alpha_{3_0}}^{\alpha_{4_0}} \dot{m}_U(\alpha) \text{ Sin } \alpha \, d\alpha \tag{B-9}$$

where α_{4_0} and α_{3_0} denote the angles α_4 $(\bar{x}, \bar{y} = 0)$ and α_3 $(\bar{x}, \bar{y}, = 0)$, respectively. Noting that for $\bar{x}' = \bar{x}''$

$$\alpha_{1_d} = 2\pi - \alpha_{4_0} \tag{B-10}$$

and

$$\alpha_{2_d} = 2\pi - \alpha_{3_0}$$

then

$$\text{Cos } \alpha_{4_0} = \text{Cos } \alpha_{1_d} \tag{B-11}$$

and

$$\text{Cos } \alpha_{3_0} = \text{Cos } \alpha_{2_d}$$

Comparing equations (B-8) and (B-9) and making use of equations (B-10) and (B-11) it can be seen that for $\bar{x}' = \bar{x}''$

$$\dot{m}_L(\bar{x}') = \dot{m}_U(\bar{x}'') \tag{B-12}$$

Introducing the new variable, $\dot{m}_w(\bar{x}')$, which denotes either $\dot{m}_L(\bar{x}')$ or $\dot{m}_U(\bar{x}'')$, and defining the nondimensional wall flux,

$$g_w(\bar{x}) \equiv \frac{\dot{m}_w(\bar{x}) - \dot{m}_2}{\dot{m}_1 - \dot{m}_2} \tag{B-13}$$

equations (B-8) and (B-9) reduce to the common integral equation

$$g_w(\bar{x}) = \frac{(1 - \text{Cos } \alpha_{1_d})}{2} + \frac{1}{2}\int_{\alpha_{1_d}}^{\alpha_{2_d}} g_w(\alpha) \text{ Sin } \alpha \, d\alpha \tag{B-14}$$

Since $\alpha_{1_d} \leq \alpha \leq \alpha_{2_d}$, the angle α satisfies the equation

$$\text{Sin } \alpha = \frac{1}{\sqrt{\tau^2(\bar{x}' - \bar{x}'')^2 + 1}} \tag{B-15}$$

where $\bar{x}''$ now denotes the wall coordinate of the opposite wall. Remembering that equation (B-14) determines the wall density at $\bar{x}'$, then as α varies from α_{1_d} to α_{2_d}, $\bar{x}''$ varies from 0 to 1. Therefore, substituting equation (B-15) into equation (B-14) and writing Cos α_{1_d} in terms of the variable $\bar{x}'$, the following integral equation for the boundary condition is obtained:

$$g_w(\bar{x}') = F(\bar{x}') + \int_0^1 g_w(\bar{x}'')\, K(\bar{x}', \bar{x}'')\, d\bar{x}'' \tag{B-16}$$

where

$$F(\bar{x}') = \frac{1}{2}\left[1 - \frac{\tau\bar{x}'}{\sqrt{\tau^2\bar{x}'^2 + 1}}\right] \tag{B-17}$$

and

$$K(\bar{x}', \bar{x}'') = \frac{\tau}{2\left[\tau^2(\bar{x}' - \bar{x}'')^2 + 1\right]^{3/2}} \tag{B-18}$$

Approximate Solution of Integral Equation

The collocation method of solving integral equations is used to obtain an approximate solution for the integral equation representing the boundary condition. In order to apply this method it is necessary to choose a series of functions which together satisfy the known properties of the exact solution. For the integral equation in equation (B-16) the following approximation was chosen:

$$g_w(\bar{x}') = \bar{x}' + \sum_{k=1}^{M} B_{2k-1}(\tau)\, \varphi_{2k-1}(\bar{x}') \tag{B-19}$$

where

$$\varphi_{2k-1}(\bar{x}') = (\bar{x}' - \tfrac{1}{2})^{2k-1} \tag{B-20}$$

and the coefficients, $B_{2k-1}(\tau)$, are functions of τ and can be obtained by satisfying the integral equation at discrete points over the inteval $0 \leq \bar{x}' < 1/2$. Substituting equation (B-19) into equation (B-16) yields

$$\sum_{k=1}^{M} B_{2k-1}(\tau) \left[\varphi_{2k-1}(\bar{x}') - \Phi_{2k-1}(\bar{x}') \right] \cong F(\bar{x}') + \Phi_{-1}(\bar{x}') - \bar{x}' \quad \text{(B-21)}$$

where

$$\Phi_{2k-1}(\bar{x}') \equiv \int_0^1 \varphi_{2k-1}(\bar{x}'') \, K(\bar{x}',\bar{x}'') \, d\bar{x}'' \quad \text{(B-22)}$$

and

$$\Phi_{-1}(\bar{x}') \equiv \int_0^1 \bar{x}'' \, K(\bar{x}',\bar{x}'') \, d\bar{x}'' \quad \text{(B-23)}$$

and the kernel, $K(\bar{x}',\bar{x}'')$, and $F(\bar{x}')$ are given by equations (B-18) and (B-17), respectively.

Consider equations (B-22) and (B-23). Making the following change of variable,

$$\xi' = \tau(\bar{x}'' - \bar{x}') \quad \text{(B-24)}$$

gives

$$\Phi_{2k-1}(\bar{x}') = \frac{1}{2} \int_{-\tau\bar{x}'}^{\tau(1-\bar{x}')} \varphi_{2k-1}(\xi',\bar{x}') \, K'(\xi') \, d\xi' \quad \text{(B-25)}$$

and

$$\Phi_{-1}(\bar{x}') = \frac{1}{2}\int_{-\tau\bar{x}'}^{\tau(1-\bar{x}')} \left(\frac{\xi'}{\tau} + \bar{x}' \right) K'(\xi')\, d\xi' \tag{B-26}$$

where

$$K'(\xi') = \frac{1}{\left[\xi'^2 + 1\right]^{3/2}} \tag{B-27}$$

and

$$\varphi_{2k-1}(\xi', \bar{x}') = \left[\xi'/\tau + (\bar{x}' - \tfrac{1}{2}) \right]^{2k-1} \tag{B-28}$$

Substituting equation (B-28) into equation (B-25) and using the binomial expansion gives

$$\Phi_{2k-1}(\bar{x}') = \frac{1}{2}\sum_{i=0}^{2k-1} \binom{2k-1}{i} \frac{(\bar{x}' - \frac{1}{2})^i}{\tau^{2k-1-i}} A_{2k-1-i}(\tau, \bar{x}') \tag{B-29}$$

where

$$A_{2k-1-i}(\tau, \bar{x}') \equiv 2\int_{-\tau\bar{x}'}^{\tau(1-\bar{x}')} \xi'^{2k-1-i} K(\xi')\, d\xi' \tag{B-30}$$

and $\binom{2k-1}{i}$ is the binomial coefficient and is defined as

$$\binom{n}{i} \equiv \frac{n!}{(n-i)!\, i\, !} \tag{B-31}$$

Making use of the definition of $A_n(\tau,\bar{x}')$ given in equation (B-30), equation (B-26) can be expressed as

$$\Phi_{-1}(\bar{x}') = \frac{1}{2\tau}\left[A_1(\tau,\bar{x}') + \tau\bar{x}' A_0(\tau,\bar{x}')\right] \tag{B-32}$$

The task of evaluating the functions $\Phi_{2k-1}(\bar{x}')$ and $\Phi_{-1}(\bar{x}')$ has now been reduced to that of determining the expressions for the functions $A_{2k-1-i}(\tau,\bar{x}')$.

Define the following indefinite integral:

$$B_m(\xi') \equiv \int \frac{\xi'^m}{\left[\xi'^2 + 1\right]^{3/2}}\, d\xi' \tag{B-33}$$

Integration by parts yields

$$B_m(\xi') = \frac{\xi'^{m+1}}{\sqrt{\xi'^2 + 1}} - m\int \frac{\xi'^m}{\sqrt{\xi'^2 + 1}}\, d\xi' \tag{B-34}$$

Noting that

$$\int \frac{\xi'^m}{\sqrt{\xi'^2 + 1}}\, d\xi = -\xi'^{m+1}\sqrt{\xi'^2 + 1} + (m+2)\int \xi'^m\sqrt{\xi'^2 + 1}\, d\xi'$$

and

$$\int \xi'^{m} \sqrt{\xi'^{2} + 1} \quad d\xi' = \frac{\xi'^{m+1}}{(m+2)} \left[\xi'^{2} + 1\right]^{3/2} -$$

$$\frac{(m-1)}{(m+1)} \int \xi'^{m-2} \sqrt{\xi'^{2} + 1} \quad d\xi'$$

then equation (B-34) can be written as

$$B_m(\xi) = \frac{\xi'^{m+1}}{\sqrt{\xi'^{2} + 1}} + m \left[\xi'^{m+1}\sqrt{\xi'^{2} + 1} - \xi^{m-1}(\xi^{2} + 1)^{3/2}\right. \quad \text{(B-35)}$$

$$\left. + (m-1) \int \xi'^{m-2} \sqrt{\xi'^{2} + 1} \quad d\xi'\right]$$

Replacing m by m + 2 in equation (B-35), making use of the integration formulas appearing after equation (B-34), and substituting equation (B-35) for the remaining integral yield the following recurrence formula:

$$B_{m+2}(\xi') = \frac{1}{m} \left[\frac{\xi'^{m+1}}{\sqrt{\xi'^{2} + 1}} - (m+1) \; B_m(\xi') \right] \quad m = 2,3,4,\ldots \quad \text{(B-36)}$$

In order to determine $B_m(\xi')$ for m = 0,1,2, and 3, which are necessary in order to determine the expressions for $B_m(\xi')$ for m = 4,5, etc. from equation (B-36), return to equation (B-33). Substituting the appropriate values of m and performing the simple integrations yield the following:

$$B_0(\xi') = \frac{\xi'}{\sqrt{\xi'^2 + 1}} \tag{B-37}$$

$$B_1(\xi') = -\frac{1}{\sqrt{\xi'^2 + 1}} \tag{B-38}$$

$$B_2(\xi') = -\frac{\xi'}{\sqrt{\xi'^2 + 1}} + \mathrm{LN}\left|\xi' + \sqrt{\xi'^2 + 1}\right| \tag{B-39}$$

$$B_3(\xi') = \sqrt{\xi'^2 + 1} + \frac{1}{\sqrt{\xi'^2 + 1}} \tag{B-40}$$

Evaluating equation (B-33) for the limits $-\tau\bar{x}'$ and $\tau(1 - \bar{x}')$ gives the functions, $A_m(\tau,\bar{x}')$. Therefore, evaluating the expressions appearing in equations (B-36) through (B-40) for these limits yields

$$A_{m+2}(\tau,\bar{x}') = \frac{1}{m}\left[\frac{[\tau(1-\bar{x}')]^{m+1}}{\sqrt{\tau^2(1-\bar{x}')^2+1}} - \frac{[-\tau\bar{x}']^{m+1}}{\sqrt{\tau^2\bar{x}'^2+1}} - (m+1)\,A_m(\tau,\bar{x}')\right] \qquad m = 2, 3, 4, \ldots \tag{B-41}$$

where

$$A_0(\tau,\bar{x}') = \frac{\tau(1-\bar{x}')}{\sqrt{\tau^2(1-\bar{x}')^2+1}} + \frac{\tau\bar{x}'}{\sqrt{\tau^2\bar{x}'^2 + 1}} \tag{B-42}$$

$$A_1(\tau,\bar{x}') = \frac{1}{\sqrt{\tau^2\bar{x}'^2 + 1}} - \frac{1}{\sqrt{\tau^2(1-\bar{x}')^2 + 1}} \qquad \text{(B-43)}$$

$$A_2(\tau,\bar{x}') = \text{LN}\left|\frac{\sqrt{\tau^2(1-\bar{x}')^2+1}+\tau(1-\bar{x}')}{\sqrt{\tau^2\bar{x}'^2+1}-\tau\bar{x}'}\right| - A_0(\tau,\bar{x}') \qquad \text{(B-44)}$$

$$A_3(\tau,\bar{x}') = \sqrt{\tau^2(1-\bar{x}')^2 + 1} - \sqrt{\tau^2\bar{x}'^2+1} - A_1(\tau,\bar{x}') \qquad \text{(B-45)}$$

Equations (B-44) and (B-45) were obtained by combining the results of equations (B-39) and (B-40) with equations (B-42) and (B-43).

Equations (B-29), (B-32), and (B-41) through (B-45) are sufficient for evaluation of the functions $\Phi_{2k-1}(\bar{x}')$. By choosing M points in the interval $0 \leq \bar{x}' < \frac{1}{2}$ and evaluating equation (B-21) at each of these points a M x M system of equations for the coefficients, $B_{2k-1}(\tau)$, is obtained. Once this system of equations has been solved, the results for the coefficients, $B_{2k-1}(\tau)$, are substituted in equation (B-19) and the approximate solution of the integral equation is completed.

For the case of M = 1 the system of equations resulting from evaluation of equation (B-21) at the point $\bar{x}' = 0$ reduces to one equation which can readily be solved. The result for the coefficient $B_1(\tau)$ is

$$B_1(\tau) = -\frac{2\left[\sqrt{\tau^2+1}(\tau+1) - 1\right]}{\left[2\sqrt{\tau^2+1}\ (\tau+1) - (\tau^2+2)\right]} \qquad \text{(B-46)}$$

APPENDIX C

DERIVATION AND APPROXIMATE SOLUTION OF INTEGRAL EQUATION REPRESENTING BOUNDARY CONDITION FOR FREE MOLECULAR FLOW THROUGH CIRCULAR TUBES

Derivation of Integral Equation

The boundary condition for free molecular flow through a circular tube of finite length is given by equation (9) of Chapter III as

$$\int_0^{\infty}\int_0^{2\pi}\int_0^{\pi} f(\bar{y}=1,\ \bar{z}',\ \theta,\ \varphi,\ \xi_\rho)\ \xi_\rho^3\ \mathrm{Sin}^2\varphi\ \mathrm{Sin}\ \theta\, d\varphi d\theta d\xi_\rho = 0 \qquad \text{(C-1)}$$

Noting that when equations (6) through (8) of Chapter III for the distribution functions are substituted into equation (C-1) the resulting expression is equivalent to setting equation (24) of Chapter III equal to zero, and observing that

$$\bar{\beta}(\theta) \equiv \bar{\bar{\beta}}(\theta) = \mathrm{Sin}\ \theta + |\mathrm{Sin}\ \theta| = \begin{cases} 2\ \mathrm{Sin}\ \theta & 0 \le \theta \le \pi \\ 0 & \pi \le \theta \le 2\pi \end{cases} \qquad \text{(C-2)}$$

$\bar{y}=1$

yield for the boundary condition

$$\int_0^{2\pi} \mathrm{Sin}\ \theta\ \mathrm{Tan}^{-1}\left(\frac{\bar{\bar{\beta}}(\theta)}{\tau\bar{z}'}\right) d\theta - \int_0^{2\pi} \frac{\tau\bar{z}'\ \bar{\bar{\beta}}(\theta)\ \mathrm{Sin}\ \theta}{[\tau^2\bar{z}'^2 + \bar{\bar{\beta}}(\theta)^2]}\ d\theta + \qquad \text{(C-3)}$$

$$2\int_0^{2\pi} \text{Sin}\ \theta d\theta \int_{\varphi_1^1(\theta)}^{\varphi_2^1(\theta)} g_w(\theta, \varphi)\ \text{Sin}^2\ \varphi\ d\varphi = 0$$

where $\varphi_1^1(\theta)$ and $\varphi_2^1(\theta)$ denote the angles $\varphi_1(\theta)$ and $\varphi_2(\theta)$ evaluated at $\bar{y} = 1$. From equations (4) and (5) of Chapter III and equation (C-2) we have

$$\varphi_1^1(\theta) = \begin{cases} \text{Tan}^{-1}\left(\dfrac{2\ \text{Sin}\ \theta}{\tau\bar{z}'}\right) & 0 \le \theta \le \pi \\ 0 & \pi \le \theta \le 2\pi \end{cases} \qquad \text{(C-4)}$$

$$\varphi_2^1(\theta) = \begin{cases} \pi - \text{Tan}^{-1}\left(\dfrac{2\ \text{Sin}\ \theta}{\tau(-\bar{z}')}\right) & 0 \le \theta \le \pi \\ \pi & \pi \le \theta \le 2\pi \end{cases} \qquad \text{(C-5)}$$

where the arctangents are defined for the principal value range of $-\pi/2$ to $\pi/2$. Introducing the expression for $\bar{\bar{\beta}}(\theta)$ into the first two integrals of equation (C-3) gives

$$\int_0^{2\pi} \text{Sin}\ \theta\ \text{Tan}^{-1}\left(\frac{\bar{\bar{\beta}}(\theta)}{\tau\bar{z}'}\right) d\theta = \int_0^{\pi} \text{Tan}^{-1}\left(\frac{2\ \text{Sin}\ \theta}{\tau\bar{z}'}\right) \text{Sin}\ \theta\ d\theta \qquad \text{(C-6)}$$

$$\int_0^{2\pi} \frac{\tau\bar{z}'\ \bar{\bar{\beta}}(\theta)\text{Sin}\ \theta\ d\theta}{[\tau^2\bar{z}'^2 + \bar{\bar{\beta}}(\theta)^2]} = \int_0^{\pi} \frac{2\tau\bar{z}'\ \text{Sin}^2\ \theta\ d\theta}{[\tau^2\bar{z}'^2 + 4\ \text{Sin}^2\ \theta]} \qquad \text{(C-7)}$$

Consider the third integral of equation (C-3). Dividing the integration with respect to θ into two parts, $0 \leq \theta \leq 2\pi$ and $\pi \leq \theta \leq 2\pi$, and using equations (C-4) and (C-5) give

$$\int_0^{2\pi} \text{Sin}\,\theta d\theta \int_{\varphi_1^1(\theta)}^{\varphi_2^1(\theta)} g_w(\theta,\varphi)\,\text{Sin}^2\,\varphi\,d\varphi = \tag{C-8}$$

$$\int_0^{\pi} \text{Sin}\,\theta d\theta \int_{\varphi_1^1(\theta)}^{\varphi_2^1(\theta)} g_w(\theta,\varphi)\,\text{Sin}^2\,\varphi\,d\varphi +$$

$$\int_{\pi}^{2\pi} \text{Sin}\,\theta\,d\theta \int_0^{\pi} g_w(\theta,\varphi)\,\text{Sin}^2\,\varphi\,d\varphi$$

where the angles $\varphi_1^1(\theta)$ and $\varphi_2^1(\theta)$ are given by equations (C-4) and (C-5) for the range $0 \leq \theta \leq \pi$. Noting that at the point under consideration, $\bar{y} = 1$ and $\bar{z} = \bar{z}'$, the wall flux is constant and given by $g_w(\bar{z}')$, then equation (C-8) becomes

$$\int_0^{2\pi} \text{Sin}\,\theta d\theta \int_{\varphi_1^1(\theta)}^{\varphi_2^1(\theta)} g_w(\theta,\varphi)\,\text{Sin}^2\,\varphi\,d\varphi = \tag{C-9}$$

$$\int_0^{\pi} \text{Sin}\,\theta d\theta \int_{\varphi_1^1}^{\varphi_2^1(\theta)} g_w(\theta,\varphi)\text{Sin}^2\,\varphi\,d\varphi - \pi\, g_w(\bar{z}')$$

Now the integral on the right-hand side of equation (C-9) is expressed in terms of the wall coordinate $\bar{z}'$. Introducing equation (C-2) into equation (2) of Chapter III and defining

$$\tau_d \equiv L/d = \tau/2 \tag{C-10}$$

the transformation from φ to $\bar{z}'$ becomes

$$\text{Tan } \varphi = \frac{\text{Sin } \theta}{\tau_d(\bar{z}' - \bar{z}'')} \tag{C-11}$$

$$\tau_d d\bar{z}' = \text{Sin } \theta \text{ Csc}^2 \varphi d\varphi \tag{C-12}$$

Since $\bar{z}'' = 0$ for $\varphi = \varphi_1(\theta)$ and $\bar{z}'' = 1$ for $\varphi = \varphi_2(\theta)$, equation (C-9) can be written as follows by using equations (C-11) and (C-12):

$$\int_0^{2\pi} \text{Sin } \theta d\theta \int_{\varphi_1(\theta)}^{\varphi_2(\theta)} g_w(\theta,\varphi) \text{ Sin}^2 \varphi \, d\varphi = \tag{C-13}$$

$$\tau_d \int_0^{\pi} d\theta \int_0^1 \frac{g_w(\bar{z}'') \text{ Sin}^4 \theta \, d\bar{z}''}{[\text{Sin}^2 \theta + \tau_d^2(\bar{z}' - \bar{z}'')^2]^2} - \pi g_w(\bar{z}')$$

Combining equations (C-6), (C-7), and (C-13) with equation (C-3) the boundary condition becomes

$$\int_0^{\pi} \text{Tan}^{-1} \left(\frac{2 \text{ Sin } \theta}{\tau \bar{z}'} \right) \text{Sin } \theta d\theta - \int_0^{\pi} \frac{2 \tau \bar{z}' \text{ Sin}^2 \theta \, d\theta}{[\tau^2 \bar{z}'^2 + 4 \text{ Sin}^2 \theta]} + \tag{C-14}$$

$$2\tau_d \int_0^{\pi} d\theta \int_0^{1} \frac{g_w(\bar{z}'') \, \mathrm{Sin}^4 \theta \, d\bar{z}''}{[\mathrm{Sin}^2 \theta + \tau_d^2(\bar{z}' - \bar{z}'')^2]^2} = 2\pi \, g_w(\bar{z}')$$

Introduce the following integration formulas:

$$\int \mathrm{Tan}^{-1}\left(a \, \mathrm{Sin} \, \theta \right) \mathrm{Sin} \, \theta \, d\theta = - \mathrm{Cos} \, \theta \, \mathrm{Tan}^{-1}\left(a \, \mathrm{Sin} \, \theta \right) - \frac{1}{a}\left[\theta - \sqrt{a^2 + 1} \; \mathrm{Tan}^{-1}\left(\sqrt{a^2 + 1} \; \mathrm{Tan} \, \theta \right) \right] \tag{C-15}$$

$$\int \frac{\mathrm{Sin}^2 \theta \, d\theta}{[a^2 + \mathrm{Sin}^2 \theta]} = \theta - \frac{a^2}{|a|\sqrt{a^2 + 1}} \mathrm{Tan}^{-1}\left(\frac{|a|\sqrt{a^2 + 1} \, \mathrm{Tan} \, \theta}{a^2} \right) \tag{C-16}$$

$$\int \frac{\mathrm{Sin}^4 \theta \, d\theta}{[\mathrm{Sin}^2 \theta + a^2]^2} = \theta - \frac{|a| \, (a^2 + 2)}{(a^2 + 1)^{3/2}} \mathrm{Tan}^{-1}\left(\frac{\sqrt{a^2 + 1} \, \mathrm{Tan} \, \theta}{|a|} \right) + \frac{a^2}{2(a^2 + 1)}\left[\frac{\mathrm{Tan} \, \theta}{[a^2 + (1 + a^2)\mathrm{Tan}^2 \theta]} + \frac{1}{|a|\sqrt{a^2 + 1}} \mathrm{Tan}^{-1}\left(\frac{\sqrt{a^2 + 1} \, \mathrm{Tan} \, \theta}{|a|} \right) \right] \tag{C-17}$$

Making use of equations (C-15) through (C-17) and expressing τ in terms of τ_d the final expression for the boundary condition becomes

$$g_w(\bar{z}') = F(\bar{z}') + \tau_d \int_0^{1} g_w(\bar{z}'') K(\bar{z}', \bar{z}'') d\bar{z}'' \tag{C-18}$$

where

$$F(\bar{z}') = \frac{\tau_d^2 \bar{z}'^2 + 0.5}{\sqrt{\tau_d^2 \bar{z}'^2 + 1}} - \tau_d \bar{z}' \tag{C-19}$$

$$K(\bar{z}', \bar{z}'') = 1 - \left|\tau_d(\bar{z}' - \bar{z}'')\right| \cdot \left[\frac{2\tau_d^2(\bar{z}' - \bar{z}'')^2 + 3}{2[\tau_d^2(\bar{z}' - \bar{z}'')^2 + 1]^{3/2}}\right] \qquad (C\text{-}20)$$

Approximate Solution of Integral Equation

The collocation method is used to obtain an approximate solution for the integral equation representing the boundary condition for free molecular flow through circular tubes. The integral equation is given by equation (C-18). In order to obtain accurate results, integrable functions are chosen to represent the nondimensional wall flux. Therefore, the following polynomial is used:

$$g_w(\bar{z}') = \frac{1}{2} + \sum_{k=1}^{M} B_{2k-1}(\tau_d)\, \varphi_{2k-1}(\bar{z}') \qquad (C\text{-}21)$$

where

$$\varphi_{2k-1}(\bar{z}') = (\bar{z}' - \frac{1}{2})^{2k-1} \qquad (C\text{-}22)$$

It should be noted that the form of equation (C-21) satisfies the antisymmetric property of the exact solution of equation (C-18).

Introduce the following transformation into equations (C-18) and (C-21):

$$\xi = \bar{z}'' - \bar{z}' \qquad (C\text{-}23)$$

The results are:

$$g_w(\xi) = \frac{1}{2} + \sum_{k=1}^{M} B_{2k-1}(\tau_d) \left[\xi + (\bar{z}' - \frac{1}{2})\right]^{2k-1} \qquad (C\text{-}24)$$

$$g_w(\bar{z}') = F(\bar{z}') + \tau_d \int_{-\bar{z}'}^{(1-\bar{z}')} g_w(\xi)K(\xi)d\xi \qquad (C\text{-}25)$$

where

$$K(\xi) = 1 - \frac{\tau_d |\xi|}{\sqrt{\tau_d^2\xi^2 + 1}} - \frac{\tau_d |\xi|}{2[\tau_d^2\xi^2 + 1]^{3/2}} \qquad (C\text{-}26)$$

Removing the absolute value signs in equation (C-26) the kernel can be expressed in two parts as

$$K^+(\xi) = 1 - \frac{\tau_d \xi}{\sqrt{\tau_d^2\xi^2 + 1}} - \frac{\tau_d \xi}{2[\tau_d^2\xi^2 + 1]^{3/2}} \quad \xi \geq 0 \qquad (C\text{-}27)$$

$$K^-(\xi) = 1 + \frac{\tau_d \xi}{\sqrt{\tau_d^2\xi^2 + 1}} + \frac{\tau_d \xi}{2[\tau_d^2\xi^2 + 1]^{3/2}} \quad \xi \leq 0 \qquad (C\text{-}28)$$

The integral equation of equation (C-25) can be written as follows by introducing equations (C-24), (C-27), and (C-28):

$$\frac{1}{2} + \sum_{k=1}^{M} B_{2k-1}(\tau_d) (\bar{z}' - \frac{1}{2})^{2k-1} \cong F(\bar{z}') + \qquad (C\text{-}29)$$

$$\tau_d \int_{-\bar{z}'}^{0} \left\{ \frac{1}{2} + \sum_{k=1}^{M} B_{2k-1}(\tau_d) \cdot [\xi + (\bar{z}' - \tfrac{1}{2})]^{2k-1} \right\} K^-(\xi)\, d\xi + \tau_d \int_{0}^{(1-\bar{z}')} \left\{ \frac{1}{2} + \right.$$

$$\left. \sum_{k=1}^{M} B_{2k-1}(\tau_d)[\xi + (\bar{z}' - \tfrac{1}{2})]^{2k-1} \right\} K^+(\xi)\, d\xi$$

Introduce the following definitions:

$$\Phi^+_{-1}(\tau_d, \bar{z}') \equiv \frac{\tau_d}{2} \int_0^{(1-\bar{z}')} K^+(\xi)\, d\xi \qquad \text{(C-30)}$$

$$\Phi^-_{-1}(\tau_d, \bar{z}') \equiv \frac{\tau_d}{2} \int_{-\bar{z}'}^{0} K^-(\xi)\, d\xi \qquad \text{(C-31)}$$

$$\Phi^+_{2k-1}(\tau_d, \bar{z}') \equiv \tau_d \int_0^{(1-\bar{z}')} [\xi + (\bar{z}' - \tfrac{1}{2})]^{2k-1} K^+(\xi)\, d\xi \quad k \geq 1 \qquad \text{(C-32)}$$

$$\Phi^-_{2k-1}(\tau_d, \bar{z}') \equiv \tau_d \int_{-\bar{z}'}^{0} [\xi + (\bar{z}' - \tfrac{1}{2})]^{2k-1} K^-(\xi)\, d\xi \quad k \geq 1 \qquad \text{(C-33)}$$

then equation (C-29) can be expressed as

$$\sum_{k=1}^{M} B_{2k-1}(\tau_d) \left\{ \varphi_{2k-1}(\bar{z}') - \left[\Phi^+_{2k-1}(\tau_d, \bar{z}') + \right. \right. \qquad \text{(C-34)}$$

$$\left. \left. \Phi^-_{2k-1}(\tau_d, \bar{z}') \right] \right\} \cong F(\bar{z}') + \left[\Phi^+_{-1}(\tau_d, \bar{z}') + \Phi^-_{-1}(\tau_d, \bar{z}') \right] - \frac{1}{2}$$

By evaluating equation (C-34) at M points for $\bar{z}'$, a M x M system of equations is obtained for a given value of τ_d. This system of equations can be solved for the M unknown coefficients, $B_{2k-1}(\tau_d)$, once the expressions for $\overset{+}{\Phi}^{-}_{2k-1}(\tau_d,\bar{z}')$ and $\overset{+}{\Phi}^{-}_{-1}(\tau_d,\bar{z}')$ are known.

The expressions for $\overset{+}{\Phi}^{-}_{-1}(\tau_d,\bar{z}')$ can be obtained directly from equations (C-30) and (C-31). Introducing equations (C-27) and (C-28) into equations (C-30) and (C-31) and performing the straightforward integrations yield

$$\overset{+}{\Phi}_{-1}(\tau_d,\bar{z}') = \frac{1}{2}\left[\tau_d(1-\bar{z}') - \sqrt{\tau_d^2\,(1-\bar{z}')^2 + 1} + \right. \tag{C-35}$$

$$\left. \frac{1}{2}\left(1 + \frac{1}{\sqrt{\tau_d^2(1-\bar{z}')^2 + 1}}\right)\right]$$

$$\overset{-}{\Phi}_{-1}(\tau_d,\bar{z}') = \frac{1}{2}\left[\tau_d\bar{z}' - \sqrt{\tau_d^2\bar{z}'^2 + 1} + \right. \tag{C-36}$$

$$\left. \frac{1}{2}\left(1 + \frac{1}{\sqrt{\tau_d^2\bar{z}'^2 + 1}}\right)\right]$$

Consider the functions $\overset{+}{\Phi}^{-}_{2k-1}(\tau_d,\bar{z}')$ given by equations (C-32) and (C-33). Using the binomial expansion for the term in brackets gives

$$\Phi^{+}_{2k-1}(\tau_d,\bar{z}') = \sum_{i=0}^{2k-1} \binom{2k-1}{i} (\bar{z}' - \tfrac{1}{2})^i \; A^{+}_{2k-1-i}(\tau_d,\bar{z}') \qquad (C\text{-}37)$$

$$\Phi^{-}_{2k-1}(\tau_d,\bar{z}') = \sum_{i=0}^{2k-1} \binom{2k-1}{i} (\bar{z}' - \tfrac{1}{2})^i \; A^{-}_{2k-1-i}(\tau_d,\bar{z}') \qquad (C\text{-}38)$$

where

$$A^{+}_{2k-1-i}(\tau_d,\bar{z}') \equiv \int_0^{(1-\bar{z}')} \xi^{(2k-1-i)} K'^{+}(\xi)\,d\xi \qquad (C\text{-}39)$$

$$A^{-}_{2k-1-i}(\tau_d,\bar{z}') \equiv \int_{-\bar{z}'}^{0} \xi^{(2k-1-i)} K'^{-}(\xi)\,d\xi \qquad (C\text{-}40)$$

and

$$K'^{\pm}(\xi) \equiv \tau_d K^{\pm}(\xi) \qquad (C\text{-}41)$$

The binomial coefficient $\binom{2k-1}{i}$ is defined in equation (B-31) of Appendix B. The task of determining the functions $\Phi^{\pm}_{2k-1}(\tau_d,\bar{z}')$ has been reduced to that of determining the functions $A^{\pm}_{(2k-1-i)}(\tau_d,\bar{z}')$ of equations (C-39) and (C-40). Combining equations (C-27), (C-28), and (C-41) with equations (C-39) and (C-40) and changing variables by introducing η as

$$\eta = \tau_d \xi \qquad (C\text{-}42)$$

yield

$$A^{+}_{2k-1-i}(\tau_d,\bar{z}') = \frac{\tau_d(1-\bar{z}')^{2k-i}}{(2k-i)} - \frac{1}{\tau_d^{(2k-1-i)}}\left\{\int_0^{\tau_d(1-\bar{z}')} \frac{\eta^{2k-i}\,d\eta}{\sqrt{\eta^2+1}} - \right. \tag{C-43}$$

$$\left. \frac{1}{2}\int_0^{\tau_d(1-\bar{z}')} \frac{\eta^{2k-i}\,d\eta}{[\eta^2+1]^{3/2}}\right\}$$

$$A^{-}_{2k-1-i}(\tau_d,\bar{z}') = -\frac{\tau_d(-\bar{z}')^{2k-i}}{(2k-i)} + \frac{1}{\tau_d^{(2k-1-i)}}\left\{\int_{-\tau_d\bar{z}'}^{0} \frac{\eta^{2k-i}\,d\eta}{\sqrt{\eta^2+1}} + \right. \tag{C-44}$$

$$\left. \frac{1}{2}\int_{-\tau_d\bar{z}'}^{0} \frac{\eta^{2k-i}\,d\eta}{[\eta^2+1]^{3/2}}\right\}$$

Define the following:

$$B_{m+1}(\eta) \equiv \int \frac{\eta^{m+1}\,d\eta}{[\eta^2+1]^{3/2}} \tag{C-45}$$

The following recurrence formula has already been derived for $B_{m+1}(\eta)$ in Appendix B:

$$B_{m+1}(\eta) = -\frac{1}{(m-1)}\left\{\frac{-\eta^m}{\sqrt{\eta^2+1}} + mB_{m-1}(\eta)\right\} \qquad m \geq 2 \tag{C-46}$$

For m = 0 and m = 1 the results can be obtained directly from the definition of equation (C-45). The results are:

$$B_1(\eta) = -\frac{1}{\sqrt{\eta^2+1}} \tag{C-47}$$

$$B_2(\eta) = -\frac{\eta}{\sqrt{\eta^2+1}} + \text{LN}\left|\eta + \sqrt{\eta^2+1}\right| \tag{C-48}$$

Introduce the following definitions:

$$B^{+}_{2k-i}(\tau_d,\bar{z}') \equiv \frac{1}{\tau^{(2k-1-i)}} \int_0^{\tau_d(1-\bar{z}')} \frac{\eta^{2k-i}\,d\eta}{[\eta^2+1]^{3/2}} = \tag{C-49}$$

$$\frac{1}{\tau^{(2k-1-i)}} \; B_{2k-i}(\eta) \Big|_0^{\tau_d(1-\bar{z}')}$$

$$B^{-}_{2k-i}(\tau_d,\bar{z}') \equiv \frac{1}{\tau^{(2k-1-i)}} \int_{-\tau_d\bar{z}'}^{0} \frac{\eta^{2k-i}\,d\eta}{[\eta^2+1]^{3/2}} = \tag{C-50}$$

$$\frac{1}{\tau^{(2k-1-i)}} \; B_{2k-i}(\eta) \Big|_{-\tau_d\bar{z}'}^{0}$$

Consider now the first integrals of equations (C-43) and (C-44). Define the following:

$$C_{m+1}(\eta) \equiv \int \frac{\eta^{m+1}\,d\eta}{\sqrt{\eta^2+1}} \tag{C-51}$$

The following recurrence formula can be derived:

$$C_{m+1}(\eta) = \frac{1}{(m+1)} \left\{ \eta^m \sqrt{\eta^2 + 1} - m\, C_{m-1}(\eta) \right\} \quad m \geq 2 \tag{C-52}$$

For m = 0 and m = 1 the results can be obtained directly from equation (C-51) by performing the necessary integrations. The results are:

$$C_1(\eta) = \sqrt{\eta^2 + 1} \tag{C-53}$$

$$C_2(\eta) = \frac{1}{2} \left[\eta \sqrt{\eta^2 + 1} - \text{LN} \left| \eta + \sqrt{\eta^2 + 1} \right| \right] \tag{C-54}$$

Introduce the following definitions:

$$C^{+}_{2k-i}(\tau_d, \bar{z}') \equiv \frac{1}{\tau^{(2k-1-i)}} \int_0^{\tau_d(1-\bar{z}')} \frac{\eta^{2k-i}\, d\eta}{\sqrt{\eta^2 + 1}} = \tag{C-55}$$

$$\frac{1}{\tau^{(2k-1-i)}} \; C_{2k-i}(\eta) \Big|_0^{\tau_d(1-\bar{z}')}$$

$$C^{-}_{2k-i}(\tau_d, \bar{z}') \equiv \frac{1}{\tau^{(2k-1-i)}} \int_{-\tau_d\bar{z}'}^{0} \frac{\eta^{2k-i}\, d\eta}{\sqrt{\eta^2 + 1}} = \tag{C-56}$$

$$\frac{1}{\tau^{(2k-1-i)}} \; C_{2k-i}(\eta) \Big|_{-\tau_d\bar{z}'}^{0}$$

Combining equations (C-43), (C-44), (C-47) through (C-50), and (C-53) through (C-56) yields:

$$\overset{+}{A}_{2k-1-i}(\tau_d,\bar{z}') = \frac{\tau_d(1-\bar{z}')^{2k-i}}{(2k-i)} - \overset{+}{C}_{2k-i}(\tau_d,\bar{z}') - \tag{C-57}$$

$$\frac{1}{2}\overset{+}{B}_{2k-i}(\tau_d,\bar{z}') \quad (2k-i) \geq 1$$

$$\overset{-}{A}_{2k-1-i}(\tau_d,\bar{z}') = -\frac{\tau_d(-\bar{z}')^{2k-i}}{(2k-i)} + \overset{-}{C}_{2k-i}(\tau_d,\bar{z}') + \tag{C-58}$$

$$\frac{1}{2}\overset{-}{B}_{2k-i}(\tau_d,\bar{z}') \quad (2k-i) \geq 1$$

where

$$\overset{+}{B}_{2k-i}(\tau_d,\bar{z}') = \frac{1}{(2k-2-i)}\left[\frac{(1-\bar{z}')^{2k-1-i}}{\sqrt{\tau_d^2(1-\bar{z}')^2+1}} - \frac{(2k-1-i)}{\tau_d^2}\cdot \tag{C-59}\right.$$

$$\left.\overset{+}{B}_{2k-2-i}(\tau_d,\bar{z}')\right] \quad (2k-i) \geq 3$$

$$\overset{-}{B}_{2k-i}(\tau_d,\bar{z}') = \frac{-1}{(2k-2-i)}\left[\frac{(-\bar{z}')^{2k-1-i}}{\sqrt{\tau_d^2\bar{z}'^2+1}} + \frac{(2k-1-i)}{\tau_d^2}\cdot \tag{C-60}\right.$$

$$\left.\overset{-}{B}_{2k-2-i}(\tau_d,\bar{z}')\right] \quad (2k-i) \geq 3$$

$$C^{+}_{2k-i}(\tau_d,\bar{z}') = \frac{1}{(2k-i)}\left[(1-\bar{z}')^{2k-1-i}\sqrt{\tau_d^2(1-\bar{z}')^2+1} - \right. \tag{C-61}$$

$$\left.\frac{(2k-1-i)}{\tau_d^2}\ C^{+}_{2k-2-i}(\tau_d,\bar{z}')\right] \qquad (2k-i) \geq 3$$

$$C^{-}_{2k-i}(\tau_d,\bar{z}') = \frac{-1}{(2k-i)}\left[(-\bar{z}')^{2k-1-i}\sqrt{\tau_d^2\bar{z}'^2+1} + \right. \tag{C-62}$$

$$\left.\frac{(2k-1-i)}{\tau_d^2}\ C^{-}_{2k-2-i}(\tau_d,\bar{z}')\right] \qquad (2k-i) \geq 3$$

$$B^{+}_{1}(\tau_d,\bar{z}') = \left[1 - \frac{1}{\sqrt{\tau_d^2(1-\bar{z}')^2+1}}\right] \tag{C-63}$$

$$B^{-}_{1}(\tau_d,\bar{z}') = \left[\frac{1}{\sqrt{\tau_d^2\bar{z}'^2+1}} - 1\right] \tag{C-64}$$

$$B^{+}_{2}(\tau_d,\bar{z}') = \left[\frac{1}{\tau_d}\ \mathrm{LN}\left|\tau_d(1-\bar{z}') + \sqrt{\tau_d^2(1-\bar{z}')^2+1}\right| - \right. \tag{C-65}$$

$$\left.\frac{(1-\bar{z}')}{\sqrt{\tau_d^2(1-\bar{z}')^2+1}}\right]$$

$$B^{-}_{2}(\tau_d,\bar{z}') = -\left[\frac{1}{\tau_d}\ \mathrm{LN}\left|\sqrt{\tau_d^2\bar{z}'^2+1} - \tau_d\bar{z}'\right| + \frac{\bar{z}'}{\sqrt{\tau_d^2\bar{z}'^2+1}}\right] \tag{C-66}$$

$$C_1^+(\tau_d,\bar{z}') = \left[\sqrt{\tau_d^2(1-\bar{z}')^2+1} - 1\right] \tag{C-67}$$

$$C_1^-(\tau_d,\bar{z}') = \left[1 - \sqrt{\tau_d^2\bar{z}'^2+1}\right] \tag{C-68}$$

$$C_2^+(\tau_d,\bar{z}') = \frac{1}{2}\left[(1-\bar{z}')\sqrt{\tau_d^2(1-\bar{z}')^2+1} - \frac{1}{\tau_d}\,LN\left|\tau_d(1-\bar{z}') + \sqrt{\tau_d^2(1-\bar{z}')^2+1}\right|\right] \tag{C-69}$$

$$C_2^-(\tau_d,\bar{z}') = \frac{1}{2}\left[\bar{z}'\sqrt{\tau_d^2\bar{z}'^2+1} + \frac{1}{\tau_d}\,LN\left|\sqrt{\tau_d^2\bar{z}'^2+1} - \tau_d\bar{z}'\right|\right] \tag{C-70}$$

Substituting equations (C-57) and (C-58) into equations (C-37) and (C-38) yields the final expressions for $\Phi^+_{2k-1}(\tau_d,\bar{z}')$. The procedure for obtaining the coefficients, $B_{2k-1}(\tau_d)$, is the same as that outlined in Appendix B for the two dimensional case.

For the case of M = 1 the system of equations resulting from evaluation of equation (C-34) at the point $\bar{z}' = 0$ reduces to one equation which can readily be solved. The result for the coefficient $B_1(\tau_d)$ is

$$B_1(\tau_d) = \frac{\left[(2\tau_d^2+1) - \sqrt{\tau_d^2+1}\;(1+2\tau_d)\right]}{\left[\sqrt{\tau_d^2+1}+1\right]} \tag{C-71}$$

This coefficient is related to the nondimensional inlet wall flux, $g_{w_0}(\tau_d)$, by the following:

$$g_{w_0}(\tau_d) = -\frac{1}{2} B_1(\tau_d) \qquad (C-72)$$

APPENDIX D

DERIVATION OF INTEGRAL EQUATIONS REPRESENTING BOUNDARY CONDITIONS FOR FREE MOLECULAR FLOW THROUGH RECTANGULAR CHANNELS

Integral Equation for the Upper and Lower Walls

The boundary condition for the upper and lower walls is represented by equation (A-36) as

$$m \int_{-\infty}^{\infty}\int_{-\infty}^{\infty}\int_{-\infty}^{\infty} f(\bar{x},\bar{y}=\begin{matrix}1\\0\end{matrix},\bar{z},\xi,\eta,\zeta)\eta \, d\xi d\eta d\zeta = 0 \qquad \text{(D-1)}$$

If one notes that equation (D-1) is identical to equation (A-68) when the latter is set equal to zero, then it can be seen that setting the right-hand side of equation (A-73) equal to zero and evaluating the resulting expressions at $\bar{y} = 0$ or $\bar{y} = 1$ yield the same result as obtained by integrating equation (D-1). Thus, referring to Figure A-2 and equations (A-12) through (A-31) and notingthat for $\bar{y} = 1$, $\alpha_{408} = 2\pi$, $\alpha_{304} = 3\pi/2$, $\alpha_{708} = \pi/2$, $\varphi_{307}(\theta) = \pi$, and $\varphi_{408}(\theta) = 0$, equation (A-73) becomes

$$\frac{\tau_d \bar{x}_T}{\sqrt{1+\tau_d^2 \bar{x}_T^2}} \left[\mathrm{Tan}^{-1}\left(\frac{\tau_d(\bar{z}_T - 1)}{\tau_b\sqrt{\tau_d^2 \bar{x}_T^2 + 1}} \right) - \mathrm{Tan}^{-1}\left(\frac{\tau_d \bar{z}_T}{\tau_b\sqrt{\tau_d^2 \bar{x}_T^2 + 1}} \right) \right] + \qquad \text{(D-2)}$$

$$\left[\operatorname{Tan}^{-1}\left(\frac{\bar{z}_T}{\tau_b \bar{x}_T}\right) - \operatorname{Tan}^{-1}\left(\frac{\bar{z}_T - 1}{\tau_b \bar{x}_T}\right)\right] + 2\left[\int_{\substack{\alpha \\ 506}}^{\frac{\pi}{2}} \operatorname{Cos}\,\theta\, d\theta \int_{\substack{\varphi\,(\theta) \\ 508}}^{\substack{\varphi\,(\theta) \\ 607}} g_{w_s}(\theta,\varphi)\, \operatorname{Sin}^2 \varphi\, d\varphi +\right.$$

$$\int_{\frac{3\pi}{2}}^{\substack{\alpha \\ 102}} \operatorname{Cos}\,\theta\, d\theta \int_{\substack{\varphi\,(\theta) \\ 104}}^{\substack{\varphi\,(\theta) \\ 203}} g_{w_s}(\theta,\varphi) \operatorname{Sin}^2 \varphi\, d\varphi + \int_{\frac{\pi}{2}}^{\frac{3\pi}{2}} \operatorname{Cos}\,\theta\, d\theta \int_{0}^{\pi} g_{w_T}(\theta,\varphi)\, \operatorname{Sin}^2 \varphi\, d\varphi +$$

$$\int_{\alpha_{102}}^{2\pi} \operatorname{Cos}\,\theta\, d\theta \int_{\substack{\varphi\,(\theta) \\ 105}}^{\substack{\varphi\,(\theta) \\ 206}} g_{w_T}(\theta,\varphi) \operatorname{Sin}^2 \varphi\, d\varphi + \int_{0}^{\alpha_{506}} \operatorname{Cos}\,\theta\, d\theta \int_{\substack{\varphi\,(\theta) \\ 105}}^{\substack{\varphi\,(\theta) \\ 206}} g_{w_T}(\vartheta,\varphi) \operatorname{Sin}^2 \varphi\, d\varphi \left.\right] = 0$$

Note that the third integral of equation (D-2) can be readily evaluated since the nondimensional wall flux is constant for the point under consideration; namely, $\bar{y} = 1$, $\bar{z} = \bar{z}''_T$, and $\bar{x} = \bar{x}''_T$. Thus,

$$\int_{\frac{\pi}{2}}^{\frac{3\pi}{2}} \operatorname{Cos}\,\theta\, d\theta \int_{0}^{\pi} g_{w_T}(\theta,\varphi) \operatorname{Sin}^2 \varphi\, d\varphi = g_{w_T}(\bar{x}''_T, \bar{z}''_T) \int_{\frac{\pi}{2}}^{\frac{3\pi}{2}} \operatorname{Cos}\,\theta\, d\theta \int_{0}^{\pi} \operatorname{Sin}^2 \varphi\, d\varphi \quad \text{(D-3)}$$

$$- \pi\, g_{w_T}(\bar{x}_T, \bar{z}_T)$$

where $\bar{x}''_T$ and $\bar{z}''_T$ have been replaced by $\bar{x}_T$ and $\bar{z}_T$, respectively. Consider now the other integrals of equation (D-2). Equations (A-4) through (A-11) can be used to transform the variables θ and φ to the appropriate wall coordinates for each integral. By applying the appropriate trans-

formation equations for each integral of equation (D-2) the following relations are deduced:

$$\text{Cos } \theta \text{ Sin}^2 \varphi \, d\varphi d\theta = \frac{\tau_d^{\,2} \tau_b^{\,3} \bar{z}_T (1-\bar{y}'_s) d\bar{x}'_s d\bar{y}'_s}{\left[\tau_d^{\,2} \bar{z}_T^{\,2} + \tau_b^{\,2} (1-\bar{y}'_s)^2 + \tau_d^{\,2} \tau_b^{\,2} (\bar{x}_T - \bar{x}'_s)^2\right]^2} \qquad \text{(D-4)}$$

for the rear side wall,

$$\text{Cos } \theta \text{ Sin}^2 \varphi \, d\varphi d\theta = \frac{\tau_d^{\,2} \tau_b^{\,3} (\bar{z}_T - 1)(1-\bar{y}''_s) d\bar{x}''_s d\bar{y}''_s}{\left[\tau_d^{\,2} (\bar{z}_T - 1)^2 + \tau_b^{\,2} (1-\bar{y}''_s)^2 + \tau_d^{\,2} \tau_b^{\,2} (\bar{x}_T - \bar{x}''_s)^2\right]^2} \qquad \text{(D-5)}$$

for the front side wall, and

$$\text{Cos } \theta \text{ Sin}^2 \varphi \, d\varphi d\theta = - \frac{\tau_d^{\,2} \tau_b^{\,3} d\bar{x}'_T d\bar{z}'_T}{\left[\tau_b^{\,2} + \tau_d^{\,2} (\bar{z}_T - \bar{z}'_T)^2 + \tau_d^{\,2} \tau_b^{\,2} (\bar{x}_T - \bar{x}'_T)^2\right]^2} \qquad \text{(D-6)}$$

for the lower wall. Introducing equations (D-4) through (D-6) into the integrals of equation (D-2) and using equations (A-4) through (A-11) to change the limits of integration yield

$$\int_{\alpha_{506}}^{\frac{\pi}{2}} \text{Cos } \theta \, d\theta \int_{\varphi_{508}(\theta)}^{\varphi_{607}(\theta)} g_{w_s}(\theta,\varphi) \text{Sin}^2 \varphi d\varphi = \int_0^1 \int_0^1 g_{w_s}(\bar{x}'_s, \bar{y}'_s) K'_{w_s}(\bar{x}_T, \bar{x}'_s, \bar{y}'_s, \bar{z}_T) d\bar{x}'_s d\bar{y}'_s \qquad \text{(D-7)}$$

$$\int_{\frac{3\pi}{2}}^{\alpha_{102}} \text{Cos } \theta \, d\theta \int_{\varphi_{104}(\theta)}^{\varphi_{203}(\theta)} g_{w_s}(\theta,\varphi) \text{Sin}^2 \varphi \, d\varphi = \int_0^1 \int_0^1 g_{w_s}(\bar{x}''_s, \bar{y}''_s) K''_{w_s}(\bar{x}_T, \bar{x}''_s, \bar{y}''_s, \bar{z}_T) d\bar{x}''_s d\bar{y}''_s \qquad \text{(D-8)}$$

$$\int_{\alpha_{102}}^{2\pi} \cos\theta\, d\theta \int_{\varphi_{105}(\theta)}^{\varphi_{206}(\theta)} g_{w_T}(\theta,\varphi)\sin^2\varphi\, d\varphi + \int_{0}^{\alpha_{506}} \cos\theta\, d\theta \int_{\varphi_{105}(\theta)}^{\varphi_{206}(\theta)} g_{w_T}(\theta,\varphi)\sin^2\varphi\, d\varphi = \tag{D-9}$$

$$\int_0^1\int_0^1 g_{w_T}(\bar{x}'_T,\bar{z}'_T)K'_{w_T}(\bar{x}_T,\bar{x}'_T,\bar{z}_T,\bar{z}'_T)d\bar{x}'_T d\bar{z}'_T$$

where $K'_{w_s}(\bar{x}_T,\bar{x}'_s,\bar{y}'_s,\bar{z}_T)$, etc. are given by equations (A-46), (A-48), and (A-50). Combining equations (D-2), (D-3), and (D-7) through (D-9) and making use of the expression for $G_{w_T}(\bar{x}_T,\bar{z}_T)$ given by equation (A-44), the following relation can be written for the boundary condition at the upper channel wall ($\bar{y} = 1$):

$$g_{w_T}(\bar{x}_T,\bar{z}_T) = G_{w_T}(\bar{x}_T,\bar{z}_T) + \frac{1}{\pi}\left[\int_0^1\int_0^1 g_{w_T}(\bar{x}'_T,\bar{z}'_T)K'_{w_T}(\bar{x}_T,\bar{x}'_T,\bar{z}_T,\bar{z}'_T)d\bar{x}'_T\, d\bar{z}'_T + \right. \tag{D-10}$$

$$\int_0^1\int_0^1 g_{w_s}(\bar{x}'_s,\bar{y}'_s)K'_{w_s}(\bar{x}_T,\bar{x}'_s,\bar{y}'_s,\bar{z}_T)\, d\bar{x}'_s d\bar{y}'_s +$$

$$\left.\int_0^1\int_0^1 g_{w_s}(\bar{x}''_s,\bar{y}''_s)K''_{w_s}(\bar{x}_T,\bar{x}''_s,\bar{y}''_s,\bar{z}_T)\, d\bar{x}''_s\, d\bar{y}''_s\right]$$

It can easily be shown that equation (D-10) is identical to that obtained for $\bar{y} = 0$. Likewise, for $\tau_b = 0$ equation (D-10) reduces to the appropriate two dimensional limit, which is given by equation (16) of Chapter II.

Integral Equation for the Side Walls

The boundary condition for the side walls is given by equation (A-37) as

$$\rho(\bar{x},\bar{y},\bar{z}=\tfrac{1}{0})w(\bar{x},\bar{y},\bar{z}=\tfrac{1}{0}) \equiv m \int_{-\infty}^{\infty}\int_{-\infty}^{\infty}\int_{-\infty}^{\infty} f(\bar{x},\bar{y},\bar{z}=\tfrac{1}{0},\ \xi,\eta,\zeta)\,\zeta\, d\xi d\eta d\zeta = 0 \qquad \text{(D-11)}$$

Noting that the result of integrating equation (D-11) is identical to equation (A-80), when the latter is set equal to zero, the following result can be written directly for $\bar{z} = 1$:

$$\frac{1}{2}\left[\frac{\tau_b \bar{x}_s}{\sqrt{1+\tau_b{}^2\bar{x}^2{}_s}}\left[\operatorname{Tan}^{-1}\left(\frac{\tau_d\sqrt{1+\tau_b{}^2\bar{x}^2{}_s}}{\tau_b \bar{y}_s}\right) - \operatorname{Tan}^{-1}\left(\frac{\tau_d\sqrt{1+\tau_b{}^2\bar{x}^2{}_s}}{\tau_b(\bar{y}_s-1)}\right)\right] + \right. \qquad \text{(D-12)}$$

$$\left.\left[\operatorname{Tan}^{-1}\left(\frac{\tau_d \bar{x}_s}{\bar{y}_s-1}\right) - \operatorname{Tan}^{-1}\left(\frac{\tau_d \bar{x}_s}{\bar{y}_s}\right)\right]\right] + \int_{\alpha_{506}}^{\alpha_{708}} \operatorname{Sin}\theta\, d\theta \int_{\varphi_{508}(\theta)}^{\varphi_{607}(\theta)} g_{w_s}(\theta,\varphi)\operatorname{Sin}^2\varphi\, d\varphi +$$

$$\int_{\pi}^{2\pi} \operatorname{Sin}\theta\, d\theta \int_{0}^{\pi} g_{w_s}(\theta,\varphi)\operatorname{Sin}^2\varphi\, d\varphi + \int_{\alpha_{708}}^{\pi} \operatorname{Sin}\theta\, d\theta \int_{\varphi_{408}(\theta)}^{\varphi_{307}(\theta)} g_{w_T}(\theta,\varphi)\operatorname{Sin}^2\varphi\, d\varphi +$$

$$\int_{0}^{\alpha_{506}} \operatorname{Sin}\theta\, d\theta \int_{\varphi_{105}(\theta)}^{\varphi_{206}(\theta)} g_{w_T}(\theta,\varphi)\operatorname{Sin}^2\varphi\, d\varphi = 0$$

The second integral of equation (D-12) can be evaluated immediately by noting that $g_{w_s}(\theta,\varphi)$ is a constant at the point $\bar{x} = \bar{x}''_s$, $\bar{y} = \bar{y}''_s$, $\bar{z} = 1$. Thus,

$$\int_{\pi}^{2\pi} \text{Sin } \theta \, d\theta \int_{0}^{\pi} g_{w_s}(\theta,\varphi)\text{Sin}^2 \, \varphi d\varphi = g_{w_s}(\bar{x}''_s,\bar{y}''_s) \int_{\pi}^{2\pi} \text{Sin } \theta d\theta \int_{0}^{\pi} \text{Sin}^2 \, \varphi \, d\varphi = \quad \text{(D-13)}$$

$$= \pi \, g_{w_s}(\bar{x}_s,\bar{y}_s)$$

where $\bar{x}''_s$ and $\bar{y}''_s$ have been replaced by $\bar{x}_s$ and $\bar{y}_s$, respectively. In order to transform the integrals of equation (D-12) from the variables θ and φ to the appropriate wall coordinates equations (A-4) through (A-11) are used. From these equations the following results are obtained directly:

$$\text{Sin } \theta \, \text{Sin}^2 \, \varphi \, d\theta d\varphi = \frac{\tau_d{}^3 \tau_b{}^2 d\bar{x}'_s d\bar{y}'_s}{\left[\tau_d{}^2+\tau_b{}^2(\bar{y}_s-\bar{y}'_s)^2 +\tau_d{}^2\tau_b{}^2(\bar{x}_s-\bar{x}'_s)^2\right]^2} \quad \text{(D-14)}$$

for the rear side wall,

$$\text{Sin } \theta \, \text{Sin}^2 \, \varphi \, d\theta d\varphi = - \frac{\tau_d{}^3 \tau_b{}^2 \bar{y}_s(1-\bar{z}'_T)d\bar{x}'_T d\bar{z}'_T}{\left[\tau_b{}^2\bar{y}_s{}^2 +\tau_d{}^2(1-\bar{z}'_T)^2+\tau_d{}^2\tau_b{}^2(\bar{x}_s-\bar{x}'_T)^2\right]^2} \quad \text{(D-15)}$$

for the lower channel wall, and

$$\text{Sin}\ \theta\ \text{Sin}^2\ \varphi\, d\theta d\varphi = -\frac{\tau_d{}^3\tau_b{}^2(\bar{y}_s-1)(1-\bar{z}''_T)d\bar{x}''_T d\bar{z}''_T}{\left[\tau_b{}^2(\bar{y}_s-1)^2+\tau_d{}^2(1-\bar{z}''_T)^2+\tau_d{}^2\tau_b{}^2(\bar{x}_s-\bar{x}''_T)^2\right]^2} \qquad \text{(D-16)}$$

for the upper channel wall. Introducing equations (D-14) through (D-16) into the integrals of equation (D-12) and using equations (A-4) through (A-11) to change the limits of integration yield

$$\int_{\alpha_{506}}^{\alpha_{708}} \text{Sin}\ \theta d\theta \int_{\varphi_{508}(\theta)}^{\varphi_{607}(\theta)} g_{w_s}(\theta,\varphi)\text{Sin}^2\ \varphi d\varphi = \int_0^1\int_0^1 g_{w_s}(\bar{x}'_s,\bar{y}'_s)K'_{w_s}(\bar{x}_s,\bar{x}'_s,\bar{y}_s,\bar{y}'_s)d\bar{x}'_s d\bar{y}'_s \qquad \text{(D-17)}$$

$$\int_0^{\alpha_{506}} \text{Sin}\ \theta d\theta \int_{\varphi_{105}(\theta)}^{\varphi_{206}(\theta)} g_{w_T}(\theta,\varphi)\text{Sin}^2\ \varphi d\varphi = \int_0^1\int_0^1 g_{w_T}(\bar{x}'_T,\bar{z}'_T)K'_{w_T}(\bar{x}_s,\bar{x}'_T,\bar{y}_s,\bar{z}'_T)d\bar{x}'_T d\bar{z}'_T \qquad \text{(D-18)}$$

$$\int_{\alpha_{708}}^{\pi} \text{Sin}\ \theta d\theta \int_{\varphi_{408}(\theta)}^{\varphi_{307}(\theta)} g_{w_T}(\theta,\varphi)\text{Sin}^2\ \varphi d\varphi = \int_0^1\int_0^1 g_{w_T}(\bar{x}''_T,\bar{z}''_T)K''_{w_T}(\bar{x}_s,\bar{x}''_T,\bar{y}_s,\bar{z}''_T)d\bar{x}''_T d\bar{z}''_T \qquad \text{(D-19)}$$

where $K'_{w_s}(\bar{x}_s,\bar{x}'_s,\bar{y}_s,\bar{y}'_s)$, etc. are given by equations (A-47), (A-49), and (A-51). Combining equations (D-12), (D-13), and (D-17) through (D-19) and making use of the expression for $G_{w_s}(\bar{x}_s,\bar{y}_s)$ given by equation

(A-45), the following result is obtained for the boundary condition at the front side wall ($\bar{z} = 1$):

$$g_{w_s}(\bar{x}_s,\bar{y}_s) = G_{w_s}(\bar{x}_s,\bar{y}_s) + \frac{1}{\pi}\left[\int_0^1\int_0^1 g_{w_s}(\bar{x}_s',\bar{y}_s')K'_{w_s}(\bar{x}_s,\bar{x}_s',\bar{y}_s,\bar{y}_s')d\bar{x}_s'd\bar{y}_s' + \right. \qquad \text{(D-20)}$$

$$\int_0^1\int_0^1 g_{w_T}(\bar{x}_T',\bar{z}_T')K'_{w_T}(\bar{x}_s,\bar{x}_T',\bar{y}_s,\bar{z}_T')d\bar{x}_T'd\bar{z}_T' +$$

$$\left.\int_0^1\int_0^1 g_{w_T}(\bar{x}_T'',\bar{z}_T'')K'_{w_T}(\bar{x}_s,\bar{x}_T'',\bar{y}_s,\bar{z}_T'')\,d\bar{x}_T''d\bar{z}_T''\right]$$

It can easily be shown that the result for the boundary condition at $\bar{z} = 0$ is identical to equation (D-20). Similarly, setting $\tau_b = 0$ it can be shown that equation (D-20) yields the result $g_{w_s}(\bar{x}_s,\bar{y}_s) = 0$. For $\tau_d = 0$ equation (D-20) reduces to the two dimensional result given by equation (16) of Chapter II with the nondimensional wall flux now given by $g_{w_s}(\bar{x}_s,\bar{y}_s)$.

BIBLIOGRAPHY

1. H. S. Tsien, "Superaerodynamics, The Mechanics of Rarefied Gases," Journal of the Aeronautical Sciences 13, Number 12 (1946).

2. M. Knudsen, "Die Gesetze der Molekularströmung und der inneren Reibungsströmung der Gasedurch Röhren,"Annalen der Physik 28, series 4, 75 (1909).

3. M. Perlmutter, "Flow and Heat Transfer Between Heated Plates of Finite Length in a Free-Molecular Flow Environment,"National Aeronautics and Space Administration, Technical Note D-2209 (1964).

4. D. R. Willis, A Study of Some Nearly-Free-Molecular Flow Problems, Princeton University Aeronautical Engineering Laboratory Report Number 440 (1958).

5. M. V. Smoluchowski, "Zur kinetischen Theorie der Transpiration und Diffusion verdünnter Gase,"Annalen der Physik 33, series 4, 1559 (1910).

6. P. Clausing, Dissertation, Amsterdam (1918).

7. P. Clausing, "Over De Stationnaire Strooming Van Zeer Verdunde Gassen," Physica 9, 65 (1929).

8. P. Clausing, "Über die Strömung sehr verdünnter Gase durch Röhren von beliebiger Lange," Annalen der Physik 12, series 5, 961 (1932).

9. W. Gaede, "Die äussere Reibung der Gase, "Annalen der Physik 41, series 4, 289 (1913).

10. R. E. H. Rasmussen, "Über die Strömung von Gasen in engen Kanälen," Annalen der Physik 29, series 5, 665 (1937).

11. A. S. D. Barrett and C. H. Bosanquet, "Resistance of Ducts to Molecular Flow," Imperial Chemical Industries Limited, Report BR-296 (1944).

12. G. P. Brown, A. DiNardo, G. K. Cheng, and T. K. Sherwood, "The Flow of Gases in Pipes at Low Pressures," Journal of Applied Physics 17, 802 (1946).

13. W. C. Demarcus, "The Problem of Knudsen Flow: Part 3. Solutions for One-Dimensional Systems," Atomic Energy Commission, Report K-1302, part 3 (1957).

14. W. Dong, Vacuum Flow of Gases Through Channels with Circular, Annular, and Rectangular Cross Sections, University of California, Ph.D. Thesis (1956).

15. H. J. Adzumi, Chemical Society of Japan 12, 285 (1937).

16. W. C. Demarcus and E. H. Hopper, "Knudsen Flow Through a Circular Capillary," Journal of Chemical Physics 23, 1344 (1955).

17. B. B. Dayton, "Gas Flow Patterns at Entrance and Exit of Cylindrical Tubes," Comm. on Vacuum Techniques, 1956 Vacuum Symposium Trans., 5 (1956).

18. L. L. Levenson, N. Milleron, and D. H. Davis, "Optimization of Molecular Flow Conductance," University of California Radiation Laboratory, Report 6014 (1960).

19. D. H. Davis, "Monte Carlo Calculation of Molecular Flow Rates Through a Cylindrical Elbow and Pipes of Other Shapes," Journal of Applied Physics 31, Number 7, 1169 (1960).

20. E. M. Sparrow, V. K. Jonsson, and T. S. Lundgren, "Free-Molecular Tube Flow and Adiabatic Wall Temperatures," Journal of Heat Transfer C 85, 111 (1963).

21. R. Narasimha, "Orifice Flow at High Knudsen Numbers," Journal of Fluid Mechanics 10, 371 (1961).

22. W. M. Howard, "Density Field for Rarefied Flow Through an Orifice," The Physics of Fluids 4, Number 4, 521 (1961).

23. W. A. Gustafson and R. E. Kiel, "Free Molecule Density Field for Orifice Flow," The Physics of Fluids 7, 472 (1964).

24. E. O. Gadamer, "Measurement of the Density Distribution in a Rarefied Gas Flow Using the Fluorescene Induced by a Thin Electron Beam," University of Toronto Institute for Aerospace Studies, Report Number 83 (1962).

25. H. Cook and E. A. Richley, "Measurements of Efflux Patterns and Flow Rates from Cylindrical Tubes in Free-Molecule and Slip Flows," National Aeronautics and Space Administration, Technical Note D-2480 (1964).

26. E. A. Richley and T. W. Reynolds, "Numerical Solutions of Free-Molecule Flow in Converging and Diverging Tubes and Slots," National Aeronautics and Space Administration, Technical Note D-2330 (1964).

27. T. W. Reynolds and E. A. Richley, "Flux Patterns Resulting from Free-Molecule Flow Through Converging and Diverging Slots," National Aeronautics and Space Administration, Technical Note D-1864 (1964).

28. E. M. Sparrow and A. Haji-Sheikh, "Velocity Profile and other Local Quantities in Free-Molecular Tube Flow," The Physics of Fluids 7, Number 8, 1256 (1964).

29. S.J. Townsend, "Free-Molecular Flow Through Axi-symmetric Tubes," University of Toronto Institute for Aerospace Studies, Report Number 106 (1965).

30. H. W. Liepmann, "Gaskinetics and Gasdynamics of Orifice Flow," Journal of Fluid Mechanics 10, 65 (1960).

31. Y. Wu, On The Internal Flow of Highly Rarefied Gases, New York University, Ph.D. Thesis (1964).

32. Y. P. Pao, Ph.D. Thesis, Princeton University (1964).

33. D. R. Willis, "Mass Flow Through a Circular Orifice and a Two-Dimensional Slit at High Knudsen Numbers," Journal of Fluid Mechanics 21, part 1, 21 (1965).

34. F. C. Hurlbut, R. G. Lord, and D. R. Willis, "Nearly Free Molecule Flow Through a Circular Orifice at High Pressure Ratios," Proceedings of the Fifth International Symposium on Rarefied Gasdynamics, Academic Press (to be published in 1966).

35. A. K. Sreekanth, "Transition Flow Through Short Circular Tubes," The Physics of Fluids 8, Number 11, 1951 (1965).

36. F. O. Smetana, W. A. Sherrill, II, and D. R. Schort, Jr., "Measurements of the Discharge Characteristics of Sharp-Edged and Round-Edged Orifices in the Transition Regime," Proceedings of the Fifth International Symposium on Rarefied Gas Dynamics, Academic Press (to be published in 1966).

37. F. B. Hildebrand, Methods of Applied Mathematics, Prentice-Hall, Inc., Englewood Cliffs, New Jersey (1952).

38. P. L. Bhatnager, E. P. Gross, and M. Krook, Physical Review 94, 511 (1954)

39. D. R. Willis, "Linearized Couette Flow for Arbitrary Knudsen Numbers, Kth Aero TN 52, Royal Institute of Technology (1960).

40. M. Abramowitz, "Evaluation of the Integral $\int_0^\infty x^n e^{-x^2 - \frac{a}{x}} dx$," Journal of Mathematics and Physics 32, 188 (1953).

41. D. R. Willis, Princeton University Aeronautical Engineering Report Number 683 (1964).

42. M. T. Chahine and R. Narasimha, "Evaluation of the Integral $\int_0^\infty v^n e^{\left[-(v-u)^2 - \frac{x}{v} \right]} dv$," Jet Propulsion Laboratory, California Institute of Technology, Technical Report Number 32-459 (1963).

43. F. I. Frankl, Trans. Acad. Sci., U.S.S.R. 58, Number 3 (1947).

VITA

Joseph Daniel Stewart was born in Savannah, Georgia, on June 20, 1941. He attended elementary and high schools in Savannah and was graduated valedictorian from Robert W. Groves High School in 1959.

In September of 1959 he entered Armstrong Junior College. After pursuing a general engineering curriculum, he transferred to the Georgia Institute of Technology in September of 1960. During the next year, he attended each school for one quarter while working part-time, and the remainder of that year was spent working full-time as a technician in the Engineering Division of the Union Bag Paper Corporation, Savannah, Georgia. In September of 1961 he returned to the Georgia Institute of Technology as a full-time student. Throughout the remainder of his undergraduate study he worked part-time as a technician in the Engineering Department of the Coca-Cola Company, Atlanta, Georgia. In December, 1963, he received the degree of Bachelor of Aerospace Engineering (with honor) and received an award for the highest grades among graduating seniors in Aerospace Engineering courses.

He continued his studies at the Georgia Institute of Technology as a graduate student, receiving a NASA Fellowship to study under the doctoral program. He received the degree of Master of Science in Aerospace Engineering in June, 1965. During the following summer he was employed as an engineer by the Aerospace Corporation in El Segundo, California. In the fall of 1965 he returned to the Georgia Institute

of Technology to complete the requirements for the doctoral degree. He is a member of Sigma Gamma Tau, Tau Beta Pi, Phi Kappa Phi, and Sigma Xi.

On September 2, 1961, he married the former Mary Agnes Scholl of Savannah, Georgia.